Water content and H-O-Li isotopes in lower crustal granulite minerals

Xiaozhi Yang

University of Science and Technology of China

Institut National Polytechnique de Lorraine

Water content and H-O-Li isotopes in lower crustal granulite minerals

Thesis by

Xiao-Zhi YANG

IN PARTIAL FULFILLMENT OF THE REQUIREMENTS FOR THE DEGREE OF DOCTOR OF PHILOSOPHY from USTC and DOCTOR from INPL

June, 2008

Committee Members

ZHANG Hongfu	*IGG/CAS Beijing*	*reviewer for INPL*
INGRIN Jannick,	*LMTG-OMP Toulous*	*reviewer for INPL*
REISBERG Laurie	*CRPG-CNRS Nancy*	
ZHENG Yongfei	*USTC Hefei*	
XU Yigang	*KLIGG/CAS Guangzhou*	
ZHENG Jiangping	*FES/CUG Wuhan*	
LI Shuguang	*USTC Hefei*	
XIA QunKe	*USTC Hefei*	*PhD director*
DELOULE Etienne	*CRPG-CNRS*	*PhD Director*

It was a long time before man came to understand that any true theory of the earth must rest upon evidence furnished by the globe itself, and that no such theory could properly be framed until a large body of evidence had been gathered together.

----Sir Archibald Geike, 1905

Acknowledgements

First and foremost, I would like to thank Qunke Xia and Etienne Deloule, my thesis advisors and trusted friends, not only for their excellent supervising and full supports on my Ph.D academic work but also for their always care on my living both at USTC and CRPG during the past several years. This thesis could not have been accomplished in this form without the scientific freedom they allowed me throughout the work.

I cannot fully express my gratitude to Shun Karato, Roberta Rudnick, David Kohlstedt, Hans Keppler, Kent Condie, Jannick Ingrin, George Rossman, John Valley, Eric Rybacki, Sylvie Demouchy, Cin-Ty Lee and Catherine McCammon for many fruitful discussions. I especially thank Shun for his always kindly guidance, encouragement and suggestions, which arose my further interest into the field of mineral physics, and Roberta for her careful opinions on many questions, which help me go deep into a lot of issues. I also thank Roland Stalder, Horst Marschall, Roland Burgmann, Attila Demeny, Luigi Dallai, Jochen Hoefs, Juan Carlos Afonso, Anne Peslier, Peter Kelemen, Jennifer Wenner, Terry Plank, John D. Clemens, John Tarney, Eugen Libowitzky, Thomas J. Shankland, Ikuo Katayama, Elizabeth Johnson, Friedemann Freund, Qicheng Fan, Yongfei Zheng, Xiaolong Huang, Yigang Xu, Xiachen Zhi, Yongsheng Liu and Peifen Xu for their suggestions and discussions on many subjects, both on geochemistry and geophysics, although many of them were not included in this thesis.

I appreciate Denis Mangin, Claire Rollion-Bard and Michael Champenois for their invaluable help, assistance and teaching on ion microprobe, and Caroline Guilmette on H extraction and isotopic analysis by H-manometry and Isotopic Ratios Mass Spectrometry (IRMS). Without their help, I could not finish the instrumental analyses and this thesis on time. I thank Romain Mathieu, Anne-Sophie Bouvier, Céline Martin, Johanna Marin, Clément Yonta Ngouné, Maxence Paul, Magali Pujol and Lei Zheng, my fellow graduate students, and

Laurent Tisssandier, a postdoc worker, and Aurelie Didot, the secretary, who helped me so much for my living and studying at CRPG.

I encountered many excellent teachers and received wonderful education for my undergraduate and graduate studies at USTC. Thanks to all of them for preparing me a good background on many disciplines, upon which I could go further and deeper into this thesis and enjoy the research. A debt of gratitude to my classmates and many friends at both Hefei and Nancy, who helped me a lot to go through this thesis, especially when I got into hard work and sometimes fell into a blue mode with my research. I thank the *Programme Sino-Français de Recherches Avancées* (PRA) program for providing me the financial support for my survival at CRPG. I also thank Bernard Marty for driving me to Cologne and and Marc Chaussidon for arranging me a car to Nancy in the *2007 Goldschmidt Conference* and CRPG for providing me the financial support.

I thank David Bell for providing me the KBH-2 opx samples, Qicheng Fan, Yigang Xu, Jianping Zheng and Xiachen Zhi for some granulite and peridotite samples. Many thanks also go to Florence Atig for translating the abstract into French.

Last, but never least, I would like to thank my parents ---- from whom the support and encouragement enables me the education in China for about 20 years. On a more personal level, I thank Li, my girlfriend, whose love and eternally optimistic perspective on life provided me the encouragement and patience I needed in order to go through this work.

Abstract

Systematic Fourier transform infrared spectrometer (FTIR) and ion microprobe (SIMS) investigations of common lower crustal minerals (pyroxenes and plagioclase: from Hannuoba, Nushan and Daoxian of eastern China), as well as mantle peridotite minerals (pyroxenes and olivine: from Hannuoba and Nushan), were undertaken to better understand the composition of structurally bound H-species within these nominally anhydrous minerals, the possible lateral and vertical variations of H_2O in the deep continental lithosphere (lower crust and upper mantle), and the H-, O-, and Li- isotopes and REE compositions of the coexisting minerals within the continental lower crust. This is the first time to document the water content and H-O-Li isotopes of the main minerals in the continental lower crust.

The nominally anhydrous minerals, such as pyroxenes and plagioclase, in the lower crustal granulites generally contain trace amounts of water in the form of structurally bound hydroxyl and less molecular H_2O, with their contents (H_2O by wt.) varying from 200 to 2330 ppm for clinopyroxene, 60 to 1875 ppm for orthopyroxene, 65 to 900 ppm for plagioclase and 155 to 1100 ppm for the estimated bulk compositions. The average bulk content is about 450 ppm, and therefore the lower crust is estimated to contain $\sim 4.26 \times 10^{18}$ kg H_2O in the nominally anhydrous minerals. A significant contrast in water content is observed between Precambrian and Phanerozoic continental deep crust, implying a more hydrous ancient lower crust relative to the modern one.

H_2O contents of the main continental lower crustal minerals, and their bulk concentrations, are obviously higher than those in the underlying lithospheric mantle, despite their large lateral variations, suggesting vertical variations of H_2O content in the deep continental lithosphere (lower crust vs. upper mantle). Such water contrast may be related with the petrogenesis of these rocks (e.g. partial melting and/or fractional crystallization), and can strongly affect the

rheological behavior of the deep continental lithosphere below the North China Craton, which probably results in different lithospheric structures and processes between different tectonic zones beneath this craton, e.g. lithospheric thinning vs. thickening.

The O-isotopic ratios of studied pyroxenes, and probably the bulk samples, range from ~4.5 to 12.5‰, higher than or nearly comparable to that of normal mantle (5.7±0.5‰) depending on the sample localities. Inter-grain $\delta^{18}O$ variations up to 2-3‰ can be observed for the same mineral even in <1 cm scale in some samples, in contrast to their nearly uniform intra-grain distribution, implying heterogeneities between different grains. Consistency between O-isotopic and cation exchange temperatures suggests the preservation of peak-metamorphic compositions.

The lower crustal granulite minerals from the North China Craton are characterized by relatively high δD values compared to the normal mantle, e.g. -80~-10‰ for the former vs. -90~-60‰ for the latter. Intra-grain variations of δD on some grains were probably caused by diffusion-induced processes shortly before or during their entrainments or exhumation, however, the minerals were usually in equilibrium with each other with respect to their average H isotopic compositions, indicating weak influences from such diffusion processes. The relatively heavier D/H ratios of the lower crustal minerals can be accounted for by melt dehydration, e.g. in the crystallization of granulite phases, but mainly through the degassing loss of reductive H-species (e.g. H_2, H_2S).

Lithium content varies from 3.2 to 34.2 ppm for cpx, 0.6 to 9.1 ppm for opx, 0.2 to 12.1 ppm for plag and ~ 1.9 to 12.6 ppm for bulk compositions, with an average bulk value of ~ 5.2 ppm in the lower crust. The studied minerals are characterized by depleted Li-isotopic values relative to normal mantle, e.g. -13 to 4.7‰ with estimated bulk values of -11 to 2‰ vs. 2 to 6‰. Large variations in δ^7Li observed on some grains were probably related with diffusion-driven

processes; however, the preservation of equilibrium δ^7Li fractionations between coexisting minerals for most samples with respect to their average compositions indicates that the initial δ^7Li compositions (reflected by the average value of multi-points and multi-grains) were not largely influenced by such diffusion-related fractionations or that the individual minerals experienced similar extents of δ^7Li resetting by Li diffusion in a closed system. The large δ^7Li compositions probably reflect their source heterogeneities and are suggested to be ultimately related with kinetic Li isotopic fractionation during the intrusion of their original melts to the preexisting lower crust or by the coupled effects from recycled crustal materials on their original melts and kinetic Li isotopic fractionation during magma underplating.

The preliminary results on the H-O-Li isotopic systematics indicate that that pervasive fluids are absent in the continental lower crust either on large or local scales. The dehydration during the formation of granulites occurs probably in their original melt prior to the crystallization of granulite minerals, mainly in the manner of degassing loss through reductive H-species (e.g. H_2 etc.). However, it has to be asserted that these conclusions are based only on samples from the North China Craton, and it is not clear that if they are applicable to the lower crust globally because of the complexities involved in the composition, formation and evolution of the deep crust.

Key words: continental lower crust, lithospheric mantle, granulite and peridotite, water content, REE, H-O-Li isotopes, FTIR, ion microprobe

摘 要

应用傅里叶变换红外光谱(FTIR)和离子探针(SIMS)技术分别对中国东部大陆下地壳麻粒岩(包括来自汉诺坝，女山和道县的捕虏体和地体样品共 4 套；以及若干来自汉诺坝和女山的地幔橄榄岩样品)主要组成矿物(单斜辉石，斜方辉石和斜长石)中的结构水含量和 REE 与 Li 含量以及 H, O, Li 同位素组成进行了系统性的测定分析，旨在更好地理解下地壳内的水含量，深部岩石圈中的水分布，下地壳的 H 和 Li 同位素组成以及可能的流体活动．本论文是国际上首次对大陆下地壳中主要组成矿物的水含量和 H-O-Li 同位素组成进行分析研究。

研究结果表明(限于本文研究的样品)：

下地壳麻粒岩中的这些名义上无水矿物普遍含有一定量以 OH 和 H_2O 形式存在的结构水，其含量(通常以 H_2O 的重量百分含量形式表示)分别为：单斜辉石，200-2330 ppm；斜方辉石，60-1875 ppm；斜长石，65-900 ppm；全岩含量可达 1000 ppm 以上(155-1100 ppm)．这表明下地壳内水的分布是显著不均一的．这些麻粒岩的平均水含量约为 450 ppm，由此估计蕴含在大陆下地壳内镁铁质麻粒岩中的水含量至少为 4.26×10^{18} kg．形成于前寒武纪和显生宙的大陆下地壳具有截然不同的水含量(前者明显较后者偏高)，可能指示早期的下地壳更加富水．

下地壳中单矿物以及估测的全岩结构水含量比岩石圈地幔中显著高的多，表明深部岩石圈中水含量的垂向不均一性．这种不均一性

可能与两个圈层中岩石的形成方式以及部分熔融过程有关. 下地壳和岩石圈地幔之间水含量的差异能对其流变性质产生直接影响, 并可能进一步影响深部岩石圈内的动力学过程, 使得岩石圈处于减薄或增厚状态.

麻粒岩中辉石的氧同位素组成为 4.5 至 12.5‰(考虑到这些共存矿物可能处于氧同位素的平衡状态, 其全岩氧同位素组成也可能在这个范围区间). 相较正常地幔而言(5.7±0.5‰), 一些产地的样品具有显著偏高的氧同位素组成, 而一些产地则与之相当; 前者可能指示了再循环的地壳物质的影响. 样品中的辉石颗粒无例外的具有均一的氧同位素组成(颗粒内部), 但颗粒之间同种矿物甚至在同一样品中 <1 cm 尺度内的差异可达 2-3‰, 暗示颗粒之间的不均一性. 辉石氧同位素平衡温度和岩石学 Fe-Mg 离子交换平衡温度之间的一致性指示样品峰期变质作用时的氧同位素组成没有被后期过程改变.

相较正常地幔而言(-90~-60‰), 下地壳中矿物的氢同位素组成显著偏高(-80~-10‰). 在仪器误差范围内, 多数颗粒氢同位素组成自核至边部均一分布, 但有少数颗粒显示较大的变化, 可能是由样品出露前(或出露过程中)一些近期事件所致; 但矿物之间的平均氢同位素组成却处于平衡状态, 暗示其初始组成并没有被显著改变. 下地壳矿物中普遍偏高的 D/H 比值可能同麻粒岩成岩过程中的脱水去气作用有关; 该作用可能发生在熔体的结晶过程中, 可能主要表现为 H 以还原性组分形式(如 H_2, H_2S 等)脱离体系.

下地壳矿物中单斜辉石最为富 Li，其次是斜方辉石，而斜长石相对最为亏损，其含量变化分别为：单斜辉石，3.2~34.2 ppm；斜方辉石，0.6~9.1 ppm；斜长石，0.2~12.1 ppm；由此估计的全岩含量为 1.9~12.6 ppm (平均含量约 5.2 ppm)．这些矿物的δ^7Li 为-13~4.7‰ (估计的全岩组成为-11~2‰)，多数明显低于正常地幔(2~6‰)．个别颗粒表现出大的δ^7Li 变化(同氢同位素结果相似)，可能是由样品出露前(或出露过程中)一些近期事件所致；但矿物间平均 Li 同位素组成多数处于平衡状态，暗示其初始组成没有显著改变或这些矿物经历了相同程度的封闭体系 Li 扩散．下地壳矿物中较大的δ^7Li 组成反映了源区的不均一性；相对较低的 Li 同位素组成可能起源于麻粒岩起始岩浆侵入到下地壳中的动力学分馏作用或原岩组成以及 Li 同位素动力学分馏作用的共同影响．

基于 H，O，Li 同位素组成的研究初步指示：无论是大尺度(如不同产地间)还是小尺度(如同一样品内部不同颗粒间)上，流体都不可能在下地壳内普遍存在；麻粒岩脱水作用可能主要发生在麻粒岩矿物自熔体中结晶之前，这意味着麻粒岩相变质作用应该是在相对干态的条件下进行的．遗憾的是，本文用于 H-O-Li 同位素研究的样品只取自华北克拉通，而下地壳的成因，组成和演化等是非常复杂的，这些结论是否具有全球尺度上的通用性还需要更多深入的研究．

关键词：下地壳，岩石圈地幔，麻粒岩，橄榄岩，水含量，H-O-Li 同位素组成，傅立叶变换红外光谱，离子探针

Résumé

Une étude par spectroscopie infrarouge à transformée de Fourrier (FTIR) et par microsonde ionique (SIMS) des minéraux majeurs de la croûte inférieure (pyroxènes et plagioclases) et des péridotites mantelliques (pyroxènes et olivine) a été entreprise afin de mieux caractérisé les mécanismes d'incorporation et les teneurs en eau de ces minéraux nominalement anhydres, et de déterminer leurs compostions isotopiques en H, O, Li et teneurs en éléments trace, pour retracer les échanges latéraux et horizontaux de l'eau dans la lithosphère continentale profonde.

Les minéraux nominalement anhydres, comme les pyroxènes et plagioclase, dans les granulites de la croûte inférieure contiennent de l'eau en trace essentiellement sous forme hydroxyles et accessoirement sous forme moléculaire, avec des concentrations (exprimées en poids H_2O) allant de 200 à 2330 ppm pour les clinopyroxènes, de 60 à 1875 ppm pour les orthopyroxènes, de 65 à 900 ppm pour les plagioclases. Les teneurs calculées en roche total de 155 à 1100 ppm, avec une concentration moyenne dans la roche de 450 ppm. A l'échelle de la terre entière, la croûte inférieure contiendrait ~ 4,26 $.10^{18}$ kgH_2O dans ses minéraux nominalement anhydres. Un contraste significatif dans la concentration d'eau est observé entre les croûtes continentales profondes du Précambrien et du Phanérozoique, impliquant une croûte inférieure ancienne plus hydrique que la récente.

Les teneurs en H_2O des minéraux principaux et en roche totale de la croûte continentale inférieure sont manifestement plus élevées que celles du manteau lithosphérique sous-jacent, malgré de grandes variations latérales, suggérant des variations verticales de la quantité d'H_2O dans la lithosphère continentale profonde (croûte inférieure vs manteau supérieur). Un tel contraste peut être du à la pétrogenèse de ces roches et peut fortement affecter le comportement rhéologique de la lithosphère continentale profonde en dessous du Craton de

Chine du Nord au cours des différents épisodes tectoniques qui l'on affecté, notamment les épisodes d'amincissement ou d'épaississement lithosphérique.

Les rapports isotopiques de l'oxygène des pyroxènes étudiés, et probablement les roches totales, vont de ~ 4,5 à 12,5‰, des valeurs comparables ou plus élevés que celles du manteau (5,7±0,5‰), Ceci indique l'implication des matériaux recyclés de la croûte durant lea pétrogenèsedes échantillons ayant un $\delta^{18}O$ élevé. Pour quelques échantillons, des variations $\delta^{18}O$ allant jusqu'à 2-3‰ ont été observées à l'échelle d'un même minéral, une échelle inférieure à 1cm, impliquant une hétérogénéité à l'échelle du grain, en contraste avec leur distribution presque uniforme sur chaque grain. La cohérence entre les températures des échanges O-isotopique et cationique suggère la préservation des compositions de pic métamorphique.

Les minéraux de la croûte inférieure sont caractérisés par des valeurs de δD relativement élevées comparées à celles du manteau, avec des valeurs de -80~-10‰ pour la première contre -90~-60‰ pour le deuxième. Les larges variations du δD au sein de quelques grains ont probablement été causées par des processus de diffusion induite peu avant ou pendant leur exhumation. Cependant, les minéraux sont le plus souvent en équilibre les uns avec les autres lorsque l'on considère leurs compositions isotopiques moyennes, indiquant une faible influence de ces processus. Les rapports D/H relativement élevés des minéraux de la croûte inférieure peuvent être considérés comme résultant soit d'une déshydratation par fusion, par exemple dans les phases de cristallisation de granulites, ou plus probablement d'une réduction de l'eau et une perte d'hydrogène sous forme réduite (par ex. H_2, H_2S).

La teneur en Lithium varie de 3,2 à 34,2 ppm pour les clinopyroxènes, 0,6 à 9,1 ppm pour les orthopyroxènes, 0,2 à 12,1 ppm pour les plagioclases et 1,9 à 12,6 ppm pour les roches totales, avec une valeur moyenne globale de ~ 5,2 ppm dans la croûte inférieure. Les minéraux étudiés sont caractérisés par des valeurs isotopiques appauvries par rapport au manteau habituel, avec des $\delta^{7}Li$

variant de -13 à 4,7‰ et des valeurs en roche totale estimées de -11 à +2‰, comparé à des valeurs de +2 à +6‰ pour le manteau. Les grandes variations en δ^7Li observées sur quelques grains sont probablement liées aux processus de diffusion. Cependant, la préservation de l'équilibre du rapport δ^7Li entre les minéraux coexistant montre que les compositions initiales en δ^7Li n'ont pas été modifiées de façon notable par une telle diffusion, dépendante des rapports élémentaires. La dispersion des valeurs reflètent l'hétérogénéité de la source des granulites, et les valeurs bassent resultent probablement de la perte par diffusion de Li pendant la mise en place des liquides silicatées provenant du manteau dans la croûte inférieure.

La grande hétérogénéité des teneurs en eau et en Lithium, et des compositions isotopiques de H-O-Li indique l'absence de circulation de fluide pervasive au travers de la croûte inférieure, qui aurait pour effet de supprimer les hétérogénéités à petite échelle et de les diminuer fortement à grande échelle.

Le mot cle: croûte continentale inférieure; manteau lithosphérique; granulites; péridotite; eau; H-O-Li isotopiques; spectroscope infrarouge (FTIR); sonde ionique (SIMS)

Table of Contents

List of Illustrations and Tables

< Chapter 2>

< Chapter 3>

< Chapter 4>

< Chapter 5>

< Chapter 6>

< Chapter 7>

< Chapter 8>

< Chapter 3>

< Chapter 5>

< Chapter 6>

< Chapter 7>

< Chapter 8>

< Appendix>

1 Introduction

The earth is distinguishable from other rocky planets in our solar system by the presence of chemically evolved crust, the continental crust, and liquid water on the surface, which promoted the later evolution and led to the appearance of human life. Without them, there would be no mountains, broad plains, green forests, rivers and oceans on the planet, neither the diversity of land-based life styles.

The continental crust covers about 40% of the Earth's whole surface area, which comprises, however, only about 0.35% of the Earth's whole mass. Relative to the thin (~ 7 km on average), basaltic and young (< 200 Ma) oceanic crust, the continental crust is thick (20-60 km, about 40 km on average), and is predominated by intermediate composition and contains almost every rock type on Earth known to geologists. The continental crust is usually divided into 3 different layers: the upper, middle and lower crust, with their variations in depth, on average, from 0 to ~15, 15 to ~25 and 25 to ~40 km, respectively. Although the continental crust constitutes one of the most accessible regions of the Earth compared to the mantle, core and even the ocean crust, there are considerable debates concerning many questions in the crust, with special respect to the lower crust, upon which the studies are still very scarce.

1.1 The continental lower crust

The continental lower crust is defined, based on the division of the crust, beneath the average depth of 20-25 km, the middle crust, and above the Moho discontinuity (Holbrook et al., 1992; Christensen and Mooney, 1995; Rudnick and Fountain, 1995). The lower crust consists mainly of granulite-facies rocks, which are accessible either as large tracts of surface outcrops (terrains) uplifted by tectonic movements or as xenoliths captured by kimberlites/alkaline basalts. The deep crust can be further divided into the upper felsic layer and the lower

mafic layer, although it is, as a whole part, proposed to be mafic to intermediate in composition (Rudnick, 1995; Rudnick and Gao, 2003). It is suggested by these available studies that the lower crust is ~ 2.8-3.1 $g \cdot cm^{-3}$ in density, ~ 6.9-7.2 $km \cdot s^{-1}$ in seismic velocity (V_p), and ductile in rheological behavior.

The lower crust is one of the most important layers inside the earth. It is the interface between the crust and upper mantle, and is the direct place where crustal accretion, magma underplating and crust-mantle exchange occur; it has critical implication for understanding the composition and evolution of the crust and even the bulk Earth. Three main approaches have been used/using for the knowledge about the composition of the lower crust (reviewed by Rudnick and Fountain (1995) and Rudnick and Gao (2003)): (1) through studying samples derived directly from the lower crust. These include uplifted terrain granulites or exposed deep-crustal sections, and deep-crustal granulite xenoliths (Harley, 1989; Percival et al., 1992; Rudnick, 1992). The former is argued that they are representative of only the middle to upper lower crust, or that they experienced slow uplift and long tectonic evolution so that they cannot record their source information in an efficient way, by contrast the latter are more representative of the lower crust since that they were transferred to the surface very quickly, e.g. several to dozens of hours. (2) by correlating seismic velocities with mineral or rock lithologies (Christensen and Mooney, 1995; Rudnick and Fountain, 1995; Wedepohl, 1995). (3) via surface heat-flow measurements (Jaupart and Mareschal, 2003). The former two are the most widely used methods until recently.

The lower crust is highly heterogeneous in both its physical and chemical compositions, properties and behaviors, as seen in exposures of granulite terrains and deep-seated granulite xenoliths, as well as by geophysical deep sounding measurements (Rudnick and Fountain, 1995; Rudnick and Gao, 2003). Heterogeneity of the deep crust is not only spatially, but also temporally. The former can be observed from the lateral variation in chemical compositions,

lithologies and geophysical behaviors, e.g. rheological strength, seismic velocity, etc. (Rudnick and Fountain, 1995; Rudnick and Gao, 2003; Afonso and Ranalli, 2004); while the latter can be seen from the notable contrast in composition between Archean and post-Archean (Kröner, 1985; Taylor and Mclennan, 1995), which may be related with different crustal-growth mechanisms and/or tectonic regimes operated in these different evolutionary stages of the Earth (Taylor and Mclennan, 1995).

1.1.1 Water in the deep crust

"There can be few topics in Earth sciences today where such totally incompatible conclusions have been reached by researchers from different disciplines as the question of the water content of the lower continental crust in stable plate interiors" ---- *Yardley and Valley (1997)*

The presence or absence, nature and compositions of water, or more commonly fluids, in the continental lower crust are crucial issues for determining the nature, structure, formation and evolution of the lower crust, the crust and even the Earth. This question, however, has been in debate for more than two decades (Yardley, 1981; Lee et al., 1983; Shankland and Ander, 1983; Haak and Hutton, 1986; Yardley, 1986; Connolly and Thompson, 1989; Hyndman and Shearer, 1989; Hyndman et al., 1993; Yardley and Valley, 1997), and has been regarded by some people as one of the most confused enigmas in geosciences as cited above (Yardley and Valley, 1997). Considering the spatial population of the lower crust, sandwiched between the overlying hydrous sphere and hydrous phases-predominated upper and middle crusts and the underlying anhydrous uppermost mantle, it may play a special role both in buffering the water content contrast between the upper crusts and mantle region and in exchanging water between them.

Debates in terms of this issue arise mainly from different approaches in the Earth sciences. Granulite consists largely and generally of nominally anhydrous

minerals, e.g. clinopyroxene, orthopyroxene, plagioclase, and minor amounts of quartz. The existence of these phases indicates the absence of fluids, or that they will react with fluids to produce hydrated (and/or carbonated) retrograde products (Yardley and Valley, 1997), for example via:

$$2\text{enstatite} + H_2O + CO_2 = \text{talc} + \text{magnetite} \quad \text{(Eq 1-a)}$$

$$2\text{K-feldspar} + 3\text{enstatite} + 2H_2O = 2\text{phlogopite} + 6\text{quartz} \quad \text{(Eq 1-b)}$$

$$3\text{enstatite} + 5\text{diopside} + 2H_2O + 2CO_2 = \text{dolomite} + 2\text{tremolite} \quad \text{(Eq 1-c)}$$

$$10\text{quartz} + 3\text{enstatite} + 4\text{dolomite} + 2H_2O = 2\text{tremolite} + 8CO_2 \quad \text{(Eq 1-d)}$$

In addition, O-isotope investigations reveal significant $^{18}O/^{16}O$ heterogeneity in lower crustal granulites or minerals, demonstrating that pervasive deep crustal fluid flow and isotopic homogenization is not a major process operating upon a regional scale (Valley and Graham, 1991; Kempton and Harmon, 1992). While on the other hand, it is suggested that, based on a popular explanation for the deep crustal high electrical conductivity, the lower crust is nearly saturated with an inter-connected pore brine, which may also account for lower crustal seismic reflectors (Hyndman et al., 1993). Furthermore, the lower crust is in equilibrium with a water fugacity of tens to hundreds of bars, it should theoretically contain remarkable amounts of water (Yardley and Valley, 1997).

Where water is stored, and what are the contents, in the continental lower crust is thus a crucial question deserving a deep and thorough investigation. One likely candidate is water incorporated in the structure of nominally anhydrous granulite minerals, as hydroxyl or less molecular H_2O.

1.1.2 Water in nominally anhydrous minerals

Knowledge of the amount of water, or hydrogen species, inside the earth at present, and in the past, is a critical issue for understanding the petrological, geochemical, geophysical and dynamical processes of the Earth, as well as for constraining the segregation, accretion and evolution model of the planet and

the whole cycle of hydrogen in its interior. This relies heavily on the well-known fact that water, even in trace amounts, has a strong influence on many chemical and physical properties of its host silicate minerals/rocks, including mechanical and rheological strength (e.g. Griggs, 1967; Kronenberg et al., 1986; Hirth and Kohlstedt, 1996), rate of ionic diffusion (Goldsmith, 1987; Elphick et al., 1988), melting behavior (Kushiro, 1972; Arndt et al., 1998) and electrical conductivity (Karato, 1990); and, if extracted from minerals, it contributes to the formation of ore deposits and hydrous fluids, and even the triggering of deep-seated earthquakes (Meade and Jeanloz, 1991).

Since the first work by Griggs and Blacic (1965) and the pioneering work by Martin and Donnay (1972), it has been gradually and widely accepted that nominally anhydrous minerals can commonly contain few to several thousand ppm water (H_2O by weight) in their structure, predominated by OH and/or less molecular H_2O, and are the main hydrogen reservoir in the deep earth, especially in the upper mantle (Bell and Rossman, 1992b; Ingrin and Skogby, 2000; Bolfan-Casanova, 2005). Such water may play crucial but diversified roles on many properties and processes in the earth (e.g. Williams and Hemley, 2001; Keppler and Smyth, 2006). Recent work on quartz, garnet and igneous feldspars in the upper and middle crust demonstrates that they contain more than ~ 1200 ppm H_2O as dispersed, structurally bound OH groups, molecular H_2O and/or NH_4^+ (Kronenberg, 1994; Johnson, 2003; Johnson and Rossman, 2003, 2004).

The continental lower crust is dominated by nominally anhydrous cpx, opx and plag in granulite facies[†], so these nominally anhydrous minerals in principle can also incorporate some water/hydroxyl in them. However, to date, there has no systematic and detailed survey on the possible water content and variation

[†] Mineral abbreviations are the same throughout this thesis: clinopyroxene, cpx; orthopyroxene, opx; plagioclase, plag; garnet, grt; amphibole, amp; magnetite, mt.

of lower crustal minerals, and it is still not clear about the hydrous status of the lower crust. These are in strong contrast to the work performed extensively on upper- and middle-crust and mantle phases. A thorough investigation about water in the lower crust is therefore necessary for a better understanding of the whole Earth system.

1.1.3 H-O-Li stable isotopes

Stable isotopes, such as hydrogen, oxygen and lithium, are powerful tools for deciphering metamorphic histories and fluid-related processes, and tracing crust-mantle recycling, although the latter is at present in kind of debate for Li-isotopes (Elliott et al., 2004; Tomascak, 2004; Rudnick and Ionov, 2007). These species, especially hydrogen and lithium isotopes, provide excellent access into how water/fluid has behaved during granulite-facies metamorphism, formation of the continental lower crust and even evolution of the Earth.

H While hydrogen in the hydrosphere, shallower upper and middle crust and upper mantle has been well characterized with respect to the mass/content and isotopic compositions (Sheppard and Epstein, 1970; Graham et al., 1984; Kyser and O'Neil, 1984; Criss and Taylor, 1986; Kyser, 1986), its amount and D/H ratios in the lower crust remain poorly constrained questions. It is well accepted that δD is from -90 to -60‰ in the normal mantle (Kyser and O'Neil, 1984), up to -9‰ for the upper oceanic and continental crust (Yui and Jeng, 1990; Putlitz et al., 2000) and about 0‰ in the ocean (Hoefs, 1997). If the crust and ocean were ultimately derived from the mantle, e.g. via differentiation and degassing, respectively, the lower crust may serve to buffer the isotopic variations between the different hydrogen reservoirs or sphere layers.

Li Lithium isotopes are a recently developed new tracer in geosciences, and are in a relatively young area of research; most of the work has been conducted during the last decade (e.g. Tomascak, 2004). Because of the incompatible and highly fluid-sensitive behavior, Li-isotopes have been widely applied/applying to

many geological processes, e.g. recycling of crustal materials during subduction, low-T alteration, partial melting and crystal fractionation, mantle metasomatism and/or peridotite-melt interaction (Tomascak, 2004; and references therein). In contrast to the comprehensive studies on the upper mantle (Rudnick and Ionov, 2007; Tang et al., 2007; Wagner and Deloule, 2007; Ionov and Seitz, 2008; and references therein), upper to middle continental crusts (Teng et al., 2004) and ocean seawater (Chan and Edmond, 1988; Chan, 2003), Li-isotopic composition of the lower crust is poorly understood, especially into its mineral assemblages; the only report is concentrated on the bulk δ^7Li budget of the lower crust (Teng et al., 2008).

O Relative to hydrogen and lithium isotopes, the continental lower crust has been better defined in terms of its oxygen isotopic compositions. Available data demonstrates that the deep crust is highly variable in the $^{18}O/^{16}O$ ratios, in the range of 5.4-13.5‰ (Kempton and Harmon, 1992), but mosty higher than that of normal mantle (Mattey et al., 1994; Harmon and Hoefs, 1995). However, previous studies were mostly performed on bulk samples, with only one report on granulite accessory magnetite (Valley and Graham, 1991), rather than on the main constitutions, e.g. pyroxenes and plagioclase.

In summary, very little work, if any, concerning H-, Li- and O-isotopes has been conducted on individual minerals in the continental lower crust, especially into the fractionations between coexisting phases and micro-scale variations. This may be caused, at least in part, by: 1) lower crustal samples, e.g. granulite xenoliths, are, if accessible, usually very small, and it is difficult, or impossible, to separate enough amounts of minerals for a common investigation; 2) poor precision and spatial resolution in the traditional techniques and instruments limited the development in these isotopic fields. In these cases, stable isotopic compositions of the lower crust are poorly constrained, especially for any possible micro-scale heterogeneities (e.g. inter- and intra-grains/minerals).

1.2 Framework of this study

Fourier transform infrared (FTIR) absorption spectroscopy is a highly sensitive, site-specific, high resolution (down to 20 μm), and non-destructive in situ method for the study of OH and molecular H_2O in minerals. It provides not only quantitative determination of the amount of structurally incorporated water and OH in the target minerals, although depending on the experimentally-calibrated absorption coefficients for given phases, but also the ability to distinguish them from water in fluid inclusions, water and hydrous minerals in cracks, alteration productions such as talc, serpentine or clays, melt inclusions and instrumental artifacts such as ice films on cryogenic detectors (Rossman, 1996). While in any studies requiring measurements of isotopic compositions and/or trace-element abundances with very high spatial resolution, Secondary ion mass spectrometry (SIMS), or ion microprobe, is still the premier tool at present for geochemistry and cosmochemistry, despite of the recent development/improvement in laser-assistant spectrometry techniques. It offers high resolution (down to ~ 1 to 20 μm), high sensitivity (ppm to ppb), and nearly non-destructive in situ analysis. These advantages are especially significant for samples that are too small/rare for the measurement by other techniques and for the determination of possible micro-scale variations (Deloule et al., 1991a; Valley et al., 1998). Using these facilities, abundances of water structurally bound into minerals, lithium and rare earth elements (REE), and isotopes of hydrogen, oxygen and lithium in samples derived from the continental lower crust can be measured precisely.

This thesis is a compilation of the studies at the University of Science and Technology of China (USTC) and the Centre de Recherches Pétrographiques et Géochimiques (CRPG), and profits ultimately from a cooperation project between China and France, *Programme Sino-Français de Recherches Avancées*. In this project, water, REE and Li contents and H-O-Li stable isotopes in lower crustal minerals have been systematically measured for the first time.

1.3 Aim of this study

In this thesis, lower crustal samples, including mainly xenolith granulites and less terrain granulites, from Hannuoba, Nushan and Daoxian in the north, east and south China, respectively, as well as some coexisting mantle peridotite xenoliths from Hannuoba and Nushan, were investigated by geochemical and isotopic methods. The petrologic, mineralogical, chronological and metamorphic characteristics of these samples are described in the thesis and form a solid basis for the interpretation and discussion of the subsequent chapters.

The aim of this thesis is to better quantify the composition and distribution of structural water in the continental lower crust, the contrast in water content between the lower crust and lithospheric mantle, partitioning of REE between lower crustal minerals, and D/H, $^{18}O/^{16}O$ and $^{7}Li/^{6}Li$ ratios of lower crustal granulite minerals. Upon these investigations, possible fluid-related processes and water activities in the lower crust are further explored. These are provided in the following chapters.

1.4 Structure of this study

This thesis is subdivided into 9 chapters, starting with the general introduction presented here. Instead of putting separate introduction, data, discussion and conclusion in each chapter as an independent one, as how many other PhD theses have been made up, the various chapters in this thesis are arranged in a slightly different way: descriptions of all the samples, illustrations of all the data and details of analytical methods are given as separate chapters, respectively; discussions about different issues are given in subsequent different chapters.

Chapter 2 gives a brief introduction to the geological setting of the studied regions (in the eastern China), including the North and South China Cratons. The former is made up of three different blocks, and the latter consists of the Yangtze and Cathaysia Cratons. Some available geological, tectonic, petrological,

dynamic and chronological knowledge/data are given in this chapter.

Chapter 3 describes the 3 sample localities, including Hannuoba, Nushan and Daoxian. The former two are located in the North China Craton, and the latter one in the Cathaysia Craton within the South China Craton. Descriptions of samples used in this thesis, including four sets of granulites and two sets of peridotites, are also given in this chapter.

Chapter 4 offers a description to all analytical methods applied during this thesis, including electrical microprobe (EMP) for chemical compositions, FTIR for hydrogen species and contents, Isotopic ratio mass spectrometry (IRMS) for H isotopic compositions in some samples, and SIMS for REE and lithium content and H-O-Li isotopes.

Chapter 5 presents all the experimental data conducted on the granulites used in this thesis, including EMP data for mineral compositions, FTIR data for H-species and contents, SIMS data for REE and Li contents and H-O-Li isotopic values, as well as EMP and FTIR data on mantle peridotites and IRMS data for H isotopes on plagioclase and feldspar samples.

Chapter 6 discusses the hydrogen species and contents in the continental deep crust, the contrast in H_2O content in the lower crust between Precambrian and Phanerozoic, and the possible influences of structural water on the high electrical conductivity in the lower crust. Parts of this work have been published in *Journal of Geophysical Research - Solid Earth* in articles entitled "Water in the lower crustal granulite xenoliths from Nushan, eastern China", and "Water contrast between Precambrian and Phanerozoic continental lower crust of eastern China", respectively.

Chapter 7 presents FTIR data for OH structurally bound to clinopyroxene and orthopyroxene in mantle peridotite xenoliths from Hannuoba and Nushan, the North China Craton. It is found that the uppermost mantle below this craton has relatively lower OH content compared to other regions globally. Comparison

in water content between the overlying lower crust and underlying lithospheric mantle reveals that, despite the lateral variations of water content in these two sphere-layers, nominally anhydrous minerals, especially pyroxenes as well as the bulk water content, in the lower crust contain obviously more water than those in the upper mantle. Based on these data, rheological structure/viscosity in different tectonic units beneath the north China is quantitatively established. The lower crust can be stronger or weaker than the lithospheric mantle, which may even result in different lithospheric processes, e.g. thinning or thickening, between different regions. This work has been submitted as a manuscript entitled "Water in minerals of the continental lithospheric mantle and overlying lower crust: a comparative study of peridotite and granulite xenoliths from the North China Craton" to *Chemical Geology*.

Chapter 8 provides the SIMS data for H-O-Li isotopes, and Li content, in 3 sets of lower crustal granulites from Hannuoba and Nushan, including 2 suites of granulite xenoliths and 1 set of terrain granulites originated from an exposed lower crustal section at Hannuoba. Minerals such as clinopyroxene, orthopyroxene and plagioclase in the lower crust beneath the north China are characterized by relatively heavier D/H ratios (mainly -80 to -10‰), rather lighter δ^7Li values (mainly -25 to 6‰) and highly variable O-isotopic values (mainly 4.5 to 12.5‰) relative to the normal mantle, e.g. -90 to -60‰, 2 to 6‰ and 5.7±0.5‰, respectively. Heterogeneities on variable scales, e.g. within subgrain or between different grains/minerals/samples/localities, can be often observed; diffusion-driven processes, shortly before or during the entrainment by host basalt, may influence to some extent the initial isotopic compositions of H and Li, the equilibrium isotopic fractionations of these species, however, exclude any significant resetting on their average compositions. Inter-grain elemental and isotopic compositions indicate the absence of a pervasive fluid in the lower crust on both regional and large scales. Compositions of the H isotopes are proposed to origin from degassing during granulite-facies metamorphism, and

the degassing possibly occurred during the crystallization of granulite minerals; compositions of the Li isotopes are suggested to relate with their protoliths, dehydration and high-T Li diffusion. Two manuscripts entitled "Ion microprobe investigation of Li content and isotopes in lower crustal granulite minerals of the North China Craton" and "H-isotopic compositions of lower crustal granulite minerals: a case study from the North China Craton" from these work will be submitted to *Geochimica et Cosmochimica Acta*.

Chapter 9 includes a summary of the results and final conclusions of these studies, as well as some perspectives on future research.

The **Appendix** includes several tables illustrating the detailed information for SIMS results on Li content, H-, O- and Li-isotopes, as well as some related publications and manuscripts in preparation for submission.

2 Geological background

The continental regions on the Earth consist mainly of several Precambrian cratons (Fig. 2-1). These cratons represent some special domains where stable "continental interiors" can be defined, in strong contrast to active areas such as "orogenic belt", and play a critical role in understanding the growth, evolution and other characteristics of the continents and the whole Earth. This thesis is focused on several typical granulite localities within the North and South China Cratons in eastern China.

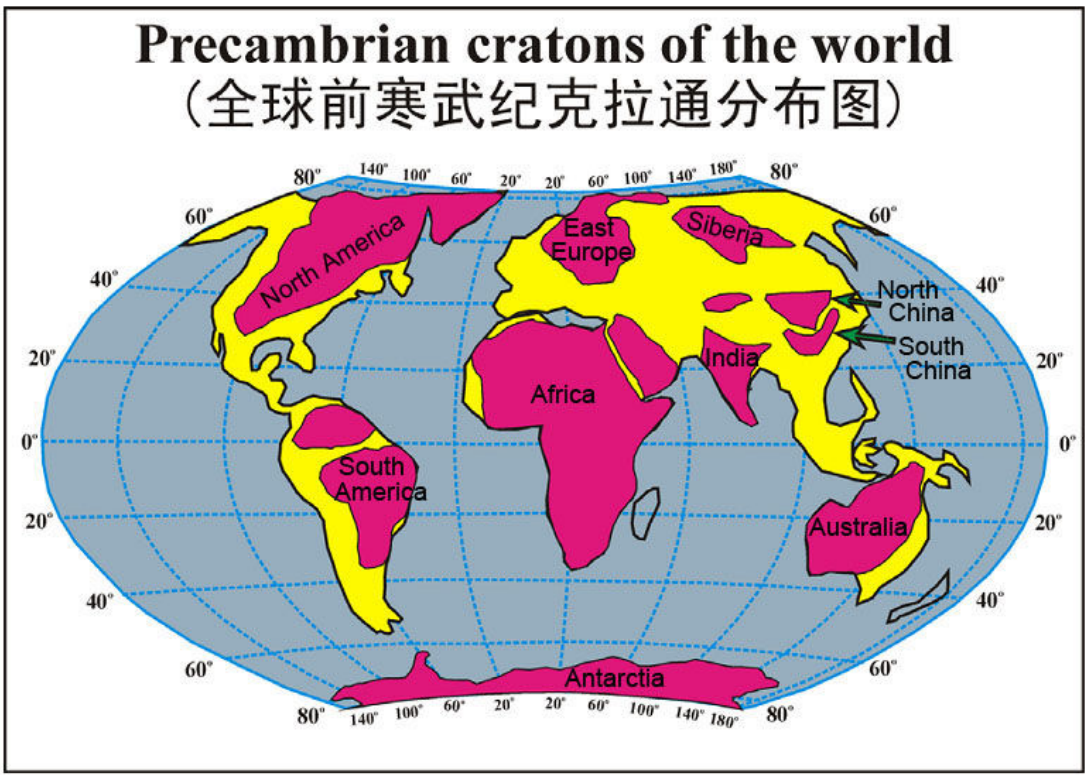

Fig. 2- 1 Precambrian cratons of the world

(after Sengör (1999))

The eastern China comprises a few different tectonic unites: from north to south, the eastern Central Asian Orogenic Belt, the North China Craton, the Dabie-Sulu ultrahigh-pressure (UHP) metamorphic belt, and the South China Craton (Fig. 2-2). These units amalgamated during the late Paleozoic to early Mesozoic. A brief description for the tectonic settings of these units is provided

here, while the emphases are focused on the North and South China Cratons (especially the former), from where the granulite samples were collected

2.1 The North China Craton

The North China Craton (NCC) is the Chinese part of the Sino-Korean craton, named sometimes the North China Block in some literatures. It is one of the most ancient cratons on the Earth, composed of early Archean and Proterozoic metamorphic rocks with the oldest recorded crustal ages >3.8 Ga (e.g. Liu et al., 1992), and is the largest craton in China, covering an area of >1,700,000 km^2. It is separated from the Mongolian Block by the eastern Central Asian Orogenic Belt in the north, and from the Yangtze Craton, part of the South China Craton, by the Triassic Dabie-Sulu UHP belt in the south (Fig. 2-2). The NCC is crosscut by two large-scale geophysical and geological linear zones. To the west, it is cut by the north-south trend Daxing'anling-Taihangshan Gravity Lineament (DTGL), which finally separates two topographically and tectonically different regions and is probably related with the diachronous lithospheric thinning of the craton (Ma, 1989; Xu, 2007); to the east, it is traversed by the Tan-Lu Fault Zone (TLFZ), which is associated with significant Cenozoic and Mesozoic volcanism.

Based on chronological ages, lithological assemblages, tectonic evolutions and P-T-t paths of metamorphic rocks, the NCC can be divided into three areas: the Eastern and Western Blocks and the intervening Central-Orogenic Belt (Fig. 2-2: Zhao et al., 1998a; Zhao et al., 2000, 2001b). The Eastern Block consists mainly of 3.5-2.5 Ga orthogneisses (dominated by tonalitic, trondhjemitic and granodioritic gneisses (TTGs)), 2.5 Ga granitoids and less amounts of ultramafic to mafic volcanics and sedimentary supracrustal rocks including banded iron formations. The Western Block is composed predominantly of late Archean TTG gneisses, together with ultramafic to felsic volcanic rocks metamorphosed at greenschist to granulite facies, and the Paleoproterozoic khondalite series and 2.5 Ga S-type granites. The Central Orogenic Belt is made up primarily of late

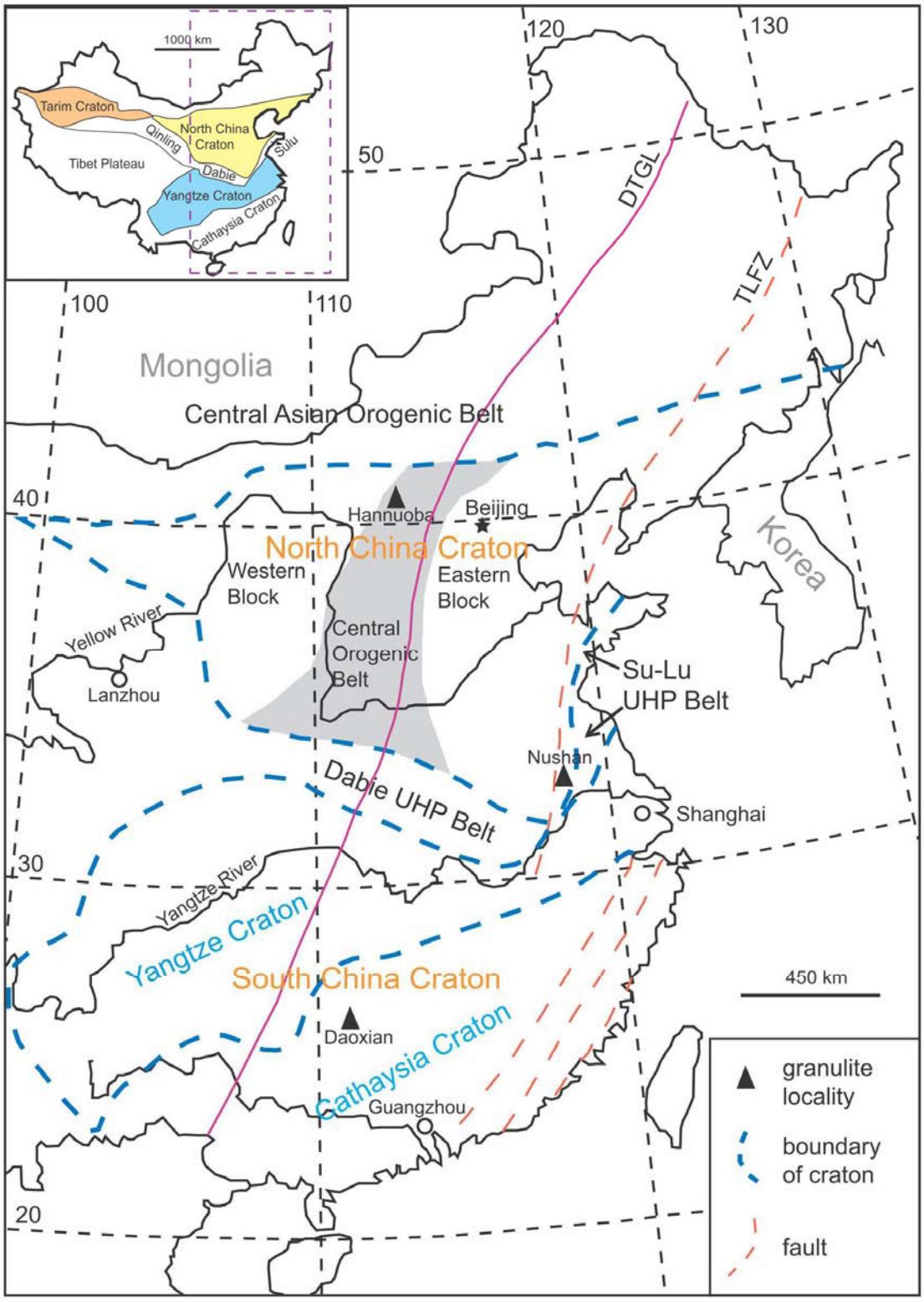

Fig. 2- 2 Simplified tectonic units of eastern China and localities of granulite xenoliths (after Xu (2007), Zhang et al. (2007a) and Zhang et al. (2007b))

Archean amphibolites and granulites and 2.5 Ga granite-greenstone terrains, overlain by 2.4-2.2 Ga bimodal volcanic rocks and thick carbonate and terrig-

neous sedimentary rocks interleaved with thin basalt flows. The collision between the Eastern and Western Blocks may have led to the formation of the Central Orogenic Belt and the final amalgamation of the NCC.

There are contrasting views towards the timing of the collision between the Eastern and Western Blocks. Multi-grain zircon U-Pb age populations from TTG gneisses of the Central Orogenic Belt have upper intercept of 2.5-2.7 Ga and lower intercept of 1.8-2.0 Ga. These younger ages are consistent with Sm-Nd ages of garnets from the high-pressure granulites in this belt and $^{40}Ar/^{39}Ar$ ages of hornblendes in amphibolites and biotites in TTGs, along with SHRIMP zircon rim ages of the TTGs and supracrustal rocks (Zhao et al., 2000, 2001b). The age of 1.8-2.0 Ga are interpreted as the age of metamorphic overgrowth. These, as well as near-isothermal decompressional clockwise P-T paths, led Zhao et al. (2000; 2001b) to propose collision occurred between the two Blocks at ~1.8 Ga. However, a recent report of a 2.5 Ga ophiolite complex in the northern Central Orogenic Belt implies a much older collisional event between these two blocks (Kusky et al., 2001). Li et al. (2000; 2001b) suggested a model that combines all these observations and assumes collision occurred between the two blocks at ~2.5 Ga followed by rifting during the 2.3-2.4 Ga with subsequent collision at 1.8-2.0 Ga representing the final amalgamation/cratonization event.

The NCC experienced widespread tectonothermal reactivation, beginning from the early Paleozoic but mainly during the late Mesozoic and Cenozoic, as manifested by the emplacement of early Paleozoic kimberlites, voluminous late Mesozoic basaltic rocks and granites and Cenozoic alkali basalts (Fan et al., 2000; Zhang et al., 2002; Yang et al., 2003; Zhang et al., 2004; Wu et al., 2005). The NCC also experienced development of extensive sedimentary basins (most of the eastern portion of the craton is covered by Quaternary sediments) and presently has higher heat flow (60 mW/m2: Hu et al., 2000) compared to other Archean and Proterozoic cratons (Nyblade et al., 1990; Jaupart and Mareschal,

2003). The changes in tectonic/magmatic activity are also reflected in a change in the type and composition of mantle xenoliths. Xenoliths carried in Ordovician kimberlites are deep-seated garnet-facies peridotites. These xenoliths, together with the appearance of diamonds in the kimberlites, indicate a cool geotherm, characterized by low heat flow of 36-40 mW/m^2, and thick lithospheric keel (~ 200 km). By contrast, xenoliths carried in Cenozoic basalts are dominated by fertile spinel peridotites, which record shallower and hotter lithospheric mantle, in good agreement with an average present-day surface heat flow of 60 mW/m^2 and thin lithosphere of 60-80 km. Collectively, these observations indicate the removal of about 80-140 km of Archean lithosphere from beneath the eastern NCC (Fig. 2-3).

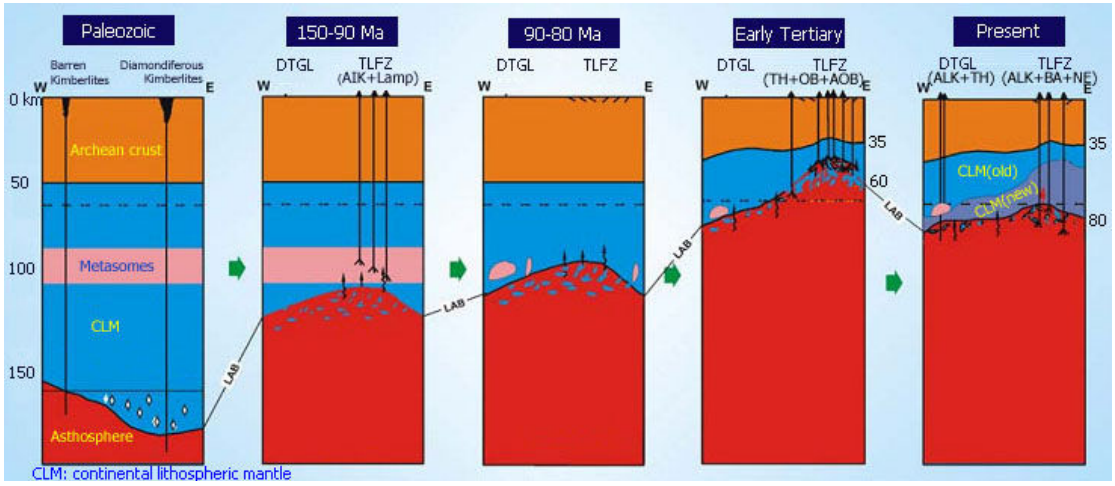

Fig. 2- 3 Schematic illustration for the thermo-tectonic evolution of the lithospheric mantle beneath the NCC.

(after Xu (2001). OB+AOB: subalkali basalts; ALK+BA+NE: alkali and strongly alkali basalts)

The lithospheric processes, such as diachronous lithospheric thinning, and structures were (or are) probably different between different regions beneath the NCC, separated especially by the DTGL. Comparison of Cenozoic basalts, and xenoliths enclosed in them, from contrasting regions reveals that the DTGL is not only a physical but also a chemical boundary that divides the NCC into two different lithospheric domains. Crustal elevation, morphology, chemical composition, crustal and lithospheric thickness, and gravity anomaly all change

remarkably across the DTGL (Xu, 2007). The evolution and composition of both basalts and the captured xenoliths, in terms of the $^{144}Nd/^{143}Nd$ and $^{187}Os/^{188}Os$ ratios, imply that the lithosphere is in progressive thinning in the western NCC, and in progressive thickening in the eastern NCC during the Cenozoic (Fig. 2-4: Xu et al., 2004a). Such contrasting lithospheric processes may be related with diachronous extension in the NCC, with initial extension in the eastern part due to the late Mesozoic Paleo-Pacific subduction and subsequent extension in the western NCC induced by the early Tertiary Indian-Eurasian collision (Xu et al., 2004a).

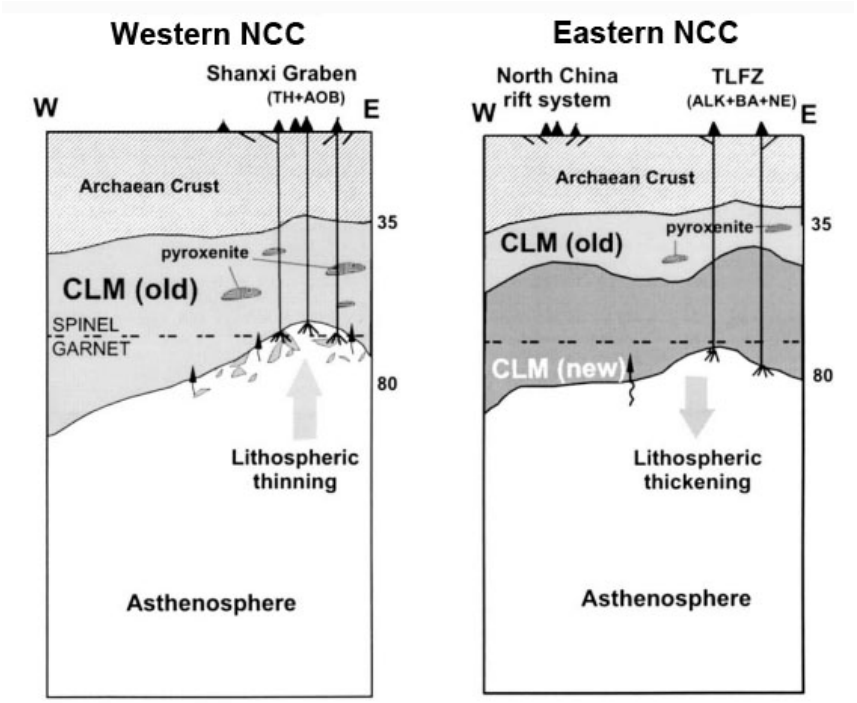

Fig. 2- 4 Schematic illustration of heterogeneous composition and structure of the present-day lithospheric mantle beneath the NCC

(after Xu et al. (2004a))

2.2 The Dabie-Sulu UHP Belt

The Dabie-Sulu UHP belt lies between the North and South China Cratons, extending from east to west for ca. 2000 km in the central-eastern China (Fig. 2-2). It is separated into two terranes by about 500 km of left-lateral strike-slip displacement along the TLFZ. The Sulu terrain in the east is segmented into a

number of blocks by several NE-SW trending faults subparallel to the TLFZ, and the Dabie terrain in the west is the major segment bounded by the TLFZ to the east and separated into a series of continuous zones by several EW-trending faults of large scales. The formation of the Dabie-Sulu UHP belt proceeded mainly in the Triassic, caused by collision between the North China and Yangtze Cratons with peak metamorphism at ~ 245 Ma (Hacker et al., 1998).

The basement of the Dabie-Sulu UHP terranes is metamorphic and igneous, such as schists, greenstones, gneisses, and rare quartzites, marbles, granulites, and eclogites, intruded by granitoids. The occurrence of eclogites first suggests that pressures of metamorphism were high. Discovery of coesite, diamond, and extreme ^{18}O-depletion, as well as exsolution of clinopyroxene, rutile and apatite, in eclogites (e.g. Okay et al., 1989; Wang et al., 1989; Xu et al., 1992; Yui et al., 1995; Zheng et al., 1996; Ye et al., 2000) demonstrates that deep subduction of continental crust to mantle depths of about 200 km and the subsequent quick exhumation (see also a review by Zheng et al., 2003).

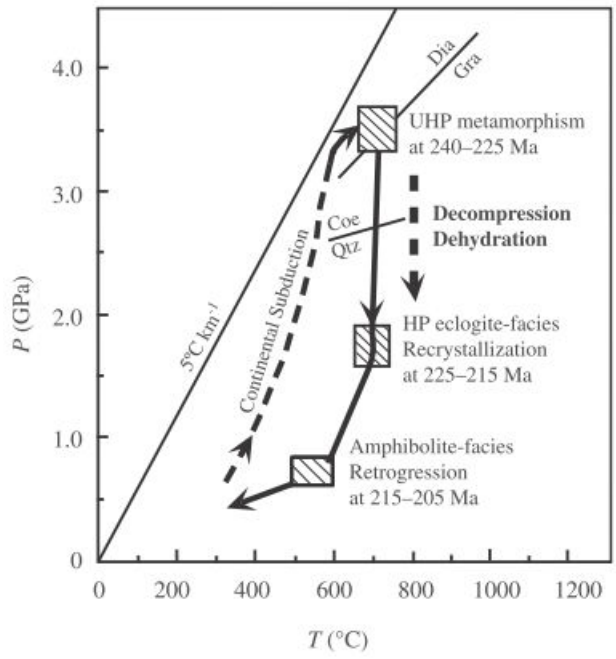

Fig. 2- 5 Schematic P-T-t diagram for subduction and exhumation of continental crust in the Dabie-Sulu orogen

(after Zhao et al. (2006)).

The chronological evolution in terms of the subduction and exhumation of the Dabie-Sulu UHP Belt can be simplified by the following (Fig. 2-5): the peak metamorphism occurred at ~ 240-245 Ma, and it experienced eclogites-facies recrystallization at ~ 225-215 Ma and amphibolite-facies retrogression at ~ 200 Ma during the exhumation to crustal levels (Zhao et al., 2006; and references therein).

2.3 The South China Craton

The South China Craton (SCC), or South China Block in some literatures, is composed of the Yangtze Craton and the Cathaysia Craton (Fig. 2-2). It was formed by the amalgamation of a collage between the two cratons during the Grenvillian-age orogeny (Chen et al., 1991; Shu and Charvet, 1996; Li et al., 2002). The Yangtze and Cathaysia Cratons are bounded by the Jiangshao fault zone in the east region, and usually by the south edge of the Jiangnan orogeny belt, exampled by some Proterozoic exposures such as Banxi Group, Lengjiaxi Group and/or Shuangqiaoshan Group, in the middle and west-south regions.

The Yangtze Craton is one of the three oldest continental blocks in China. The recent advances, especially some chronological work, greatly improved our knowledge about the geological and tectonic evolution of this craton. These include mainly the following several aspects: (1) The existence of a widespread Archean basement with ages up to >3.2 Ga, as indicated Sm-Nd and Hf model ages and SHRIMP zircon U-Pb ages (Gao et al., 1999; Qiu et al., 2000; Zhang et al., 2006; Zheng et al., 2006b). The most ancient exposed rocks are found in the west and north edges of this craton, exampled remarkably by Kangding Group in west Sichuan Province and Kongling Group in west Hubei Province (Fig. 2-6). (2) Paleo- to Meso-Proterozoic magmatisms are widely distributed in the south edge of this craton (Zhang et al., 2006; Zheng et al., 2006b), indicating the wide presence of Proterozoic basement. (3) Neo-Proterozoic mafic and granitic magmatisms are widely found in the margins of this craton (Li, 1999;

Zhou et al., 2002a; Li et al., 2003a; Li et al., 2003b; Zheng et al., 2004b), but the age-populations are markedly different, e.g. 720-770 Ma in the north margin (Zheng et al., 2004b) vs. 820-830 Ma in the others. (4) This craton possesses abundant ore deposits, especially rare metals, such as gold, copper, etc., in its central and east regions (e.g. Zhai et al., 1996).

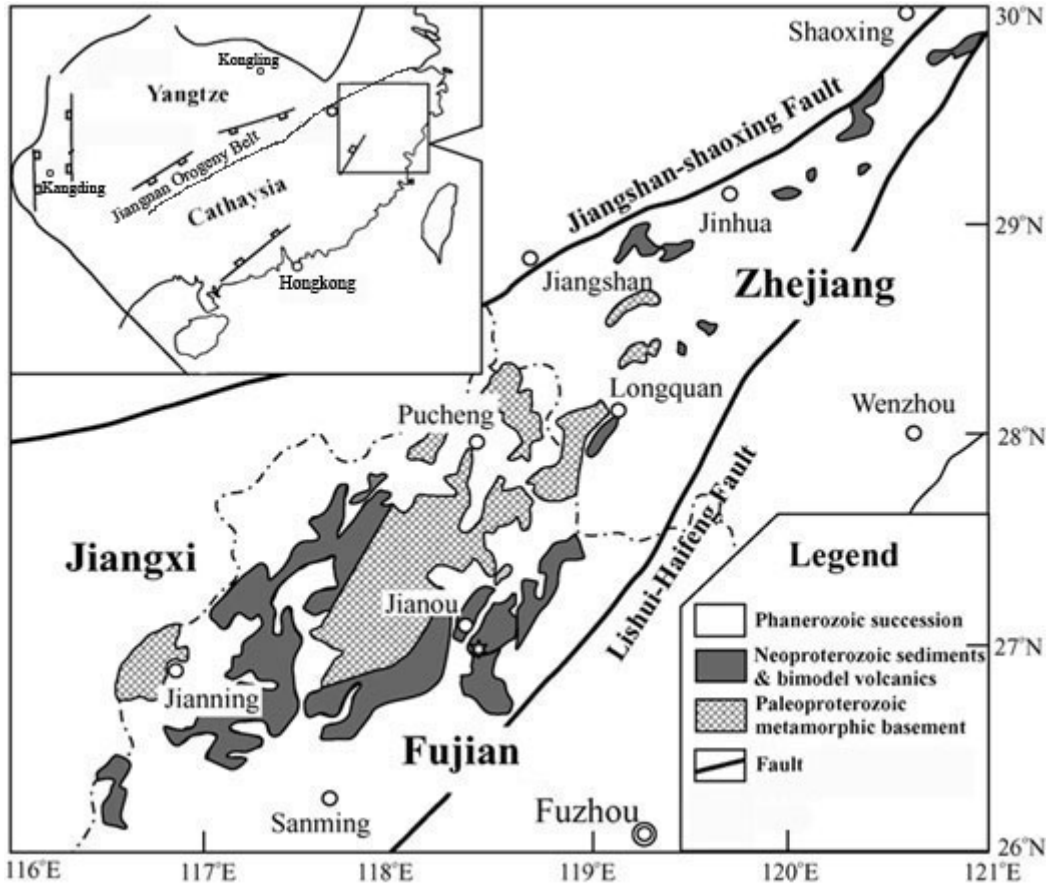

Fig. 2- 6 Schematic geology of the Cathaysia Craton

(after Li et al. (2005) and Zheng et al. (2006b))

The Cathaysia Craton is a relatively young craton compared to the NCC and the Yangtze Craton. The basement of this craton is dominantly Paleo- to Meso-Proterozoic, with some local late Archean component (Chen and Jahn, 1998). The exposed terrains in this craton are mainly sedimentary rocks, derived from variable time-periods, and magmatic rocks dominated by Mesozoic granitites. Precambrian basement rocks in this craton are exposed mainly in an area between the Phanerozoic Jiangshao and Lishui-Haifeng faults in northwestern

Fujian and southwestern Zhejiang Provinces (Fig. 2-6). Late Meso-Proterozoic igneous rocks have been recently documented in southwest of this region, e.g. southern Jiangxi and northeastern Guangdong Provinces (Xie et al., 2001), implying a possible southwestern extension of the basement. The Precambrian basement in this craton has been divided into two subunits based on lithologic and structural features and metamorphic grades (Li, 1997): (1) The older unit, named the Mayuan complex in northwestern Fujian and the badu complex in southwestern Zhejiang, consists mainly of leptynites, schists, gneissic granites and mafic and felsic meta-volcanic rocks. All these rocks were metamorphosed to amphibolite-facies at 4-6.5 kbar and 550-650 °C (Jin and Sun, 1997). The formation age of this unit is about 1.7-1.9 Ga by zircon U-Pb method (Gan et al., 1993; Li, 1997), however, there are as yet no metamorphic ages available for this unit. (2) The younger unit, named the Mamianshan Group in northwestern Fujian and the Longquan Group in southwestern Zhejiang (Fig. 2-6), consists mainly of micaceous-/quartz-schist and micaceous leptynites, meta-volcanic rocks, and banded Fe-bearing marbles and quartzites. These rocks underwent intense deformation, and were metamorphosed to upper-greenschist to lower-amphibolite facies at 3-4.5 kbar and 530-600 °C (Jin and Sun, 1997). The formation age of this unit is about 818 Ma from SHRIMP U-Pb dating on zircon in rhyolite (Li et al., 2005).

After the collision, or amalgamation, of the Yangtze and Cathaysia Cratons, a failed rifting was developed roughly along the suture between them during the Neoproterozoic and Paleozoic, geographically through Hunan, Jiangxi, west Guangdong and east Guangxi Provinces. The rifting was manifested by the >13 km thick deposition of Neoproterozoic to Paleozoic abyssal marine carbonatitic / clastic sequence in the center and the 2-5 km shallow-sea carbonate deposits in the rifting margins (Wang and Li, 2003). These pre-Mesozoic sequences were overprinted by the Indosinian tectonothermal events and unconformably overl-ain by the late Mesozoic terrestrial clastics. The Indosinian mafic magmatism, ~

224 Ma, is missing except for some gabbroic xenoliths hosted by Mesozoic basalts in Daoxian, southern Hunan Province (Guo et al., 1997b).

2.4 Lithospheric thinning in eastern China

The lithospheric thinning in eastern China is a warmly and widely discussed topic in the last decade (Fan and Menzies, 1992; Menzies et al., 1993; Griffin et al., 1998; Menzies and Xu, 1998; Menzies et al., 2007). It is not clear, however, about its scale, mechanism and timing, as well as tectonic controlling factors, for this geodynamical process.

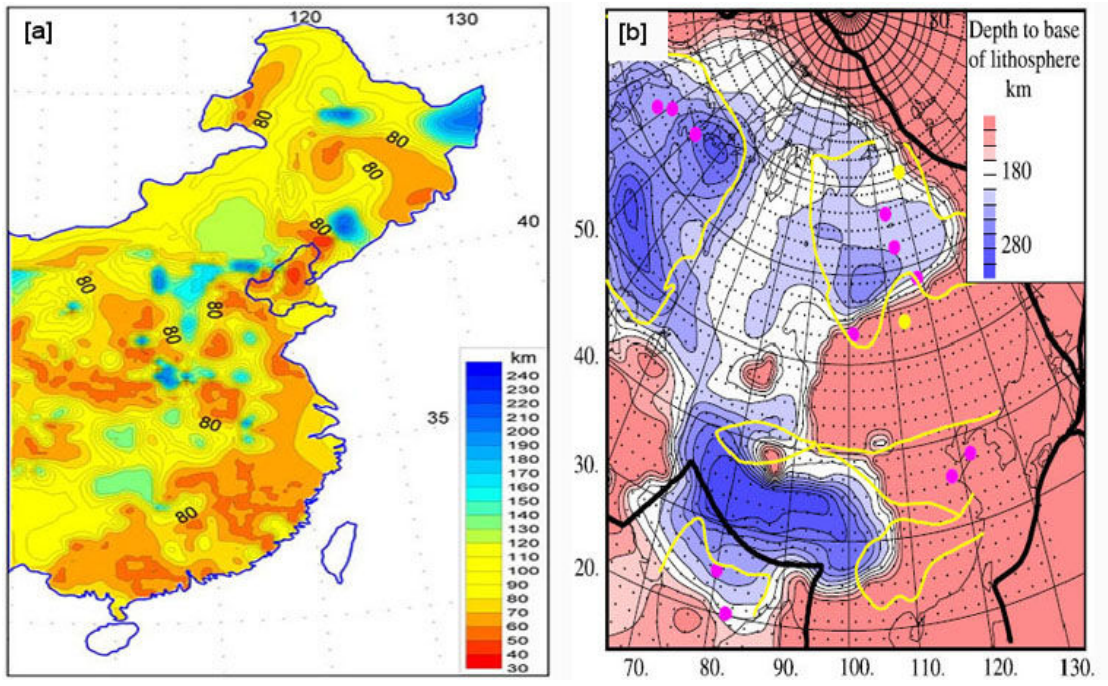

Fig. 2- 7 Thermal (a) and tomography (b) structure of the upper mantle in eastern China (after He et al. (2001) and Priestley et al. (2006), respectively)

The scale for the lithospheric thinning involves both its spatial and vertical distribution, which indicates how wide and how thick the lithosphere has been removed, respectively. There is at present a general consensus that the NCC, as noted in the first section in this chapter, has experienced significant lithospheric thinning, especially its eastern domain. Recent studies show that, not only the NCC, but also the north-east and south-east China are characterized by rather

thin lithosphere relative to other ancient cratons on the Earth (Xu et al., 2000; Zou, 2001; Xu et al., 2002; Wu et al., 2003). Based on these work, it seems that the entire eastern China, to the east of the DTGL, has experienced lithospheric thinning. This can be further supported by the thermal structure (Fig. 2-7a: He et al., 2001) and seismic tomography (Fig. 2-7b: Priestley et al., 2006) of the upper mantle below eastern China. The issue for the vertical thinning involves the removal of either only the lithospheric mantle or both part of the lower crust and the whole lithospheric mantle, which is still a debate until recently (Menzies et al., 1993; Griffin et al., 1998; Menzies and Xu, 1998; Zheng, 1999; Xu, 2001; Wu et al., 2003; Gao et al., 2004; Xu and Bodinier, 2004; Menzies et al., 2007).

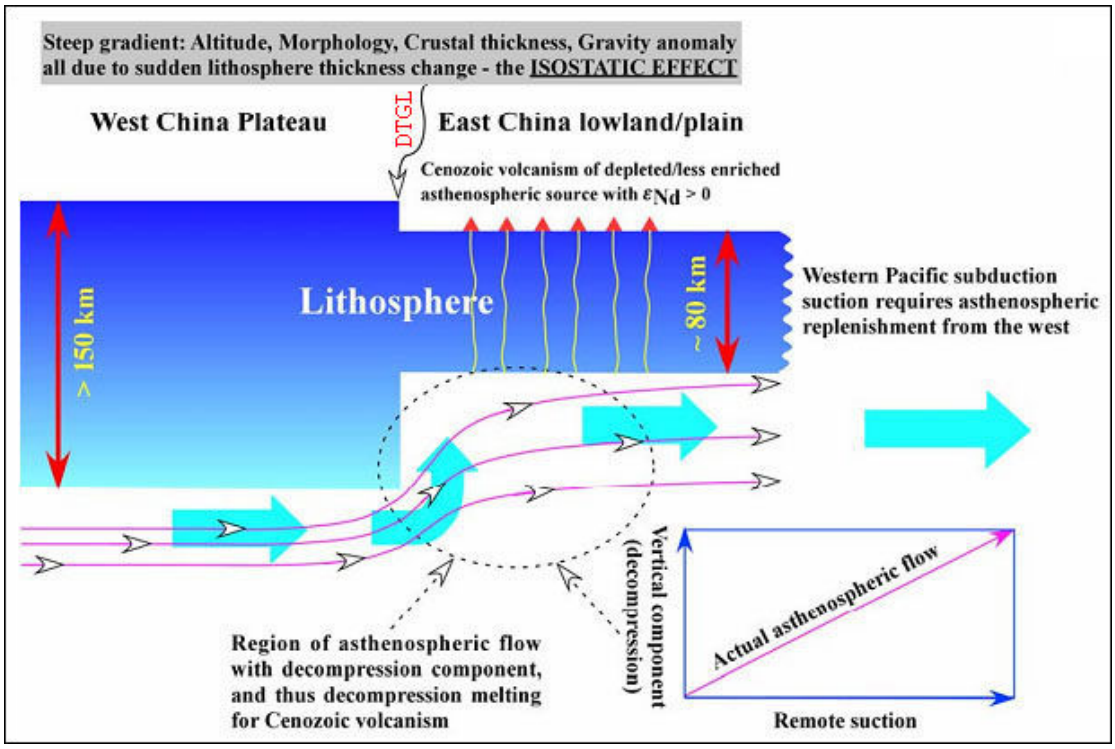

Fig. 2- 8 Lithospheric thinning of east China and subduction/dehydration of the Pacific plate (after Niu (2005))

How the lithospheric keel below eastern China had been lost has been the subject of considerable debate during the past 20 years, among which previous studies are largely concentrated on the eastern NCC. Various mechanisms have been proposed to explain this process below the NCC, the most prevailing are: (1) Delamination in a short period (Yang et al., 2003; Gao et al., 2004). Yang et

al. (2003) suggested that lithospheric delamination took place primarily in the early Cretaceous, based on the evidence for widespread crustal melting during 130-110 Ma which would require thinning of the lithosphere. By contrast, Gao et al. (2004) argued for Jurassic delamination of the lower crust, based on their discovery that Jurassic andesites, dacites and adakites from Xinglonggou (north NCC) have chemical signatures consistent with their derivation as partial melts of eclogites that interacted with mantle peridotite; in this case, they proposed that lithospheric thinning had reached such a stage by the late Jurassic that lower crustal rocks could be delaminated, converted to eclogites, incorporated into the convecting mantle and melted. The latter model, however, is difficult to reconcile the fact that Mesozoic mafic and felsic magmatism peaked in the early Cretaceous (Yang et al., 2003; Xu et al., 2004b; Wu et al., 2005) rather than the Jurassic; furthermore, rapid delamination is clearly at odds with the protracted Mesozoic magmatism (~100 Ma) in the NCC (e.g. Xu et al., 2004b), and it is not easy to explain satisfactorily the linear thinning along the whole east China (Fig. 2-7a & b). (2) Thermal-mechanical erosion (e.g. Griffin et al., 1998; Xu, 2001). Within this scheme, lithospheric thinning proceeded by heat transport into the lithosphere and small-scale asthenospheric convection induced by extension. Once lithospheric mantle is thermally converted to asthenosphere, it can convectively mix with, and eventually be replaced by, asthenosphere (Davis, 1994). A recent hypothesis suggests that the lithospheric thinning has been initiated by hydration weakening—correspondingly the base of the old lithospheric mantle has been transformed into the convective asthenosphere, for which the water required may come from dehydration of the subducted Paleo-Pacific lithosphere that lies horizontally in the 410-660 km transition zone beneath eastern China (Fig. 2-8: Niu, 2005). The westward thrust of the Pacific plate into, not penetrating, the transition zone underneath east China, with the coincidence in the position between its west end and the DTGL, has been recently observed by high-resolution seismic tomography (Huang and Zhao, 2006). Furthermore, the subduction may even lead to the Bouguer gravity anomaly in eastern China and

the formation of the DTGL in the early Cretaceous (e.g. Niu, 2005; Xu, 2007). This subduction-related mechanism is also supported by evidence from mineral compositions of mantle peridotites with different formation ages (Zheng et al., 2006a).

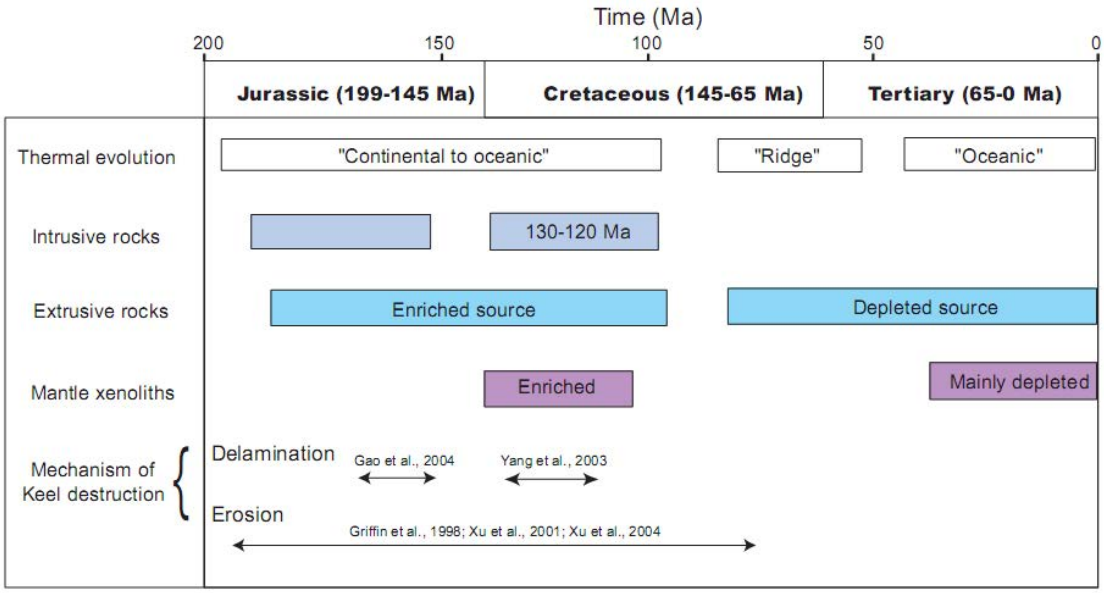

Fig. 2- 9 A 200 Ma event history for the NCC

(after Menzies et al. (2007))

Although the lithospheric thinning in east China has been well recognized for more than a decade, debate continues on the time-scale of such destruction, in especial terms of its beginning, peak-period and ending. This, however, relies fundamentally, or at least in part, on the understanding of how the lithosphere keel has been removed. A short time interval of only 10-20 Ma, or even less, for delamination-induced thinning (Yang et al., 2003; Gao et al., 2004) is in strong contrast to that of over 100 Ma for erosion-induced thinning (Griffin et al., 1998; Xu, 2001; Xu et al., 2004a; Xu et al., 2004b). Some relevant geological, geochemical and geophysical data on a 200 Ma time scale for the NCC is summarized in Fig. 2-9 so that these events can be cross-correlated. The presence of mantle derived plutonic rocks around 180-190 Ma is believed to mark the reactivation of the cratonic lithosphere, the early Cretaceous is widely agreed to mark a key period, and the thinning is probably very weak, if any, in the Cenozoic (Menzies

et al., 2007; and references therein).

3 Localities and samples

Lower crustal and mantle xenolith localities are widely distributed in the north, east and south China, which provide direct windows into the deep continental lithosphere below the eastern China. Among these places, Hannuoba in the northern NCC, Nushan in the southern NCC and Daoxian in the middle SCC (at the north edge of the Cathaysia Craton) are the most famous, especially for the presence of abundant lower crustal granulites. This thesis is focused on 4 sets of granulites and 2 sets of peridotites from these 3 localities, a brief description of each locality and the nature of samples are provided below.

3.1 Hannuoba

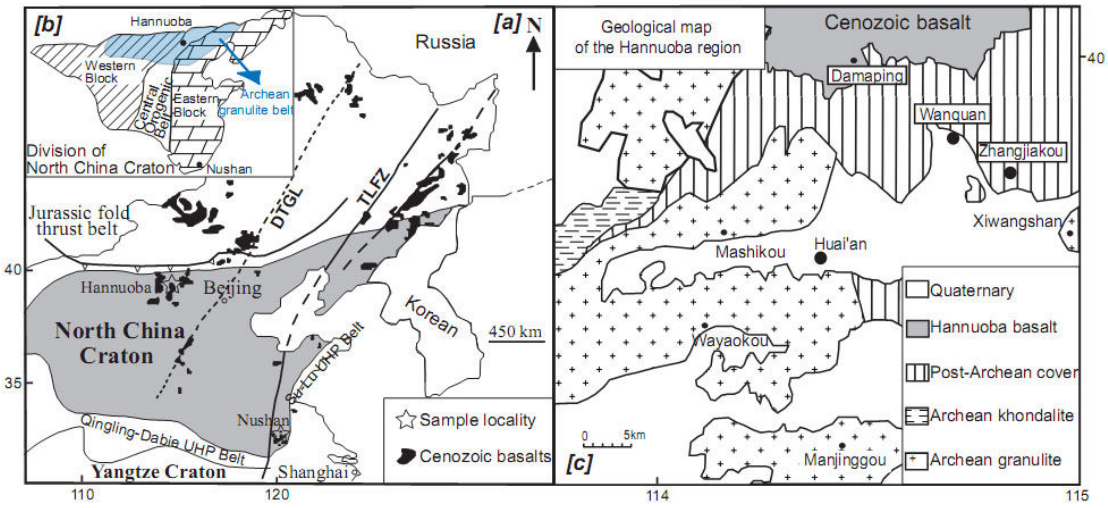

Fig. 3- 1 Sketch map showing simplified tectonic units and granulite localities in the NCC (after Zhao et al. (1998a; 2000; 2001b), Liu et al. (2001), Huang et al. (2004))

Hannuoba in the Hebei Province is located to the west of the DTGL, at the northern boundary of the Central Orogenic Belt (Figs. 2-2 and 3-1). It is a unique area where xenolith-bearing basalts are underlain and surrounded by Archean granulite terrains. The Hannuoba basalts, covering an area of > 1700 km^2, are composed mainly of intercalated tholeiitic and alkali basalts, with their age dated to be 14-27 Ma by the K-Ar method (Zhu, 1998). A remarkable va-

riety of deep-seated xenoliths derived from both the lower crust and upper mantle are widely distributed in this region, where extremely abundant and fresh xenoliths have been found at Damaping (Fig. 3-1). The xenoliths entrained in the Hannuoba basalts include peridotites (harzburgites, spinel lherzolites and spinel-garnet lherzolites), pyroxenites (websterites, spinel- and garnet-bearing pyroxenites) and mafic to felsic granulites (Song and Frey, 1989; Tatsumoto et al., 1992; Chen et al., 2001; Liu et al., 2001; Gao et al., 2002; Xu, 2002; Zhou et al., 2002b; Wilde et al., 2003; Wu et al., 2003; Liu et al., 2004; Rudnick et al., 2004; Liu et al., 2005; Zheng et al., 2006a; Zhang et al., 2007a). The estimated geothermal structure, coupled with the seismic velocity measurements and regional seismic refraction detections, indicates that, beneath this region, the lower crust extends from 24 to ~ 42 km, divided further into the upper, 24-35 felsic layer and lower, 35-42 km, mafic layer, whereas the lithospheric mantle extends from about 45 to 100 km (Fig. 3-2). A sharp contrast in seismic velocity between the lower crust and upper mantle, ranging in V_p from 7.0 to 8.0 km/s from the bottom of the former to the top of the latter, is observed beneath this area, indicating the presence of a narrow crust-mantle transitional zone (~ 3-5 km: Fig. 3-2), which was probably formed through Mesozoic magmatic underplating. Adjacent to the Hannuoba basalts is a belt of exposed Archean terrain granulites (Fig. 3-1), which extends east-west for >1000 km in the northern edge of the NCC. Detailed geological studies suggest that the rock sequence from Manjinggou-Wayaokou-Mashikou, namely the Huai'an high pressure (HP) granulite terrains in some literatures, represents an exposed lower crustal section (Zhai, 1996; Zhai et al., 2001).

Granulite xenoliths found in the Hannuoba basalts, especially those from Damaping, are dominated by mafic compositions, although intermediate and felsic granulites are common and metapelite xenoliths are also present. The mafic and intermediate granulites are cumulates interpreted to have formed by

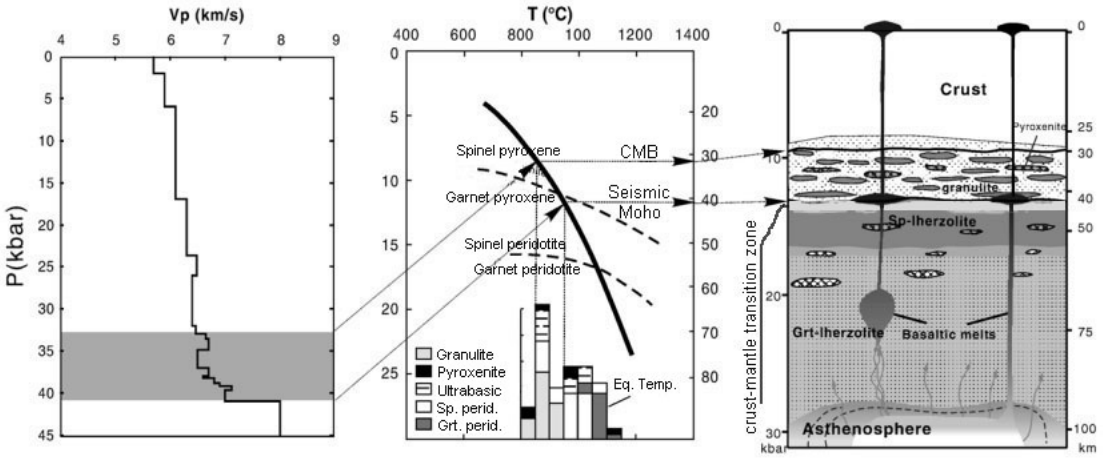

Fig. 3- 2 Seismic, geothermal and lithologic profile for the lithosphere below Hannuoba (after Xu (2007))

magmatic underplating and subsequent fractional crystallization at the base of the lower crust (Chen et al., 2001; Liu et al., 2001; Zhou et al., 2002b), possibly during the Mesozoic (~ 180-80 Ma), based on zircon U-Pb ages (Fan et al., 1998; Liu et al., 2001; Wilde et al., 2003). Equilibrium T-P conditions are estimated to be mainly 800-950 °C and 0.9-1.2 GPa for these granulites (Chen et al., 2001; Liu et al., 2001; Fan et al., 2005). Mantle-derived xenoliths captured in the Hannuoba basalts, especially those from Damaping, are chiefly spinel peridotites and rarely harzburgites (e.g. <5% clinopyroxene), although garnet peridotites are also found in small amount. Os isotope studies conducted on the Hannuoba peridotites demonstrate that they formed ~ 1.9 Ga ago as residues of partial melting (Gao et al., 2002); trace element and Sr-Nd-Pb isotopic compositions of whole rock and clinopyroxene separates reflect recent metasomatic overprinting (Song and Frey, 1989; Tatsumoto et al., 1992; Rudnick et al., 2004). Equilibrium T-P conditions are in the range of 800-1150 °C, but mainly 850-1100 °C, and 1.2-2.5 GPa for these peridotites (Chen et al., 2001; Rudnick et al., 2004).

The Huai'an gneiss terrane, separated from the usually referred Khondalite Series by a detachment fault in the west, is mainly composed of gneisses and granulites of TTG composition (Dirks et al., 1997). HP granulites are distributed

around the outer part of the Huai'an gneiss dome (Guo et al., 1993; Dirks et al., 1997; Zhai et al., 2001), and the most famous areas are Manjinggou, Wayaokou, Mashikou and Xiwangshan (Fig. 3-1). HP granulites occur usually as small sheet-like and lenticular bodies in highly deformed tonalitic gneisses and granulites (Guo et al., 1993; Zhai, 1996; Li et al., 1998; Zhai et al., 2001), implying that they were initially mafic dykes intruded into the pre-existing lower crust (e.g. Guo et al., 2002). These granulites have clockwise P-T paths, with moderate temperatures of 750-850 °C and high pressures of 1.1-1.5 GPa, implying that they are products of continental collision (Zhao et al., 2001a; Guo et al., 2002; O'Brien and Otzler, 2003). In these granulites, garnet porphyroblasts with well-preserved kelyphite textures, consisting of extremely fine-grained minerals (e.g. cpx + opx + plag) around fresh garnet cores, can be frequently observed (Guo et al., 1993), implying that they experienced rapid decompression and rapid cooling during their ascent (Rudnick, 1992). Geochronological studies by Sm-Nd and U-Pb dating indicate that these granulites experienced two important metamorphic events at about 2.6-2.5 Ga and 1.9-1.8 Ga, and were uplifted to the surface at ~ 1.8 Ga, which may be related with the final amalgamation of the NCC (Guo et al., 2005).

3.2 Nushan

Nushan in the Anhui Province lies to the east of the TLFZ, at the southern margin of the eastern cratonic block (Figs. 2-2 and 3-1). Nushan volcanism began in the Paleocene (~ 65 Ma) and continued in the Quaternary. The Nushan lavas are mainly alkali olivine basalts, basanites and nephelinites, with their age dated to be 0.53-0.73 Ma by the K-Ar method (Chen and Peng, 1988). Abundant peridotite, pyroxenite and granulite xenoliths, as well as some mineral megacrysts (e.g. clinopyroxene, orthoclase, etc.), have been found in the basaltic flow and scoria (Xu et al., 1998; Yu et al., 2003; Huang et al., 2004; Xu and Bodinier, 2004; Xia et al., 2006). The established lithospheric structure underneath this area indicates that the lower crust extends from 20 to ~ 31 km,

with the mafic layer or the lowermost crust likely in the 25-31 km depth range, the upper mantle extends from ~ 31 to 80 km, and no transitional zone is observed in this region (Fig. 3-3: Xu et al., 1998; Huang et al., 2004).

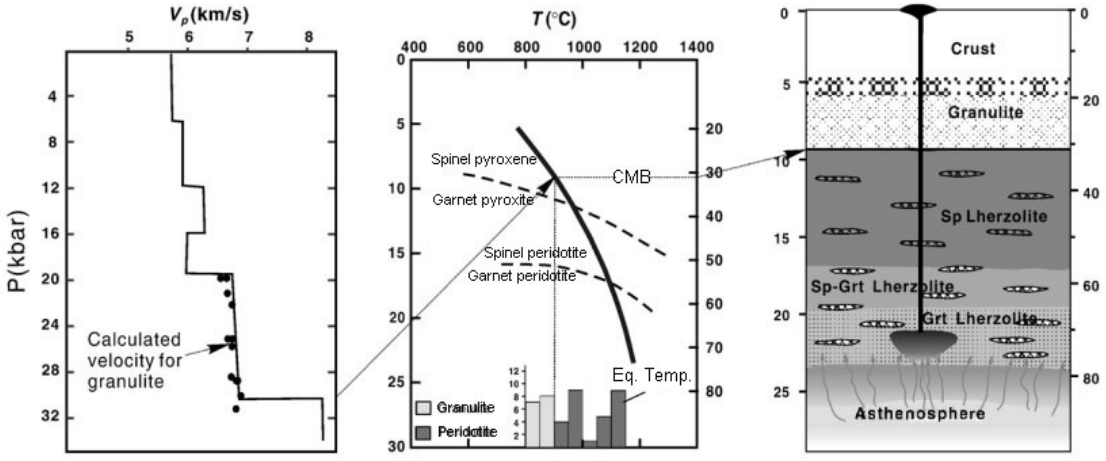

Fig. 3- 3 Seismic, geothermal and lithologic profile for the lithosphere below Nushan (after Xu (2007))

Granulite xenoliths found in the Nushan basalts are dominated by mafic to intermediate compositions. The Nushan granulites were carried to the surface by Cenozoic basalts, however, zircon U-Pb dating indicates two evident episodes of about 2.5 and 1.9 Ga for their formation, significantly different from those from Hannuoba but instead resembling the Huai'an HP terrain granulites (Huang et al., 2004). This, combined with trace-element modeling, Sr-Nd isotopic models and similarities in seismic velocities and major element and whole rock compositions, led Huang et al. (2004) to suggest that the Nushan granulites were primarily derived from the late Archean crystalline basement and only subordinately from the mafic layer newly accreted during the late Mesozoic, and that they can be used as a proxy for early lower crust.

Peridotite xenoliths enclosed in the Nushan basalts are mainly spinel peridotites, although garnet peridotites are also present in rare amount (Xu et al., 1998; Xu and Bodinier, 2004). It is suggested that these peridotites formed as mantle residues of 0 to 25% partial melting overprinted by mantle metasoma-

tism, and possibly originated from a mixture of old lithospheric relicts and newly accreted mantle after the removal of ancient lithospheric keel (Xu et al., 2000; Xu and Bodinier, 2004). The metasomatic events may be related to subducted oceanic slab, as revealed by Sr-Nd and H-O isotopic analyses of mantle samples from this region (Xia et al., 2004). Equilibrium T-P parameters shown by previous investigations range from ~ 850 to 1100 °C and from ~ 1.0 to 2.5 GPa for these peridotites (Xu et al., 1998; Xu and Bodinier, 2004).

3.3 Daoxian

Daoxian in the Hunan Province lies at the north margin of the Cathaysia Craton (Figs. 2-2 and 3-4). This region, as well as the adjacent Ningyuan area, is unique in the west Cathaysia Craton for the presence of various kinds of lower crust and mantle xenoliths. The Daoxian basalts are dominated by alkaline basalts, with their ages ranging from 150 to 130 Ma determined by K-Ar and Ar-Ar method (Guo et al., 1996; Zhao et al., 1998b; Li et al., 2004). Among more than 120 small basaltic outcrops in this area, Huziyan (25°31′7″N, 111°37′1″E) is the only one where both lower crustal and mantle xenoliths have been found, which include granulite, gabbro, spinel lherzolite, garnet lherzolite, dunite and pyroxenite (Guo et al., 1996; Guo et al., 1997a; Li et al., 2001a; Zheng et al., 2004a; Dai et al., 2008). At present there is no available geotherm for this region, however, if we can assume that the lower crustal structure is similar to the average as revealed by seismic refraction profiles across this craton (Gao et al., 1998), the lower crust extends from ~ 30 to 40 km at Daoxian, and, in this case, the upper mantle is in the depth range of ~ 40-100 km if using a reference frame that the lithospheric thickness beneath this region is ~ 100 km (see chapter 2).

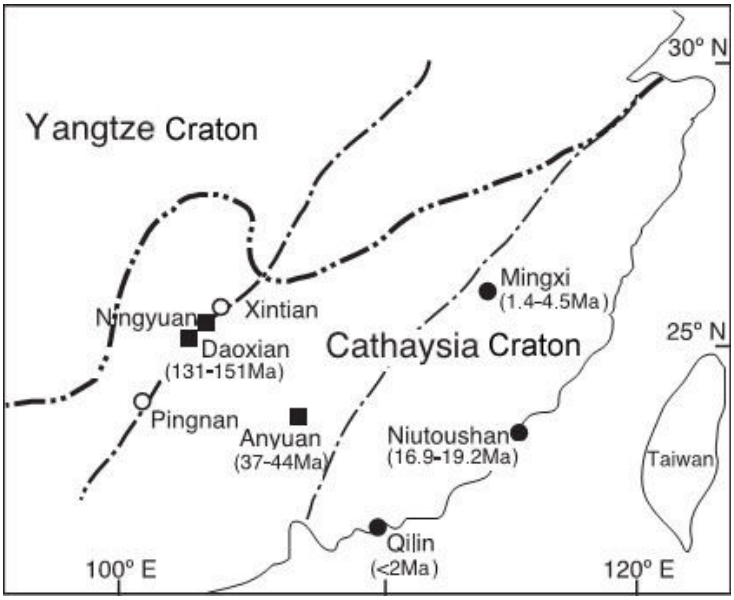

Fig. 3- 4 Sketch map for xenolith locations in the Cathaysia Craton

(after Zheng et al. (2004a))

Lower crustal xenoliths entrained in the Daoxian (or Huziyan) basalts are predominated by mafic granulite and gabbro, which were transferred to the surface during the middle Mesozoic (~ 150-130 Ma). These xenoliths were probably formed through accumulation of pyroxene and plagioclase from underplating mafic melts, followed by subsequent lower crustal metamorphism in multiple episodic periods, as revealed by their ~ 220 and 800 Ma ages, but dominated by the relatively young age of about 220 Ma, from Sm-Nd isochron method obtained from whole rock and separated minerals and zircon SHRIMP U-Pb method (Guo et al., 1997b; Kong et al., 2002; Dai et al., 2008). Large variations in Hf isotopic compositions for zircons of the same age, e.g. $\varepsilon_{Hf}(t)$=-5.4 to 20.8 for 220Ma and -8.3 to 10.0 for 800 Ma zircons, respectively, suggests wide mixing and interaction between depleted mantle and old crustal components involved in the genesis of the juvenile crust (Dai et al., 2008).

3.4 Samples

This section offers a detailed description for the samples used in this thesis. Totally 4 suites of granulites, as xenoliths from Hannuoba, Nushan and Daoxian

and old terrains from Hannuoba, and 2 sets of peridotites, as xenoliths from Hannuoba and Nushan, have been collected, in which EMP and FTIR studies have been conducted on all of them and SIMS on 3 sets of selected granulites. All the samples are very fresh, except that some Daoxian granulites are partly altered. Descriptions for each set of these samples are provided separately as following.

3.4.1. Hannuoba xenolith granulites

(8 samples: WD9520, WD9522, WD9530, WD9532, WD9546, DM9855, DM9871, HD71)

The Hannuoba xenolith granulites were collected from Damaping. They are all two-pyroxene granulites, dominated by the paragenesis of cpx + opx + plag. These xenoliths, ranging from about 5 to 18 cm in size, are usually enriched in pyroxenes, with their fractions up to 90%, and are characterized by medium to coarse-grained granoblastic fabrics and heteroblastic and/or near-equigranular textures (Table 3-1); mineralogical banding of pyroxene-rich and plag-rich layers can be found frequently, and triple junctions of pyroxenes or plag are very common in these xenoliths.

Table 3- 1 Summary of petrographic features for Hannuoba xenolith granulites

	cpx	opx	plag	Description
WD9520	45	20	35	banded, medium to coarse grain, near-equigranular texture
WD9522	30	50	20	banded, medium grain, granoblastic, heteroblastic texture
WD9530	45	25	30	banded, medium to coarse grain, near-equigranular texture
WD9532	55	25	20	banded, medium grain, granoblastic, near-equigranular texture
WD9546	55	35	10	less banded, medium grain, granoblastic, heteroblastic texture
DM9855	30	25	45	banded, medium to coarse grain, near-equigranular texture
DM9871	25	10	65	banded, medium grain, granoblastic, near-equigranular texture
HD71	50	35	15	banded, medium grain, near-equigranular texture

3.4.2. Hannuoba terrain granulites

(10 samples: MJ9801, MJ9803, MJ9805, MJ9806, MJ9807, MJ9808, MJ9810, MJ9811, SX-1, SX-2)

These terrain granulites were collected from Manjinggou and Xiwangshan,

with their label as MJ and SX, respectively. They are mainly garnet-free/bearing two-pyroxene granulites, and usually contain some amphibole; oxides (e.g. *mt*) are common in them, and some samples also contain a few sulfides (Table 3-2). The mineral assemblages are cpx + opx + plag + mt ±grt ± amphibole, with their abundances variable between different samples; amphibole is probably secondary in origin, although no evident alteration can be observed for other phases. These granulites are composed of very fine to fine grains, and banded distributions of pyroxene-rich and plag-rich layers, although not that obvious as observed in the other three sets of granulites, and triple junctions and smooth boundaries can be frequently, if not always, observed in them. Sample MJ9803 contains relatively large cpx grains (e.g. >1 mm) with spinel exsolutions.

Table 3- 2 Summary of petrographic features for Hannuoba terrain granulites

	lithos	cpx	opx	plag	grt	mt	amp	Description
MJ9801	a	30	12	30	23	2	3	fine grain, near equigranular texture
MJ9803	b	30	13	55		2		banded, fine grain
MJ9805	a	30	10	40	15	5		banded, fine grain
MJ9806	b	30	7	55		5	3	less banded, fine grain
MJ9807	b	35	10	50		5		banded, fine grain
MJ9808	b	40	7	50		3		fine grain, near equigranular texture
MJ9810	a	45	20	25	5	3	2	banded, fine grain
MJ9811	a	35	12	45	5	3		fine grain, near equigranular texture
Sx-1	a	25	5	50	15	3	2	banded, fine grain with large grt grains
SX-2	a	28	5	40	23	3	1	banded, fine grain

Note: a, grt-bearing two-pyroxene granulite; b, grt-free two-pyroxene granulite.

3.4.3. Nushan xenolith granulites

(10 samples: 04NS1, 04NS5, 04NS8, 04NS9, 04NS11, 04NS12, 04NS13, 04NS14, 04NS15, 04NS16)

The Nushan xenolith granulites are two-pyroxene granulites and hypersthene-bearing granulites. These granulites, ranging 5-15 cm in diameter, all show a foliated structure in hand-specimens, due to oriented distribution of tabular plag crystals relative to other minerals, and a fine-grained granoblastic texture, in which pyroxene and plag grains are mostly 0.1-0.7 mm in size. They

usually contain the mineral assemblages of opx + plag ± cpx ± quartz (qtz) ± mt. Description for these samples is summarized in Table 3-3, while oxides are excluded in the modal mineral estimation. Mineralogical banding composed of pyroxene-rich and plag-rich layers can be observed in all these samples. Pyroxenes are usually surrounded by anhydral opaque oxides, which is distinctively different from the other granulites in this thesis. Triple junctions of plag and/or pyroxenes are often observed in the Nushan granulites.

Table 3- 3 Summary of petrographic features for Nushan xenolith granulites

	lithos	cpx	opx	plag	qtz	Description
04NS1	c		10	85	5	banded, fine-rain granoblastic texture with triple junction
04NS5	d	15	25	60		banded, fine-grain granoblastic texture with triple junction
04NS8	d	5	10	60	25	banded, fine-grain granoblastic texture, partially altered
04NS9	d	30	10	60		banded, fine-grain granoblastic texture with triple junction
04NS11	c		20	72	8	banded, heteroblastic texture
04NS12	d	10	10	80		fine-grain texture with triple junction
04NS13	c		15	80	5	banded, heteroblastic texture
04NS14	c		10	83	7	banded, fine-grain granoblastic texture
04NS15	d	10	5	82	3	banded, fine-grain granoblastic texture with triple junction
04NS16	d	5	10	80	5	banded, fine-grain granoblastic texture with triple junction

Note: c, hypersthene-bearing granulite; d, two-pyroxene granulite.

3.4.4. Daoxian xenolith granulites

(14 samples: DX01, DX03, DX04, DX06, DX10, DX12, DX13, DX19, DX20, DX28, DX31, DX34, DX40, DX44)

The Daoxian xenolith granulites were collected from Huziyan, round or elliptical in shape and 5 to 15 cm in diameter. They are all two-pyroxene granulites, with the mineral phases of cpx + opx + plag ± spinel. Small amounts of spinel can be often found as vermicular symplektite associated with pyroxenes or as individual grains in these xenoliths (Table 3-4), which is different from the other 3 groups of granulites. The grain size of pyroxenes is usually smaller than that of plag (~0.6-2.4 mm in the former vs. ~0.5-4 mm in the latter). Alteration of opx in these granulites, with their products mainly of chlorite/serpentine, is very common, while cpx is generally fresh in strong contrast (see also Dai et al.,

2008). Exsolution of opx and spinel in cpx and of spinel in opx and plag can be observed frequently within these xenoliths (Fig. 3-5), indicating decompression during their paragenesis. Possible origins accounting for these mineral exsolution will be discussed in the subsequent chapters.

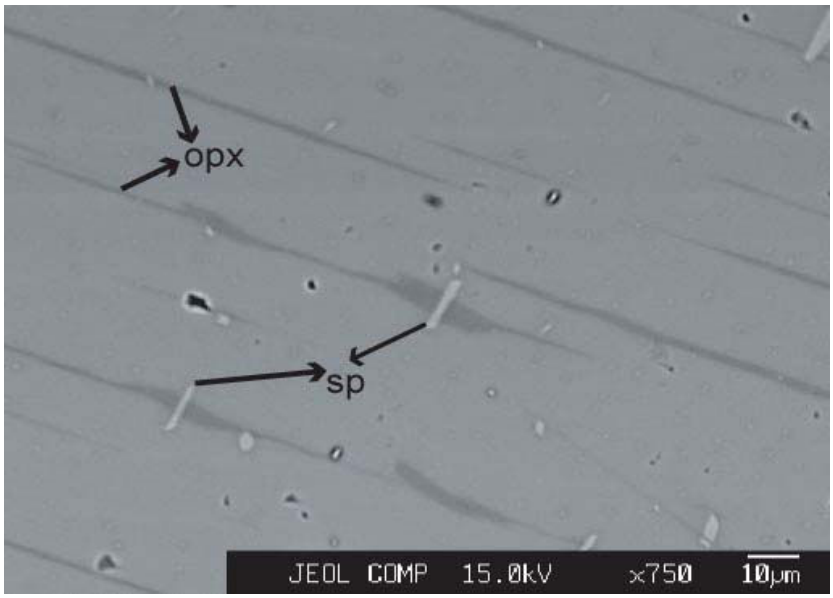

Fig. 3- 5 Mineral exsolution within cpx in Daoxian granulites

Table 3- 4 Summary of petrographic features for Daoxian xenolith granulites

	cpx	opx	plag	sp	Description
DX01	40	30	30		medium to fine grain, near equigranular texture
DX03	35	10	54	1	banded, medium to coarse grain
DX04	20	20	60		banded, medium to fine grain
DX06	30	20	49	1	banded, medium to fine grain
DX10	30	25	44	1	banded, medium to fine grain
DX12	25	10	64	1	banded, medium to fine grain
DX13	40	19	40	1	banded, medium to coarse grain
DX19	30	15	54	1	banded, medium to coarse grain
DX20	30	15	54	1	banded, medium to fine grain
DX28	35	20	45		less banded, fine grain
DX31	65	20	14	1	medium to fine grain, heteroblastic texture
DX34	20	10	70		less banded, fine grain
DX40	30	10	59	1	less banded, coarse grain
DX44	35	20	44	1	banded, medium to coarse grain

3.4.5. Hannuoba xenolith peridotites

(12 samples: P1, P2, P3, P4, P6, P8, P11, P12, P13, P14, P15, P17)

The Hannuoba xenolith peridotites were collected from Damaping, coexisting with granulites and other xenoliths. They are all spinel lherzolites, ranging up to 30 cm in diameter. Mineral abundances by volume are 55-75% for olivine, 15-25% for opx, 5-13% for cpx and 1-3% for spinel (Table 3-5). Mineral grains are relatively large (> 1 mm), and olivine, opx and cpx can reach ~ 1 cm in size. An unusual feature of these xenoliths is the presence of trace amounts of sulfides in some of them, occurring as tiny inclusions (5-10 μm) within glass that coats grain boundaries, as large grains (20-40 μm) at triple junctions and/or as large isolated inclusions (50-70 μm).

Table 3- 5 Modal proportions for Hannuoba xenolith peridotites

	cpx	opx	ol	sp
P1	9	18	71	2
P2	10	25	63	2
P3	10	24	65	1
P4	5	18	74	3
P6	7	20	72	1
P8	7	20	71	2
P11	9	15	75	1
P12	13	20	65	2
P13	15	27	55	3
P14	9	25	65	1
P15	7	23	68	2
P17	8	15	74	3

3.4.6. Nushan xenolith peridotites

(15 samples: NS01, NS03, NS06, NS07, NS08, NS12, NS13, NS14, NS16, NS21, NS22, NS24, NS25, NS29, NS30)

The Nushan xenolith peridotites are dominated by spinel lherzolites, with one spinel harzburgite. Amphibole can occur as small grains surrounding spinels, as large grains enclosing spinels, and/or as either interstitially at grain

boundaries or as small inclusions in large olivines in some of these samples. According to the presence/absence of amphibole, these peridotites are divided into two groups: amphibole-free and amphibole-bearing peridotites. The dominant texture is tabular equigranular for the former, and protogranular to porphyroclastic textures for the latter. Modal compositions are estimated to be 51-75% for olivine, 16-30% for opx, 0-18% for cpx and 1-3% for spinel, while amphibole in the amphibole-bearing samples is usually less than 3% (Table 3-6). In these samples olivine and orthopyroxene grains are usually larger than 1 mm, whereas clinopyroxene grains are generally smaller than 1 mm (although some can be up to ~ 0.5 cm in diameter).

Table 3- 6 Modal proportions for Nushan xenolith peridotites

	Lithos	cpx	opx	ol	sp	amp
NS01	e	9	25	64	1	1
NS03	e	10	27	61	2	
NS06	e	5	24	70	1	
NS07	e	10	25	62	3	
NS08	f		25	72	1	2
NS12	e	7	28	63	2	
NS13	e	12	25	61	2	
NS14	e	18	30	51	1	
NS16	e	9	20	70	1	
NS21	e	9	22	65	2	2
NS22	e	15	27	56	1	1
NS24	e	18	25	55	2	
NS25	e	7	18	73	2	
NS29	e	13	20	64	1	2
NS30	e	5	16	75	1	3

Note: e, spinel lherzolite; f, spinel harzburgite.

4 Analytical methods

4.1 Petrography and sample documentation

Totally 69 samples of different rock types, including both lower crustal granulites and mantle peridotites, have been studied in this thesis. Because the employed analytical methods, e.g. EMP, FTIR and SIMS, are all high-resolution and in-situ, several thin sections for each sample have been carefully prepared. For the treatment of sections, only the inner part of xenoliths and the freshest regions of terrains have been saw/cut. Usually 3 thin sections for each sample, including 2 double-polished sections (~ 2 × 1 cm in length × width and ~ 0.2 mm in thickness) and 1 single-polished thin section (~ 0.03 mm in thickness), have been prepared.

All the samples have been performed the petrographic observation in thin sections, EMP analysis for their chemical compositions and FTIR determination for water content of their main constitutive minerals. Out of these, a suite of 10 representative granulite samples from the NCC, including 4 Hannuoba xenoliths (DM9855, DM9871, WD9532 and WD9546), 4 Nushan xenoliths (04NS9, 04NS11, 04NS13 and 04NS16) and 2 Hannuoba terrains (MJ9801 and MJ9805), have been further selected for the measurement by SIMS of their REE and Li contents and H-O-Li isotopic compositions of the main mineral phases, e.g. cpx, opx and plag.

Microanalysis by SIMS requires detailed petrographic documentation of the samples. Therefore, optical images for selected grains were taken from the thin sections using the polarization microscope in combination with a digital camera, and these grains were carefully checked for their homogeneities in composition by EMP and qualities of purity by back-scattered electron (BSE) imaging on a Cameca SX50 microprobe (University Henri Poincaré, Nancy) and by FTIR.

4.2 Electron microprobe (EMP)

Chemical compositions of constitutive mineral phases were determined by different instruments for different samples: a Cameca SX100 EMP for the Hannuoba xenolith granulites and a Cameca SX50 EMP for the Hannuoba terrain and Nushan xenolith granulites at University Henri Poincaré, Nancy; and a JEOL JXA-8100 superprobe for the Daoxian xenolith granulites and the Nushan and Hannuoba xenolith peridotites at Nanjing University, China. Duplicate analyses on the same granulite samples by different apparatus did not show notable differences beyond analytical uncertainties, implying good consistency and reproducibility. 2-3 points from core to rim region for each grain and 2-5 grains for each mineral in each sample were performed the analyses. Except for the 10 selected granulite samples, for which the EMP, FTIR and SIMS analyses were conducted on the same double-polished thin sections, all the others were measured by EMP using the ~ 0.03 mm single-polished thin section.

The experimental conditions were similar for the different EMP instruments and different samples: 15 kV accelerating voltage, 20 nA beam current, <5 μm beam size, natural minerals and synthetic oxides as standards. However, the methods used for data correction were different: it is a program based on PAP procedure (Pouchou and Pichoir, 1985) for the Cameca SX 50 and 100 EMP, and on ZAF procedure (in reference to the three factors of matrix effects: atomic number (Z), absorption (A) and fluorescence (F)) for the JEOL JXA-8100 EMP.

Equilibrium temperatures and pressures were calculated according to the protocols suggested by Xu et al. (1998): the two-pyroxene geothermometers of Wood and Banno (1973) and Wells (1977) for all the granulites, the Ca-in-opx geothermometer of Brey and Kohler (1990) for the xenolith peridotites, and the geobarmometer of Wood (1974) for the garnet-bearing terrain granulites. The equilibrium pressures for the Hannuoba and Nushan garnet-free granulite and peridotite xenoliths were estimated by the geotherm established by Chen et al. (2001) for Hannuoba and by Huang et al. (2004) for Nushan, respectively.

4.3 Fourier transform infrared spectroscopy (FTIR)

4.3.1 Spectrometer and measurement parameters

Double-polished thin sections with the thickness of ~0.2 mm were used for the FTIR investigation. The cleaning procedure of the sections prior to measurements included 10 to 20 hours dissolution in ethanol or acetone to remove the residual epoxy, followed by heating in an oven at ~ 100 °C for 3 to 10 hours to remove the surface absorbed water.

All the samples were investigated under a microscope coupled to the FTIR spectrometer (Fig. 4-1). The principal advantages of such treatment are that:

- It is easy to observe the sample spot and to check the quality optically before the measurements;
- The liquid-N_2 cooled detector placed over the microscope is optimized for a focused beam;
- The focused IR beam yields higher intensities than a measurement in the sample chamber of the spectrometer.

Fig. 4- 1 Picture for the Nicolet 5700 FTIR spectrometer coupled with a microscope

The Nushan xenolith granulites were measured using a Brucker Equinox 55 FTIR spectrometer coupled with a Hyperion 2000 microscope at Tongji University, China, and a Nicolet 5700 FTIR spectrometer coupled with a Continuμm microscope at USTC; duplicate analyses show that consistencies between these two instruments are within 10-20%, which were likely produced by different grains used in the measurements. All the other samples were investigated by the Nicolet 5700 FTIR spectrometer coupled with a Continuμm microscope at USTC. Infrared spectra were obtained at wave number between 650 and 6000 cm^{-1}, except that the Nushan xenolith granulites were in the range of 570-7500 cm^{-1} by the Brucker FTIR spectrometer, using unpolarized radiation with an IR light source, a KBr beam-splitter and a narrow-band, high-sensitivity MCT-A detector cooled by liquid-N_2 at room temperature and pressure. A total of 128 or 256 scans were accumulated for each spectrum at a 2 or 4 cm^{-1} resolution; the aperture was 30 × 30, 50 × 50 or 100 × 100 μm, depending critically on the size and quality of the mineral grains. Measurements were generally performed in optically clean, inclusion- and crack-free areas, usually in the core region of selected grains. A wire-grid polarizer was applied on some oriented grains for a better understanding of the hydrogen species incorporated in the structure of minerals.

Quantitatively accurate measurement for the content of hydrogen species in anisotropic minerals requires the preparation of oriented single crystals along (i) three crystallographic axes, (ii) three random, but orthogonal sections of a crystal, or (iii) two orthogonal sections oriented parallel to each of the two axes of the indicatrix ellipsoid and the using of polarized IR radiation (Libowitzky and Rossman, 1996). However, conducting such treatments on fine-grained natural rocks is extremely difficult, if not impossible. In this case, we instead measured a statistically significant number of individual grains, e.g. 8-30, for each mineral in the same sample, and their average value was used to determine the water content. This approach has been widely used in recent reports on natural rocks

(Asimow et al., 2006; Katayama et al., 2006; Grant et al., 2007a). Some oriented grains were selected for a polarized analysis, and some high-quality grains were conducted the profile determination either from core to rim region or over the whole grain.

4.3.2 Calculation of water content

Water content of minerals in the granulites and peridotites was calculated by a modified form of the Beer-Lambert Law:

$$\Delta = I \times c \times t \times \gamma$$

where Δ is the total integrated absorbencies of absorption bands in the region of interest (cm^{-1}), I is the integral specific absorption coefficient ($ppm^{-1} \cdot cm^{-2}$), c is the content of hydrogen species (ppm H_2O by wt.), t is the thickness of the target sample (cm), and γ is the orientation factor from Paterson (1982). In this thesis, the integral region was set mostly in the range of 3000 to 3750 cm^{-1}, although it could be down to ca. 2700 cm^{-1} for some plag spectra. The mineral specific calibration coefficient used in the calculation is 7.09 $ppm^{-1} \cdot cm^{-2}$ for cpx, 14.84 $ppm^{-1} \cdot cm^{-2}$ for opx and 1.36 $ppm^{-1} \cdot cm^{-2}$ for grt from Bell et al. (1995), and 15.3 $ppm^{-1} \cdot cm^{-2}$ for plag from Johnson and Rossman (2003). The thickness was measured using a digital micrometer and reported as the average of 20-40 measurements covering the whole thin section. An orientation factor of 1/3 was applied for anisotropic cpx, opx and plag, and of 1 for isotropic grt (Paterson, 1982). Baseline corrections for the obtained IR spectra were carried out with a spline fit method.

Several factors have to be taken into consideration during the integration of IR spectra: (i) The Nicolet 5700 FTIR spectrometer occasionally suffers from an intrinsic problem, in that it can randomly produce positive, neutral or negative absorptions in 3700-3900 cm^{-1}, usually peaked at ~ 3740 and ~ 3850 cm^{-1} (Fig. 4-2). These absorptions can change from one type to another in very short time, e.g. in less than a few minutes, so that they are probably caused by

an artifact of the instrument, e.g. by the silicon carbide source, rather than by the instabilities of the background (*G.R. Rossman, personal communication, 2005*). (ii) The application of liquid-N_2 on the coupled microscope can sometimes lead to the formation of invisible water film on the detector, and thus result in a weak absorption peak at about 3250 cm^{-1}. (iii) Some secondary phases even in trace amounts, e.g. invisible amphibole/mica lamellae, may contribute to the absorption of hydrogen-related species in the 3000-3700 cm^{-1} region, e.g. a weak band at ~ 3660 cm^{-1} observed in some Nushan samples (see also the next chapter). (iv) Residual traces of epoxy on the sample wafers can generate minor absorptions between 2800 and 3000 cm^{-1} because of influences from C-H bands; this contribution should not be included in the calculation of the total integrated OH absorbance, especially for some spectra of plag which can extend down to ~ 2700 cm^{-1}. The influences from the above mentioned 4 aspects are actually, in most cases, very little or negligible to the final total integrated area related with the absorption of OH/water molecular structurally bound to the host minerals; but there are a few occasions that their influences are so evident that they have to be treated separately. We attempted to resolve and fit the individual peaks manually on each background-subtracted spectrum, of which the bands from non-structural OH/H_2O are notably visible (in this case, the contributions are mostly beyond 5%), by using the Peakfit V4.12 program (Jandel Scientific). The Gaussian form was used to fit the spectra, and the results were usually assured by $r^2 > 99.9\%$ at 95% confidence level. The above case (iii) is a little complicated, because altered hydrous products may produce, in addition to the ~ 3660 cm^{-1} peak, absorption bands at other positions, which may superimpose on the typical peaks from structural hydrogen-species. In this case, it is impossible to separate the superimposed peak at present. Fortunately, in samples where case (iii) cannot be avoided, the altered products (amphibole/mica) usually show only one single band at ~ 3660 cm^{-1}, which will also be discussed in the next chapter.

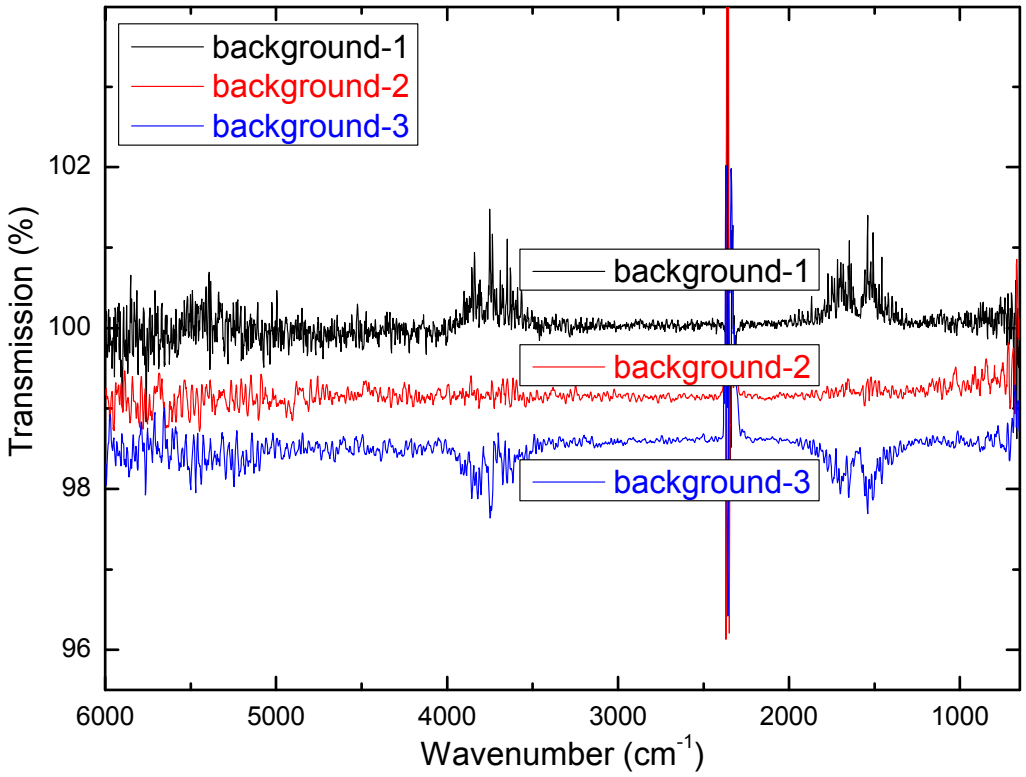

Fig. 4- 2 Absorption artifact of the Nicolet 5700 FTIR spectrometer

(The spectra were obtained for a blank, and were vertically offset for the illustration)

The interference from the FTIR spectrometer, mentioned above as artifact of the instrument, has fundamental influences on the baseline treatment of the IR spectra, in that it produces absorption in the 3700-3850 cm^{-1} range (see also the next chapter for details). Therefore, this problem must be treated carefully. We try to resolve this by the following procedure illustrated in Fig. 4-3: firstly, a blank background spectrum was obtained (Fig. 4-3a); secondly, a subtraction was carried out on a normal spectrum with many noisy bands in the 3700-3850 cm^{-1} area (Fig. 4-3b) relative to the blank, and a new spectrum with very weak or relatively simple absorptions in this region was produced (Fig. 4-3c); finally, a linear replacement was performed on the yielded spectrum between ~ 3750 and 3900 cm^{-1} for an approximation, which was processed by a "Straight Line" function provided in the Omnic software (Nicolet), and a relatively high-quality spectrum was made (Fig. 4-3d), on which the band at ~ 3740 cm^{-1}, if present, can be easily resolved by Peakfit software. According to the curve trend of the

spectrum (Fig. 4-3d), this approach, in most cases, contributes very little (e.g. < 2% or even less) uncertainty to the final calculated water content.

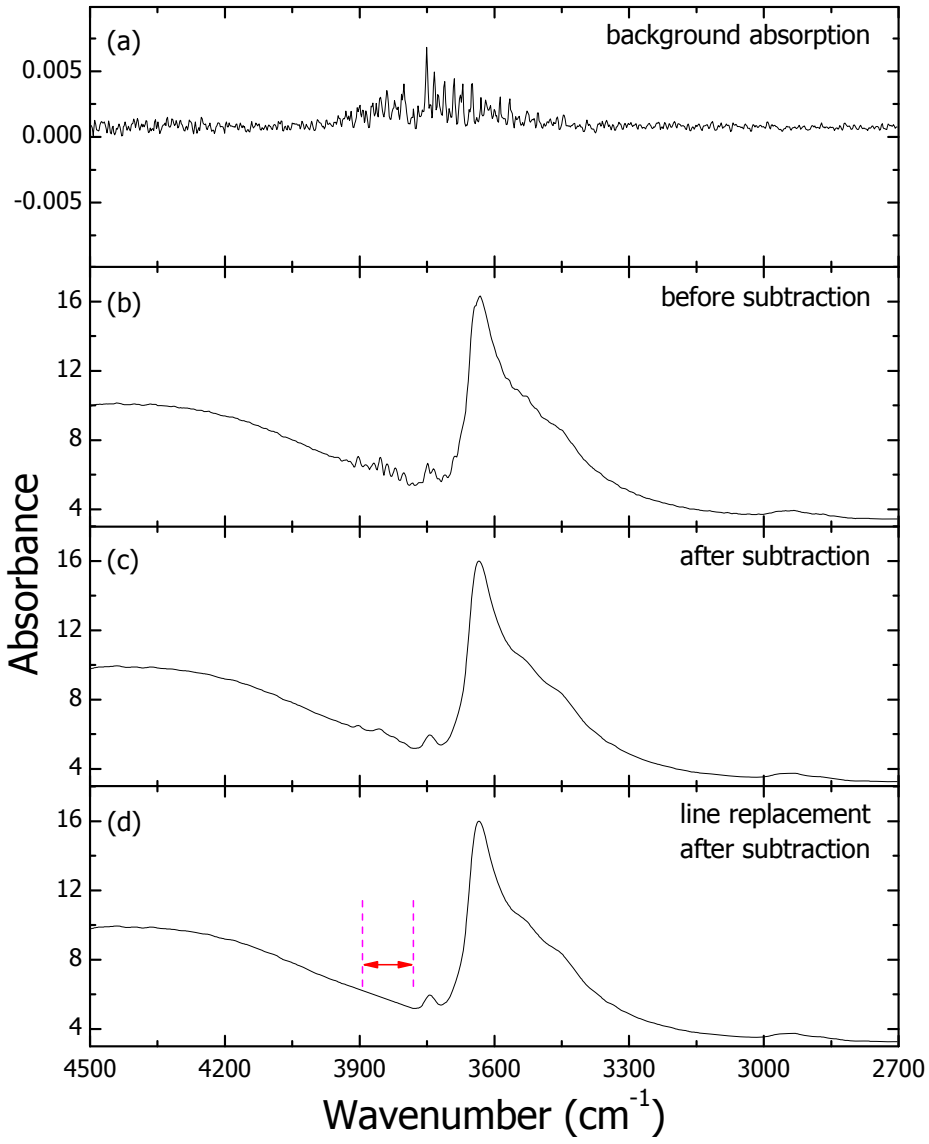

Fig. 4- 3 Interference treatment from the instrumental artifact

Possible factors influencing the calculated results include: (1) Unpolarized light. This is the main uncertainty during the analysis but it is estimated to be mostly less than 10% considering the treatment in this thesis and the recent approach from Asimow et al. (2006). (2) Baseline correction. This is actually not that difficult to control, because the background could be treated as a flat curve along the trend of our spectra in most cases, and the difference between different baseline corrections, e.g. spline-fit or polynomial-fit or slightly changing

the points during the fitting, is usually < 3%. (3) Variation of sample thickness on the thin sections. It is difficult to keep the sample sections totally parallel on both sides, but the variation is mostly less than 6% in our samples as shown by 30-40 measurements. (4) Extinction coefficients. There are slight differences between cpx, opx and grt in our granulite samples and those used to determine the mineral specific absorption coefficients (Bell et al., 1995), but the variation is generally < 8% in their compositions and densities, and it is even less for cpx and opx in mantle xenoliths relative to those used in Bell et al. (*1995*) and for plag relative to those used in Johnson and Rossman (2003). The error caused by the coefficients is therefore estimated to be < 10%. In an attempt to further constrain this estimated uncertainty, some minerals with high quality spectra were processed for their OH contents by using the wavenumber-dependent calibration coefficient (Libowitzky and Rossman, 1997) and by estimating the mineral density from its chemical composition and the end-member densities from Deer et al. (1992). The H_2O contents obtained by the two different approaches are mostly within 12% variation. In summary, the total uncertainty during our analysis is estimated to be better than 30%.

The bulk water concentration for each sample was estimated from the H_2O content (determined by FTIR), volume fraction (provided in a series of Tables in Chapter 3) and mineral density of each constitutive phase, by

$$c_{bulk} = \frac{\sum \rho_i c_i v_i}{\sum \rho_i v_i}$$

where ρ_i, c_i and v_i are the density, water content and volume fraction of phase i, respectively. The density of each mineral was determined from its composition from EMP and the densities of its end-member minerals from Deer et al. (1992), the latter are Wo-2.98 g/cm^3, En-3.21 g/cm^3 and Fs-3.96 g/cm^3 for cpx and opx and An-2.76 g/cm^3, Ab-2.55 g/cm^3 and Or-2.63 g/cm^3 for plag. For each set of granulite, the average density of certain mineral from all that suite of samples was used in the calculation. Actually, the variations in mineral density between

different groups of granulites are very small, e.g. <5 % (see also next Chapter).

4.4 Isotopic ratio mass spectrometry (IRMS)

The hydrogen isotopic composition of plag in sample 04NS9 was determined by hydrogen extraction and mass spectrometric techniques at the CRPG (Nancy), which was used later as a standard for the calibration of D/H ratios of plag in granulites measured by SIMS. In an attempt to check if the IRMS result is reliable, an alkaline feldspar megacryst from the Massif Central France was performed the same procedure in parallel.

About 0.5 g plag in the sample 04NS9 and 2.5 g feldspar in the megacryst were separated by handpicking under a binocular microscope, with the purities > 99% for the former and 99.9% for the latter. The former was ground quickly into fine powder using an agate mortar; while the latter was first divided into 3 aliquots with the mass of ~ 1 g, 1 g and 0.5 g, respectively, and the 3 aliquots were then subjected to different treatments: the first one was not powdered, and the latter two were crushed in the same way as that conducted on the plag in 04NS9. The same subsequent processes were applied to both the separated plag and 3 feldspar aliquots: the mineral separate was first loaded into a clean glass tube and pre-dried under vacuum at about 150°C for a whole night, it was then heated in an induction furnace at about 1100°C for several hours, with the temperature increased incrementally to this value, until no more hydrogen was liberated even the temperature was further raised to more than 1200°C, as monitored by a high-sensitivity hydrogen manometer; the released hydrogen was converted to H_2 and collected quantitatively in a glass ampule using an automatic Toepler pump, followed by the determination using a VG354 Gas Chromatograph-Isotopic Ratio Mass Spectrometer (GC-IRMS). A distilled ocean water was used as working standard. The results are shown in the δ-notation ($\delta = (R_1/R_2 - 1) \times 1000$, where R_1 and R_2 are the D/H ratios in the sample and standard, respectively) in permil relative to SMOW. There is no memory effect

on the VG354 IRMS in the CRPG and the precision is within 2‰ reproducibility for hydrogen isotopic analysis.

(Two double-polished thin sections of the feldspar megacryst were made for a quantitative determination of the incorporated water content by FTIR).

4.5 Secondary ion mass spectrometry (SIMS)

The SIMS measurements of REE contents and H-O-Li isotopic compositions by both Cameca IMS 3f and 1270 ion microprobe were performed at the CRPG, Nancy.

All these measurements were conducted on the same thin sections used by FTIR. After FTIR analyses, the sections were mounted on individual glass slices using epoxy, saw carefully so that the size is suitable for the insertion into a commercial Cameca sample holder, polished and coated by carbon film for the EMP analysis. Whereafter, these sections were polished again using diamond paste, cleaned by ultrasonic washing and coated by gold film for the SIMS determination of REE contents and H-O-Li isotopic ratios. The ion microprobe analyses were performed in the same regions, or at least in the same mineral grains, as those studied by EMP, and these regions were carefully examined under a binocular microscope to be free of cracks and by FTIR to be free of any alterations or possible inclusions. Because SIMS analyses usually suffer notably from matrix effects, the outmost rims (~ 10 to 30 μm depending on the size of beam) of the studied grains were deliberately avoided in the measurements. During the isotopic analyses of oxygen, lithium and hydrogen, selected standards were loaded and duplicately measured once the sample was changed, prior to the loading of new samples, to check the stability of the instrument.

4.5.1 Rare earth elements

REE contents of cpx, opx and plag in the granulites were analyzed by the Cameca IMS 3f ion microprobe. Analytical procedure follows Fahey et al. (1987)

and Hinton (1990). A 10 kV O^- primary beam of 15-30 nA intensity was focused to a spot of 20 μm in diameter. Secondary ions were accelerated to 4500 eV and analyzed at a mass resolution of ~ 300 with an energy filtering at -60 ± 10 V. This low energy filtering offered the advantage to keep the counting rate high while removing complex molecular interferences. Remaining interferences on REE (e.g. LREE oxides interfering with HREE) were eliminated by deconvolution techniques (Fahey et al., 1987) by the measurement of 31 atomic masses from 138 to 180. Secondary ion currents were normalized to Si, and secondary yields relative to Si determined on standard. A glass standard of KL2-G from Jochum et al. (2006) was used in the SIMS measurements. The analytical precision and reproducibility for the different elements range between 10 and 20%. For each sample, 1-3 points from core to rim zone for each grain and 1-3 grains for each mineral were determined.

4.5.2 Hydrogen isotopes

Hydrogen isotopic compositions of cpx and plag in the granulites were determined by the Cameca IMS 1270 ion microprobe. The analytical procedure is referred to that of Deloule et al. (1991b) and Xia et al. (2004). A 13 kV O^- primary beam of 5-10 nA intensity was focused to a spot of ~20 μm in diameter. The positive secondary ions of H^+, D^+ and H_2^+ were measured through 24 successive cycles, at a mass resolution of 2000, for ~25 min by ion counting and peak switching, with an energy window of 55 eV and no energy offset. Moisture is removed by baking the sample and ion probe at 120°C, and using a liquid-nitrogen trap. Under the analytical conditions, count rates on H^+ (IsH) varied from 1.2×10^4 to 6.5×10^5 counts per second, depending on the mineral and sample analyzed. The H_2^+/H^+ ratios were always in the range of 0.3 to 2×10^{-3}, reflecting minimal or no instrumental contributions (Deloule et al., 1991b). Cpx and plag of known D/H ratios were used as standards for these minerals. Instrumental D/H fraction factor for cpx was calculated as a function of the Mg# value, as used recently by Xia et al. (2004), and Mg# values for cpx

in both the samples and standards were obtained from their EMP data. Instrumental D/H fractionation factors for plag were assumed the same as that obtained on the standards ($\Delta_{ins}=\delta_{ims} - \delta_{ms}$, where Δ_{ins} is the instrumental fractionation factor, δ_{ims} and δ_{ms} are the δD values measured by ion microprobe and mass spectrometer, respectively). If applying the latter method to the calibration of cpx, similar δD values (i.e. within ~ 7‰ variation) can be acquired relative to those obtained by the Δ_{ins}-Mg# relation. The results are expressed in the δ-notation ($\delta = (R_1/R_2 - 1) \times 1000$, where R_1 and R_2 are the D/H ratios in the sample and standard, respectively) in permil relative to V-SMOW. Reduplicate analyses of both standards and pyroxenes and plag in sample DM9855 prior to, in the middle of and after the measurement of the samples show that the precision is from 3 to 16‰, including the possible microscale heterogeneities of the standards. 1-4 points in the same grain and 1-3 grains for each mineral in each sample were performed the analysis.

4.5.3 Oxygen isotopes

Oxygen isotopic compositions of cpx and opx in the granulites were analyzed using the Cameca IMS 1270 ion microprobe. The analytical procedure is similar to that used by Rollion-Bard et al. (2003) and Vielzeuf et al. (2005). Oxygen isotopes were measured as O^- ions produced by the bombardment of the target by a Cs^+ primary beam at 10 kV with a 5 nA sample current. The size of spots is about 10 μm with a depth of ~ 2 μm. The normal incidence electron was used to compensate sample charging during analysis. Secondary $^{16}O^-$ and $^{18}O^-$ ions were accelerated at 10 kV and analyzed at a mass resolution of 4000 using the circular focusing mode of the IMS 1270 and a transfer optic of 150 μm. There is no interference from other species on the $^{16}O^-$ and $^{18}O^-$ peaks at this mass resolution. O isotopes were measured in multicollection mode using two off-axis Faraday cups (L'2 and H1), of which the gains were calibrated at the beginning of the analytical session using the Cameca built-in amplifier calibration routine. 40 cycles of successive measurements were accumulated for each

session, with ion intensities of 3-8 $\times 10^6$ counts per second on the $18O^-$ peak so that an internal 1σ error of 0.05-0.14‰ was reached for each session (see also data in the next chapter). The calibration of matrix effects on the $^{18}O/^{16}O$ ratios of pyroxenes is referred to that suggested by Vielzeuf et al. (2005) for garnet: 3 cpx standards with variable compositions but similar to those in the granulites were used for their correction of cpx, and 1 opx standard with the composition close to those in the Hannuoba xenolith granulites was used for their calibration (see also the next chapter for details). The results are given in the δ-notation ($\delta = (R_1/R_2 - 1) \times 1000$, where R_1 and R_2 are the $^{18}O/^{16}O$ ratios in the sample and standard, respectively) in permil relative to V-SMOW. The precision by reduplicate analyses on standards varies 0.6-1‰. Multi-point (e.g. 4-18) profiling for each grain and 1-3 grains for each mineral were performed the analysis.

4.5.4 Lithium contents and isotopic compositions

Lithium concentrations and isotopic compositions of the granulite minerals were measured by the Cameca IMS 3f ion microprobe, following the procedure developed by Chaussidon and Robert (1998) and Decitre et al. (2002). A 10 kV, 10-20 nA O^- primary beam was focused on an area of 10-25 μm in diameter on the sample surface. Positive secondary ions accelerated through 4.5 kV were analyzed at low mass resolution of ~ 500 with an energy offset of 80 ± 20 eV for abundance determination, and at high mass resolution of ~ 1100 without energy offset for isotopic determination. Secondary ions were counted with an electron multiplier in pulse counting mode. The lithium contents and isotopic compositions were determined in different sessions and using different settings so that they do not correspond to the same sputtered spots. For Li-content analyses, counting times were 4 s for ^7Li and ^{30}Si over 40 cycles, the measured Li/Si ratios were corrected for the relative useful yields of Li and Si determined on 5 standards (glasses Nazca, ATHO and UTR-2 and cpx BZCG and BZ226, see Decitre et al. (2002) and Jochum et al. (2006)) in the same analytical session.

The analytical precision, including counting statistics and reproducibility, ranges from ~ 5 to 20% relative. In order to obtain Li-isotopic data, 100 cycles were accumulated with counting time of 12 s for ^{6}Li and 3 s for ^{7}Li. The ion intensities on ^{7}Li peak range from 3000 to 66000 counting per second, depending on the sample Li content and the intensity of primary beam. Cpx BZ226 and BZCG, opx BZ226 and glass BHVO and Nazca (Decitre et al., 2002) were used as standards for the calibration of the instrumental measured data. It has been established that there is an absence of matrix effects on the lithium instrumental isotopic fractionation using the same IMS 3f in the CRPG (Decitre et al., 2002; Beck et al., 2004), and this approach has been widely applied in recent ion microprobe investigations of mineral ^{7}Li/^{6}Li ratios in both CRPG and other SIMS laboratories, such as cpx, opx and olivine (e.g. Decitre et al., 2002; Beck et al., 2004, 2006; Lundstrom et al., 2005; Parkinson et al., 2007; Tang et al., 2007; Wagner and Deloule, 2007) ; Beck et al. (2004) also argues against an important additional matrix effect on the δ^{7}Li determination of plag (maskelynite) and phosphate by ion microprobe, however the obtained δ^{7}Li data are probably not as precise as those of pyroxenes due to the absence of available standards for these phases (to check the possible matrix effects). And consequently, cpx and opx in these granulites were the main objects for the SIMS determination of their Li-isotopic compositions, and only a few plag and grt grains were measured for their δ^{7}Li values to check that at first order no unexpected δ^{7}Li anomalies were present. The yielded results are given in the traditional δ-notation ($\delta = (R_1/R_2 - 1) \times 1000$, where R_1 and R_2 are the ^{7}Li/^{6}Li ratios in the sample and standard, respectively) in permil relative to L-SVEC (7Li/6LiLSVEC = 12.0191: Flesh et al., 1973). The analytical precision, including (1) the counting statistics, (2) the determination of instrumental mass fractionation of Li-isotopes, and (3) the external standard reproducibilities, ranges from 1 to 2.5‰ (1 sigma) depending on the mineral Li contents.

5 Results

This chapter compiles all the experimental results, including EMP, FTIR and SIMS data for both granulites and peridotites as well as IRMS data for hydrogen isotopic ratios of feldspars. These data are provided separately in the following sections.

5.1 EMP results

5.1.1 Granulites

EMP measurements show no inter- and intra-grain heterogeneities for individual minerals in each granulite sample, and the average data of multi-point analyses are given in Table 5-1 for the Hannuoba xenolith granulites, Table 5-2 for the Hannuoba terrain granulites, Table 5-3 for the Nushan xenolith granulites and Table 5-4 for the Daoxian xenolith granulites. These results are similar to previous investigations conducted on the same kind of sample from the same locality (e.g. Chen et al., 2001; Huang et al., 2001; Huang et al., 2004; Fan et al., 2005; Dai et al., 2008).

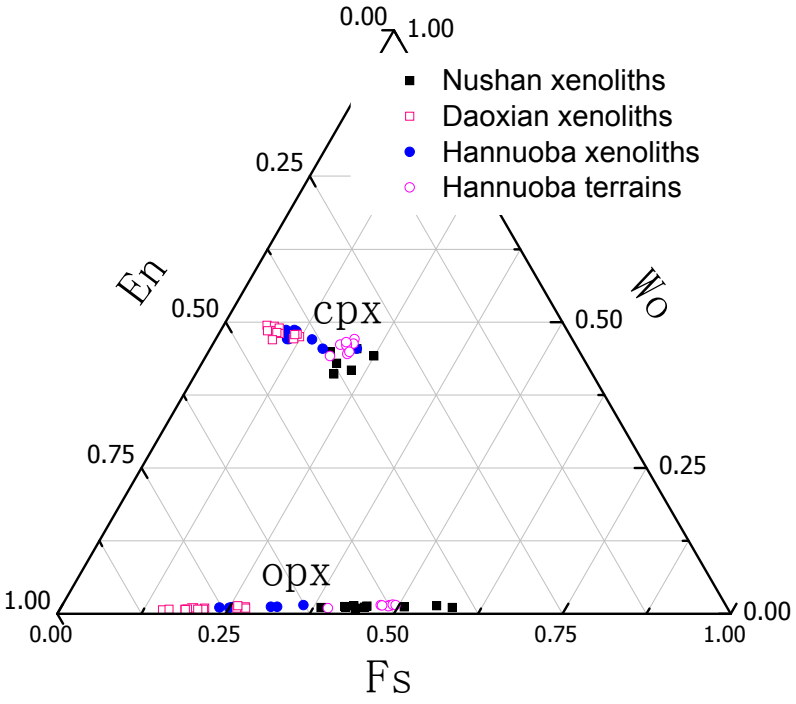

Fig. 5- 1 End-member compositions of pyroxenes in the studied granulites

The EMP data demonstrate that almost all the studied granulites are mafic in composition. The mineral chemistry reveals very limited variation for each set of granulites; and as a whole, the Hannuoba terrain granulites resemble more the Nushan xenolith granulites but differ strongly from the Hannuoba xenolith granulites with respect to the mineral composition; pyroxenes in the Hannuoba terrain and Nushan xenolith granulites are depleted in Al, Mg and Na and enriched in Fe relative to the other two suites, while plagioclases are depleted in Al and Ca and enriched in Na; Mg# (=Mg/(Mg + Fe)) values of either cpx or opx are usually highest in the Daoxian xenolith granulites and lowest in the Nushan xenolith and Hannuoba terrain granulites, with the Hannuoba xenolith granulites falling between them (Tables 5-1, 5-2, 5-3 and 5-4; Fig. 5-1). On the basis of these data and the petrogenetic discrimination methods of opx proposed by Rietmejir (1983), almost all these granulites project into the region defined by metamorphic origin.

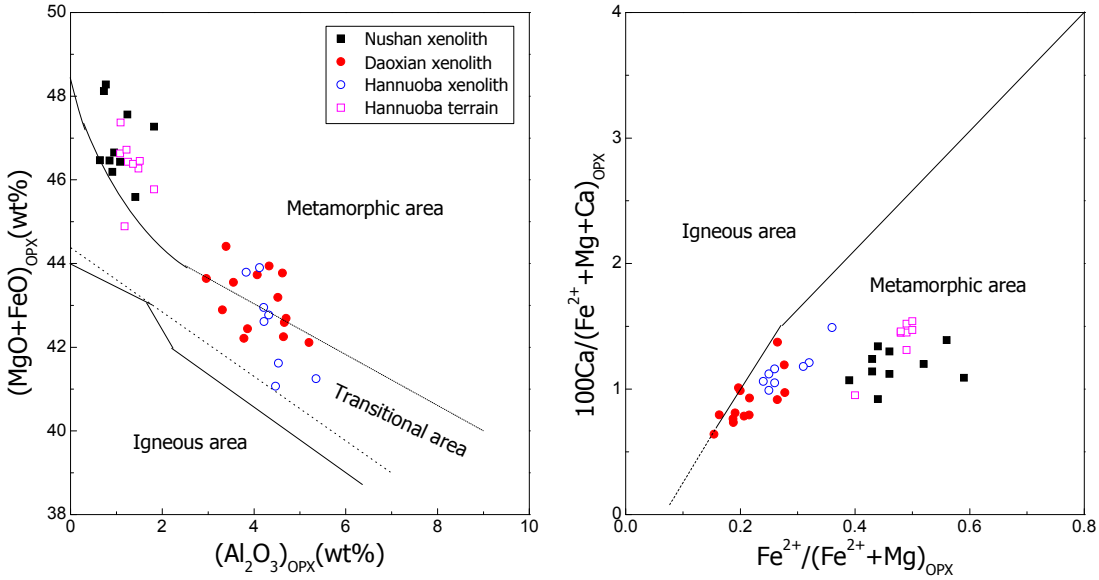

Fig. 5- 2 Petrogenetic discrimination diagrams of opx in the studied granulites

The equilibrial temperatures obtained by the two-pyroxene geothermeters of Wood and Banno (1973) and Wells (1977) are mostly falling into ± 50 °C variation with each other, consistent with the uncertainty of these two methods, and are ~ 860-920 °C for the Hannuoba xenolith granulites, ~ 760-900 °C for

Table 5- 1 Mineral compositions of the Hannuoba xenolith granulites

	Mineral	SiO_2	TiO_2	Al_2O_3	Cr_2O_3	FeO	MnO	MgO	CaO	Na_2O	K_2O	Total	Mg#	Wo(An)	En(Ab)	Fs(Or)	T_1(°C)	T_2(°C)
	cpx	49.59	0.81	5.80	0.06	8.17	0.18	13.33	21.14	0.94	0.02	100.0	0.74	45.88	40.27	13.85		
WD9520	opx	50.49	0.14	4.12	0.03	20.06	0.34	23.84	0.60	0.03	0.01	99.67	0.68	1.21	66.75	32.05	885	894
	plag	54.62	0.00	27.98	0.00	0.19	0.00	0.01	10.90	5.33	0.34	99.37		52.02	46.05	1.93		
	cpx	50.27	0.80	5.76	0.11	6.47	0.10	14.05	21.86	0.84	0.01	100.2	0.79	47.06	42.07	10.87		
WD9522	opx	52.35	0.13	4.22	0.05	16.61	0.24	26.00	0.52	0.05	0.01	100.2	0.74	1.05	72.57	26.38	903	887
	plag	53.82	0.01	28.53	0.00	0.06	0.03	0.02	11.66	4.96	0.29	99.39		55.58	42.80	1.62		
	cpx	49.55	0.73	5.79	0.07	9.67	0.18	12.28	20.51	1.18	0.04	100.0	0.69	45.44	37.84	16.72		
WD9530	opx	50.92	0.11	3.83	0.01	21.90	0.37	21.89	0.72	0.06	0.01	99.81	0.64	1.48	62.72	35.80	862	879
	plag	57.63	0.01	26.29	0.00	0.08	0.00	0.01	8.03	6.30	1.17	99.51		38.58	54.73	6.69		
	cpx	50.12	0.97	6.45	0.08	8.20	0.13	12.40	20.97	1.04	0.01	100.4	0.73	46.99	38.67	14.34		
WD9532	opx	51.80	0.16	4.21	0.03	19.18	0.30	23.76	0.57	0.05	0.01	100.1	0.69	1.17	67.69	31.13	875	874
	plag	56.61	0.10	27.74	0.00	0.09	0.09	0.02	9.98	5.64	0.36	100.6		48.43	49.52	2.06		
	cpx	50.69	0.81	6.51	0.11	5.60	0.12	13.54	21.97	0.82	0.00	100.2	0.81	48.63	41.71	9.67		
WD9546	opx	53.35	0.14	4.53	0.07	14.75	0.23	26.86	0.52	0.02	0.01	100.5	0.76	1.06	75.36	23.59	902	869
	plag	51.68	0.00	30.51	0.00	0.13	0.08	0.01	13.72	3.68	0.35	100.2		65.98	32.03	1.99		
	cpx	49.94	1.13	7.33	0.09	6.37	0.12	12.69	21.27	1.04	0.01	99.99	0.78	48.46	40.21	11.32		
DM9855	opx	52.51	0.16	5.35	0.04	15.37	0.24	25.88	0.48	0.04	0.01	100.1	0.75	0.99	73.99	25.03	896	871
	plag	55.99	0.02	27.85	0.00	0.10	0.01	0.03	10.30	5.20	0.88	100.4		49.63	45.34	5.03		
	cpx	50.71	0.97	6.59	0.02	6.27	0.13	12.99	21.74	0.91	0.01	100.4	0.79	48.63	40.43	10.94		
DM9871	opx	53.47	0.12	4.47	0.01	15.44	0.31	25.63	0.54	0.04	0.01	100.0	0.75	1.12	73.54	25.35	888	861
	plag	54.86	0.02	28.42	0.00	0.00	0.12	0.02	10.88	4.91	0.32	99.55		53.98	44.11	1.90		
	cpx	49.90	0.81	6.07	0.12	6.31	0.13	14.14	21.86	0.76	0.01	100.1	0.80	47.05	42.34	10.60		
HD71	opx	52.39	0.11	4.32	0.05	16.22	0.25	26.55	0.58	0.03	0.01	100.5	0.74	1.15	73.34	25.51	913	896

	plag	53.67	0.01	28.43	0.00	0.14	0.02	0.02	11.61	4.83	0.32	99.05		55.98	42.18	1.84

$Mg\# = Mg/(Mg + Fe^{2+})$, assuming all Fe as Fe^{2+}. Ab, albite; An, anorthite; En, enstatite; Fs, ferrosilite; Or, orthoclase; Wo, wollastonite. T1, by Wood and Banno (1973); T2, by Wells (1977).

Table 5- 2 Mineral compositions of the Hannuoba terrain granulites

	Mineral	SiO_2	TiO_2	Al_2O_3	FeO	MnO	MgO	CaO	Na_2O	K_2O	Total	Mg#	Wo(An)	En(Ab)	Fs(Or)	T_1(°C)	T_2(°C)	P(GPa)
MJ9801	cpx	49.67	0.35	3.65	12.75	0.35	11.69	21.35	0.50	0.03	100.30	0.62	44.88	34.19	20.93	825	867	1.3
	opx	50.29	0.03	1.48	28.61	0.72	17.66	0.69	0.02	0.01	99.51	0.52	1.42	51.02	47.55			
	grt	38.58	0.06	21.41	25.63	1.66	5.57	6.73	0.08	0.04	99.85	0.28						
	plag	54.20	0.00	28.70	0.07	0.02	0.01	11.62	4.91	0.22	99.77		55.99	42.77	1.24			
MJ9803	cpx	51.18	0.24	1.74	11.64	0.35	12.01	22.11	0.43	0.01	99.71	0.65	46.15	34.88	18.96			
	opx	49.98	0.05	1.08	29.57	0.93	17.05	0.69	0.02		99.39	0.51	1.45	49.95	48.59	791	820	
	plag	57.07	0.02	27.58	0.13	0.00	0.01	8.73	6.49	0.26	100.3		42.01	56.48	1.51			
MJ9805	cpx	51.35	0.26	2.23	12.05	0.52	11.49	21.56	0.50	0.02	99.98	0.63	45.92	34.03	20.03			
	opx	51.22	0.09	1.18	28.10	1.10	16.80	0.66	0.00	0.02	99.16	0.52	1.42	49.90	48.68	801	833	
	plag	57.52	0.03	26.58	0.05	0.00	0.01	8.76	6.43	0.41	99.79		41.95	55.74	2.31			
MJ9806	cpx	50.43	0.27	2.38	12.68	0.48	11.83	21.16	0.47	0.00	99.73	0.62	44.52	34.65	20.82			
	opx	50.08	0.04	1.25	29.41	1.23	17.02	0.72	0.01	0.00	99.77	0.51	1.49	49.01	49.50	827	872	
	plag	57.32	0.01	26.17	0.12	0.00	0.01	8.75	6.35	0.78	99.54		41.34	54.27	4.39			
MJ9807	cpx	50.93	0.23	1.85	12.35	0.34	11.76	22.22	0.49		100.2	0.63	46.07	33.94	20.00			
	opx	49.48	0.10	1.09	30.29	0.75	17.09	0.74	0.04	0.02	99.58	0.50	1.54	49.37	49.09	779	803	
	plag	55.71	0.01	27.76	0.13	0.02		8.46	6.51	0.57	99.16		40.44	56.30	3.26			
MJ9808	cpx	50.88	0.28	2.36	12.67	0.33	11.18	21.94	0.49	0.01	100.1	0.61	46.29	32.84	20.86	782	806	
	opx	50.88	0.08	1.22	29.57	0.87	17.15	0.62	0.03	0.02	100.4	0.51	1.31	50.17	48.51			

	plag	54.60	0.02	28.50	0.20	0.02	0.02	9.50	5.87	0.50	99.25		45.85	51.50	2.85			
MJ9810	cpx	50.76	0.24	2.61	11.80	0.42	11.38	21.81	0.46	0.01	99.48	0.63	46.55	33.80	19.65	788	813	1.2
	opx	50.95	0.09	1.36	28.86	0.95	17.52	0.70			100.42	0.52	1.46	51.22	47.32			
	grt	37.56	0.10	21.46	26.71	2.29	5.38	6.72	0.01	0.01	100.2	0.26						
	plag	54.20		28.77	0.19	0.03		11.85	4.74	0.37	100.1		56.79	41.12	2.08			
SX-1	cpx	49.49	0.56	3.87	11.00	0.13	12.54	20.62	0.68	0.03	98.98	0.67	44.20	37.40	18.40	866	900	1.4
	opx	51.24	0.07	1.82	24.72	0.39	21.05	0.47	0.01	0.02	99.80	0.60	0.95	59.34	39.71			
	grt	38.61	0.14	21.31	23.83	1.20	7.65	7.75	0.01	0.03	100.5	0.36						
	plag	54.92	0.03	28.49	0.08	0.02	0.01	11.10	5.36	0.12	100.2		52.98	46.32	0.70			
SX-2	cpx	50.59	0.28	2.93	12.51	0.21	11.00	22.32	0.56	0.01	100.4	0.61	47.10	32.29	20.61	762	779	1.1
	opx	50.94	0.04	1.51	29.65	0.55	16.80	0.70	0.03	0.02	100.2	0.50	1.47	49.52	49.01			
	grt	37.66	0.06	21.58	28.54	1.41	4.26	6.95	0.04	0.02	100.5	0.21						
	plag	54.88	0.01	28.79	0.21	0.01		10.37	5.36	0.37	100.0		50.58	47.25	2.17			

$Mg\# = Mg/(Mg + Fe^{2+})$, assuming all Fe as Fe^{2+}. Ab, albite; An, anorthite; En, enstatite; Fs, ferrosilite; Or, orthoclase; Wo, wollastonite. T1, by Wood and Banno (1973); T2, by Wells (1977); P, by Wood (1974).

Table 5- 3 Mineral compositions of the Nushan xenolith granulites

	Mineral	SiO_2	TiO_2	Al_2O_3	Cr_2O_3	FeO	MnO	MgO	CaO	Na_2O	K_2O	Total	Mg#	Wo(An)	En(Ab)	Fs(Or)	T_1(°C)	T_2(°C)
04NS1	opx	49.23	0.00	0.73	0.00	33.58	1.27	14.55	0.65	0.00	0.00	100.0	0.44	1.39	42.97	55.64		
04NS5	cpx	51.24	0.23	2.13	0.02	11.03	0.14	12.64	21.31	0.46	0.01	99.21	0.67	44.86	37.01	18.12	842	886
	opx	50.60	0.05	1.24	0.00	28.49	0.51	19.07	0.55	0.00	0.00	100.5	0.54	1.12	53.80	45.08		
	plag	57.85	0.04	26.23	0.00	0.05	0.04	0.00	8.15	5.94	0.68	98.99		41.37	54.54	4.09		
04NS8	cpx	51.19	0.16	1.90	0.00	14.56	0.49	10.12	20.15	0.65	0.00	99.23	0.55	44.19	30.88	24.93	812	886

	opx	48.95	0.12	0.77	0.00	34.65	1.33	13.64	0.51	0.00	0.00	99.96	0.41	1.09	40.78	58.13		
04NS9	cpx	51.39	0.28	2.22	0.01	12.34	0.79	12.93	19.25	0.62	0.04	99.88	0.65	41.08	38.37	20.55	892	958
	opx	50.54	0.01	0.85	0.00	27.21	1.37	19.25	0.45	0.00	0.00	99.68	0.56	0.92	55.26	43.82		
	plag	58.92	0.00	25.15	0.01	0.00	0.00	0.01	6.25	6.36	1.82	98.53		31.36	57.78	10.86		
04NS11	opx	51.47	0.04	0.91	0.00	26.32	1.29	19.87	0.61	0.01	0.03	100.5	0.57	1.24	56.65	42.11		
	plag	59.02	0.00	24.99	0.00	0.16	0.00	0.04	7.17	6.49	1.21	99.09		35.19	57.71	7.09		
04NS12	cpx	49.22	0.21	3.32	0.00	12.87	0.14	10.86	20.92	0.54	0.00	98.07	0.60	45.40	32.80	21.80	810	853
	opx	48.75	0.10	1.82	0.00	30.95	0.71	16.32	0.57	0.00	0.00	99.21	0.48	1.20	47.88	50.93		
04NS13	opx	50.08	0.16	1.08	0.00	27.06	1.13	19.37	0.65	0.00	0.02	99.55	0.56	1.34	55.30	43.36		
	plag	59.70	0.00	25.01	0.00	0.03	0.00	0.04	6.34	6.96	0.72	98.79		32.01	63.67	4.32		
04NS14	opx	51.22	0.13	1.41	0.00	24.31	0.69	21.28	0.53	0.04	0.02	99.62	0.61	1.07	60.28	38.64		
04NS15	cpx	51.51	0.16	2.07	0.00	12.30	0.33	12.78	20.58	0.71	0.00	100.4	0.65	42.92	37.07	20.01	860	902
	opx	50.99	0.02	0.95	0.00	26.62	0.56	20.03	0.56	0.03	0.00	99.76	0.57	1.14	56.63	42.23		
	plag	60.26	0.05	23.97	0.00	0.05	0.08	0.02	5.96	6.85	1.27	98.51		29.99	62.40	7.61		
04NS16	cpx	50.74	0.24	1.93	0.00	13.29	0.69	11.56	18.96	1.10	0.03	98.54	0.61	41.74	35.42	22.84	849	897
	opx	50.50	0.01	0.64	0.00	28.00	2.35	18.47	0.63	0.00	0.00	100.6	0.54	1.30	53.33	45.37		
	plag	59.19	0.09	24.32	0.00	0.18	0.00	0.02	6.17	8.21	1.37	99.55		32.82	59.72	7.47		

$Mg\# = Mg/(Mg + Fe^{2+})$, assuming all Fe as Fe^{2+}. Ab, albite; An, anorthite; En, enstatite; Fs, ferrosilite; Or, orthoclase; Wo, wollastonite. T1, by Wood and Banno (1973); T2, by Wells (1977).

Table 5- 4 Mineral compositions of the Daoxian xenolith granulites

	Mineral	SiO_2	TiO_2	Al_2O_3	FeO	MnO	MgO	CaO	Na_2O	K_2O	NiO	Total	Mg#	Wo(An)	En(Ab)	Fs(Or)	T_1(°C)	T_2(°C)
DX01	cpx	49.75	1.62	6.46	3.71	0.16	14.18	22.14	1.28	0.00	0.02	99.33	0.87	49.45	44.08	6.46	869	779
	opx	52.34	0.06	3.86	10.40	0.20	32.04	0.34	0.08	0.00	0.04	99.35	0.85	0.64	84.05	15.31		

	plag	53.81	0.02	29.14	0.02		0.01	11.83	5.12	0.10		100.1		90.51	9.21	0.28		
	cpx	49.40	1.09	6.44	7.09	0.17	13.04	21.42	1.06		0.02	99.74	0.77	47.50	40.24	12.26		
DX03	opx	50.25	0.20	4.62	17.75	0.34	26.01	0.60	0.05	0.01	0.02	99.87	0.72	1.19	71.46	27.35	869	849
	plag	53.80	0.03	29.38	0.01		0.02	11.70	5.05	0.26	0.01	100.3		90.29	9.02	0.69		
	cpx	49.54	0.95	6.47	5.13	0.12	14.18	22.43	1.23	0.00	0.01	100.1	0.83	48.59	42.73	8.68		
DX04	opx	51.16	0.18	4.52	13.30	0.26	29.89	0.52	0.05	0.02	0.00	99.90	0.80	0.99	79.23	19.78	854	787
	plag	52.24	0.04	30.37	0.07	0.02	0.01	12.80	4.43	0.16		100.1		91.88	7.70	0.42		
	cpx	51.19	0.73	6.70	4.32	0.14	13.72	21.82	1.36		0.01	99.99	0.85	49.27	43.12	7.61		
DX06	opx	53.64	0.11	5.20	12.81	0.26	29.31	0.52	0.10	0.00	0.04	101.9	0.80	1.01	79.51	19.48	876	813
	plag	52.44	0.00	29.99	0.05	0.03	0.01	12.48	4.53	0.15	0.03	99.68		91.63	7.96	0.40		
	cpx	50.31	0.71	6.17	4.69	0.13	14.27	22.20	1.10	0.01	0.03	99.60	0.84	48.56	43.44	8.00		
DX10	opx	52.21	0.09	4.64	12.31	0.22	29.94	0.39	0.07		0.01	99.87	0.81	0.76	80.64	18.60	890	824
	plag	51.33	0.01	30.30	0.07		0.02	12.88	4.50	0.18		99.28		91.71	7.82	0.47		
	cpx	50.54	0.70	6.65	4.69	0.16	14.14	21.92	1.16		0.03	99.96	0.84	48.44	43.48	8.08		
DX12	opx	52.57	0.04	3.31	12.70	0.25	30.19	0.42	0.04		0.06	99.58	0.81	0.81	80.26	18.93	898	837
	plag	51.91	0.00	30.59	0.08		0.01	13.10	4.12	0.12		99.93		92.56	7.13	0.31		
	cpx	50.44	0.86	6.10	4.92	0.07	13.81	22.11	1.28		0.02	99.61	0.83	48.95	42.55	8.50		
DX13	opx	51.50	0.16	4.66	14.04	0.26	28.56	0.48	0.08	0.00	0.05	99.77	0.78	0.93	77.66	21.41	848	790
	plag	52.86	0.00	29.90	0.07	0.02	0.01	12.37	4.61	0.13	0.01	99.97		91.53	8.13	0.34		
	cpx	50.12	1.03	6.44	5.21	0.12	14.07	21.84	1.09	0.01	0.03	99.94	0.83	48.02	43.04	8.94		
DX19	opx	52.35	0.08	3.55	14.31	0.28	29.24	0.42	0.05	0.00	0.03	100.3	0.79	0.79	77.83	21.37	897	851
	plag	52.74	0.04	29.76	0.04	0.01	0.01	12.29	4.50	0.18		99.56		91.55	7.97	0.48		
	cpx	51.49	0.58	5.61	4.12	0.10	14.72	22.31	1.15	0.01	0.01	100.1	0.86	48.49	44.51	7.00		
DX20	opx	52.75	0.06	3.78	10.90	0.24	31.31	0.42	0.07	0.00	0.04	99.54	0.84	0.79	83.00	16.21	901	823
	plag	51.73		30.77	0.02	0.00		13.37	4.12	0.07	0.01	100.1		92.72	7.09	0.19		
	cpx	49.89	1.11	6.03	6.74	0.16	13.54	21.49	1.04	0.00	0.04	100.0	0.78	47.14	41.32	11.55	885	863

DX28	opx	50.94	0.02	4.33	17.16	0.27	26.77	0.47	0.06	0.00	0.02	100.0	0.74	0.92	72.88	26.21		
	plag	54.15	0.03	29.08	0.08	0.02	0.01	11.38	5.26	0.25		100.2		89.87	9.45	0.67		
	cpx	50.79	0.77	6.12	4.97	0.13	14.18	21.98	1.04		0.05	100.0	0.84	48.22	43.28	8.51		
DX31	opx	51.87	0.04	4.70	13.53	0.25	29.17	0.40	0.05	0.00	0.03	100.0	0.79	0.78	78.74	20.48	902	852
	plag	53.04	0.03	29.83	0.03	0.02	0.01	12.63	4.50	0.14		100.2		91.70	7.94	0.37		
	cpx	50.52	0.52	5.12	5.03	0.17	14.84	21.76	1.19	0.03	0.03	99.18	0.84	46.97	44.56	8.47		
DX34	opx	52.41	0.14	2.96	12.75	0.25	30.89	0.39	0.07	0.00	0.03	99.82	0.81	0.73	80.61	18.66	908	847
	plag	51.94	0.01	30.91	0.02	0.03	0.00	12.45	4.53	0.18		100.1		91.75	7.79	0.46		
	cpx	49.84	1.22	6.33	6.72	0.18	13.03	21.52	1.20	0.01	0.01	100.0	0.78	47.93	40.39	11.68		
DX40	opx	51.36	0.02	3.39	18.06	0.31	26.35	0.50	0.06	0.01	0.03	100.1	0.72	0.97	71.54	27.49	850	824
	plag	54.17	0.03	29.15	0.05		0.00	11.64	4.92	0.24	0.02	100.2		90.47	8.87	0.66		
	cpx	49.97	1.08	6.35	6.49	0.18	13.08	21.34	1.24			99.75	0.78	47.84	40.81	11.35		
DX44	opx	51.55	0.18	4.07	17.09	0.36	26.63	0.70	0.05	0.02	0.02	100.7	0.74	1.37	72.52	26.11	863	834
	plag	53.87	0.03	29.05	0.05	0.01	0.01	11.50	4.99	0.26	0.00	99.75		90.28	9.00	0.72		

$Mg\# = Mg/(Mg + Fe^{2+})$, assuming all Fe as Fe^{2+}. Ab, albite; An, anorthite; En, enstatite; Fs, ferrosilite; Or, orthoclase; Wo, wollastonite.

T1, by Wood and Banno (1973); T2, by Wells (1977).

the Hannuoba terrain granulites, ~ 810-900 °C for the Nushan xenolith granulites and ~ 850-900 °C for the Daoxian xenolith granulites (Tables 5-1, 5-2, 5-3 and 5-4). The equilibrium pressures are ~ 1.1-1.4 GPa for the Hannuoba terrain granulites; combined with the established geothermal gradients by Chen et al. (2001) and Huang et al. (2004), the Hannuoba xenolith granulites are equilibriated at ~ 0.9-1.2 GPa and the Nushan xenolith granulites are at ~ 0.6-0.9 GPa; compared with the P-T variations from Dai et al. (2008), the Daoxian xenolith granulites are equilibriated at ~ 0.9-1.2 GPa. These P-T data agrees well with available reports (Chen et al., 2001; Huang et al., 2001; Huang et al., 2004; Fan et al., 2005; Dai et al., 2008). Based on the P-T results and the lithospheric structure beneath each locality documented in Chapter 3, as well as the mineral and compositional characteristics of these samples, the investigated granulite xenoliths were probably derived from the lower and lowermost crusts at each locality, which is ~ 35-42 km at Hannuoba, ~ 25-30 km at Nushan and ~ 30-40 km at Daoxian.

5.1.2 Peridotites

EMP investigations show that the mineral chemistry is inter- and intra-grain homogeneous for each peridotite xenolith, and the average data of multi-point determinations are reported in Table 5-5 for Hannuoba xenolith peridotites and Table 5-6 for Nushan xenolith peridotites. These results are similar to previous studies on the same type of peridotites from the same location (Rudnick et al., 2004; Xu and Bodinier, 2004).

In the Hannuoba peridotites, there is no evident variation in the composition of the individual minerals; but in the Nushan peridotites, slight differences can be observed between the *amp*-bearing and *amp*-free samples: the former is depleted in Al and Ti and enriched in Mg and Na for cpx, depleted in Al and Ti and enriched in Mg for opx, depleted in Mg and enriched in Fe for spinel and depleted in Ca for olivine relative to the latter. Some notable variation can also

be found between the Hannuoba and Nushan samples: the former is depleted in Al and Na for pyroxenes and in Al and Ca for olivine compared with the latter (Tables 5-5 and 5-6). These characteristics are consistent with available reports (Rudnick et al., 2004; Xu and Bodinier, 2004).

Mg# values range from 0.89 to 0.91 for cpx, 0.90 to 0.92 for opx and 0.89 to 0.91 for olivine in the Hannuoba peridotites and 0.86 to 0.90 for cpx, 0.87 to 0.91 for opx and 0.88 to 0.91 for olivine in the Nushan peridotites (Tables 5-5 and 5-6). The good correlations between some major elements for pyroxenes in the Hannuoba samples, e.g. negative relationship between Al_2O_3 (and FeO) and Mg# in cpx and opx and positive relationship between CaO and Mg# in cpx (Fig. 5-3), indicate that these xenoliths were probably evolved from the same mantle source experiencing variable extents of partial melting, and similar observations and conclusions can be acquired for the Nushan samples (Fig. 5-3).

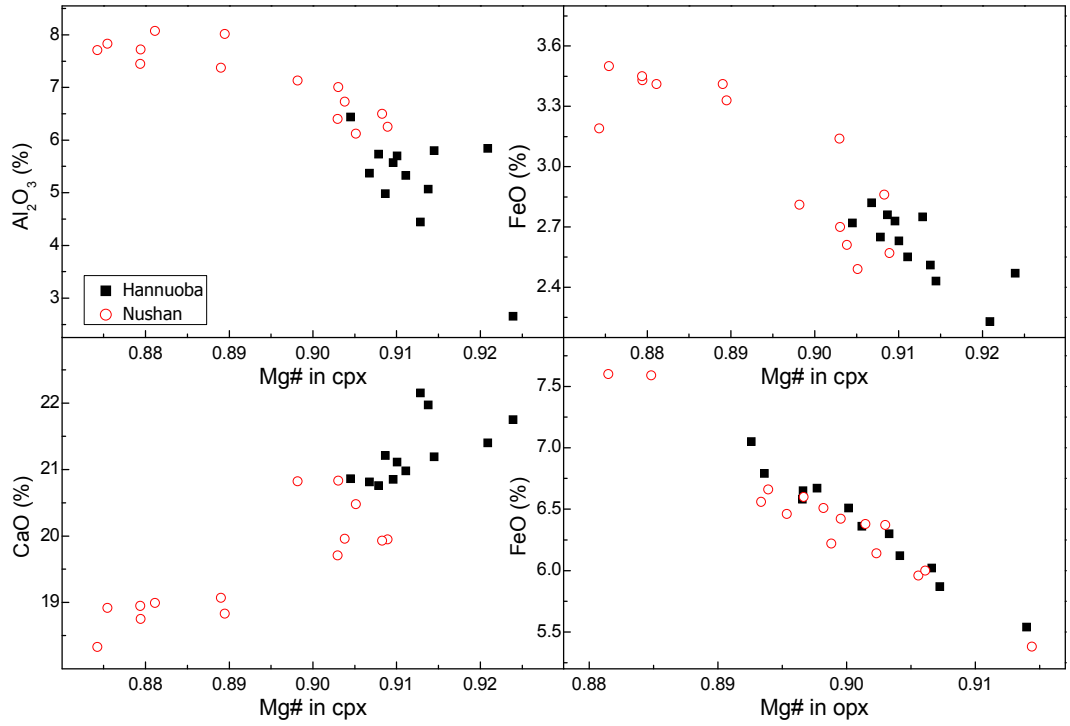

Fig. 5- 3 Correlations between major elements of pyroxenes in the studied peridotites

The estimated temperatures are 850-1050 °C for the Hannuoba peridotites and 900-1100 °C for the Nushan peridotites (Tables 5-5 and 5-6), agreeing well

Table 5- 5 Mineral compositions of Hannuoba xenolith peridotites

	P1	P2	P3	P4	P6	P8	P11	P12	P13	P14	P15	P17
	clinopyroxene											
SiO_2	53.04	53.02	52.15	53.66	52.52	52.06	52.06	52.24	53.13	52.51	52.28	52.94
TiO_2	0.53	0.41	1.05	0.20	0.35	0.19	0.47	0.50	0.58	0.68	0.59	0.45
Al_2O_3	5.80	5.73	5.07	2.65	4.98	4.44	5.57	5.37	6.44	5.84	5.70	5.33
Cr_2O_3	0.77	0.93	0.89	1.24	0.92	0.74	0.74	0.80	0.69	0.89	0.66	0.81
FeO	2.43	2.65	2.51	2.47	2.76	2.75	2.73	2.82	2.72	2.23	2.63	2.55
MnO	0.23	0.30	0.37	0.33	0.38	0.31	0.28	0.33	0.24	0.33	0.41	0.36
MgO	14.56	14.65	14.89	16.83	15.43	16.13	15.38	15.38	14.44	14.55	14.92	14.67
CaO	21.19	20.76	21.97	21.75	21.21	22.15	20.85	20.81	20.86	21.40	21.11	20.98
Na_2O	1.07	1.16	0.97	0.72	0.99	0.54	0.98	0.98	1.24	1.12	1.12	0.92
K_2O	0.00	0.02	0.01	0.00	0.00	0.00	0.01	0.01	0.00	0.00	0.00	0.01
Total	99.63	99.62	99.88	99.85	99.55	99.3	99.06	99.24	100.3	99.54	99.43	99.01
Mg#	0.91	0.91	0.91	0.92	0.91	0.91	0.91	0.91	0.90	0.92	0.91	0.91
	orthopyroxene											
SiO_2	56.33	56.21	55.86	56.31	55.54	55.03	55.12	55.00	56.19	56.03	55.26	55.98
TiO_2	0.10	0.07	0.26	0.11	0.10	0.05	0.12	0.14	0.11	0.12	0.14	0.11
Al_2O_3	3.50	3.57	3.20	2.72	3.65	4.07	4.15	3.90	4.02	3.40	3.82	3.92
Cr_2O_3	0.26	0.33	0.33	0.59	0.46	0.39	0.40	0.36	0.26	0.25	0.30	0.33
FeO	6.51	6.58	7.05	5.54	6.12	6.67	6.02	6.36	6.79	6.30	6.65	5.87
MnO	0.60	0.54	0.47	0.57	0.47	0.50	0.55	0.57	0.56	0.40	0.60	0.50
MgO	32.92	31.99	32.86	33.00	32.40	32.85	32.76	32.55	31.97	33.01	32.37	32.23
CaO	0.38	0.43	0.37	0.81	0.68	0.74	0.70	0.63	0.49	0.36	0.57	0.62
Na_2O	0.05	0.06	0.03	0.06	0.05	0.05	0.06	0.04	0.07	0.05	0.06	0.06
K_2O	0.01	0.00	0.00	0.01	0.01	0.00	0.00	0.01	0.00	0.00	0.01	0.00
Total	100.7	99.77	100.4	99.71	99.49	100.3	99.86	99.55	100.5	99.91	99.78	99.63
Mg#	0.90	0.90	0.89	0.91	0.90	0.90	0.91	0.90	0.89	0.90	0.90	0.91

T(°C)	866	887	858	1027	988	1006	992	969	915	857	947	965
	spinel											
SiO_2	0.00	0.05	0.01	0.03	0.02	0.03	0.02	0.00	0.02	0.00	0.02	0.05
TiO_2	0.06	0.15	0.36	0.35	0.18	0.07	0.19	0.23	0.12	0.17	0.21	0.15
Al_2O_3	57.27	53.96	51.00	51.11	50.10	54.03	54.39	53.93	58.84	55.74	57.68	53.00
Cr_2O_3	11.00	13.27	17.07	14.81	17.60	14.75	13.82	14.53	9.25	11.88	10.07	14.52
FeO	11.68	12.35	12.61	15.63	11.87	12.13	11.82	11.21	11.62	11.20	10.94	12.00
MnO	0.57	0.50	0.62	0.89	0.56	0.59	0.45	0.40	0.48	0.46	0.37	0.51
MgO	18.39	19.24	18.45	16.90	19.25	19.71	19.96	19.64	20.14	19.70	20.32	19.74
CaO	0.00	0.00	0.00	0.00	0.01	0.00	0.00	0.00	0.00	0.00	0.00	0.00
Na_2O	0.00	0.01	0.02	0.00	0.02	0.02	0.02	0.00	0.03	0.00	0.00	0.02
K_2O	0.00	0.00	0.00	0.01	0.00	0.00	0.01	0.01	0.00	0.00	0.00	0.00
Total	98.96	99.52	100.1	99.73	99.6	101.3	100.7	99.95	100.5	99.14	99.6	99.98
Mg#	0.74	0.74	0.72	0.66	0.74	0.74	0.75	0.76	0.76	0.76	0.77	0.75
	olivine											
SiO_2	40.31	41.25	40.64	40.99	40.63	40.31	40.62	40.27	40.37	40.83	40.47	40.66
TiO_2	0.01	0.00	0.00	0.01	0.00	0.02	0.03	0.00	0.01	0.00	0.00	0.00
Al_2O_3	0.01	0.02	0.00	0.01	0.01	0.02	0.01	0.01	0.01	0.01	0.01	0.01
Cr_2O_3	0.01	0.03	0.00	0.03	0.00	0.00	0.00	0.03	0.00	0.01	0.01	0.01
FeO	10.44	10.36	11.02	8.73	9.64	9.89	9.86	10.16	10.89	10.15	10.68	9.56
MnO	0.49	0.46	0.47	0.49	0.53	0.46	0.51	0.48	0.48	0.52	0.52	0.65
MgO	48.53	47.71	48.10	49.74	48.86	49.03	48.93	48.91	48.38	48.76	48.28	48.76
CaO	0.02	0.03	0.01	0.08	0.06	0.05	0.04	0.04	0.04	0.03	0.04	0.05
Na_2O	0.01	0.00	0.02	0.01	0.01	0.00	0.00	0.01	0.01	0.00	0.01	0.01
K_2O	0.00	0.00	0.02	0.00	0.00	0.00	0.00	0.01	0.00	0.00	0.01	0.01
Total	99.82	99.85	100.3	100.1	99.74	99.78	100.0	99.92	100.2	100.3	100.0	99.72
Mg#	0.89	0.89	0.89	0.91	0.90	0.90	0.90	0.90	0.89	0.90	0.89	0.90

$Mg\# = Mg/(Mg + Fe^{2+})$, assuming all Fe as Fe^{2+}. T, by Brey and Kohler (1990).

Table 5- 6 Mineral compositions of Nushan xenolith peridotites

	NS01	NS03	NS06	NS07	NS08	NS12	NS13	NS14	NS16	NS21	NS22	NS24	NS25	NS29	NS30
	clinopyroxene														
SiO_2	54.95	52.02	52.00	51.82	-	51.98	51.96	52.18	51.47	52.70	51.98	51.92	51.66	52.98	53.38
TiO_2	0.17	0.36	0.36	0.57	-	0.64	0.59	0.41	0.58	0.27	0.45	0.37	0.55	0.26	0.29
Al_2O_3	6.25	6.40	6.50	7.72	-	7.83	7.01	7.45	8.02	6.73	7.13	7.37	8.07	6.12	7.71
Cr_2O_3	1.03	1.03	1.08	0.73	-	0.58	0.63	1.08	0.79	0.96	0.74	0.97	0.72	0.93	0.89
FeO	2.57	3.14	2.86	3.43	-	3.50	2.70	3.45	3.33	2.61	2.81	3.41	3.41	2.49	3.19
MnO	0.10	0.10	0.08	0.11	-	0.11	0.09	0.17	0.11	0.06	0.13	0.09	0.13	0.08	0.08
MgO	14.41	16.37	15.90	14.04	-	13.81	14.09	14.11	15.04	13.75	13.90	15.34	14.16	13.31	12.42
CaO	19.95	19.71	19.93	18.75	-	18.92	20.83	18.95	18.83	19.96	20.82	19.07	18.99	20.48	18.33
Na_2O	2.53	1.59	1.59	2.02	-	1.88	1.98	1.81	1.99	2.55	2.15	1.93	1.94	2.44	3.30
K_2O	0.01	0.02	0.01	0.00	-	0.00	0.00	0.02	0.03	0.01	0.00	0.01	0.02	0.00	0.00
Total	101.9	100.7	100.3	99.2	-	99.25	99.88	99.62	100.2	99.59	100.1	100.5	99.64	99.09	99.58
Mg#	0.91	0.90	0.91	0.88	-	0.88	0.90	0.88	0.89	0.90	0.90	0.89	0.88	0.91	0.87
	orthopyroxene														
SiO_2	56.24	54.78	54.37	54.22	55.62	54.47	55.38	54.56	53.90	55.53	55.01	53.99	54.09	55.97	55.52
TiO_2	0.00	0.13	0.12	0.20	0.02	0.20	0.11	0.06	0.00	0.07	0.06	0.11	0.21	0.04	0.05
Al_2O_3	3.27	5.15	5.08	5.79	3.44	5.77	4.53	5.66	6.21	3.87	4.28	5.67	6.19	3.67	3.10
Cr_2O_3	0.35	0.59	0.55	0.38	0.35	0.40	0.20	0.09	0.48	0.33	0.25	0.50	0.37	0.30	0.27
FeO	6.38	5.38	5.96	6.66	7.60	6.14	6.51	6.00	6.46	6.42	6.60	6.56	6.22	6.37	7.59
MnO	0.18	0.10	0.11	0.18	0.18	0.14	0.15	0.11	0.09	0.09	0.18	0.15	0.15	0.11	0.15
MgO	32.74	32.23	32.08	31.46	31.70	31.80	32.20	32.48	31.01	32.25	32.10	30.80	30.99	33.25	32.71
CaO	0.49	1.07	1.01	1.11	0.48	0.97	0.53	1.04	1.03	0.54	0.56	1.07	1.03	0.52	0.45
Na_2O	0.13	0.19	0.19	0.23	0.18	0.22	0.10	0.07	0.20	0.13	0.13	0.19	0.22	0.15	0.19
K_2O	0.02	0.02	0.01	0.00	0.00	0.00	0.00	0.00	0.00	0.01	0.02	0.00	0.00	0.02	0.02
Total	99.8	99.63	99.48	100.2	99.56	100.1	99.72	100.1	99.38	99.24	99.19	99.06	99.47	100.4	100
Mg#	0.90	0.91	0.91	0.89	0.88	0.90	0.90	0.91	0.90	0.90	0.90	0.89	0.90	0.90	0.88

T(°C)	913	1099	1084	1107	912	1073	931	1089	1090	937	945	1101	1090	973	899
	spinel														
SiO_2	0.12	0.02	0.07	0.02	0.00	0.00	0.01	0.02	0.14	0.02	0.03	0.09	0.09	0.00	0.00
TiO_2	0.21	0.24	0.19	0.27	0.01	0.22	0.09	0.21	0.24	0.06	0.10	0.16	0.23	0.07	0.03
Al_2O_3	59.14	51.59	51.99	58.42	47.35	59.36	59.96	54.87	58.34	53.26	58.41	55.30	59.27	53.03	49.89
Cr_2O_3	6.96	16.44	16.05	8.97	19.59	8.61	8.37	11.88	10.09	15.86	10.09	13.17	9.04	16.00	17.78
FeO	11.11	11.48	11.25	11.29	15.17	10.59	10.56	12.08	10.51	11.81	11.65	11.73	11.49	12.03	14.79
MnO	0.02	0.12	0.18	0.12	0.25	0.07	0.08	0.16	0.12	0.06	0.11	0.11	0.06	0.16	0.10
MgO	21.29	20.58	20.80	21.11	17.56	21.30	20.65	20.78	20.12	19.33	19.54	19.71	19.33	18.02	18.09
CaO	0.00	0.01	0.01	0.00	0.00	0.00	0.00	0.00	0.00	0.00	0.00	0.00	0.00	0.00	0.00
Na_2O	0.00	0.00	0.03	0.00	0.23	0.00	0.06	0.01	0.03	0.00	0.07	0.02	0.02	0.02	0.04
K_2O	0.01	0.00	0.01	0.01	0.06	0.00	0.00	0.00	0.01	0.00	0.01	0.01	0.00	0.00	0.00
Total	98.86	100.5	100.6	100.2	100.2	100.2	99.78	100	99.59	100.4	100.0	100.3	99.52	99.32	100.7
Mg#	0.77	0.76	0.77	0.77	0.67	0.78	0.78	0.75	0.77	0.74	0.75	0.75	0.75	0.73	0.69
	olivine														
SiO_2	40.65	41.08	40.21	41.16	40.71	n.a.	40.58	41.25	41.22	41.00	40.73	40.96	40.48	40.48	40.78
TiO_2	0.00	0.00	0.00	0.00	0.00	n.a.	0.01	0.01	0.02	0.01	0.01	0.00	0.01	0.00	0.00
Al_2O_3	0.01	0.04	0.02	0.06	0.01	n.a.	0.01	0.03	0.03	0.01	0.01	0.03	0.02	0.01	0.00
Cr_2O_3	0.01	0.03	0.01	0.00	0.01	n.a.	0.01	0.00	0.04	0.02	0.00	0.05	0.02	0.01	0.02
FeO	10.40	10.52	10.28	11.76	13.37	n.a.	10.36	11.00	11.43	10.36	11.70	11.10	11.55	10.15	12.97
MnO	0.18	0.14	0.48	0.11	0.11	n.a.	0.50	0.14	0.15	0.09	0.08	0.06	0.13	0.42	0.17
MgO	48.50	48.27	48.32	47.15	46.61	n.a.	48.75	47.49	47.40	47.62	47.52	47.20	47.84	48.67	46.40
CaO	0.02	0.09	0.06	0.11	0.02	n.a.	0.02	0.12	0.09	0.03	0.05	0.09	0.09	0.01	0.04
Na_2O	0.00	0.05	0.01	0.03	0.03	n.a.	0.00	0.02	0.03	0.01	0.04	0.02	0.01	0.01	0.04
K_2O	0.01	0.01	0.00	0.01	0.01	n.a.	0.01	0.01	0.01	0.01	0.01	0.01	0.02	0.00	0.02
Total	99.72	99.72	99.72	99.72	99.72	n.a.	99.72	99.72	99.72	99.72	99.72	99.72	99.72	99.72	99.72
Mg#	0.89	0.89	0.89	0.88	0.86	n.a.	0.89	0.88	0.88	0.89	0.88	0.88	0.88	0.90	0.86

$Mg\# = Mg/(Mg + Fe^{2+})$, assuming all Fe as Fe^{2+}. T, by Brey and Kohler (1990). -: this mineral is free in the sample; n.a.: not analyzed.

with previous investigations (Rudnick et al., 2004; Xu and Bodinier, 2004). In combination with the established geothermal gradients for the Hannuoba and Nushan regions by Chen et al. (2001) and Huang et al. (2004), respectively, the investigated peridotite xenoliths probably originated from the uppermost mantle, at an estimated depth of ~ 45-65 km and ~ 30-55 km, respectively.

5.2 FTIR results

5.2.1 Granulites

5.2.1.1 Near-IR absorption

In the near-IR region (4000 to 6500 cm^{-1}), the minerals under investigation display quite different absorption behavior: a broad band peaked at ~ 4400 and 5100 cm^{-1} can be observed for cpx and opx, respectively; by contrast, no such band can be found for plag, and grt generally show two broad bands peaked at ~ 4150 and 5800 cm^{-1} (Fig. 5-4). So broad are these bands that they cannot be ascribed to either combination or overtones of the fundamental (e.g. stretching and bend vibration) modes. Actually, the position and shape of these bands are similar to the corresponding minerals reported by Burns (1993), and therefore, it is suggested that they are produced by the electronic absorption or transition of Fe^{2+} in the crystal field of the hosted minerals.

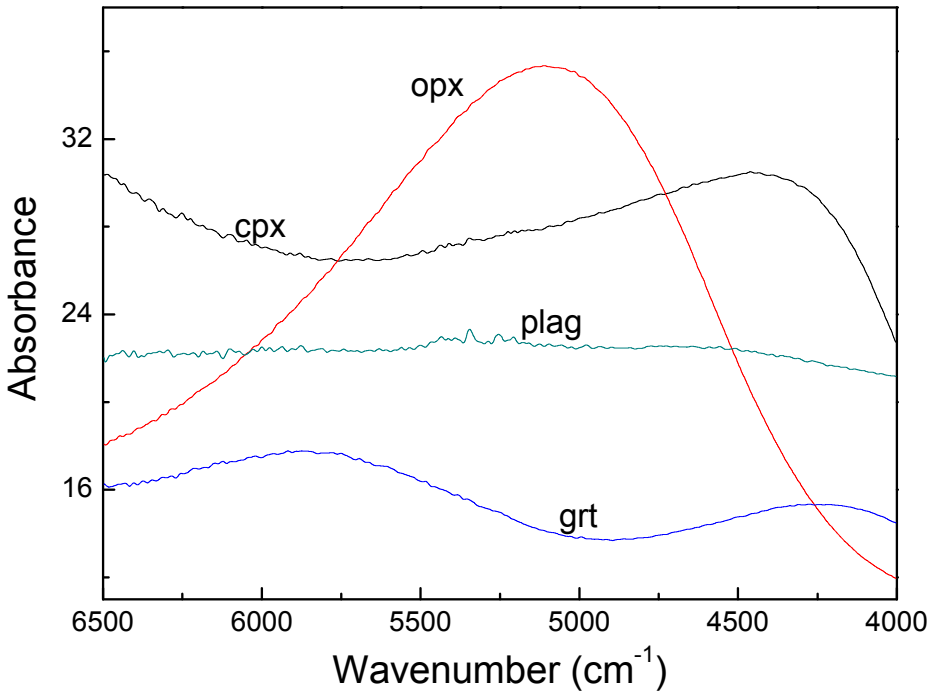

Fig. 5- 4 Representative spectra of cpx, opx, plag and grt in the near-IR region

(All the spectra were normalized to 1 cm thickness and were vertically offset. These illustrations are also applicable to the following spectra figures)

5.2.1.2 Hydrogen-related species

In the middle-IR region (3000 to 3650 cm^{-1}), all the spectra of analyzed cpx, opx, plag and grt exhibit several H-related absorption bands. Representative IR spectra of these minerals are illustrated individually for the 4 suites of granulites (Figs. 5-5, 5-6, 5-7 and 5-8), because noticeable differences in the shape, position and absorption intensity of these bands can be observed for samples from different localities.

Based on the position, these absorption bands can be divided into several different groups for different minerals. Briefly, they are usually in the range of (1) 3620-3635, 3510-3530, 3450-3470 cm^{-1} for cpx, (2) 3595-3610, 3570-3590, 3510-3525, 3395-3430, 3295-3315, 3195-3220, 3055-3070 cm^{-1} for opx (the latter 3 are relatively rare), (3) 3610-3630, 3580-3600, 3480-3520, 3420-3445, 3380-3406, 3180-3230 cm^{-1} for plag, and (4) 3610-3630, 3570-3600, 3420-3450 cm^{-1} for grt. All these bands are relatively common in the samples, with the exception that a few opx spectra of high absorption were only found in some terrain granulites (Fig. 5-6). The relative absorbances of these bands are highly variable for different grains even within the same sample, which is attributed to different orientations of different grains with respect to the infrared beam direction. The position and shape of these absorption bands are mostly similar to available results for the corresponding minerals (i.e. Aimes and Rossman, 1984; Skogby and Rossman, 1989; Skogby et al., 1990; Bell and Rossman, 1992a, 1992b; Stalder and Skogby, 2002; Johnson and Rossman, 2004; Stalder, 2004), while slight differences for some spectra may be associated with the chemical composition and crystal structure of the hosted phases. Correspondingly, it is suggested that these absorption bands are mainly related with the stretching vibration of structural hydroxyl (however, the 3420-3450 cm^{-1} band of grt is out of the energy range of structural hydroxyl, usually 3500-3700 cm^{-1}, in previous studies on both natural and synthesized garnets, which is commonly ascribed to

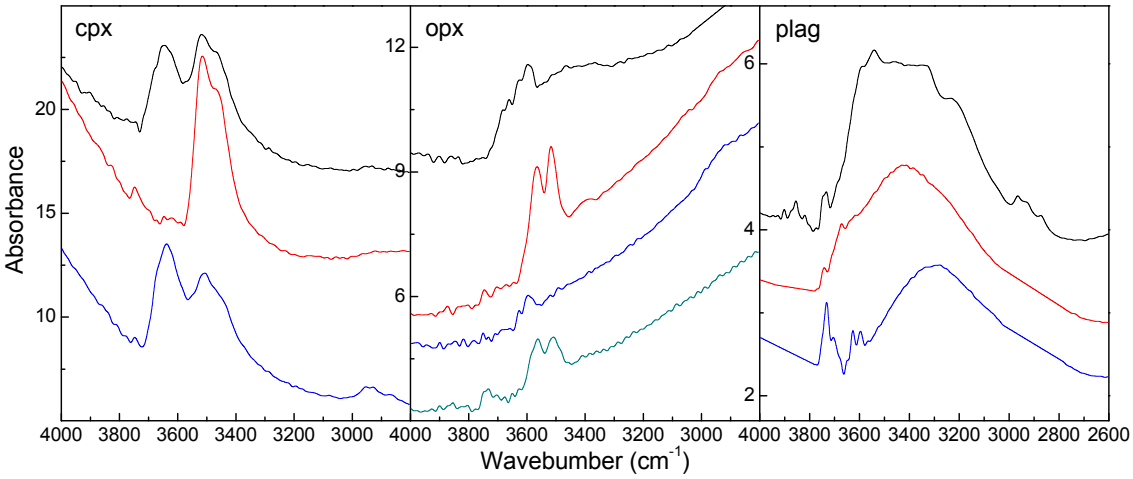

Fig. 5- 5 Representative IR spectra for cpx, opx and plag in Hannuoba xenolith granulites

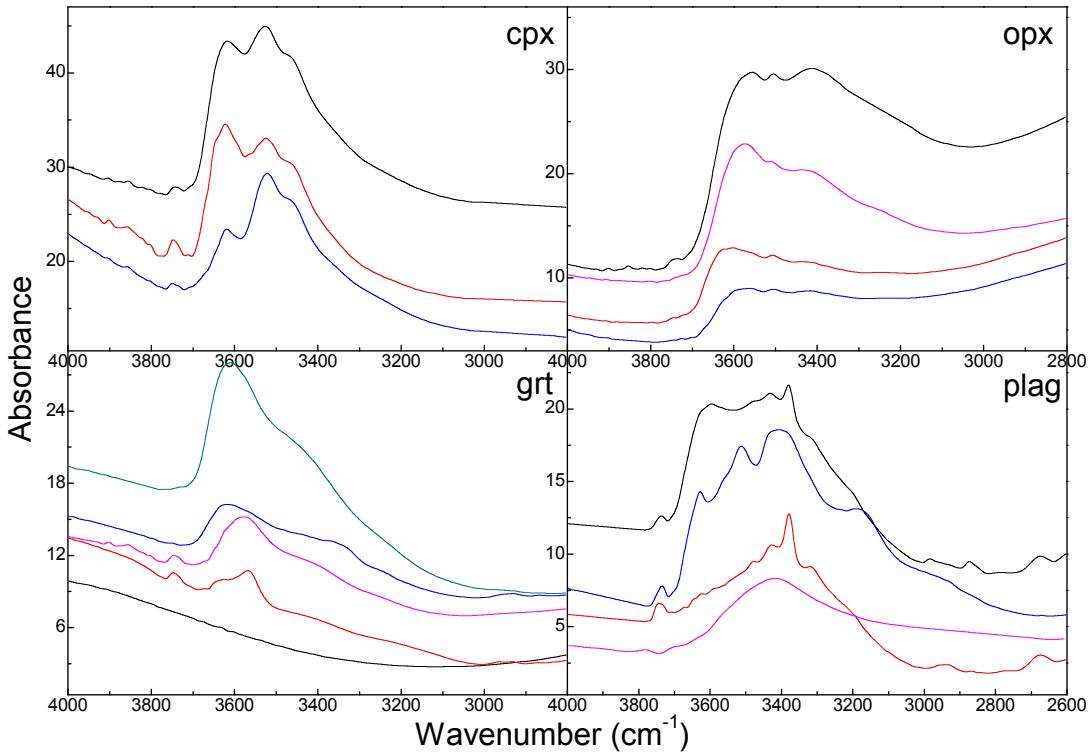

Fig. 5- 6 Representative IR spectra for cpx, opx, plag and grt in Hannuoba terrain granulites

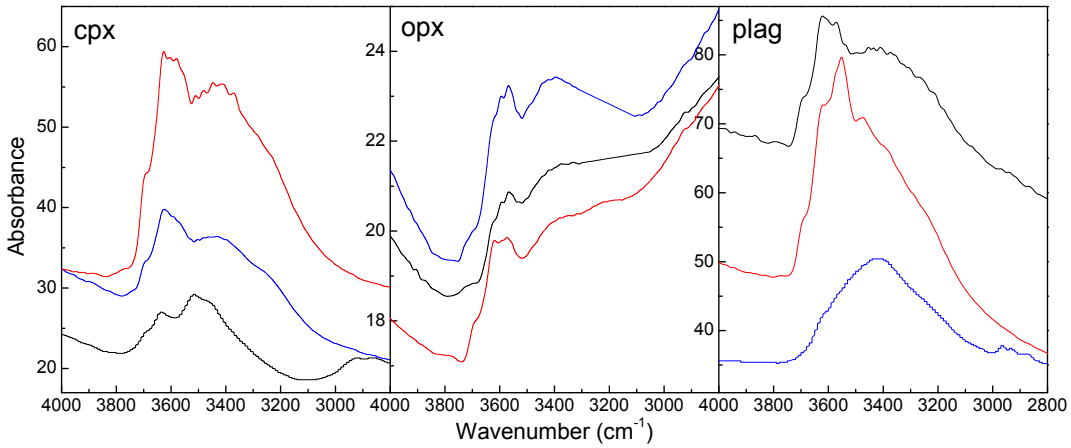

Fig. 5- 7 Representative IR spectra for cpx, opx and plag in Nushan xenolith granulites

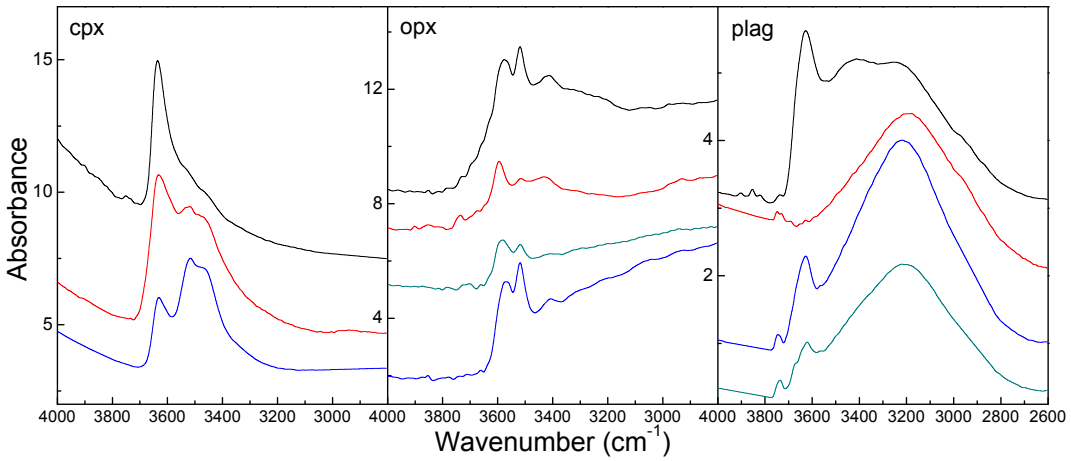

Fig. 5- 8 Representative IR spectra for cpx, opx and plag in Daoxian xenolith granulites

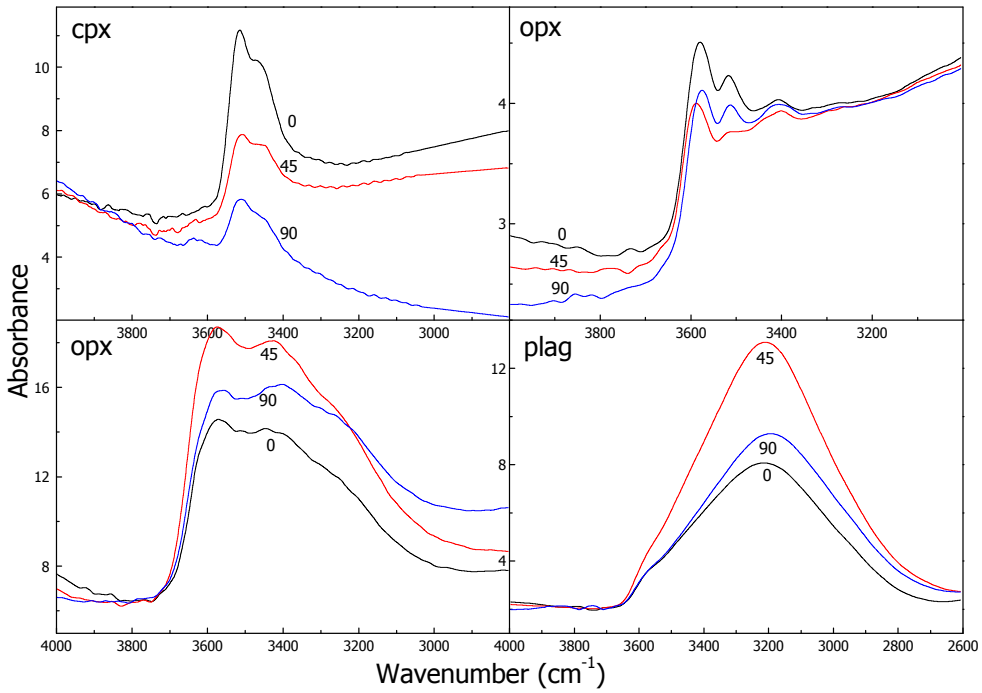

Fig. 5- 9 Representative polarized IR spectra for minerals in granulites

tiny fluid inclusions (Rossman et al., 1989; Rossman and Aines, 1991; Langer et al., 1993), and they were therefore removed from the calculation of H_2O content by the Peakfit treatment). This can be further supported by the polarized analyses on some oriented grains (Fig. 5-9), which reveal that the absorption intensity of individual bands for each mineral vary significantly with the angle of incident IR light. Furthermore, the inconsistent variations between these bands of each mineral, or say independent variations, shown in Fig. 5-9 indicate that different kinds of H-defects are involved, e.g. the polarized behavior of the ~ 3620 cm^{-1} band of cpx is markedly different from that of the ~ 3520 and 3460 cm^{-1} bands, which may reflect the presence of at least two distinct types of H incorporated into the mineral. The H-related species bound to the structure of plag in granulites is a little complicated, they may contain OH, H_2O molecular and/or NH_4^+ according to the characteristic bands observed in our samples and those in igneous feldspars reported by Johnson and Rossman (2004).

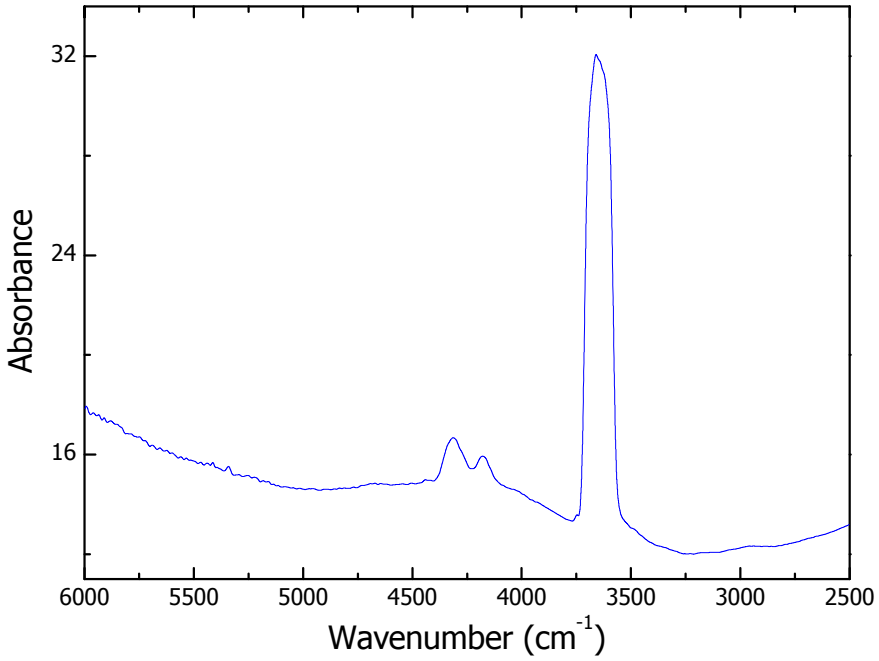

Fig. 5- 10 IR spectra of secondary amphibole in granulites

The IR spectra of minerals in some Hannuoba terrain, Nushan and Daoxian xenolith granulites are of special attention for the presence of a weak band at ~ 3660 cm^{-1} (e.g. Fig. 5-7), which is ascribed to amphibole/mica lamellae. In order to figure out the possible effects from these altered products on the final integrated absorption area, we have to know that if there are other bands from

these hydrous phases, which may superimpose on the peaks of the investigated minerals. Therefore, a few grains of secondary amphibole/mica were performed the FTIR determination, and it was shown that there is usually only one single band peaked at ~ 3660 cm^{-1}, with very weak absorption in the 3570-3200 cm^{-1} range (Fig. 5-10). In this case, for the spectra displaying weak absorption at ~ 3660 cm^{-1}, the secondary amphibole/mica probably contributes little to the total integral absorption area, and their influences can be quantitatively resolved and removed by Peakfit treatments.

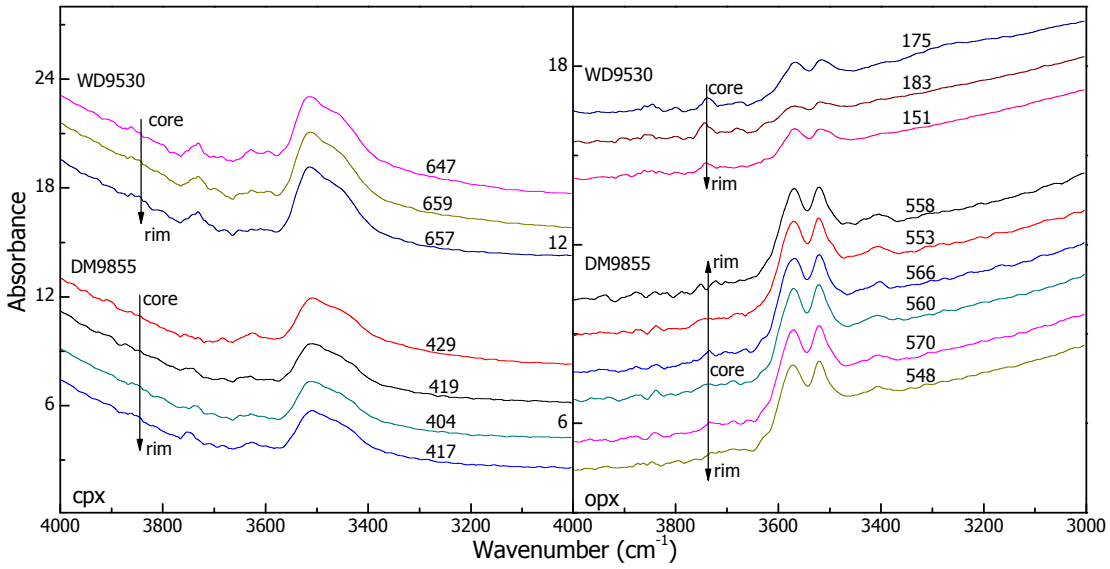

Fig. 5- 11 Profile analyses of H absorption in the Hannuoba xenolith granulites

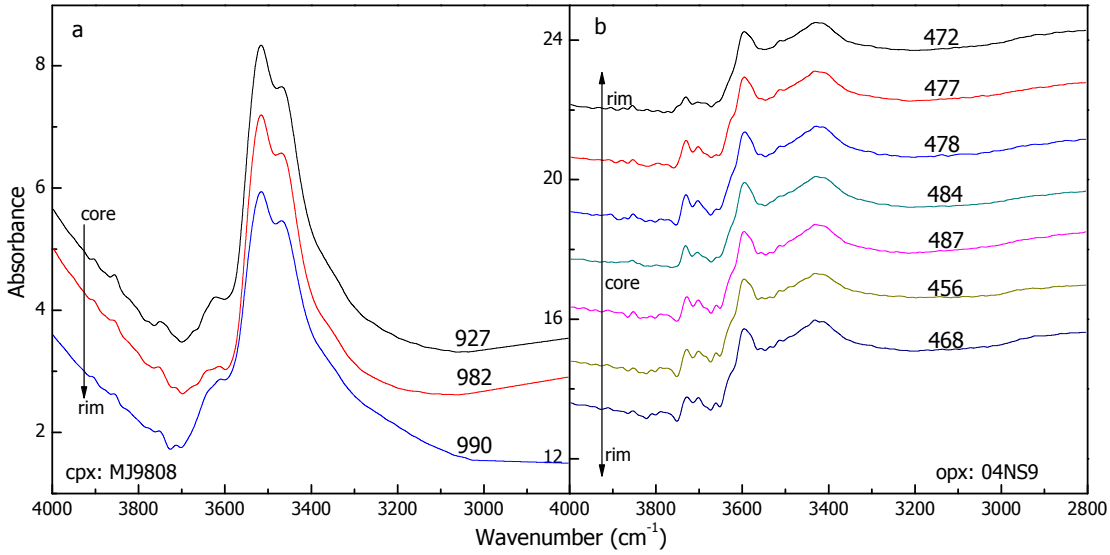

Fig. 5- 12 Profile analyses of H absorption in the (a) Hannuoba terrain and (b) Nushan xenolith granulites

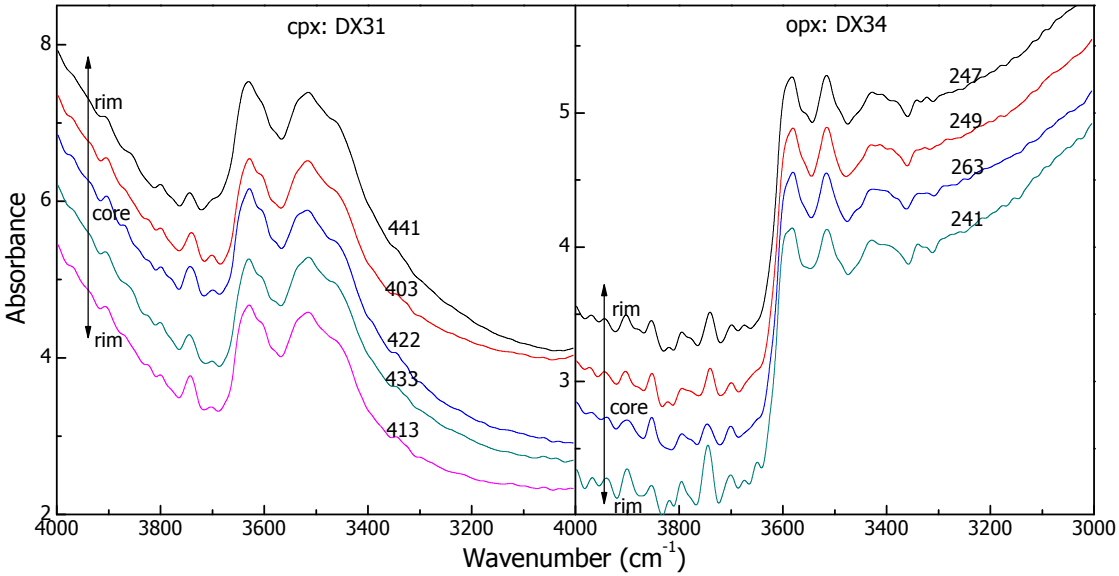

Fig. 5- 13 Profile analyses of H absorption in the Daoxian xenolith granulites

Note: Numbers above each spectrum in Figs. 5-11, 5-12 and 5-13 are the integral absorption area of H-species in the 3000-3650 cm^{-1} range, which is the same as those in the following profile illustrations for xenolith peridotites.

In an attempt to understand whether the water content of these samples was significantly modified during their transport to the surface, profile analyses have been conducted on abundant selected cpx and opx grains for each suite of granulites (almost all these samples have been subjected to such investigation). Because cpx in the Nushan xenolith and opx in the Hannuoba terrain samples are extremely fine-grained, it is not easy to find large, gem-quality transparent and clear grains in them (especially in the terrain samples), and therefore only opx in the former and cpx in the latter were performed the analyses. The results are shown in Fig. 5-11 for the Hannuoba xenolith granulites, Fig. 5-12a for the Hannuoba terrain granulites, Fig. 5-12b for the Nushan xenolith granulites and Fig. 5-13 for the Daoxian xenolith granulites. These observations imply that pyroxene grains in the granulites are mostly unzoned in terms of their hydrogen FTIR absorption from the core to rim region. However, we did determine some grains which, in very fewer cases, display variable hydroxyl absorption between their core and rim region; while no regular populations were found, they can be either enriched or depleted in the core relative to the rim with respect to the IR absorption.

5.2.1.3 Water content

The determined water concentrations, and the estimated bulk contents, for the 4 suites of granulites are given in Table 5-7, the water contents of analyzed garnet grains in 5 Hannuoba terrain granulites are provided in Table 5-8 and the profile-measurements across 7 garnet grains in SX-1 are summarized in Table 5-9.

These water contents are highly variable. It ranges in average from 275 to 720 ppm for cpx, 60 to 185 ppm for opx, 65 to 205 ppm for plag and 165 to 355 ppm for bulk rock in the Hannuoba xenolith granulites, from 585 to 1480 ppm for cpx, 230 to 1875 ppm for opx, 175 to 895 ppm for plag, 290 to 620 ppm for grt and 405 to 1120 ppm for bulk rock in the Hannuoba terrain granulites, from 200 to 2330 ppm for cpx, 140 to 1270 ppm for opx, 145 to 900 ppm for plag and 155 to 970 ppm for bulk rock in the Nushan xenolith granulites, and from 285 to 500 ppm for cpx, 65 to 135 ppm for opx, 205 to 345 ppm for plag and 200 to 360 ppm for bulk rock in the Daoxian xenolith granulites (Table 5-7).

Water contents of the Nushan xenolith granulites are notably different from those of the Hannuoba and Daoxian xenolith granulites, they instead resemble more those of the Hannuoba terrain granulites for their especially high contents (Table 5-7). Such similarity between the Nushan xenolith and Hannuoba terrain granulites is in good agreement with the major and trace element compositions (Huang et al., 2004; and this study). In addition to the contrast in H_2O content of both minerals and bulk rocks between different localities, the large variation is also observed for individual minerals within each group of granulites, e.g. it is >200% for cpx and >100% for opx in the Hannuoba xenolith granulites and >150% for cpx and >100% for opx in the Daoxian xenolith granulites, and is even larger in the other two suites of granulites (Table 5-7). These variations are far beyond the experimental uncertainty (~ 30%), implying heterogeneities of water content on macro scales, e.g. between different samples and localities.

Because of its isotropic characteristic, garnet provides a special probe into the microscale distribution of water in these granulites for the unpolarized FTIR analyses. The H_2O content in grt can be down to about 0 ppm, for the presence

of some grains without evident hydrogen-related IR absorption (Fig. 5-6), and up to more than 1400 ppm (Tables. 5-8 and 5-9). This variation is also observed between different grains within the same sample, e.g. it ranges from about 90 to 1330 ppm in MJ9801 and from 230 to 1240 ppm in MJ9811 (Table 5-8); even within the same grain, the difference in water content between different zones can be a factor of 10-20 (Table 5-9). The wide variation of water content in the grt is similar to those reported in eclogites from the Central Dabieshan by Xia et al. (2005), which experienced quick deep subduction, UHP metamorphism and subsequent exhumation in a cycle of 10 to 20 Ma (Zheng et al., 2003), and to those reported in grossular-andradite garnet from the skarn belt in Oak Hill and Willsboro, Adirondacks by Johnson (2003), which experienced a spatially and temporally complicated fluid and metamorphic history (Valley and O'Neil, 1982, 1986), although the H_2O concentrations in the latter are much higher even if we re-calculated them by the same method in this study.

The above documented variations indicate that the distribution of water in the granulites is variable on both large and small scales, e.g. within sub-grain / between different grains/samples/localities.

No simple correlations in H_2O content, in terms of the partitioning of water between the coexisting mineral pairs, can be observed in the studied granulites (Table 5-7; see also Chapter 6 for a detailed discussion).

Table 5- 7 H_2O content (ppm by wt.) of individual minerals and bulk rock in the studied granulites

	cpx	opx	plag	grt	bulk
Hannuoba xenolith					
WD9520	440	65	180		275
WD9522	600	185	135		300
WD9530	470	140	205		310
WD9532	480	70	85		300
WD9546	570	90	140		355
DM9855	275	135	100		165
DM9871	720	70	90		260
HD71	470	60	65		265
Hannuoba terrain					
MJ9801	1480	1875	895	560	1120
MJ9803	665	310	265	-	405
MJ9805	1250	1480	580	-	795
MJ9806	820	1325	795	-	855
MJ9807	780	306	274	-	480
MJ9808	585	620	325	-	470
MJ9810	1175	885	345	430	875
MJ9811	1100	365	245	620	615
SX-1	1365	1285	445	290	725
SX-2	885	230	175	430	465
Nushan xenolith					
04NS1		290	460		435
04NS5	2330	665	725		970
04NS8	2030	590	710		790
04NS9	215	445	365		325
04NS11	-	465	450		455
04NS12	200	160	145		155
04NS13	-	140	290		260
04NS14	-	1270	900		950
04NS15	1245	550	565		645
04NS16	2330	525	820		870
Daoxian xenolith					
DX01	445	110	350		310
DX03	285	70	205		220
DX04	335	65	205		200
DX06	390	90	295		280
DX10	345	90	345		270
DX12	435	120	265		295
DX13	310	110	290		260
DX19	430	140	305		315
DX20	425	85	250		280
DX28	435	135	260		295
DX31	285	80	225		235
DX34	350	85	275		270
DX40	500	70	340		360
DX44	370	135	330		300

Average densities used in the calculation are:

Hannuoba xenoliths:

cpx, 3.20 g/cm^3; opx, 3.47 g/cm^3; plag, 2.69 g/cm^3

Hannuoba terrains:

cpx, 3.26 g/cm^3; opx, 3.60 g/cm^3; plag, 2.68 g/cm^3; grt, 3.9 g/cm^3

Nushan xenoliths:

cpx, 3.28 g/cm^3; opx, 3.60 g/cm^3; plag, 2.65 g/cm^3

Daoxian xenoliths:

cpx, 3.17 g/cm^3; opx, 3.43 g/cm^3; plag, 2.70 g/cm^3

Actually, the variation in density of the same mineral is very small (<4%) between the 4 groups of granulites.

Note: the data are average values of 8-30 grains, and are rounded to the nearest 5 ppm. -: this mineral is free in the sample.

Table 5- 8 H_2O content (ppm by wt.) of garnet grains in terrain granulites

	1	2	3	4	5	6	7	8	9	10
MJ9801	982	1114	949	787	287	354	882	1337	933	618
	140	89	143	237	362	105	439	281		
MJ9810	635	569	953	558	1477	955	1132	1253		
MJ9811	490	1243	229	794	761	523	285			
SX-1	62	167	124	142	191	24	140	206	60	157
	54	147	95	68	142	90	156	175	63	173
	297	322	365	358	209	581	165	79	133	408
	174	556	211	349	151					
SX-2	481	199	336	406	654	584	273	552	404	392

Note: nearly 40 grains in sample SX-1 were analyzed because it is especially rich in garnet; some grains in these samples actually contain no water, which were not illustrated here.

Table 5- 9 Profile analyses of H across several garnet grains in SX-1

	1	2	3	4	5	6	7	8	9	10
Grain 1	681	438	87	427	155	284	386	204	83	1735
Grain 2	56	322	609	110	1087					
Grain 3	91	263	123	328	744	886	367			
Grain 4	62	167	124							
Grain 5	142	191	24	140						
Grain 6	206	60	157	54						
Grain 7	147	95	68							

Note: grain 1, a nearly linear profile along rim-core-rim; grain 2 to 7, nearly linear profile from core to rim region.

5.2.2 Peridotites

5.2.2.1 H-related species

In the middle-IR region (3000 to 3650 cm^{-1}), all the spectra of analyzed cpx and opx grains display several H-related absorption bands. Representative IR spectra of cpx and opx are shown in Fig. 5-14 for the Hannuoba peridotites and Fig. 5-15 for the Nushan peridotites (All the spectra were normalized to 1 cm thickness and were vertically offset). In strong contrast to the general H-related absorption observed in cpx and opx, olivine in both these 2 suites of peridotites usually shows no, or in rare cases very weak (< 1 but mostly < 0.1 ppm H_2O according to Bell et al. (2003)), H-absorption (Fig. 5-16). Such difference may be caused by the relatively faster diffusion rate of H in olivine than in pyroxenes

(Kohlstedt and Mackwell, 1998, 1999; Hercule and Ingrin, 1999; Woods et al., 2000), and correspondingly the diffusion loss of H is significant in the former.

The absorption bands of pyroxenes can be divided into different groups for each mineral: (1) 3600-3635, 3510-3550 and 3445-3470 cm^{-1} for cpx, and (2) 3570-3595, 3500-3525, 3390-3415 and 3300-3315 cm^{-1} for opx, the last one is very rare. The relative absorbances of these bands vary among grains even in the same sample due to the variable orientation of grains with respect to the IR beam direction. The positions and shape of these bands are similar to previous studies on mantle pyroxenes (Skogby and Rossman, 1989; Skogby et al., 1990), suggesting that they are caused by the vibration of structural OH. This is even supported by the polarized analysis of some oriented grains: the IR absorption intensity of each band varies with the polarizing direction (Fig. 5-17). Similar to granulite minerals, the different polarized behavior between different bands can

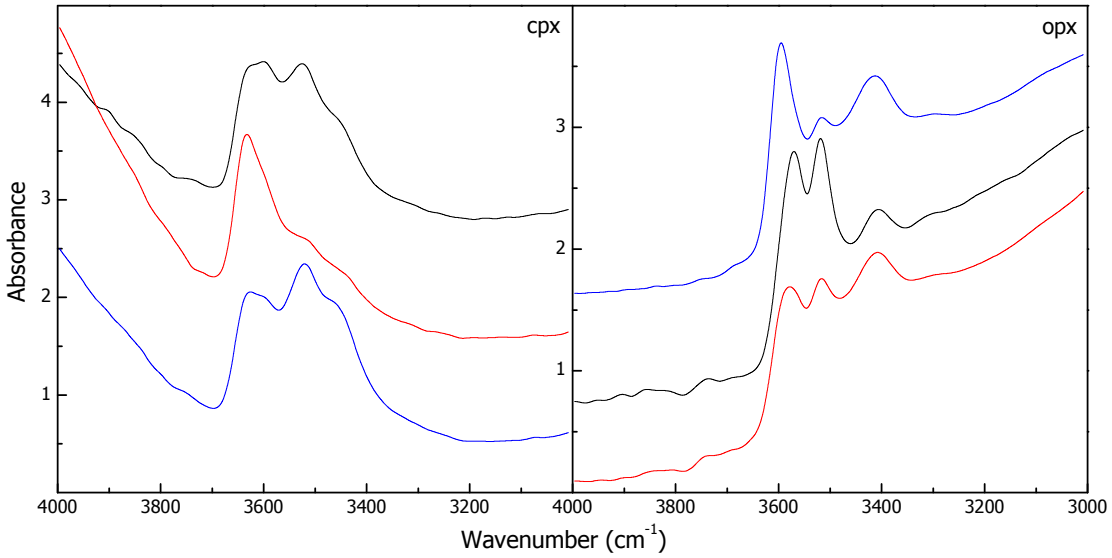

Fig. 5- 14 Representative IR spectra of pyroxenes in the Hannuoba xenolith peridotites

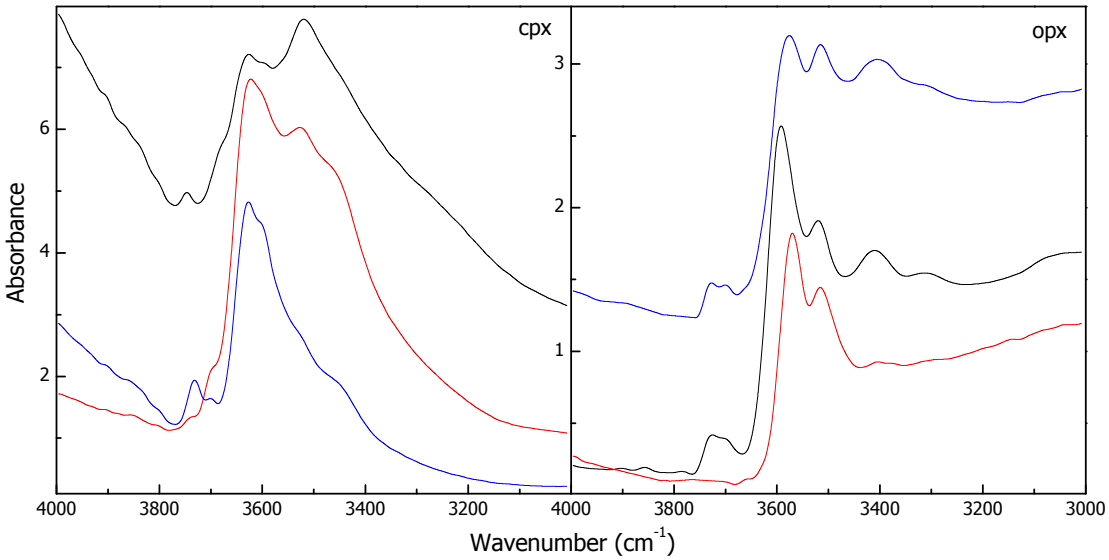

Fig. 5- 15 Representative IR spectra of pyroxenes in the Nushan xenolith peridotites

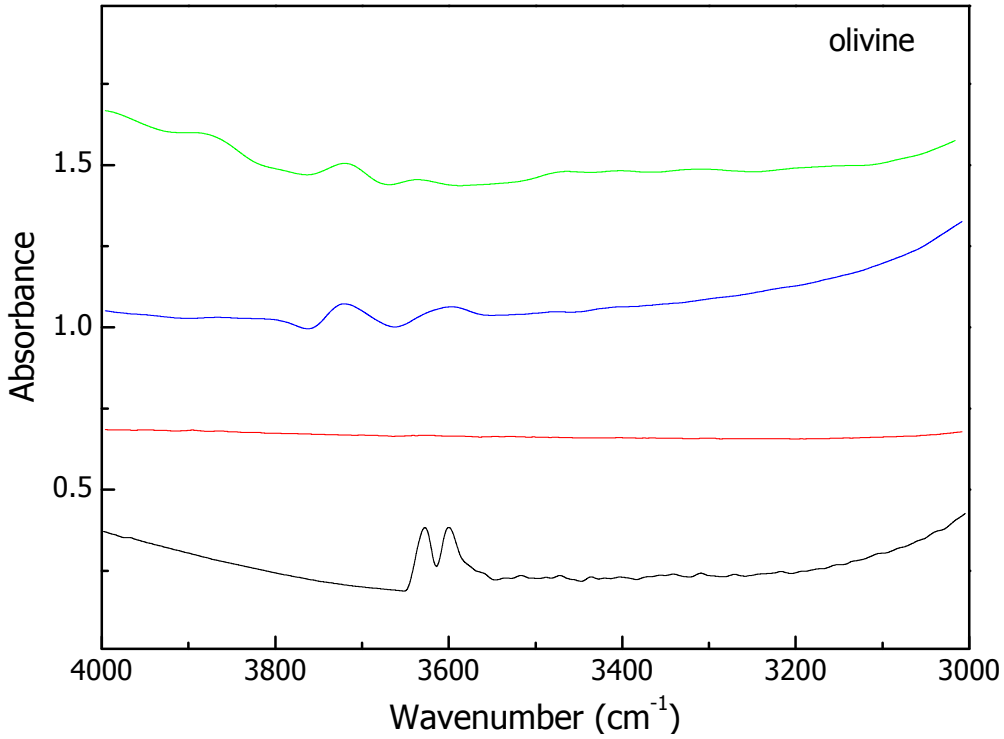

Fig. 5- 16 Representative IR spectra of olivine in the Hannuoba and Nushan peridotites

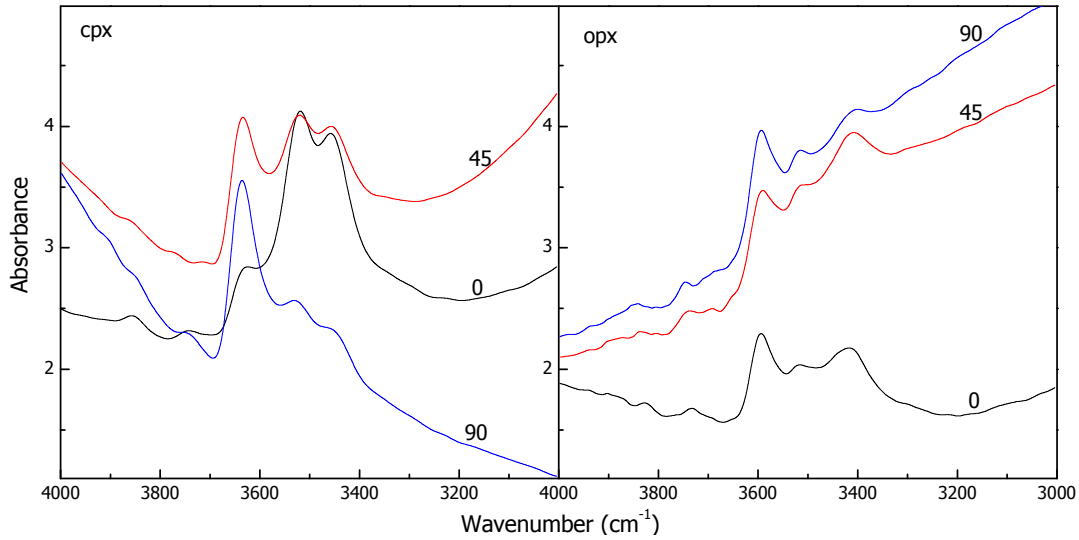

Fig. 5- 17 Polarized IR spectra of cpx and opx in the Hannuoba and Nushan peridotites

also be observed in mantle pyroxenes, indicating the presence of distinct hydrogen-related defects for the incorporation of H into the structure of cpx (or opx).

Profile analyses across many oriented grains show that hydrogen-induced IR absorption is usually homogeneous from the core to rim region for both cpx and opx within the two sets of peridotites (Figs. 5-18 and 5-19). This strongly suggests that, during the transport to the surface carried by the hosted basalts, the hydrogen information of pyroxenes in these samples were not significantly modified, similar to what has been observed in granulites.

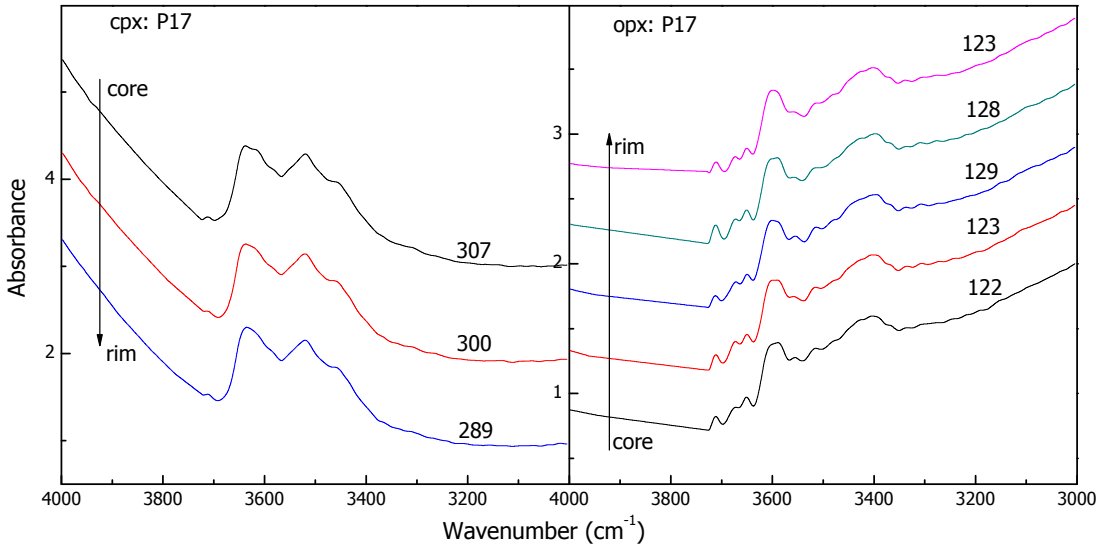

Fig. 5- 18 Profile analyses of H-absorption in Hannuoba peridotites

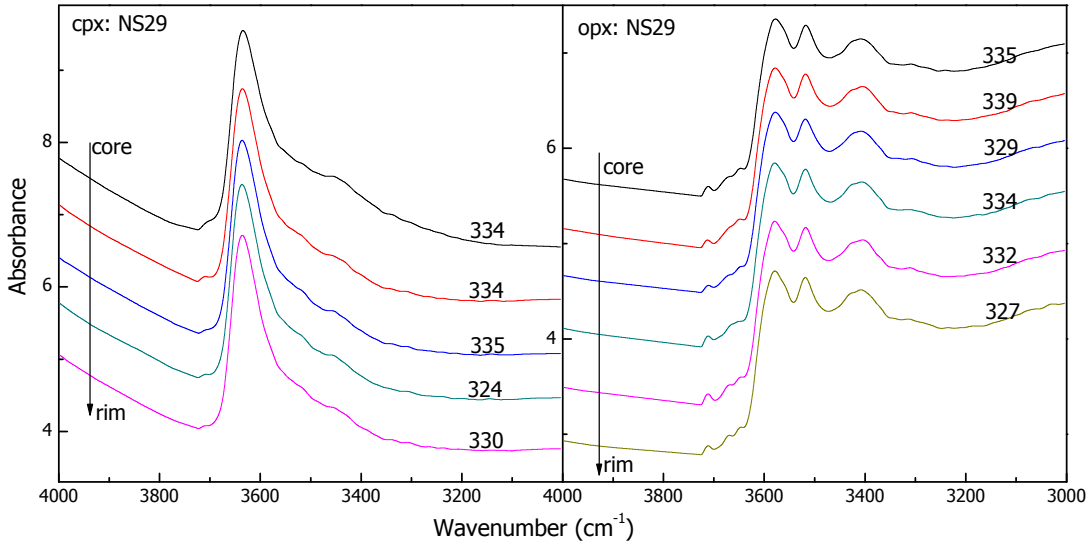

Fig. 5- 19 Profile analyses of H-absorption in Nushan peridotites

5.2.2.2 Water content

The measured water contents for cpx and opx were compiled in Table 5-10. OH content varies from 5 to 355 ppm for cpx and 5 to 140 ppm for opx in these peridotites, and the Nushan samples exhibit a much wider range in water concentrations than the Hannuoba ones. The large variations in these contents, far beyond the analytical uncertainty, strongly suggest heterogeneities between samples and localities.

Distinctively different from granulites, pyroxenes in the peridotites define a

Table 5- 10 H_2O (ppm wt.) content of minerals in mantle peridotites

	cpx	opx	ol	bulk		cpx	opx	ol	bulk*
Hannuoba xenoliths					*Nushan xenoliths*				
P1	85	25	10	20	NS01	190	105	20	55(260)
P2	90	40	10	25	NS03	95	55	10	30
P3	60	20	5	15	NS06	40	40	5	15
P4	50	20	5	10	NS07	115	80	10	40
P6	150	55	15	30	NS08	-	15	5	5(420)
P8	85	35	10	20	NS12	165	110	15	50
P11	70	35	5	15	NS13	15	20	5	10
P12	110	35	10	30	NS14	215	95	20	80
P13	100	45	10	35	NS16	240	115	25	60
P14	140	55	15	35	NS21	215	90	20	50(470)
P15	125	55	15	30	NS22	5	5	0	0(205)
P17	100	35	10	20	NS24	245	110	25	85
					NS25	355	140	35	75

	NS29	240	105	25	70(480)
	NS30	55	40	5	15(635)

Note: all the data were rounded to the nearest 5 ppm. The contents were determined by FTIR for cpx and opx, and were calculated by assuming equilibrium partitioning between pyroxenes and olivine and using the coefficient of ~ 0.1 between olivine and cpx (Hirth and Kohlstedt, 1996; Aubaud et al., 2004; Hauri et al., 2006). Densities used in the calculation are 3.28 g/cm^3 for cpx, 3.13 g/cm^3 for opx and 3.3 g/cm^3 for olivine.

*: data in the parentheses are the contents considering the water in amphibole (assuming 2% water concentration and density of 3.3 g/cm^3).

-: this mineral is free in the sample.

good correlation between their water contents (Fig. 5-20). The yielded coefficient is ~ 2.1, agreeing well with available reports on both natural and synthetic samples (e.g. Bell and Rossman, 1992b; Peslier et al., 2002; Koga et al., 2003; Aubaud et al., 2004; Bell et al., 2004; Grant et al., 2007a). The water content in olivine, calculated from equilibrium partitioning between olivine and pyroxenes using the partitioning coefficient, $D_{cpx/olivine} \approx 10$, in Hirth and Kohlstedt (1996), Aubaud et al. (2004) and Hauri et al. (2006) (see also Chapter 8), ranges from ~ 0 to 35 ppm and yields bulk content in the range of 10-85 ppm if considering the water only in the main constitutions (pyroxenes and olivine: Table 5-10).

Water content of opx in the two suites of samples correlates with their Al^{3+} content (Fig. 5-21), implying that the incorporation of hydrogen into mantle opx is related with coupled substitution of $H^+ + Al^{3+} = Si^{4+}$ (e.g. Rauch and Keppler, 2002; Stalder et al., 2005). The deviation of the amphibole-bearing peridotites from Nushan from the trend may be caused by the formation of the hydrous amphibole (Andrut et al., 2003; Peslier and Luhr, 2006)

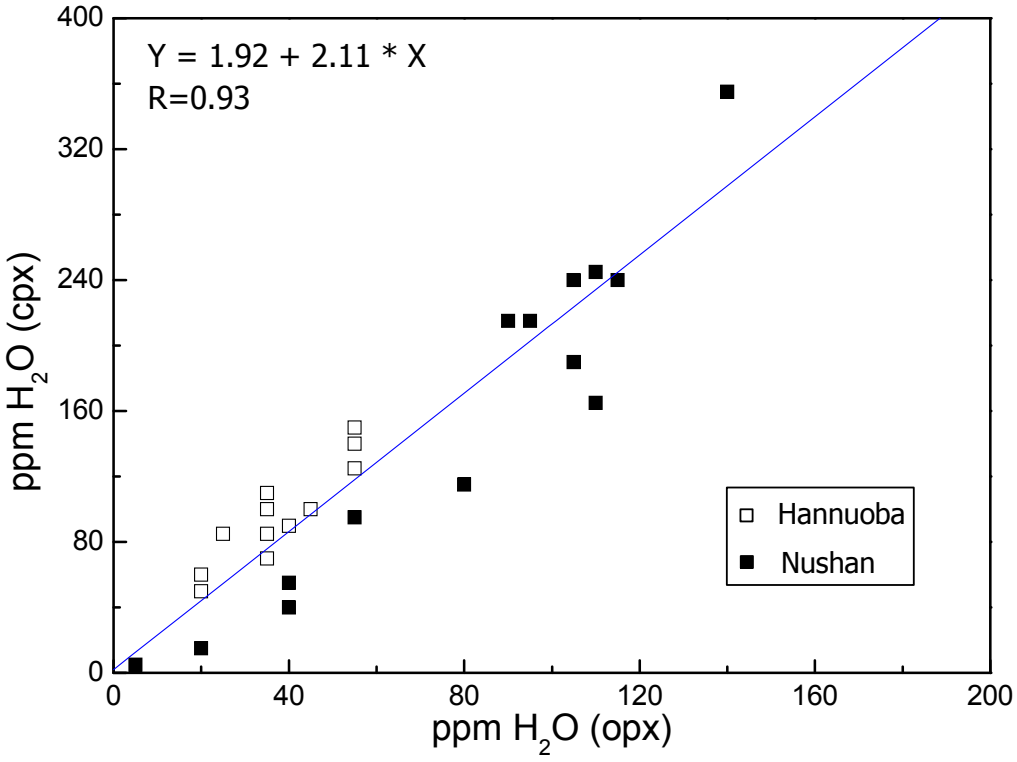

Fig. 5- 20 Water content of cpx and opx in the Hannuoba and Nushan peridotites

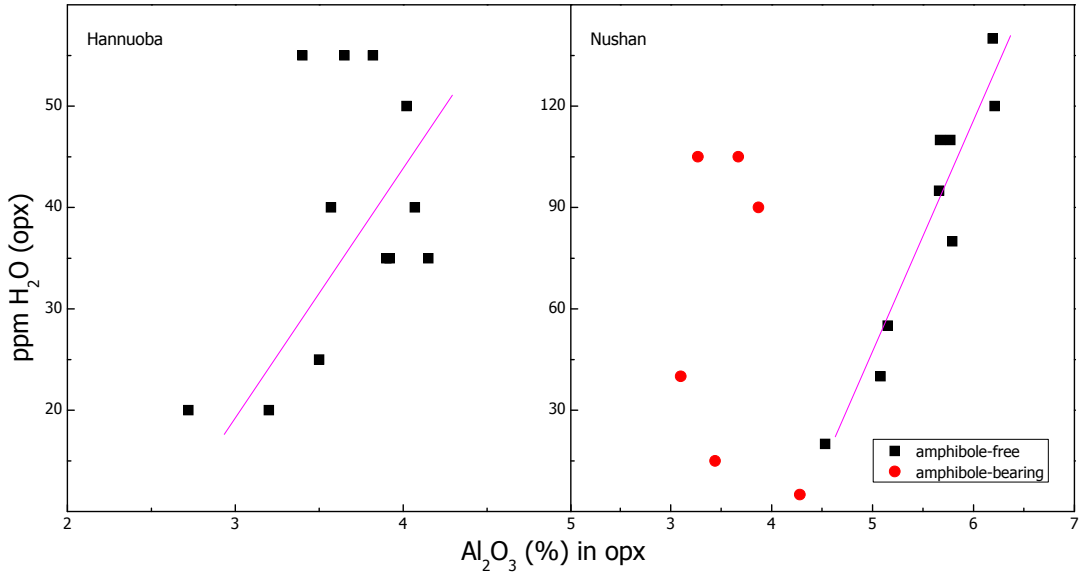

Fig. 5- 21 Correlation between H_2O (ppm) and Al_2O_3 (%) in peridotite opx

5.3 IRMS results

The amount of hydrogen for plag in 04NS9 and the 3 aliquots of feldspar megacryst extracted by hydrogen manometer and the δD values measured by IRMS are given in Table 5-11.

Table 5- 11 Hydrogen yields and δD values of feldspar samples

	aliquot	mass (mg)	H yield (mbar)	δD (SMOW)
feldspar	grain	1000.99	221.8	-69.3
	power	1146.28	257	-83.8
	power	472.81	80.6	-78.8
04NS9	power	511.48	106.4	-72.3

A good correlation (R^2=0.9941) is observed between the yielded hydrogen (mbar, determined by manometry) and the mass (mg) of feldspar samples (Fig. 5-22). This has at least the following two implications:

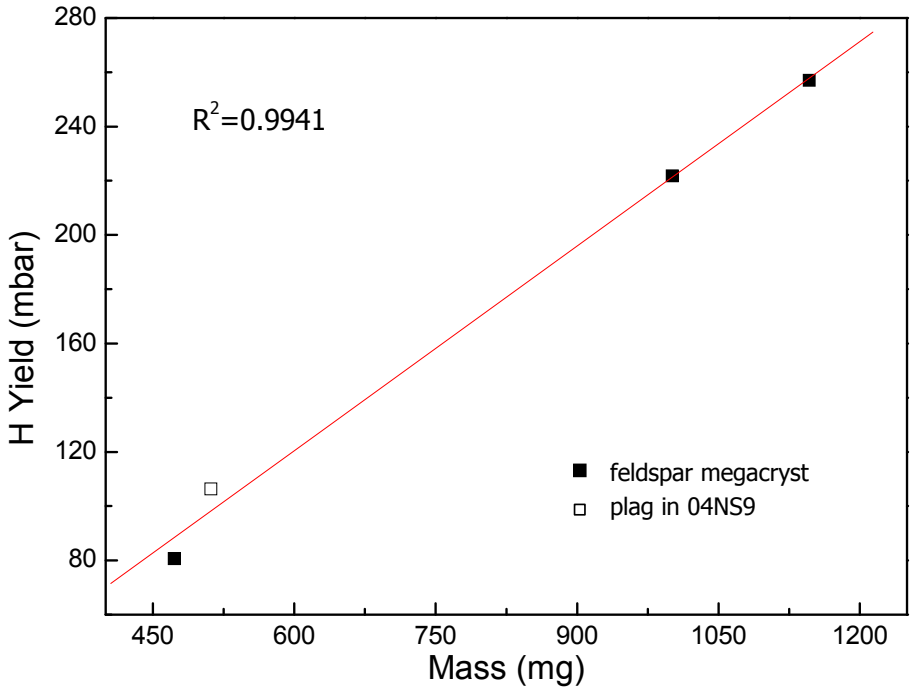

Fig. 5- 22 Yields of hydrogen as a function of aliquot mass of samples

(1) The H_2O concentration of plag in 04NS9 is similar to that in the feldspar megacryst. This has also been confirmed by FTIR measurements, which show that the water content is 365 ppm for the former (Table 5-7) and 410 ppm for the latter, falling within the analytical uncertainty (30%);

(2) There is no notable influence from adsorbed water on the sample surface. One possibility is that the adsorbed water was totally removed during the pre-treatment (heating) processes, because it is well known that the more one sample is ground, the more it will increase the surface to volume ratio and the more it will adsorb water on the surface; and thus the powered sample will

release more water than the non-powered at the same mass, this is, however, not observed.

The IRMS analyses show that the δD is -69.3‰, -83.8‰ and -78.8‰ for the three feldspar aliquots, and is -72.3‰ for the plag in 04NS9.

5.4 SIMS results

5.4.1 REE contents

In situ REE analyses show that they are generally inter- and intra-grain homogeneous for each mineral in each sample, and their average values are presented in Table 5-12. In terms of the total contents (ΣREE) for each mineral, they are usually higher in the Nushan and lower in the Hannuoba xenolith granulites, with the Hannuoba terrain granulites falling between them or close to the Nushan samples. Despite the variation of each mineral between different samples, the ΣREE generally follows a sequence of cpx >(grt ?) >plag >opx. This resembles the result from Pride and Muecke (1981), which yields the same sequence for granulite-facies minerals from Scourian Complex, NW Scotland.

Chondrite-normalized REE data exhibit regular and consistent distribution for individual minerals (Fig. 5-23). Cpx are characterized by no or very slight LREE/HREE fractionation except the two terrain samples, the latter show visible HREE enrichment and very low $(La/Yb)_N$ ratio; a significant concave-downward pattern can be observed for cpx in all the samples peaked in the LREE to Middle-REE region, which may be related with the preferential partition of REE into the M2-site of diopside (Reiitan et al., 1980); cpx in the granulites usually show no obvious Eu anomalies (Fig. 5-23, Table 5-12). Opx are characterized by the enrichment of HREE relative to LREE with very low $(La/Yb)_N$ ratios (Table 5-12), and they mostly exhibit very weak positive Eu anomalies (Fig. 5-23, Table 5-12). Plag display remarkable enrichment in LREE relative to HREE with specially high $(La/Yb)_N$ ratios; the most distinguishing feature of the plag REE patterns is the ubiquitous large positive Eu anomaly, reflected by their Eu/Eu^* ratios from 10.7

Table 5- 12 In situ REE contents (ppm) of cpx, opx, plag and grt in the granulite samples

	Sample	La	Ce	Pr	Nd	Sm	Eu	Gd	Dy	Er	Yb	Lu	∑REE	Eu/Eu*	$(La/Yb)_N$
cpx	04NS9	35.83	118.0	29.35	158.6	37.40	5.31	17.58	29.71	15.86	21.75	2.83	472.2	0.63	1.12
	04NS16	38.66	150.4	34.90	182.7	42.42	5.94	20.12	37.41	17.83	25.60	3.12	559.1	0.62	1.03
	MJ9801	11.51	41.58	9.97	49.22	13.36	2.39	9.59	21.56	12.98	16.91	1.78	190.8	0.64	0.46
	MJ9805	10.57	34.26	8.24	43.36	12.76	2.88	8.03	19.39	12.58	21.84	2.47	176.4	0.87	0.33
	DM9855	6.10	22.97	5.94	33.49	8.43	2.53	4.69	7.34	3.73	4.76	0.63	100.6	1.23	0.87
	DM9871	2.58	10.06	2.60	18.49	5.05	1.32	3.46	4.00	2.26	2.74	0.46	53.0	0.96	0.64
	WD9546	2.63	10.33	2.59	16.36	4.66	1.45	2.81	4.80	2.12	2.75	0.39	50.9	1.22	0.65
	WD9532	3.25	12.24	3.39	20.22	5.60	1.95	3.49	6.06	3.09	2.94	0.45	62.7	1.35	0.75
opx	04NS11	0.06	0.33	0.17	0.39	0.23	0.14	0.16	0.66	0.94	2.56	0.27	5.9	2.19	0.02
	04NS13	0.07	0.34	0.15	1.08	0.39	0.10	0.17	0.84	0.75	1.83	0.28	6.0	1.21	0.03
	04NS9	0.04	0.11	0.09	0.20	0.19	0.09	0.19	0.87	1.05	3.44	0.39	6.7	1.50	0.01
	04NS16	0.04	0.29	0.08	0.67	0.54	0.15	0.22	0.86	0.90	2.20	0.43	6.4	1.31	0.01
	MJ9801	0.04	0.08	0.09	0.26	0.14	0.08	0.17	0.65	0.70	1.45	0.16	3.8	1.63	0.02
	MJ9805	0.06	0.08	0.10	0.16	0.12	0.05	0.29	0.98	1.39	1.29	0.13	4.6	0.82	0.03
	DM9855	0.02	0.02	0.03	0.09	0.09	0.08	0.14	0.18	0.20	0.51	0.07	1.4	2.25	0.03
	DM9871	0.05	0.05	0.04	0.09	0.06	0.04	0.13	0.11	0.17	0.31	0.07	1.1	1.31	0.11
	WD9546	0.03	0.03	0.01	0.10	0.07	0.08	0.08	0.14	0.14	0.32	0.08	1.1	3.37	0.05
	WD9532	0.01	0.02	0.02	0.08	0.10	0.09	0.08	0.14	0.16	0.38	0.07	1.2	2.98	0.02
plag	04NS11	26.35	23.63	2.13	5.47	0.35	1.92	0.53	0.27	0.51	0.70	0.19	62.1	13.54	25.65
	04NS13	24.49	21.92	1.94	4.89	0.37	2.59	0.21	0.05	0.13	0.41	0.10	57.1	28.13	40.88
	04NS9	25.66	22.92	2.07	5.23	0.54	3.18	0.46	0.22	0.19	0.68	0.19	61.3	19.38	25.82
	04NS16	26.17	21.47	1.97	4.96	0.47	2.36	0.15	0.23	0.32	0.49	0.05	58.6	27.00	36.07
	MJ9801	9.27	10.59	0.97	2.51	0.21	1.13	0.12	0.10	0.08	0.12	0.01	25.1	21.48	54.27
	MJ9805	8.08	7.71	0.67	1.76	0.17	1.38	0.07	0.07	0.10	0.13	0.02	20.1	38.39	43.37
	DM9855	5.82	6.66	0.69	2.04	0.14	0.53	0.09	0.11	0.11	0.21	0.06	16.5	14.40	18.61
	DM9871	2.47	2.94	0.37	1.38	0.14	0.41	0.10	0.07	0.16	0.38	0.06	8.5	10.73	4.42
	WD9546	2.31	3.04	0.39	1.32	0.19	0.56	0.04	0.10	0.10	0.18	0.03	8.3	20.62	8.65
	WD9532	2.50	2.89	0.34	1.04	0.07	0.35	0.02	0.07	0.09	0.16	0.02	7.5	26.37	10.67
grt	MJ9801	0.04	0.16	0.14	2.44	4.94	1.56	13.08	78.19	69.44	59.78	14.61	244.4	0.59	0.0004

Note :

Eu/Eu* and $(La/Yb)_N$ are the Chondrite-normalized ratios.

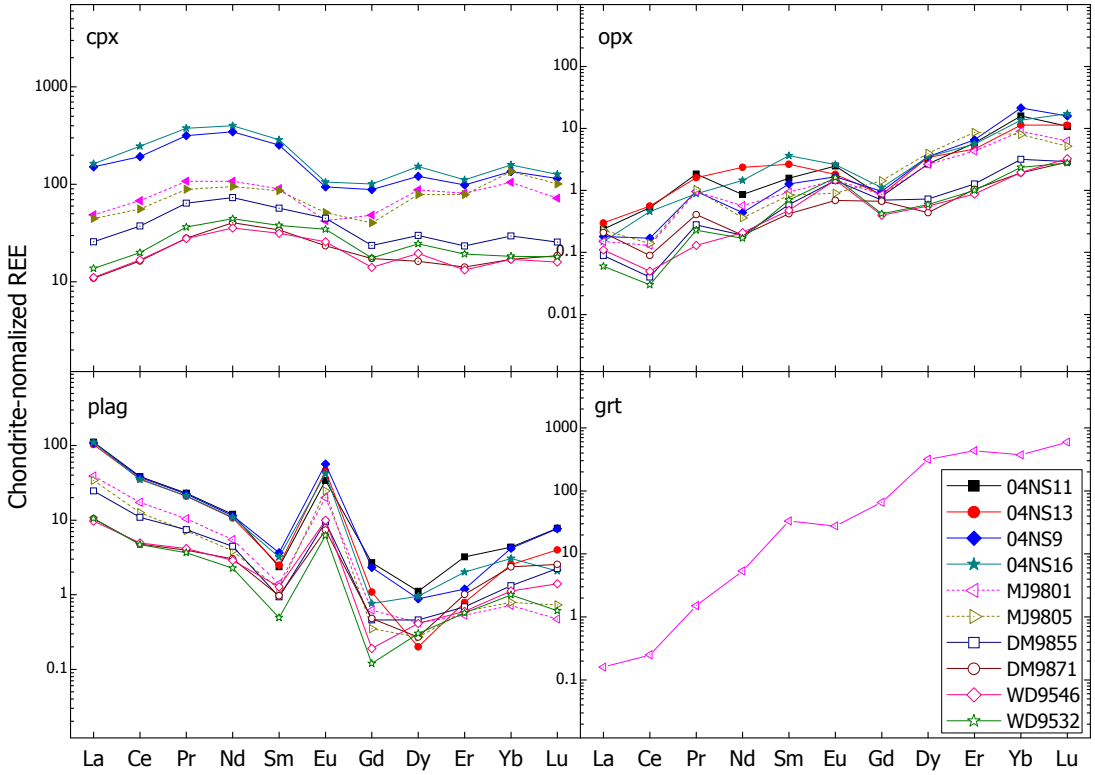

Fig. 5- 23 Chondrite-normalized REE patterns for individual minerals in granulite samples

to 38.4, and it is the only major mineral to have a positive Eu anomaly in these granulites (Fig. 5-23, Table 5-12). Grt is present only in MJ9801, and it exhibits nearly linear enrichment of HREE relative to LREE with extremely light $(La/Yb)_N$ ratio (Table 5-12). The REE patterns of these granulite minerals, except minor differences in opx, are very similar to those observed in the granulites from the Scourian Complex, NW Scotland (Pride and Muecke, 1981).

5.4.2 Hydrogen isotopic compositions

The in situ hydrogen isotopic compositions of cpx and plag in these lower crustal granulites are provided in Table 5-13 (details are available in Table A1 within the appendix).

Table 5- 13 In situ H-isotopic compositions of cpx and plag in the granulite samples

	Mineral	Point*	IsH	D/H	s.d.	δD	Mean
Nushan xenolith granulites							
04NS11	plag	1-c	1.9E+05	99.20	1.05	-32	-55
		1-m	1.8E+05	93.91	1.03	-66	
		1-r	1.7E+05	94.42	1.17	-63	
		2-c	1.8E+05	96.33	1.17	-50	
		2-m	1.7E+05	93.93	1.17	-66	
		2-r	1.7E+05	98.38	0.93	-37	

		3-c	1.4E+05	96.73	0.81	-48	
		3-m	1.5E+05	94.19	0.78	-64	
		3-r	1.4E+05	94.19	1.18	-64	
04NS13	plag	1-c	6.8E+04	91.08	1.52	-84	-69
		1-m	7.8E+04	91.96	1.65	-79	
		1-r	7.4E+04	86.33	2.03	-115	
		2-c	4.1E+04	93.50	2.58	-69	
		2-m	4.3E+04	92.18	1.85	-77	
		2-r	5.0E+04	98.22	2.20	-38	
		3-c	4.9E+04	100.25	2.12	-25	
		3-m	6.0E+04	96.02	1.37	-52	
		3-r	5.8E+04	92.01	1.29	-78	
04NS9	cpx	1-c	3.0E+05	89.57	0.70	-58	-42
		1-m	2.8E+05	96.60	0.76	-13	
		1-r	2.7E+05	95.93	0.58	-17	
		2-c	2.4E+05	88.45	0.94	-65	
		3-c	2.7E+05	89.68	0.95	-57	
	plag	1-c	1.4E+05	95.38	1.10	-57	-72
		1-m	1.2E+05	91.89	1.33	-79	
		1-r	1.2E+05	91.41	1.29	-82	
		2-c	1.1E+05	93.02	1.44	-72	
04NS16	cpx	1-c	1.4E+05	84.60	1.30	-89	-96
		1-r	1.4E+05	82.32	1.19	-104	
	plag	1-c	6.5E+04	93.67	2.62	-68	-57
		1-r	6.6E+04	97.01	1.99	-46	
Hannuoba terrain granulites							
MJ9801	cpx	1-c	9.1E+04	90.48	1.70	-80	-44
		1-m	9.0E+04	91.55	1.35	-73	
		1-r	9.5E+04	92.10	1.19	-70	
		2-c	7.8E+04	94.55	1.48	-54	
		2-m1	5.6E+04	103.63	2.12	4	
		2-m2	7.8E+04	98.77	1.36	-27	
		2-r	6.8E+04	101.29	1.63	-11	
	plag	1-c	1.6E+04	102.09	3.39	-13	-43
		1-m	1.6E+04	94.24	2.73	-64	
		1-r	1.7E+04	95.92	2.40	-53	
MJ9805	cpx	1-c	5.7E+05	89.33	0.56	-59	-55
		1-m	5.4E+05	89.69	0.61	-57	
		1-r	5.3E+05	90.07	0.54	-54	
		2-c	3.2E+05	89.96	0.93	-55	
		2-r	2.6E+05	90.94	1.13	-49	
	plag	1-c	6.6E+05	91.83	0.39	-79	-61
		1-r	5.5E+05	93.68	0.37	-67	
		2-c	3.9E+05	96.62	0.82	-49	
		2-m	3.9E+05	95.03	0.60	-59	
		2-r	3.8E+05	96.04	0.53	-52	
Hannuoba xenolith granulites							
DM9855	cpx	1-c	4.1E+05	91.84	0.69	-45	-55
		1-m	4.1E+05	93.48	0.66	-34	
		1-r	4.0E+05	94.58	0.63	-27	
		2-c	6.2E+05	87.90	0.55	-70	
		2-m	6.1E+05	87.13	0.58	-75	
		2-r	6.1E+05	86.96	0.52	-76	
	plag	1-c	3.3E+05	98.02	0.66	-40	-53
		1-m	3.2E+05	98.19	0.51	-39	
		1-r	3.0E+05	97.50	0.82	-43	
		2-c	2.8E+05	94.48	0.92	-62	
		2-m	2.5E+05	93.90	0.79	-66	
		2-r	2.3E+05	93.24	0.73	-70	
DM9871	cpx	1-c	7.8E+04	93.91	2.04	-32	-42
		1-m	7.1E+04	95.25	1.41	-23	
		1-r	6.8E+04	96.28	1.09	-16	
		2-c	3.9E+04	89.45	2.50	-60	
		2-m	4.1E+04	90.99	2.01	-50	
		2-r	3.9E+04	87.97	2.38	-70	
	plag	1-c	2.3E+04	89.21	1.56	-96	-86
		1-m	2.1E+04	88.94	3.35	-98	
		1-r	2.1E+04	94.44	3.39	-63	
WD9532	cpx	1-c	3.8E+05	95.54	0.72	-20	-17

		1-m	3.6E+05	98.07	0.74	-4	
		1-r	3.5E+05	94.91	0.59	-24	
		2-c	2.6E+05	96.55	0.95	-14	
		2-r	2.6E+05	95.17	1.03	-23	
	plag	1-c	1.6E+05	95.63	1.14	-55	-49
		1-m	1.6E+05	98.07	0.83	-39	
		1-r	1.6E+05	95.63	0.84	-55	
		2-c	1.3E+05	96.58	0.95	-49	
		2-r	1.4E+05	96.80	1.11	-47	
WD9546	cpx	1-c	5.4E+04	90.21	1.63	-56	-10
		2-r	6.9E+04	99.61	1.04	5	
		2-m	6.0E+04	100.24	1.97	9	
		2-c	5.4E+04	99.57	2.65	4	
	plag	1-c	1.6E+04	96.08	2.42	-52	-55
		1-m	1.4E+04	103.59	3.49	-4	
		1-r	1.4E+04	91.97	3.13	-78	
		2-r	1.3E+04	90.58	3.39	-87	

*: numbers denote different grains; c, r and m are core, rim and in the middle between them, respectively; IsH, the counts on hydrogen per second; D/H and δD are the measured and instrumental calibrated H-isotopic compositions on each analytical point, respectively; the last column corresponds to the average value for the studied phases in each sample.

In strong contrast to their inter- and intra-grain identical compositions of both major elements and REE for each mineral in each sample, the hydrogen isotope compositions of these minerals show significant differences. They can be nearly homogeneous for some samples, e.g. cpx in MJ9805 and plag in WD9532, highly variable between some grains in the same sample, e.g. plag in 04NS13 and cpx in DM9871, and even in the same grain for certain mineral, e.g. varying within < 200 μm scale from -54 to 4‰ on cpx grain 2 in MJ9801 and from -78 to -4‰ on plag grain 1 in WD9546. Variations for the latter two are well beyond the analytical uncertainty (<16‰), indicating variable scales of heterogeneities. Similar or larger fractionations on such scales have only previously been reported for mantle amphibole and K-richterite from xenoliths in alkali basalts/kimberlites and mantle-derived melts emplaced in the crust (Deloule et al., 1991a; Graham et al., 1994; Xia et al., 2002; Stone et al., 2005). The IsH (a semi-quantitative index of H_2O content at the analyzed point (Deloule et al., 1991a) from the core to rim profile mostly show limited variations over the grains, supporting the FTIR results that no significant zones in OH/H_2O in the studied mineral grains.

The D/H ratios are variable for each mineral. Overall, they range from -104 to 9‰ for cpx and from -115 to -4‰ for plag, and most of them fall outside

the zone of accepted normal mantle values (-90 to -60‰: e.g. Sheppard and Epstein, 1970; Kyser and O'Neil, 1984; Feldstein et al., 1996). Under most cases, minerals in these samples are characterized by relatively higher δD values (e.g. -80 to -10‰: Figs. 5-24 and 5-25). Although similarities in δD values for each mineral can be observed between the 3 types of granulites, the Nushan xenolith and Hannuoba terrain granulites are more analogous in terms of their mineral D/H ratios, which are moderately different from those in the Hannuoba xenolith samples (Table 5-13, Figs. 5-24 and 5-25).

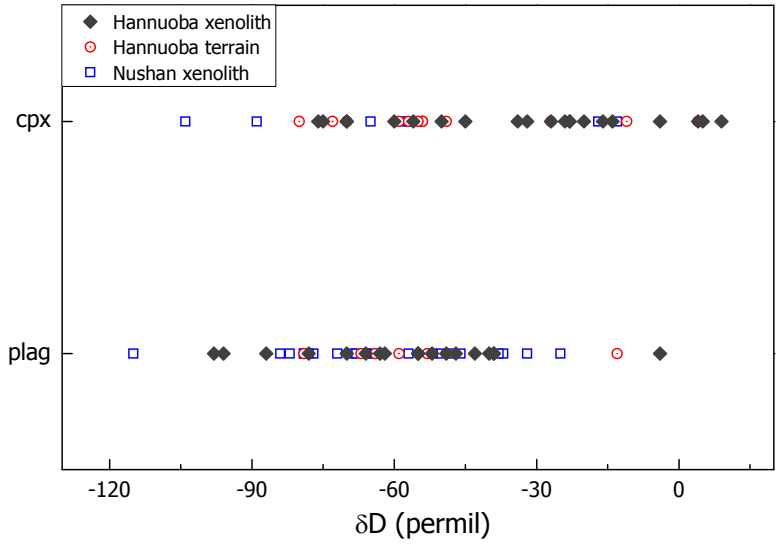

Fig. 5- 24 Variations in δD of cpx and plag in the granulites.

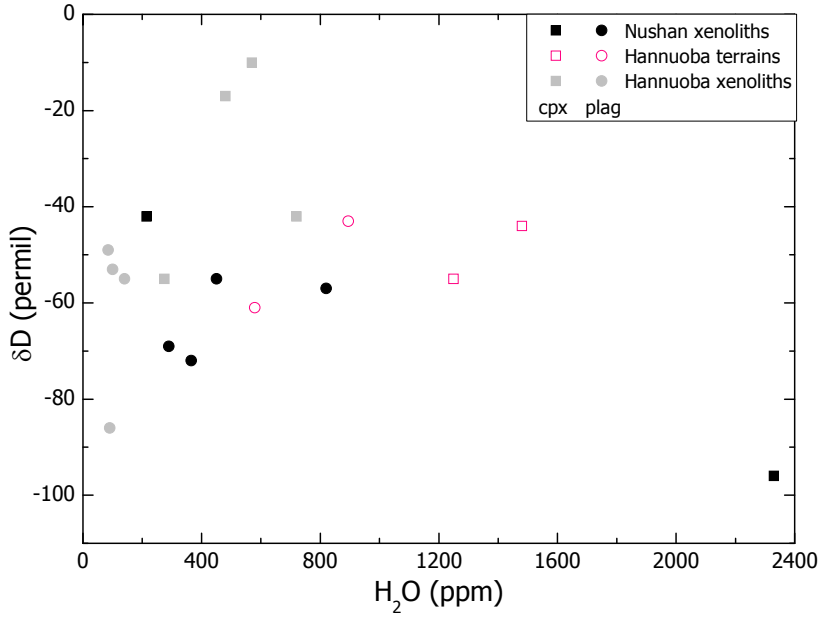

Fig. 5- 25 Relationship between δD and H_2O for minerals in the granulites

5.4.3 Oxygen isotopic compositions

Compositions of the standards, as well as the samples, are shown in Fig. 5-26 for an illustration. In summary, the cpx standards exhibit visible variation in their chemistry but close to the studied cpx, and the opx standard resembles more opx in the Hannuoba xenolith samples relative to those in the Hannuoba terrain and Nushan xenolith granulites.

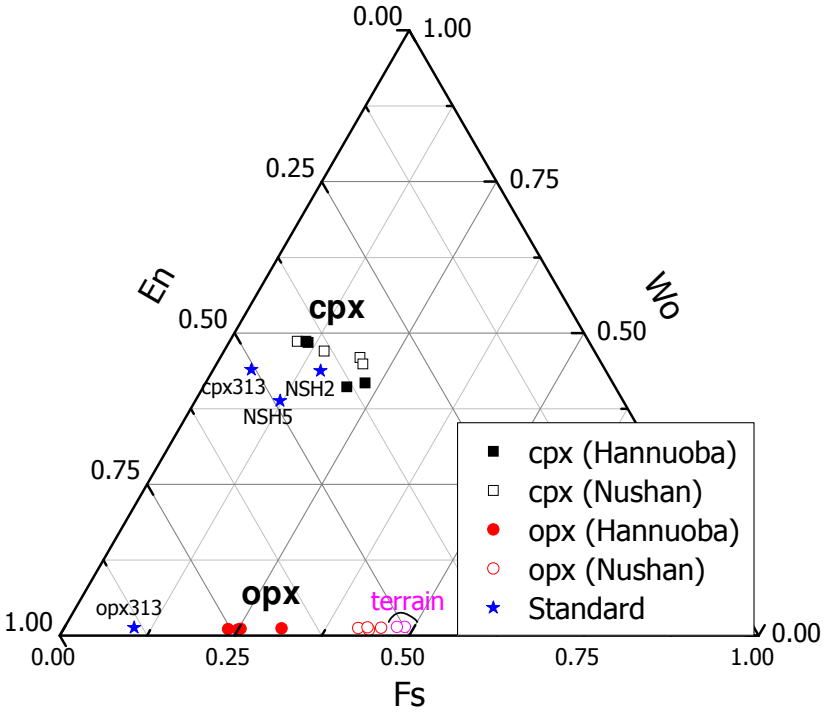

Fig. 5- 26 Comparison in the compositions of standards and samples

The determined $\delta^{18}O$ values of the cpx and opx standards are presented in Table 5-14. The results show that, in spite of variation in their chemical compositions, the instrumental fractionations ($\Delta_{ins} = \delta^{18}O_{sims} - \delta^{18}O_{true}$) are almost the same for the 3 cpx standards, implying no significant matrix effects on the $\delta^{18}O$ analyses for them. This rule has been applied to the measurements of cpx in the samples for the similarities in their mineral chemistry. Since the composition of the opx standard is more close to those in the Hannuoba xenolith granulites and there is at present no suitable standards covering the whole variation of the studied opx (e.g. to see if matrix effects are present), the $\delta^{18}O$ measurements were focused on opx only in the Hannuoba xenolith samples and in one Nushan sample, and the opx standard was used for the calibration.

Table 5- 14 ^{18}O determination of the cpx and opx standards by SIMS

	$\delta^{18}O_{true}$	$\delta^{18}O_{sims}$	n	$\delta^{18}O_{sims}$	n	$\delta^{18}O_{sims}$	n
cpxNSH2	5.46	5.91 (0.13)	6	5.85 (0.25)	5	6.14 (0.48)	7
cpxNSH5	5.88	6.37 (0.26)	6	5.79 (0.34)	5		
cpx-313	5.5	5.84 (0.13)	5				
opx-313	5.8	3.7 (0.23)	4	4.14 (0.16)	5	3.72 (0.20)	4

Note: $\delta^{18}O$ values (‰) are relative to V-SMOW; n, numbers of independent spot analyses on a given standard. $\delta^{18}O_{sims}$ are measured by ion microprobe; numbers in the parentheses are the standard deviation of n duplicate analyses.

Table 5- 15 In situ O-isotopic compositions of cpx and opx in the granulite samples

	$\delta^{18}O$	2σ	$\delta^{18}O$-corr	mean	spot		$\delta^{18}O$	2σ	$\delta^{18}O$-corr	mean	spot
04NS9						cpx3_1	7.95	0.09	7.52		c
cpx1_1	7.39	0.08	6.45		c	cpx3_2	8.19	0.10	7.76		
cpx1_2	7.56	0.09	6.62			cpx3_3	7.97	0.11	7.54		
cpx1_3	8.50	0.12	7.56			cpx3_4	8.19	0.11	7.76		
cpx1_4	8.53	0.12	7.59		r	cpx3_5	7.83	0.11	7.40		r
										8.76	
cpx2_1	6.14	0.11	5.20		c	opx1_1	6.17	0.13	8.72		r
cpx2_2	6.63	0.09	5.69			opx1_2	5.95	0.13	8.50		
cpx2_3	6.31	0.11	5.37			opx1_3	5.84	0.11	8.39		
cpx2_4	6.04	0.09	5.10		r	opx1_4	6.04	0.12	8.59		
						opx1_5	6.24	0.12	8.79		
cpx3_1	8.50	0.09	7.56		c	opx1_6	6.26	0.12	8.81		
cpx3_2	8.03	0.11	7.09			opx1_7	6.19	0.10	8.74		
cpx3_3	8.37	0.09	7.43			opx1_8	6.23	0.12	8.78		c
cpx3_4	8.32	0.08	7.38		r	opx1_9	6.84	0.14	9.39		
						opx1_10	6.63	0.13	9.18		
cpx4_1	8.50	0.11	7.56		c	opx1_11	6.56	0.13	9.11		
cpx4_2	8.25	0.10	7.31		r	opx1_12	5.67	0.12	8.22		
				6.71		opx1_13	6.71	0.13	9.26		
opx1_1	3.72	0.11	6.27		c	opx1_14	6.60	0.09	9.15		
opx1_2	4.56	0.11	7.11			opx1_15	5.58	0.10	8.13		
opx1_3	4.18	0.12	6.73			opx1_16	6.55	0.12	9.10		
opx1_4	4.66	0.12	7.21			opx1_17	6.49	0.08	9.04		
opx1_5	10.18	0.07	6.06			opx1_18	6.32	0.08	8.87		r
opx1_6	10.09	0.07	5.97							8.82	
opx1_7	9.9	0.06	5.78		r	**WD9546**					
				6.45		cpx1_1	9.30	0.12	8.36		c
04NS16						cpx1_2	10.12	0.12	9.18		
cpx1_1	10.10	0.08	9.16		c	cpx1_3	10.24	0.12	9.30		
cpx1_2	9.67	0.08	8.73		r	cpx1_4	10.26	0.13	9.32		
cpx1_3	9.87	0.09	8.93		r	cpx1_5	9.60	0.11	8.66		r
cpx1_4	9.64	0.09	8.70		r					8.96	
						opx1_1	5.98	0.08	8.53		c
cpx2_1	9.63	0.11	8.69		c	opx1_2	7.00	0.10	9.55		
cpx2_2	10.14	0.09	9.20			opx1_3	7.15	0.12	9.70		

cpx2_3	9.73	0.10	8.79		r
				8.88	
MJ9801					
cpx1_1	7.6	0.1	6.66		r
cpx1_2	8.09	0.08	7.15		
cpx1_3	7.42	0.08	6.48		c
cpx1_4	8.02	0.06	7.08		
cpx1_5	7.8	0.09	6.86		r
cpx2_1	8.02	0.08	7.08		c
cpx2_2	8.03	0.08	7.09		
cpx2_3	8.33	0.09	7.39		
cpx2_4	8.37	0.08	7.43		r
cpx3_1	11.49	0.08	5.09		c
cpx3_2	12.01	0.07	5.61		
cpx3_3	12.46	0.09	6.06		r
				6.66	
MJ9805					
cpx1_1	11.32	0.09	4.92		c
cpx1_2	10.86	0.06	4.46		
cpx1_3	10.91	0.08	4.51		r
cpx2_1	11.24	0.09	4.84		c
cpx2_2	11.51	0.09	5.11		r
cpx3_1	7.9	0.09	6.96		c
cpx3_2	8.28	0.08	7.34		
cpx3_3	8.55	0.08	7.61		
cpx3_4	8.37	0.09	7.43		
cpx3_5	8.81	0.12	7.87		r
				6.10	
WD9532					
cpx1_1	8.67	0.08	8.24		c
cpx1_2	8.84	0.10	8.41		
cpx1_3	8.88	0.08	8.45		
cpx1_4	9.49	0.15	9.06		
cpx1_5	9.32	0.14	8.89		r
cpx2_1	9.83	0.11	9.40		c
cpx2_2	10.17	0.07	9.74		
cpx2_3	10.16	0.12	9.73		
cpx2_4	10.64	0.12	10.21		
cpx2_5	10.52	0.09	10.09		
cpx2_6	10.39	0.12	9.96		r

opx1_4	7.02	0.11	9.57		
opx1_5	6.73	0.1	9.28		r
				9.33	
DM9855					
cpx1_1	8.23	0.06	7.80		c
cpx1_2	8.33	0.08	7.90		
cpx1_3	8.02	0.11	7.59		
cpx1_4	8.59	0.20	8.16		
cpx1_5	7.94	0.15	7.51		
cpx1_6	8.51	0.12	8.08		
cpx1_7	8.98	0.09	8.55		r
cpx2_1	9.35	0.08	(7.41)		c
cpx2_2	9.52	0.08	8.58		
cpx2_3	9.79	0.06	8.85		
cpx2_4	10.03	0.08	9.09		
cpx2_5	11.22	0.08	(11.28)		r
				8.21	
opx1_1	6.38	0.09	8.93		c
opx1_2	6.11	0.08	8.66		
opx1_3	6.22	0.06	(7.77)		
opx1_4	7.20	0.11	9.75		
opx1_5	7.48	0.09	(11.03)		
opx1_6	7.41	0.09	9.96		r
				9.33	
DM9871					
cpx1_1	13.42	0.14	12.48		c
cpx1_2	12.49	0.10	11.55		
cpx1_3	12.43	0.13	11.49		
cpx1_4	12.80	0.14	11.86		
cpx1_5	12.16	0.10	11.22		r
cpx2_1	13.35	0.11	12.41		c
cpx2_2	12.99	0.11	12.05		
cpx2_3	12.84	0.14	11.90		r
				11.87	
opx1_1	9.05	0.14	11.60		r
opx1_2	9.08	0.13	11.63		
opx1_3	9.44	0.07	11.99		
opx1_4	9.15	0.11	11.70		
opx1_5	8.76	0.10	11.31		c
opx2_1	7.82	0.09	10.37		r
opx2_2	7.72	0.08	10.27		c
				11.27	

Note: the oxygen isotopic data are reported in the unit of ‰.

$\delta^{18}O$ is the SIMS measured oxygen isotopic data, and $\delta^{18}O$-corr is the calibrated data for matrix effects; data in the mean column are the average for each mineral within each sample; c and r show the position of core and rim during the profile analyses.

The in situ oxygen isotopic compositions of cpx and opx in the lower crustal

granulites are summarized in Table 5-15 (details are available in Table A2 within the appendix). It is demonstrated that these $\delta^{18}O$ values are highly variable, in the range of ~ 4.5 to 12.5‰, agreeing well with previous reports upon lower crustal granulites (Kempton and Harmon, 1992), indicating large scale heterogeneities. Pyroxenes in the Hannuoba xenolith granulites are characterized by markedly higher $\delta^{18}O$ relative to the normal mantle of 5.7±0.5‰ (Mattey et al., 1994; Harmon and Hoefs, 1995; Eiler, 2001), while those in the Hannuoba terrain and Nushan xenolith granulites generally have $\delta^{18}O$ similar to or slightly higher than the normal mantle. Profile measurements reveal that nearly all the mineral grains are uniform with their $^{18}O/^{16}O$ ratios from core to rim areas. The only exceptions were observed on one cpx and opx grain in sample DM9855, which yield large variations up to about 3‰; the extreme values of 7.41 and 11.28‰ in the cpx grain and 7.77 and 11.03‰ in the opx grain are in strong contrast with other data obtained on the same grains and on the other grains in the same and other samples (Table 5-15); a careful re-check found that this sample suffered most seriously from a charging problem during the SIMS analyses among all the samples, and that these 4 analytical points with exceptional $\delta^{18}O$ data were mostly situated on the charged regions; therefore, these four data appear to be erroneous and they were excluded from the calculation of the average $\delta^{18}O$ values of cpx and opx in this sample. Pyroxenes in the Nushan xenolith and Hannuoba terrain granulites are similar in their oxygen isotopic compositions, which are relatively lower than those observed in the Hannuoba xenolith granulites.

5.4.4 Lithium contents and isotopic compositions

The in situ lithium contents and isotopic compositions of cpx and opx in the lower crustal granulite samples are given in Table 5-16 (details are available in Tables A3 and A4 within the appendix); the average lithium concentrations and isotopic compositions for all the samples from these multi-point and multi-grain analyses are also compiled in Table 5-17 for a better illustration.

Table 5- 16 In situ Li-contents and isotopic data of minerals in the granulite samples

	$^{7}Li/^{30}Si$	2σ	Li-corr	mean	spot
04NS11					
opx1_1	1.58	0.04	2.37		r
opx1_2	1.58	0.04	2.37		
opx1_3	1.59	0.04	2.39		c
opx1_4	1.86	0.05	2.79		
opx1_5	2.31	0.05	3.47		
opx1_6	2.2	0.06	3.30		r
opx2_1	4.2	0.11	6.31		c
opx2_2	4.3	0.1	6.46	opx	c
				3.7	
plag1_1	0.72	0.03	1.24		r
plag1_2	0.75	0.02	1.29		c
plag1_3	0.8	0.03	1.38		
plag1_4	0.71	0.02	1.22	plag	r
				1.3	
04NS13					
opx1_1	2.9	0.08	4.24		r
opx1_2	3.09	0.06	4.52		
opx1_3	2.92	0.05	4.27		c
opx1_4	3.33	0.05	4.87		
opx1_5	3.37	0.04	4.92		r
opx2_1	2.48	0.03	3.62		r
opx2_2	2.3	0.06	3.36		
opx2_3	2.47	0.04	3.61	opx	c
				4.2	
plag1_1	0.68	0.03	1.18		c
plag1_2	1.21	0.04	2.11		r
plag2_1	1.09	0.03	1.90		c
plag3_1	0.52	0.04	0.91		c
plag3_2	0.58	0.03	1.01		
plag3_3	0.73	0.03	1.27		
plag3_4	0.81	0.03	1.41	plag	r
				1.4	
04NS9					
cpx1_1	5.68	0.05	9.29		c
cpx1_2	6.68	0.05	10.92		
cpx1_3	6.32	0.07	10.33		
cpx1_4	5.04	0.09	8.24		
cpx1_5	7.65	0.05	12.51		r
cpx2_1	4.32	0.01	7.06		r
cpx2_2	4.93	0.17	8.06	cpx	c
				9.5	
opx1_1	2.53	0.02	4.07		c
opx1_2	2.39	0.04	3.84		
opx1_3	2.15	0.02	3.46		
opx1_4	2.44	0.02	3.92	opx	r
				3.8	
plag1_1	1.66	0.02	3.11		r
plag1_2	1.46	0.02	2.74		
plag1_3	1.6	0.01	3.00		c
plag2_1	1.42	0.01	2.66		r
plag2_2	1.98	0.02	3.71		c
plag2_3	1.65	0.02	3.09	plag	
				3.1	
04NS16					
cpx1_1	7.79	0.06	12.58		c
cpx1_2	8.86	0.24	14.30		r

	$\delta^{7}Li$	2σ	$\delta^{7}Li$-corr	mean	spot
04NS11					
opx1_1	30.14	0.89	4.9		c
opx1_2	31.00	0.81	5.8		r
opx2_1	22.34	0.86	-2.9		c
opx2_2	24.52	0.95	-0.7		r
opx2-1 #	23.83	0.88	-0.6		r
opx2-2 #	10.94	1.13	-13.5		
opx2-3 #	4.19	1.69	-20.2		
opx2-4 #	6.20	2.30	-18.2		
opx2-5 #	10.73	1.56	-13.7		
opx2-6 #	16.92	0.88	-7.5		c
opx2-7 #	25.76	1.22	1.3		
opx2-8 #	33.85	1.04	9.4		
opx2-9 #	35.08	1.63	10.6		r
opx3-1	25.25	1.04	0.8		r
opx3-2	10.25	0.89	-14.2		
opx3-3	34.25	0.62	9.8		c
opx3-4	21.45	0.81	-3.0		r
opx4-1	32.21	1.10	7.8		r
opx4-2	28.16	1.02	3.7		
opx4-3	14.39	1.10	-10.0	opx	c
				-2.5	
04NS13					
opx1_1	27.49	0.70	2.3		c
opx1_2	25.10	0.69	-0.1		
opx1_3	25.35	0.61	0.2		
opx1_4	29.09	0.78	3.9		
opx1_5	21.09	0.74	-4.1		
opx1_6	20.96	0.75	-4.2		
opx1_7	25.78	0.64	0.6		
opx1_8	24.96	0.62	-0.2		r
opx2_1	12.53	0.47	-12.7		c
opx2_2	12.88	0.57	-12.3	opx	r
				-2.7	
04NS9					
cpx1_1	30.71	1.22	5.5		c
cpx1_2	27.75	0.92	2.6		
cpx1_3	28.31	1.08	3.1		
cpx1_4	30.84	1.21	5.6		
cpx1_5	26.48	1.80	1.3	cpx	r
				3.6	
opx1_1	31.27	0.92	6.1		c
opx1_2	28.61	1.15	3.4	opx	r
				4.7	
04NS16					
cpx1_1	28.10	0.64	2.9		c
cpx1_2	25.65	0.62	0.4	cpx	r
				1.7	
opx1_1	26.84	0.84	1.6		c
opx1_2	20.85	0.88	-4.4		r
				opx	
				-1.4	
MJ9801					
cpx1_1	27.39	0.84	2.2		r
cpx1_2	24.68	1.04	-0.5		c

cpx2_1	7.09	0.08	11.45	cpx 12.8	c
opx1_1	3.77	0.04	6.06		c
opx2_1	1.95	0.03	3.13	opx 4.6	c
plag1_1	1.26	0.01	2.37		c
plag2_1	0.87	0.02	1.64		c
plag3_1	0.93	0	1.75	plag 1.9	c
MJ9801					
cpx1_1	15.76	0.32	22.84		r
cpx1_2	20.65	0.23	29.93		
cpx1_3	22.83	0.18	33.09		c
cpx1_4	21.07	0.87	30.54		
cpx1_5	21.05	0.12	30.51		r
cpx1_6	19.19	0.16	27.82		r
cpx1_7	17.19	0.43	24.92		
cpx1_8	23.6	0.52	34.21		c
cpx1_10	13.9	0.41	20.15		
cpx1_11	15.86	0.36	22.99	cpx 27.7	r
opx1_1	1.9	0.07	2.79		c
opx1_2	2.7	0.1	3.96	opx 3.4	r
plag1_1	4.01	0.05	6.34		r
plag1_2	4.84	0.08	7.65		c
plag2_1	6.81	0.16	10.77		r
plag2_2	7.49	0.11	11.85		
plag2_3	7.67	0.07	12.13		
plag2_4	6.31	0.07	9.98	plag 9.8	c
grt1_1	1.9	0.04	2.14		c
grt1_2	2.28	0.04	2.57		
grt1_3	2.4	0.04	2.70		
grt1_4	2.72	0.06	3.06		r
grt2_1	2.83	0.06	3.19		c
grt2_2	3.47	0.04	3.91		
grt2_3	3.3	0.06	3.71	grt 3.0	r
MJ9805					
cpx1_1	17.21	0.27	25.79		r
cpx1_2	18.56	0.19	27.81		c
cpx1_3	18.87	0.18	28.27		r
cpx2_1	18.58	0.17	27.84		r
cpx2_2	19.71	0.18	29.53	cpx 27.8	c
opx1_1	1.33	0.05	1.99		c
opx2_1	1.17	0.03	1.75		r
opx2_2	0.82	0.05	1.23		
opx2_3	1.22	0.04	1.82		c
opx3_1	2.35	0.05	3.51		r
opx3_2	1.79	0.04	2.68		c
opx3_3	1.33	0.03	1.99	opx 2.1	r
plag1_1	0.31	0.01	0.52		r
plag1_2	0.55	0.04	0.92		
plag1_3	1	0.05	1.68		c

cpx2_1	27.07	1.01	1.9		c
cpx2_2	19.81	0.73	-5.4		
cpx2_3	25.41	0.96	0.2	cpx -0.3	r
opx1_1	20.86	1.34	-4.3		c
opx1_2	18.36	1.32	-6.8	opx -5.6	r
grt1	21.88	1.21	-3.3		c
plag1_1	12.01	1.60	-13.2		c
plag1_2	11.44	1.38	-13.8	plag -13.5	r
MJ9805					
cpx1_1	22.17	1.02	-3.0		r
cpx1_2	21.34	1.12	-3.9		c
cpx2_1	20.98	0.99	-4.2		c
cpx2_2	20.07	0.95	-5.1	cpx -4.1	r
opx1_1	20.21	1.08	-5.0		c
opx1_2	17.66	0.78	-7.5		r
opx2	28.85	1.40	3.7	opx -3.0	c
DM9855					
cpx1_1	20.40	0.91	-4.8		c
cpx1_2	14.82	0.79	-10.4		r
cpx1-1 #	12.04	0.79	-12.4		r
cpx1-2 #	20.38	1.10	-4.1		
cpx1-3 #	25.44	1.08	1.0		
cpx1-4 #	16.21	1.14	-8.2		
cpx1-5 #	26.28	1.39	1.8		
cpx1-6 #	32.65	1.43	8.2		c
cpx1-7 #	35.36	1.31	10.9		
cpx1-8 #	10.80	1.22	-13.6		
cpx1-9 #	16.80	1.56	-7.6		r
cpx1-10 #	30.16	1.81	5.7		r
cpx2_1	22.84	0.87	-2.4		c
cpx2_2	21.69	0.98	-3.5		
cpx2_3	23.29	0.89	-1.9		
cpx2_4	20.46	0.96	-4.7		
cpx2_5	21.62	0.95	-3.6		
cpx2_6	11.21	1.05	-14.0		r
cpx2-1 #	25.54	0.54	1.1		r
cpx2-2 #	26.65	0.67	2.2		
cpx2-3 #	21.88	0.57	-2.6		
cpx2-4 #	20.12	0.55	-4.3		
cpx2-5 #	21.80	1.11	-2.6		c
cpx2-6 #	15.86	0.63	-8.6		
cpx2-7 #	12.14	0.67	-12.3		
cpx2-8 #	11.37	0.62	-13.1		
cpx2-9 #	14.72	0.54	-9.7	cpx -4.2	r
opx1_1	10.91	0.64	-14.3		c
opx1_2	26.46	0.72	1.3		
opx1_3	24.53	0.78	-0.7		r
opx1-1 #	20.53	0.71	-3.9		r
opx1-2 #	11.16	0.44	-13.3		c
opx1-3 #	20.56	0.48	-3.9		r

plag2_1	0.14	0.01	0.24		r
plag2_2	0.65	0.02	1.09		
plag2_3	1.96	0.04	3.29		
plag2_6	0.35	0.01	0.59		c
plag3_1	1.4	0.03	2.35		r
plag3_2	1.8	0.03	3.02		
plag3_3	0.8	0.04	1.34		
plag3_4	0.96	0.02	1.61		
plag3_5	1.16	0.01	1.95		
plag3_6	0.98	0.02	1.65	plag 1.6	c
DM9855					
cpx1_1	3.53	0.04	5.61		r
cpx1_2	3.9	0.01	6.20		
cpx1_3	3.9	0.02	6.20		c
cpx1_4	3.93	0.03	6.24		
cpx1_5	3.7	0.03	5.88		
cpx1_6	4.6	0.03	7.31		r
cpx2_1	5.08	0.29	8.07		c
cpx2_2	6.29	0.04	9.99		r
cpx3_1	5.71	0.05	9.07		
cpx3_2	6.48	0.09	10.30	cpx 7.5	
opx1_1	2.36	0.02	3.94		r
opx1_2	5.44	0.03	9.09		
opx1_3	4.97	0.01	8.30		
opx1_4	4.34	0.04	7.25		
opx1_5	4.83	0.05	8.07		c
opx1_6	4.55	0.02	7.60		
opx1_7	0.34	0.01	0.57		r
opx1_8	1.23	0.01	2.05		
opx2_1	1.04	0.02	1.74		r
opx2_2	1.3	0.01	2.17		
opx2_3	0.56	0.01	0.94		c
opx3_1	5.25	0.02	8.77		c
opx3_2	3.51	0.02	5.86		
opx3_3	0.98	0.01	1.64	opx 4.9	r
plag1_1	0.48	0.07	0.86		c
plag1_2	0.55	0.01	0.98		
plag1_3	0.52	0.01	0.93		
plag1_4	0.5	0.01	0.89		
plag1_5	0.38	0.01	0.68		r
plag2_1	0.43	0.01	0.77		r
plag2_2	0.48	0.01	0.86		
plag2_3	0.52	0.01	0.93		c
plag3_1	0.91	0.01	1.62		
plag3_2	0.94	0.03	1.67	plag 1.0	
DM9871					
cpx2_1	6.41	0.08	9.48		r
cpx2_2	3.11	0.05	4.60		
cpx2_3	2.19	0.03	3.24		c
cpx2_4	2.28	0.06	3.37		
cpx2_5	2.98	0.03	4.41		
cpx2_6	5.25	0.09	7.77	cpx 5.5	r
opx2_1	2.14	0.06	3.34		r

opx1-4 #	12.27	0.62	-12.2		r
opx2-1	18.32	0.55	-6.1		r
opx2-2	10.10	0.58	-14.3		
opx2-3	8.32	0.57	-16.1		
opx2-4	37.04	0.76	12.6		
opx2-5	17.50	1.54	-6.9		
opx2-6	28.89	0.46	4.5		
opx2-7	27.96	0.58	3.5		
opx2-8	32.42	0.54	8.0	opx -4.1	c
DM9871					
cpx1_1	29.29	1.07	4.1		c
cpx1_2	26.52	1.17	1.3		r
cpx1_1 #	32.78	1.11	8.3		c
cpx1_2 #	29.71	0.99	5.3		
cpx1_3 #	24.86	0.90	0.4		
cpx1_4 #	12.50	0.72	-11.9		
cpx1_5 #	7.34	0.62	-17.1		
cpx1_6 #	10.12	0.51	-14.3		
cpx1_7 #	10.01	0.58	-14.4		r
cpx2_1	9.77	0.68	-15.4		c
cpx2_2	10.10	1.47	-15.1		
cpx2_3	8.78	0.80	-16.4		
cpx2_4	4.96	0.62	-20.2		
cpx2_5	0.28	0.58	-24.9		
cpx2_6	0.31	0.44	-24.9		
cpx2_7	5.88	0.32	-19.3		
cpx2_8	7.10	0.34	-18.1		r
cpx2-1 #	13.05	1.05	-11.4		*c*
cpx2-2 #	0.91	0.78	-23.5		
cpx2-3 #	8.52	0.70	-15.9	cpx -12.2	*r*
opx1_1	21.11	0.91	-4.1		r
opx1_2	29.29	1.07	4.1		c
opx1_1 #	23.58	0.68	-0.9		r
opx1_2 #	22.53	0.72	-1.9		
opx1_3 #	18.27	1.18	-6.2		
opx1_4 #	23.94	1.47	-0.5		
opx1_5 #	21.37	1.45	-3.1		
opx1_6 #	30.29	1.24	5.9		c
opx1_7 #	29.70	0.94	5.3		
opx1_8 #	28.20	1.42	3.8		
opx1_9 #	21.37	0.89	-3.1		
opx1_10 #	20.39	0.92	-4.0		r
opx2_1	8.76	0.93	-16.4		
opx2_2	7.85	1.11	-17.4		
opx3_1	25.83	0.65	0.6		r
opx3_2	31.59	0.68	6.4		
opx3_3	31.61	0.62	6.4		c
opx3_1 #	42.28	0.74	8.0		*c*
opx3_2 #	42.00	0.61	7.7		
opx3_3 #	35.36	0.72	1.1	opx -0.4	*r*
WD9532					
cpx1_1	20.34	1.32	-4.9		c
cpx1_2	15.52	1.55	-9.7		r

opx2_2	1.94	0.05	3.03			cpx1-1 #	22.24	1.38	-2.2		r
opx2_3	2.08	0.04	3.25		c	cpx1-2 #	24.78	0.84	0.3		c
opx2_4	2.4	0.07	3.74								
opx2_5	2.64	0.04	4.12								
opx2_6	1.57	0.05	2.45	opx 3.3	r	cpx2_1	21.92	1.94	-3.3		c
						cpx2_2	23.30	1.48	-1.9		r
plag1_1	0.32	0.03	0.51		r						
plag1_2	0.34	0.02	0.54			cpx2-1 #	21.38	2.25	-3.1		r
plag1_3	0.28	0.02	0.45			cpx2-2 #	24.64	2.33	0.2		
plag1_4	0.34	0.02	0.54	plag 0.5	c	cpx2-3 #	15.96	1.80	-8.5		
						cpx2-4 #	8.59	2.28	-15.9		
WD9532						cpx2-5 #	25.27	1.96	0.8		c
cpx1_1	3.45	0.08	5.05		r	cpx2-6 #	21.64	1.63	-2.8		
cpx1_2	3.29	0.05	4.81			cpx2-7 #	17.54	1.66	-6.9	cpx -4.4	r
cpx1_3	3.52	0.07	5.15								
cpx1_4	3.35	0.06	4.90	cpx 5.0	c	opx1_1	15.38	1.38	-9.8		c
						opx1_2	8.43	1.01	-16.8		r
opx1_2	2.61	0.05	3.94		r						
opx1_3	2.49	0.04	3.76			opx1-1 #	7.67	0.80	-16.8		r
opx1_4	2.44	0.03	3.69		c	opx1-2 #	25.76	0.85	1.3		
						opx1-3 #	25.76	0.82	1.3		
opx2_1	1.6	0.03	2.42		r	opx1-4 #	22.70	0.70	-1.7		
opx2_2	1.33	0.04	2.01			opx1-5 #	18.75	0.68	-5.7		c
opx2_3	1.54	0.03	2.33	opx 3.0	c	opx1-6 #	18.78	0.66	-5.7		
						opx1-7 #	10.03	0.63	-14.4		r
plag1_1	0.25	0.04	0.41		r						
plag1_2	0.26	0.04	0.43			opx2_1	17.56	1.39	-7.6		r
plag1_3	0.24	0.04	0.40		c	opx2_2	21.88	1.38	-3.3		c
plag2_1	0.17	0.02	0.28	plag 0.4		opx2-1 #	16.95	0.77	-7.5		r
						opx2-2 #	28.16	0.90	3.7		
WD9546						opx2-3 #	29.41	0.76	5.0		
cpx1_1	3.74	0.09	5.53		r	opx2-4 #	28.85	0.84	4.4		
cpx1_2	4.58	0.08	6.77			opx2-5 #	31.32	0.78	6.9		c
cpx1_3	4.65	0.07	6.88			opx2-6 #	29.47	0.80	5.0	opx -3.6	
cpx1_4	4.61	0.07	6.82		c						
						plag1_1	24.76	1.09	-0.4		c
cpx2_1	4.77	0.09	7.05		r						
cpx2_2	4.48	0.07	6.63								
cpx2_3	4.86	0.07	7.19			**WD9546**					
cpx2_4	4.7	0.07	6.95		c	cpx1_1	14.59	1.42	-10.6		c
cpx2_6	4.59	0.07	6.79			cpx1_2	15.43	1.39	-9.8		
cpx2_7	4.66	0.05	6.89	cpx 6.7	r	cpx1_3	16.00	1.49	-9.2		r
opx1_1	3.28	0.07	5.11		r	cpx2_1	16.77	1.46	-8.4	cpx -9.5	c
opx1_3	3.2	0.05	4.98								
opx1_4	3.15	0.05	4.91		c	opx1_1	12.04	1.59	-13.2		c
opx1_5	3.23	0.05	5.03	opx 5.0		opx1_2	5.76	1.66	-19.4		
						opx1_3	6.56	2.22	-18.6		
plag1_1	0.25	0.01	0.38		r	opx1_4	9.62	2.19	-15.6		
plag1_2	0.33	0.02	0.50		c	opx1_5	15.61	1.88	-9.6		
						opx1_6	7.13	2.11	-18.1		
plag2_1	0.28	0.02	0.42		r	opx1_7	17.01	1.56	-8.2		
plag2_2	0.25	0.01	0.38		c	opx1_8	15.25	1.58	-10.0		
						opx1_9	12.62	1.57	-12.6		
plag3_1	0.18	0.01	0.27		r	opx1_10	13.06	1.68	-12.1		
plag3_2	0.17	0.01	0.26		c	opx1_11	14.39	0.88	-10.8		
plag3_3	0.17	0.01	0.26		r	opx1_12	12.72	0.74	-12.5	opx -13.4	r
plag4_1	0.25	0.01	0.38		r						
plag4_2	0.22	0.01	0.33	plag 0.4	c						

Note: the left half panel is for Li-contents (in ppm), and the right for Li-isotopes (‰). The grain numbers for each mineral within each sample are of the same sequence for both their

contents and isotopic compositions.

$^{7}Li/^{30}Si$ (in the 10^{-3} units) is the SIMS measured Li-index, which is used for the correction of the its true content, Li-corr; δ^{7}Li is the SIMS measured data, and δ^{7}Li-corr is the calibrated data for the possible matrix effects during the analyses; the mean value yields the average for all the measurements of the same mineral in each sample, in terms of the contents and isotopic data, respectively; c and r denote core and rim, respectively (during the profile determination); #, duplicate analyses on the same grain.

Table 5- 17 Average lithium data in the studied granulites

	Abundance (ppm)					Isotope (d7Li, ‰)			
	cpx	opx	plag	grt	wr*	cpx	opx	plag	grt
04NS11		3.68	1.28		1.94		-2.52		
04NS13		4.18	1.40		1.96		-2.68		
04NS9	9.49	3.82	3.05		5.31	3.62	4.74		
04NS16	12.78	4.6	1.92		2.96	1.68	-1.36		
MJ9801	27.70	3.38	9.79	3.04	12.58	-0.33	-5.59	-13.5	-3.3
MJ9805	27.85	2.14	1.56	-	12.31	-4.06	-2.96		
DM9855	4.98	3.03	0.38		2.59	-4.2	-4.13		
DM9871	6.75	5.01	0.35		2.68	-12.18	-0.42		
WD9532	7.49	4.86	1.02		5.67	-4.44	-3.63	-0.4	
WD9546	5.48	3.32	0.51		4.26	-9.51	-13.39		

Note: the left and right panels are for Li contents and isotopic compositions, respectively, which are compiled from Table 5-16. *: the estimated whole rock contents based on the constitutive minerals.

The results show that, as a whole, cpx are commonly rich in Li, following by opx, and plag are usually depleted in Li, with their contents ranging from 3.2 to 34.2 ppm for cpx, from 0.6 to 9.1 ppm for opx, from 0.2 to 12.1 ppm for plag and from 2.1 to 3.9 ppm for grt, the latter one is in only one sample (Table 5-16). The profile analyses on the mineral grains usually show limited, or nearly constant, variation in the Li abundance, although they can be significantly different from grain to grain even in the same sample; however, intra-grain variations beyond the analytical uncertainty can also be observed in these samples: they can be either enriched or depleted in the core relative to the rim area (Table 5-16). The Li contents of cpx and plag in the Nushan xenolith and Hannuoba terrain granulites are similar to some extent to each other and higher than those in the Hannuoba xenolith granulites; however, no such contrast can be found within opx in these samples, instead the average concentration of opx

is similar between them (Table 5-17). The estimated bulk Li concentrations are highly variably, ranging from ~1.9 to 12.6 ppm, between different samples, and the highest contents are observed in the Hannuoba terrain granulites, which is similar to those observed for cpx and plag (Table 5-17).

The measurements of lithium isotopic compositions demonstrate that they are highly variable on the inter- and intra-grain scale, with their total variation of -24.9 to 10.9‰ for cpx and -20.2 to 12.6‰ for opx (Table 5-16). In some samples, the mineral grains didn't display any obvious distinction in their $^{7}Li/^{6}Li$ ratios between the core and rim area, as revealed by the two-point analyses in these regions, e.g. cpx in MJ9805, or by profile analyses on some grains, e.g. cpx1 in 04NS9 (if considering the uncertainty). However, the profile analyses in most cases show complex but no general variation: they can be heavier in the core than in the rim, e.g. cpx1 and 2 in DM9855 and opx3 in 04NS11, lighter in rare cases in the core than in the rim, e.g. opx1 in DM9855, or in a few cases a low δ^{7}Li trough in the intermediate of core and rim region, e.g. cpx2 in WD9532, opx in DM9871 and opx in DM9855 (Table 5-16). The duplicate measurements across the same grains usually yield similar isotopic values if the analyzed spots are close to each other, whereas the variations observed on some grains were probably related to the heterogeneous distribution of δ^{7}Li within the sub-grain scale. The average δ^{7}Li of cpx and opx in the Nushan samples resemble those in the Hannuoba terrain samples, and are higher than those in the Hannuoba xenolith granulites, e.g. -4.1~3.62‰ for cpx and -5.6~4.7‰ for opx in the former vs. -12.2~-4.2‰ for cpx and -13.4~-0.4‰ for opx in the latter (Table 5-17). The δ^{7}Li of plag measured in two samples are about -13.4‰ and -0.4‰, respectively, and about -3.3‰ for grt in MJ9801 (Table 5-16); in fact, the δ^{7}Li values of plag and grt, theoretically, cannot be assumed as precise as those of pyroxenes before the establishment of standards for the corresponding phases, however, the similarity between the δ^{7}Li of plag and grt with coexisting cpx and opx, e.g. generally depleted relative to the normal mantle, suggests no notable matrix effects on them according to Beck et al. (2004) and Decitre et al. (2002) that no significant matrix effects on the instrumental mass fractionation of a wide spectrum of minerals and glasses.

In summary, except only one sample 04NS9 whose cpx and opx have δ^7Li values falling in the range of normal upper mantle, e.g. 2-6‰ defined by the isotopic compositions of oceanic basalts (Elliott et al., 2004; Tomascak, 2004; and references therein) and "equilibrated" intra-plate mantle peridotites (Seitz et al., 2004; Magna et al., 2006; Jeffcoate et al., 2007; Ionov and Seitz, 2008), minerals (cpx and opx in majority) in all the other samples are characterized by relatively depleted Li-isotopic compositions (Table 5-17). The profile Li isotopic variations on most grains in contrast to the limited variations of Li contents on most grains observed in the ten granulites are actually similar to some extent to those found in minerals from meteorites (Beck et al., 2004, 2006; Lundstrom et al., 2005) and intra-plate mantle peridotite xenoliths (Tang et al., 2007; Wagner and Deloule, 2007) and mineral phenocrysts from primitive arc lavas (Parkinson et al., 2007).

6 Water in the continental lower crust

In this chapter, the water content of lower crustal granulite minerals given in Chapter 5 will be used towards a detailed, although very preliminary to some extent, discussion about their distribution, evolution and possible effects on the high electrical conductivity in the continental lower crust. For the first time, the water budget in the lower crust and the contrast in water content between Precambrian and Phanerozoic lower crust are documented.

6.1 Preservation of initial hydrogen information

Whether or not deep-seated minerals brought to the surface by kimberlite or alkaline basalts can preserve their original hydrogen information is an issue in debate. It is argued by some scholars that minerals can record their initial OH contents (Peslier et al., 2002; Bell et al., 2004; Grant et al., 2007a), but there are also some studies suggesting that the water content of minerals can be modified during eruption, especially by H diffusion and/or exchange between crystals and melts (e.g. Ingrin and Skogby, 2000).

For our results, the following reasons are proposed that these water data may preserve their source information, or at least record the minimum estimate of their initial contents:

(1) Each of the phases in the same sample is chemically identical. No major element compositional zoning was observed for any studied grains in all the samples, and no REE compositional zoning was observed in individual grains within the Hannuoba xenolith and terrain and Nushan xenolith granulites.

(2) The FTIR measurements were usually conducted in the core region of clean, crack- and inclusion-free grains of relatively large size. It is therefore inferred that the loss of hydrogen caused by diffusion during the ascent would be very small (Peslier and Luhr, 2006).

(3) Profile analyses on many grains in all the 4 sets of granulites show that the H-related IR absorption is mostly homogeneous between their core and rim regions (Figs. 5-11, 5-12 and 5-13), indicating negligible depletion or enrichment of H from diffusion or exchange. This has also been verified by H counts of SIMS during the hydrogen isotopic analyses, which in most cases reveal no significant zoning across the grain (Table 5-13).

(4) The studied samples are usually very fresh, and all the spectra show no signal of any evident hydrous phases, which would produce sharp bonds in the region of > 3660 cm^{-1}. In this case, there is no evident interference from other H-bearing phases, neither any marked exchange of H between them.

(5) The hydrogen isotopic measurements by SIMS for both profile analyses across mineral grains and the average compositions of individual minerals in the 10 selected granulites from the NCC favor the preservation of their initial hydrogen information (which will be discussed in Chapter 8).

The above discussions suggest that the measured water concentrations of the granulite minerals (cpx, opx, plag and grt) reflect their original contents in the lower crust. These data will be used in the subsequent discussions in terms of the nature, behavior and implications of water in the deep continental crust.

One potential issue needing further consideration is the mineral exsolution in some samples, such as in the Daoxian xenolith granulites (Fig. 3-5). In fact, mineral exsolution is very common in high-temperature metamorphic rocks, e.g. exsolution of quartz in cpx (Gayk et al., 1995), pyroxenes in cpx (Sandiford and Powell, 1986) and spinel in plagioclase (Rudnick et al., 1986) of granulites, and is usually interpreted as a response of a cooling process (e.g. Jaffe et al., 1975; Harley, 1987). As to the mineral exsolutions in the xenolith granulites, it is difficult to imagine that they were formed during the entrainment of the xenoliths and/or during their transport to the surface -- so quick are these processes (e.g. from several hours to a few days) that there is no time available for a general

development of the exsolutions, as observed in the Daoxian samples. Therefore, a more likely explanation is that these exsolutions reflect cooling and metamorphic recrystallization in the lower crust prior to the entrainment (Roberta Rudnick, person. comm., 2007). Accordingly, the water content recorded in these granulites can be used as an index of their source hydrogen-composition. This is also supported by the nearly uniform profile analyses (Fig. 5-13) across mineral grains, by the indistinguishable FTIR-absorption bands and intensities (e.g. the integral area) between exsolution-free and exsolution-bearing areas within the same grain and by the similar average water content between exsolution-absent and exsolution-common Daoxian xenolith granulites.

6.2 Distribution of water within sub-grain scale

The within-grain variations of water content in the lower crustal granulites can be accessed according to the FTIR profile analyses conducted on selected oriented mineral grains. For pyroxenes, the mineral grains are mostly unzoned with respect to their hydroxyl abundances, as revealed by the FTIR absorption measurements (Figs. 5-11, 5-12 and 5-13), indicating that the pyroxene grains within the lower crust have usually acquired their hydrogen equilibrium driven by diffusion. However, a few grains with either higher or lower FTIR absorption in the core relative to the rim region, in other words heterogeneous, were also found in these granulites (mentioned in Chapter 5). Such micro-heterogeneities can not exist in the lower crust for long duration and they will be homogenized in very short interval (e.g. in several thousands of years or even less), because of the very high mobility of hydrogen under the deep crustal high temperatures; accordingly, it is suggested that these within-grain variations were produced in the entrainment of the samples by mantle melts or shortly before such events.

For grt in the Hannuoba terrain samples, the heterogeneity in H_2O content between different grains in each sample and between different zones in each grain are especially significant, with the variation up to a factor of 10-20 (Tables

5-8 and 5-9). The profile measurements of garnet in SX-1 demonstrate that the distribution of water in the sub-grain scale is irregular: they can be either lower or higher in the core than in the rim region, and, in most cases, no general variation in water content from core to rim can be observed (Table 5-9). These terrain granulites were uplifted to the surface by complex tectonic movements, however, the preservation of fresh kelyphite in them (Guo et al., 1993) indicates a rapid decompression during their exhumation (Rudnick, 1992), and the FTIR profile analyses of pyroxenes in them (Fig. 5-12), the SIMS counts on hydrogen across the most mineral grains (Table 5-13) and the SIMS investigations of H, O and Li isotopic compositions for their individual minerals (Tables 5-13, 5-15 and 5-16; and the discussions in Chapter 8) also favor that they were probably not significantly influenced by later/secondary processes to a large extent. In this case, the large variations of water content in garnet in the terrain samples are difficult to explain by a simple and unique explanation, as proposed by Johnson (2003) for garnets from the Adirondacks. The contrast between pyroxenes and grt could be related with their different hydrogen diffusion coefficients (Ingrin and Blanchard, 2006), however, many questions remain and further studies are necessary, especially in the incorporation mechanisms of water into garnets.

It is difficult to constrain the ascent rate of the exposed Archean granulite terrains. However, The preservation of fresh kelyphite, consisting of extremely fine-grained cpx+ opx+ plag around fresh garnet cores, in these high pressure terrain granulites (Guo et al., 1993) indicates rapid decompression and cooling during their uplift (Rudnick, 1992). Unfortunately, there is no available study for an exact time constraint for the Hannuoba terrain granulites. Perusal of many literatures reveals that the presence of fresh kelyphite in "terrain-type" samples roughly implies an rapid cooling and exhumation rate of about 200-350 °C/Ma (e.g. Morishita et al., 2001). Applying such estimation to the Hannuoba terrain granulites, an ascent time of ~ 2-4 Ma could be obtained. During such interval, it is very likely that the original hydrogen information was preserved, as those

proposed for the quickly subducted and exhumed eclogites in the central Dabie Mountains (Xia et al., 2005). Given these possibilities, the heterogeneous water distribution within garnet in the terrain granulites, whether initial or secondary-modified, rules out the possibility that the terrain granulites were infiltrated by a pervasive fluid during their uplift.

6.3 Partitioning of water between lower crustal phases

The partitioning of water between lower crustal granulite mineral pairs, e.g. cpx-opx, cpx-plag and opx-plag, define very poor correlations (Fig. 6-1a, b and c). Although roughly positive relationship can be observed for the plag-cpx and plag-opx pairs (Fig. 6-1b and c), the data points are very scattering for the cpx-opx pair (Fig. 6-1a); the partitioning coefficient of water content between cpx and opx varies in the range of 0.48 to 10.28, with an average of 3.24, in contrast with that of 0.55 between plag and cpx and of 1.67 between plag and opx (Table 5-7).

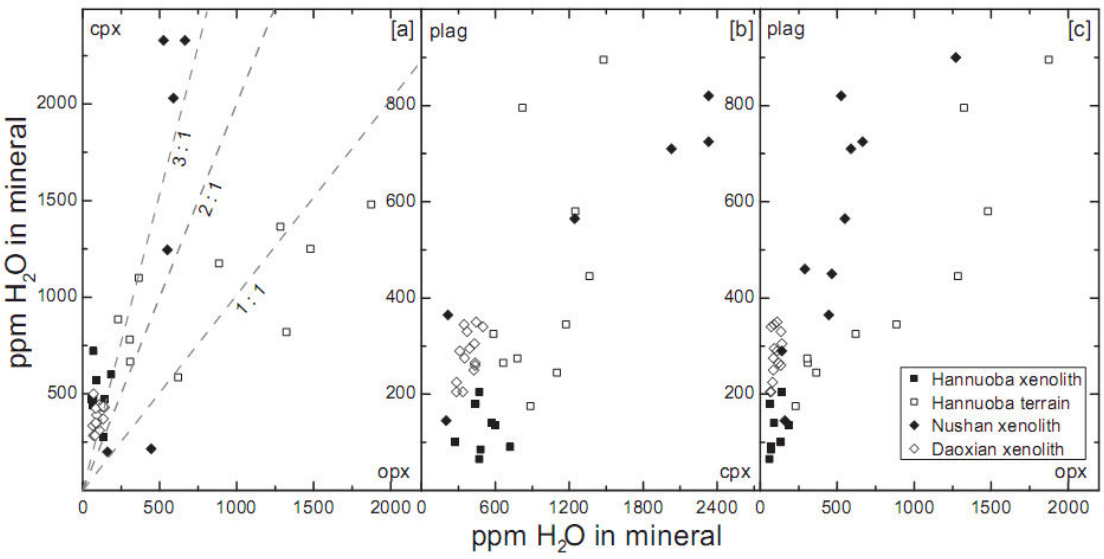

Fig. 6- 1 Partitioning of water between (a) cpx-opx, (b) plag-cpx and (c) plag-opx pairs in the lower crustal granulites

The partitioning of water between these coexisting minerals display significant variation from locality to locality (Fig. 6-1). For example, the partition

coefficient of water between cpx and opx is ~6 for the Hannuoba xenolith granulites, ~1 for the Hannuoba terrain granulites, ~2.5 for the Nushan xenolith granulites and ~4 for the Daoxian xenolith granulites (Table 5-7). Similar variations can also be observed for the plag-cpx and plag-opx pairs (Fig. 6-1).

Although the lack of data on water partitioning between plagioclase and pyroxenes makes it hard for a quantitative comparison with our data, available studies on natural and synthesized mantle samples have documented that the equilibrium partition coefficient of water between cpx and opx, $D_{cpx/opx}^{water}$, is about 1.9-2.3 (Bell and Rossman, 1992b; Peslier et al., 2002; Koga et al., 2003; Aubaud et al., 2004; Bell et al., 2004; Hauri et al., 2006; Grant et al., 2007a; and this study on the Hannuoba and Nushan peridotites). The values measured in our samples (in particular Nushan and Daoxian granulites; Fig. 6-1) are similar to those mentioned above. Deviation from the equilibrium trend may be ascribed to water loss from individual grains/minerals during granulite-facies metamorphism (e.g. via mineral degassing after crystallization or water loss from the original mantle melts). These processes could certainly modify the initial water content of minerals inherited from their original melts or even the water content in the melts, and therefore produce the observed disequilibrium. However, there are also several other scenarios which can result in such disequilibrium: (1) the equilibrium could not be acquired under the lower crustal T and P conditions, (2) the water content of lower crustal minerals was not inherited from their originated mantle source, (3) closed-system re-distribution of H between coexisting minerals altered their partitioning as a function of the different mineralogical composition (e.g. plagioclase- vs. pyroxene-rich samples).

Alternatively, the equilibrium partition coefficient between pyroxenes obtained from mantle samples cannot be applied directly to crustal samples, because: (1) the chemical composition and crystal structure between crustal and mantle minerals/rocks are so different, e.g. rich in Fe in granulites vs. Mg in

peridotites, which may influence greatly the incorporation of H (e.g. Skogby and Rossman, 1989; Stalder, 2004), and the less close-packed structures of Fe-rich pyroxenes in granulites relative to the Mg-rich ones in mantle samples theoretically allow a greater range of substitutions of trivalent and quadrivalent ions, even of large size such as OH, although this is not well constrained by experiments at present; (2) the incorporation behavior of H into minerals is probably different between lower crust and mantle T and P conditions, this has actually been verified recently by experimental investigations performed on Al-rich orthopyroxene (Mierdel et al., 2007), which contain apparently more water (up to ~ 7000 ppm) under lower crustal than mantle conditions. Under these cases, further investigations are necessary for a better knowledge of the partitioning of water between lower crustal assemblages.

6.4 Water budget in the lower crust

During the last several decades, many efforts have been devoted to the knowledge of water content/solubility in the upper mantle, transition zone and lower mantle (Table 6-1). These studies suggest that, in spite of some possible uncertainties, the total water stored in the earth's mantle is about a few ocean masses (e.g. Bolfan-Casanova et al., 2003), although it was argued recently that the mantle transition zone is probably in dry status instead of containing a large amount of water in wadsleyite and ringwoodite (Yoshino et al., 2008).

Table 6- 1 Mineralogy and water capacity of the Earth's mantle

Layer	Depth (km)	T (^{o}C)	P (Gpa)	Mineralogy	H_2O (ppm)
upper mantle	~50-410	1000-1400	1.3-13	olivine, pyroxenes, garnet	~ 250
transition zone	410-670	1400-1600	13-23	wadsleyite, majorie, ringwoodite	~ 1400
lower mantle	670-2900	1600-3500	23-135	perovskites, magnesiowüstitie	~ 10

Data source: Bolfan-Casanova et al (2003); and references therein.

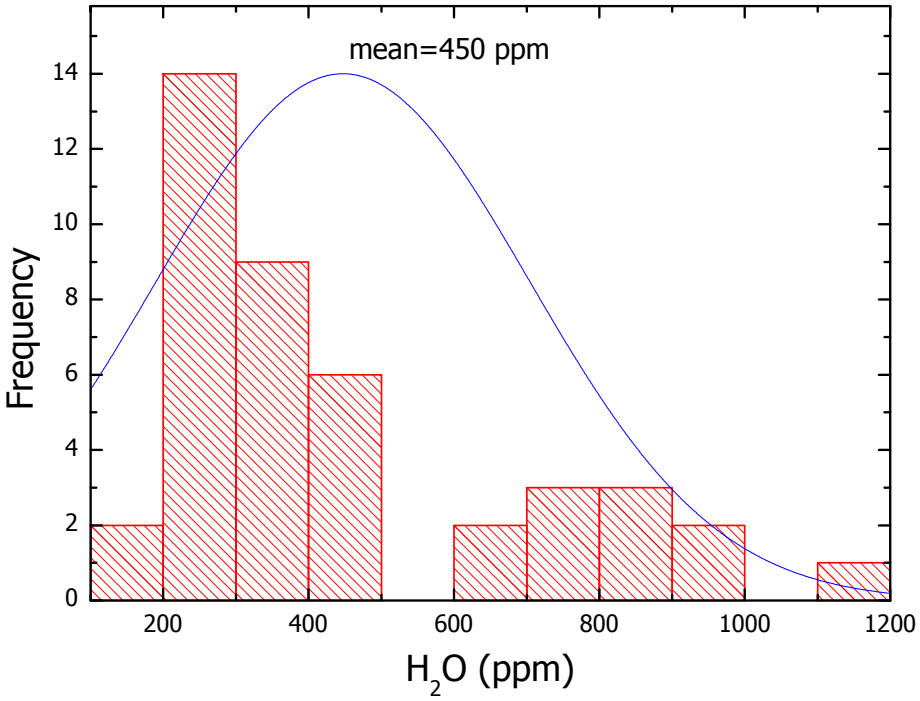

Fig. 6- 2 Bulk water content in the lower crust and the normal pattern

In contrast to the numerous studies toward the Earth's mantle, there is no previous investigation on the water budget in the continental lower crust. On the basis of our data, the distribution of water in the lower crust seems highly variable. This is shown not only on large scales, e.g. between different samples/localities, but also on small scales, e.g. within the subgrain of garnet, as discussed in the Chapter 5 (Tables 5-7, 5-8 and 5-9). The total variation of water content is from 200 to 2330 ppm for cpx, 60 to 1875 ppm for opx and 65 to 900 ppm for plag between different samples, and ~ 50 to 1700 ppm for grt between different analytical points. The estimated bulk water content varies from about 150 to more than 1000 ppm, with an average content of around 450 ppm (Fig. 6-2).

This average bulk value is used for an approximation of water in the lower crust. If assuming that: (1) the mass of the bulk continental crust is 2.44×10^{22} kg (McLennan and Taylor, 1999); (2) the weight proportion of the upper, middle and lower crusts is 0.317 : 0.295 : 0.388 (Rudnick and Gao, 2003); and (3) felsic granulites in the deep crust contain similar water content as the mafic ones, we

can obtain that the amount of water stored in the lower crust is about 4.26 × 10^{18} kg. This amount of water is small compared to the 1.35 × 10^{21} kg of water in the oceans and the maximum water mass of 4 × 10^{20} kg stored in the upper mantle within nominally anhydrous minerals (using the estimate of Ingrin and Skogby (2000) of 600 ppm for an estimation). However, we have to emphasize that (1) the volume, and mass, of the lower crust is very small compared to that of the upper mantle; and (2) the presence of fluids and/or hydrous phases was not considered, but these phases do present in some regions of high water flux, such as in island arc settings where hydrous oceanic lithosphere is subducted and dewatered (e.g. Kushiro, 1990).

6.5 Water content contrast between Precambrian and Phanerozoic lower crust

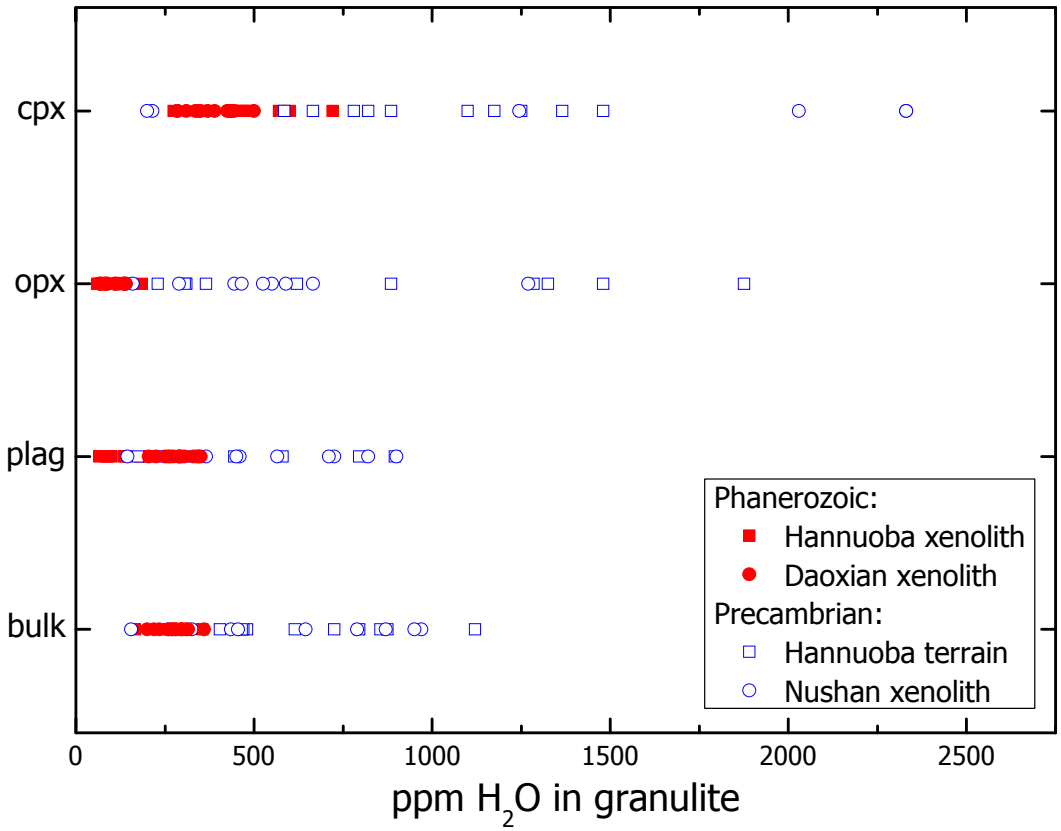

Fig. 6- 3 Water content contrast between Precambrian and Phanerozoic lower crust

According to the formation ages determined by zircon U-Pb dating, the four

suites of granulite samples can be roughly divided into two different categories: the Precambrian and Phanerozoic group. The former consists of the Hannuoba and Daoxian xenolith granulites, and the latter includes the Hannuoba terrain and Nushan xenolith granulites. The division is actually not that strict and works under the assumption that the Nushan granulites are predominated by ancient ages and the Daoxian granulites by young ages.

Under this division, a very interesting result is that the water content in the Precambrian granulites is significantly higher than that in the Phanerozoic ones, in terms of both individual minerals and bulk rocks and in spite of the possible heterogeneities between different samples (Fig. 6-3). Such obvious contrast in water content can be produced by differences in the pressure, or in the derived depth, which would affect the solubility of H_2O in minerals. This, however, can not contribute a lot to the variation of water content in the granulites, because the pressure of these granulites varies only from about 0.8 to 1.5 GPa (and they mostly vary in a even narrower range); in this range, variation of water content caused by pressure is relatively small, e.g. <15% for cpx and <30% for opx on the basis of experimental studies by Rauch and Keppler (2002) and Bromiley et al. (2004) (or for opx by a recent report by Mierdel et al. (2007)), respectively.

In this case, it is proposed that the continental lower crust is more hydrous in the Precambrian than in the Phanerozoic. This wetter condition would exert profound influences on many physical and chemical properties of ancient lower crustal, e.g. lowering rheological strength and melting temperatures, modifying seismic velocity, and so on.

The strong contrast in water content between the Precambrian and Phanerozoic lower crust can be accounted for by the following possibilities:

(1) Re-equilibration of Precambrian granulites with mantle melts and increase of their OH contents. There is no evidence that these Precambrian granulites were affected by mantle melts (Huang et al., 2004; Zhai et al., 2005).

Furthermore, the ability for melt to percolate within a rock matrix is controlled by the dihedral angle (θ) between solid and melt, and for θ>60º, small melt fractions cannot percolate (Waff and Bulau, 1979). θ between lower crustal assemblages and melt are usually larger than 60º (e.g. θ is 98º between cpx and melt), and is 76º between opx and melt (Toramaru and Fujii, 1986). Thus melt percolation through the lower crust is unlikely and so rehydration of the lower crust by mantle melts.

(2) De-hydration of the Phanerozoic granulites via heating and partial melting from an underplated mantle. This would make sense if these granulites were associated with volcanism due to the underplating episode, which may have extracted the most differentiated magma with a large part of water to the surface, leaving the residues depleted in water in their source. In this scenario, two independent processes may exert some influences: fractional crystallization prior to and/or partial melting after the formation of these granulites can lower their OH contents; and if the initial water contents in both the Precambrian and Phanerozoic granulites (or original melts) were similar, relatively high degree of such dehydration is required. However, the extent of fractional crystallization for the Hannuoba xenolith granulites is only very low to medium (5-40%: Liu et al., 2001). While on the other hand, the lacking of depletion in LREE and other incompatible elements in both individual minerals (this study) and bulk rocks of the Hannuoba xenolith granulites (Liu et al., 2001) and of the Daoxian xenolith granulites (Dai et al., 2008) does not support notable partial melting after their formation; and furthermore, it is suggested that the incompatible behavior of H_2O during melting and crystallization is equally comparable to Ce (*e.g. Michael, 1995; and references therein*), so if partial melting happened to the Phanerozoic granulites after their formation, there should be correlation between Ce content and indices of melting (e.g. Mg#), which is absent in the Hannuoba xenolith granulites for pyroxenes (Fig. 6-4) and in the Daoxian xenolith granulites for their bulk compositions (*Dai et al., 2008*). This possibility is therefore not fa-

vored (the reason why we choose Ce instead of H_2O for such illustrations is that the H_2O content might be reset during the degassing processes without changing other elements).

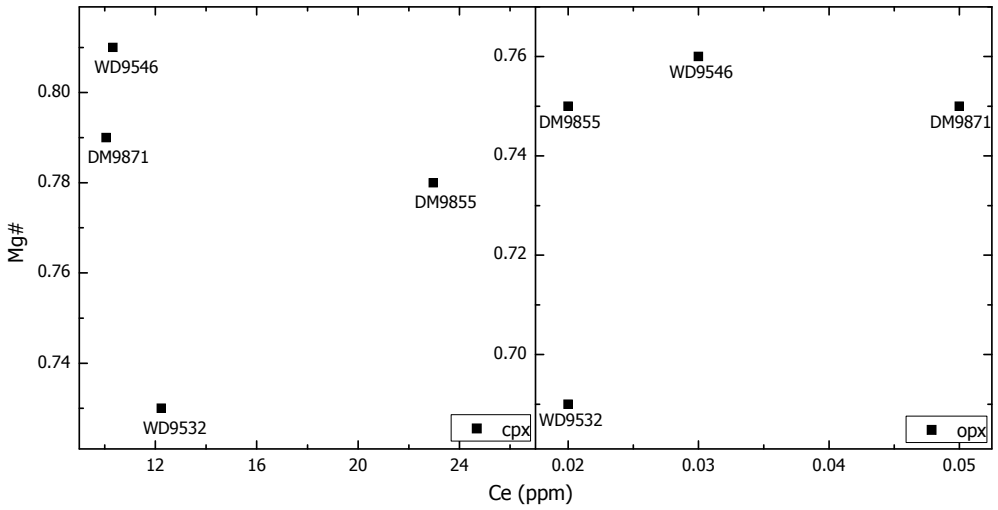

Fig. 6- 4 Mg# vs. Ce content for pyroxenes in the Hannuoba xenolith granulites

(3) It is possible that the heat provided by underplating melts induced significant H loss, e.g. through dehydration, in the Phanerozoic lower crust, but such thermal events did not produce any visible partial melting of the granulites (e.g. the above discussed (2)). In this case, the dehydration loss of H in the Phanerozoic granulites would be evidently larger than in the Precambrian ones. Nonetheless, the estimated difference in the extent of dehydration from their H-isotopic data, mainly in the manner of H_2 loss, between the Hannuoba xenolith granulites and the Hannuoba terrain and Nushan xenolith granulites is on the first-order of only about 10% (see also Chapter 8), which would have no way accounting for the observed large difference in their water contents if their original concentrations were similar. This possibility is thus excluded.

(4) Percolation of fluids dominated by CO_2 was suggested by Newton et al. (1980) for the formation of granulites, and such percolation would effectively remove most of the water without changing major/trace elements markedly. The effects of CO_2 on granulite-facies metamorphism have been debated, as it

is argued recently that CO_2 probably plays a consequential rather than causal role on the genesis of granulites (Cesare et al., 2005). On the other hand, a pervasive percolation of CO_2 in the lower crust is in conflict with the observed inter-grain $\delta^{18}O$ heterogeneity, up to 2-3‰, on intra-grain homogenous samples even in <1 cm scale – – such micro-scale variations would be erased by the fluids (Chapter 8; see also Valley and O'Neil (1984)). And furthermore, if granulites were really involved with CO_2 for their genesis (e.g. influx of CO_2 produces the lower water content in granulites), it would be difficult to imagine that only the Phanerozoic granulites were markedly influenced by CO_2 to lower their water contents relative to the Precambrian ones. This possibility is therefore not favored.

(5) Secondary metasomatism by melts/fluids, responsible for the formation of amphibole in the Hannuoba terrain granulites, may play some roles in buffering/increasing the water content of the coexisting cpx, opx and plag. However, it has been suggested that the formation of secondary hydrous amphibole through later alterations or metasomatism consumes nearly all of the water available in the fluid phase (Andrut et al., 2003) or even in the coexisting NAMs (Peslier et al., 2002). In the former case the H content in the NAMs will remain unmodified while in the latter they can be notably lowered, e.g. via closed-system H re-distribution. In addition, the REE patterns of mineral grains in the Hannuoba terrain samples resemble those in the Hannuoba and Nushan xenolith granulites and no extreme variations in $(La/Yb)_N$ ratios of individual minerals can be observed between them, implying that these grains were not modified by later alteration or metasomatism (see Chapter 5 and 8). Finally, no hydrous phases occurring in the Nushan xenolith granulites show higher water contents. In addition, there is no apparent variation in water content between amphibole (chlorite or other hydrous phases)-bearing and –free samples, e.g. in the terrain granulites (*this study*), xenolith peridotites (*Peslier et al., 2002*) and granitic pegmatites (*Filip et al., 2006*)

(6) The water contrast was inherited from their original melts/protoliths. In this case, if the melts derived from the upper mantle, the water content of the upper mantle may have been higher in the Precambrian than in the Phanerozoic, which was then inherited by the lower crust formed from them. It is interesting to note that if the water content of the lower crust decreased from Proterozoic to Phanerozoic era, this could explain the large dispersion of water content observed for the Nushan granulites, which resided in the lower crust during this time interval. That is, the Nushan granulites may represent a mixture of Precambrian and newly formed Phanerozoic lower crust (Huang et al., 2004). Differently, water in the Hannuoba terrain granulites could be preserved from late re-equilibration due to its early exhumation.

In summary, our data suggest that the Precambrian continental lower crust in eastern China was more hydrous than the Phanerozoic one, and that the contrast in water contents may relate ultimately with the difference of water content in the original melts/protoliths. This may indicate that the ancient upper mantle in China was more hydrous, in agreement with the hypothesis that the upper mantle was more hydrous in the Precambrian than in the Phanerozoic (e.g. Stone et al., 1997). Several other implications from our data include: if the granulites formed during mantle upwelling and the source of upwelling was the deep mantle, our results would make a real difference between the upper and lower mantle degassing; alternatively, if formation of the early lower crust was related to the occurrence of superplumes, as proposed by Condie (2004), and buildup of the NCC was also related to a plume, as suggested by Zhao et al. (2001b), our results indicate that these plume-related melts were rich in water. So if superplumes accounted for the growth of the early lower crust in the NCC, the Precambrian upper mantle was not necessarily H2O-richer than the Phanerozoic one. Future research on the lower crustal granulites may shed light into which one of these hypotheses is correct.

6.6 Speculation on the high electrical conductivity in the lower crust

Magneto-telluric deep sounding measurements around the world have well demonstrated that the stable continental crust generally contains a broad zone, with the thickness of 10-20 km, where the electrical conductivity is anomalously high and then drops again to greater depth (e.g. Jones, 1992; Hermance, 1995; Glover, 1996). This anomalous zone is often well recognized in ancient cratons and typically appears in the middle to lower crusts, although its nature, depth and extent vary from place to place.

Many mechanisms have been suggested for interpreting the high electrical conductivity in the deep continental crust, chief of which are the presence of an interconnected network of aqueous fluids (Brace, 1971; Olhoeft, 1981; Lee et al., 1983; Hyndman and Shearer, 1989; Hyndman et al., 1993), of a continuous network of intergranular carbon or graphite films (Alabi et al., 1975; Duba and Shankland, 1987; Frost et al., 1989; Glover and Vine, 1992, 1994; Mareschal et al., 1992, 1995; Katsube and Mareschal, 1993), and of positive hole pairs (PHP) in NAMs recently proposed by Freund (2003). However, none of these models can be applied satisfactorily, because (1) it is now widely accepted that hydrous fluids will always be consumed through retrograde reactions (Yardley and Valley, 1997), as a result, no free fluid phases can present in the deep continental crust for a long duration; (2) there is no visible carbon or graphite film observed on deep crustal samples (Yardley and Valley, 1997), furthermore, a major problem is that interconnected carbon/graphite films, if present, would have to become disconnected worldwide at a depth of around 20 km — such a uniform loss of connectivity is highly unimaginable (Freund, 2003); and (3) PHP charge carriers dominate their electrical conductivity in the temperature range of 400-600 °C, and their conductivities decrease significantly above ~ 800 °C (Freund, 2003), which temperatures are, however, very common in the lower continental crust. Besides, the anisotropic behavior of the deep crustal electrical anomaly, at least horizontally in some areas (Hyndman et al., 1993), is difficult to explain by any of these three models.

Other models that have been investigated include the presence of hydrous minerals such as amphibole (Stesky and Brace, 1973; Van Zijl, 1978) or of melts (Hermance, 1979, 1995), and solid state conduction by other accessory phases such as magnetite (Parkhomenko, 1982; Duba et al., 1994) or clay minerals (Toussaint-Jackson, 1984). Each of these may be important locally but cannot explain the wide distribution of highly conducting electrical anomaly in the mid- to lower crust (Hyndman et al., 1993; Glover, 1996; Yardley and Valley, 1997).

The above discussions imply that, confronted with a choice for explaining the high electrical conductivity in the deep crust, none of the available models seems fully satisfactory. Therefore, we have to seek a new explanation. What is the way out?

In addition to the deep continental crust, the asthenospheric mantle is also characterized by high electrical conductivity (e.g. Hermance, 1995; see also the supplementary figure in the end of this chapter). The electrical anomaly in the upper mantle has been accepted to result from enhanced hydrogen diffusion in olivine (Karato, 1990), and the possible effects of H_2O or H on electrical conductivity in the upper mantle have been well documented by recent experimental studies (Huang et al., 2005; Wang et al., 2006). This has initiated a series of investigations on the remote sensing of water in the deep earth (e.g. Tarits et al., 2004; Ichiki et al., 2006). Logically, can this approach be applied to the deep continental crust?

The effects of hydrogen species on the electrical conductivity of a solid can be approximated by the Nernst-Einstein relation (Mott and Gurney, 1948)

$$\sigma = fDcq^2/kT$$

where σ is the electrical conductivity, f is a numerical factor (correlation) nearly equal to unity, D is the diffusivity, c is the content, q is the electrical charge of the charged H species, k is the Boltzmann constant and T is the temperature. This equation will be used in the subsequent calculations towards a theoretical

approximation about the possible influence of H-species in nominally anhydrous granulite minerals on the high electrical conductivity in the deep continental crust.

Table 6- 2 Estimated water content for granulite cpx, opx and plag from conductivity

Mineral	References	Orientation	D (m^2/s)	Calculated water content (ppm)			
				0.0001S/m		0.01S/m	
				H/Si	H_2O	H/Si	H_2O
cpx	Woods et al. (2000)	[100]	3.03E-11	7.12E+01	5	7.12E+03	457
		[001]	3.04E-11	7.08E+01	5	7.08E+03	454
opx	Stalder & Skogby (2003)	[001]	5.89E-12	3.66E+02	23	3.66E+04	2347
plag	Kronenberg et al. (1996)	[001]	1.36E-11	1.59E+02	10	1.59E+04	1017

The calculations were applied on the individual cpx, opx and plag minerals, respectively. The diffusion coefficient for cpx is from Woods et al. (2000), opx from Stalder and Skogby (2003), and plag from Kronenberg et al. (1996). The report of Kronenberg et al. (1996) is actually for K-feldspar, and there is at present no available data about hydrogen diffusion in plag, so an assumption is made that the diffusion rate of hydrogen in plag is similar to that in K-feldspar. The other parameters are set as temperature of 900°C (based on the equation, the content (c) increases linearly with T if the other variables were given, slight variation in T, e.g. 100°C, leads to minor change in c) and electrical conductivity of 10^{-4} to 10^{-2} S/m (http://www.ees11.lanl.gov/EES11/Staff/Shankland/conductivity.html), and the results are provided in Table 6-2.

The yielded data demonstrate that, in order to produce the 10^{-4} to 10^{-2} S/m electrical conductivity in the deep crust, the required water content is about 5 to 450 ppm for cpx, 20 to 2350 ppm for opx and 10 to 1020 ppm for plag. These data are nearly consistent with the measured water contents (Table 5-7), indicating the likelihood that H-species structurally bound to granulite minerals can result in the high electrical conductivity in the deep continental crust. This model would have many advantages relative to the other available mechanisms, especially in terms of the possible anisotropic behavior of the conductivity in

the deep crust.

However, the above calculations are only from a theoretical approximation, further experimental studies about the relationships between H_2O content and electrical conductivity of deep crustal samples are necessary for casting light on the hypothesis. In fact, we have to admit that there are many assumptions and simplifications during the computation, such as (1) the influence of pressure on the diffusion rate of hydrogen and solubility of water content was not taken into consideration; (2) the diffusion coefficient used in the calculation should be the self-diffusion coefficient of hydrogen but not the chemical-diffusion coefficient, as used in our calculation and in that of Karato (1990); and (3) it was suggested that only proton, rather than all the structurally dissolved hydrogen, contribute to the enhancement of electrical conductivity inside the deep Earth (e.g. Huang et al., 2005), while this was not strictly differentiated in the above calculations.

For a reference, electrical conductivity anomalies inside the deep earth are illustrated in the figure below:

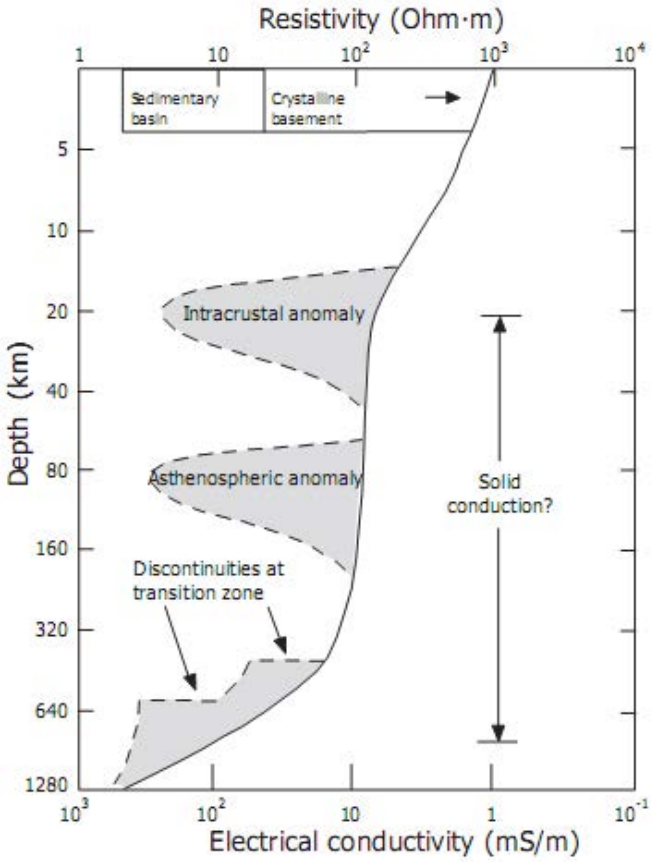

Figure illustration:

Two most significant electrical conductivity anomalies in the deep Earth were found by magneto-telluric measurements (Hermance, 1995): one in the middle to lower but mostly in the lower crust, the other one in the asthenospheric mantle.

7 Water in the deep continental lithosphere beneath the North China Craton

In this chapter, the attention is focused on the water content of minerals in the mantle peridotites from the NCC and on the variation of water content, both laterally and vertically, in the deep continental lithosphere. For the 1st time, the vertical contrast in water content between the lower crust and the underlying lithospheric mantle is discussed, and their possible influences on the rheological viscosity of the deep continental lithosphere beneath the NCC are quantitatively estimated.

7.1 Preservation of initial water content in mantle minerals

Similar to the discussions in the Chapter 6, in terms of the preservation of initial water content in the granulite minerals, the following evidences suggest that the pyroxenes in the peridotite samples record their original H information.

(1) All the samples are chemically homogeneous for individual phases, and no major element compositional zoning was observed for each studied grain.

(2) The FTIR analyses were usually performed in the core region of clean, crack- and inclusion-free grains of relatively large size. It is thus inferred that the loss of hydrogen caused by diffusion during the quick ascent would be very small (Peslier and Luhr, 2006).

(3) Profile analyses across some grains in these peridotites reveal that the H-related IR absorption is usually homogeneous between their core and rim region (Figs. 5-18 and 5-19), indicating negligible depletion or enrichment of H from diffusion or exchange.

(4) The studied samples are usually very fresh, and all the spectra show no signal of any evident hydrous phases, which would produce sharp bonds in the region of >3660 cm^{-1}. In this case, there is no evident interference from

other H-bearing phases, neither any exchange of H between them.

(5) The excellent correlation with respect to the H_2O content between cpx and opx (Fig. 5-20), with a linear coefficient of ~ 2.1, favors the preservation of their original water content (Grant et al., 2007a).

(6) The relationships between Al_2O_3 (%) and H_2O (ppm) in opx for the two suites of peridotites (Fig. 5-21) indicates that the dissolution of hydrogen in these minerals is combined with that of Al^{3+}, whose diffusion coefficient is so low that significant loss is unlikely, neither the hydrogen abundance.

The above discussions imply that the pyroxenes in the peridotite samples mostly preserve their source H_2O concentrations. By contrast, the olivine grains in these samples generally show no or only very weak IR absorption (Fig. 5-16). The very low, if present, H_2O content of olivine relative to pyroxenes is actually very common in natural mantle peridotites (Demouchy et al., 2006; Peslier and Luhr, 2006; Grant et al., 2007a), and is usually ascribed to a significant diffusion loss of initial water during their ascent to the surface (Ingrin and Skogby, 2000; Demouchy et al., 2006; Peslier and Luhr, 2006), because of the faster H diffusion in olivine than in pyroxenes (Kohlstedt and Mackwell, 1998, 1999; Hercule and Ingrin, 1999; Woods et al., 2000).

7.2 Estimation of the ascent rate of xenolith/ hosted alkaline basalts

If assuming that cpx, opx and olivine in the studied peridotites were initially in equilibrium with each other in terms of their H_2O content and that pyroxenes mostly preserve their initial H_2O content as noted above, we can estimate the original water concentration of olivine in the mantle source, based on the water data in the coexisting pyroxenes and if the partition coefficient of H_2O between pyroxenes and olivine are given.

However, the available partition coefficient between pyroxenes and olivine, $D_{cpx/olivine}$ and $D_{opx/olivine}$, obtained from both natural samples and experimental

investigations are highly variable between different publications, e.g. Koga et al. (2003) determined $D_{opx/olivine}$ of 12±2, Aubaud et al. (2004) measured $D_{cpx/olivine}$ of 12±1 and $D_{opx/olivine}$ of 9±1, Bell et al. (2004) quantified $D_{cpx/olivine}$ of 3.0±0.5 and $D_{opx/olivine}$ of 1.6±0.2, Hauri et al. (2006) presented $D_{cpx/olivine}$ of 9-21 and $D_{opx/olivine}$ of 1-16 and Grant et al. reported $D_{cpx/olivine}$ of 88.1±47.8 and $D_{opx/olivine}$ of 40.7±19.8 for spinel peridotites and of 22.4±24.1 and 11.7±9.5 for garnet peridotites in (2007a) and $D_{opx/olivine}$ of 25±1 in (2007b). Instead of using these coefficients, we assume a value of 10 for $D_{cpx/olivine}$ or of 5 for $D_{opx/olivine}$ as those discussed by Hirth and Kohlstedt (1996), which seems reasonable estimate for the upper-most mantle (e.g. <100 km) according to Hirschmann et al. (2005).

By using these partition coefficients, we were able to recover the original water content of olivine, ranging from ~ 0 to 35 ppm (Table 5-10).

A simplified form of the Fick's second law for one-dimensional diffusion in a solid was employed for the estimation, it can be expressed by (Ingrin et al., 1995)

$$C_{\mathrm{av}} = \frac{8C_0}{\pi^2}\sum_{n=0}^{\infty}\frac{1}{(2n+1)^2}\exp(-\frac{Dt(2n+1)^2\pi^2}{4L^2})$$

where C_{av} is the water concentration at time t, C_0 is the initial concentration, D is the diffusion coefficient of H, and 2L is the width of grain along the diffusional direction. Parameters for the approximation are: D is estimated, for a minimum value, ~ 5.0×10^{-11} m^2/s at 1250°C and 1.0×10^{-10} m^2/s at 1300°C, based on the recent compiled data in Ingrin and Blanchard (2006); the average width is ~ 2.4 mm as estimated on many grains; C_{av} contained in the olivine is estimated ~ 0.01-0.1 ppm from FTIR detection for a boundary condition, instead of 0 ppm for a use in the diffusion equation; C_0 is assumed 20-35 ppm and homogeneous across the grain. The yielded average duration time is ~ 8 to 26 hours for all the cases covering by the above starting conditions, and the average ascent rate is, assuming a depth origin is 60-70 km, approximated ~ 1-2 m/s for the xenolith

samples and, by extension, their hosted alkaline basalts (for a nearly adiabatic ascent). This estimate is probably a minimum for the basaltic magma, because the xenoliths are denser than the hosted magma. Such rapid ascent toward the surface is consistent with the fresh aspect of various xenoliths. The ascent rates are slower than the 4 m/s rate for volatile-rich kimberlitic magmas based on Ar diffusion profiles in phlogopite-bearing ultramafic xenoliths (Kelley and Wartho, 2000), but similar to the about 1 m/s rate estimated for xenolith granulites from Pali-Aike, Patagonia, Chine (Selverstone and Stern, 1983).

7.3 Lateral variation of water content in the continental lithosphere

The FTIR results show that the H_2O content of cpx and opx in the xenolith peridotites from Hannuoba and Nushan varies evidently, ranging from 5 to 350 ppm and from 5 to 140 ppm, respectively, and that the samples from Hannuoba are relatively drier than those from Nushan (Table 5-10; Fig. 5-20). The latter is probably due to metasomatism of subducted oceanic crust in the Nushan area (Xia et al., 2004). Subduction hydrates the upper mantle above the downgoing plate, as hydrothermally altered oceanic crusts or water-saturated sediments undergo dehydration and metamorphism, forcing water out of the subducting slab and into the overlying mantle wedge (Peacock, 1993). As a possible result, peridotites in the subduction-modified mantle wedge areas are virtually wetter than in other normal mantle regions (Peslier et al., 2002; Dixon et al., 2004).

Water content for cpx and opx in mantle peridotite xenoliths from different regions, including data from this study on Hannuoba and Nushan and those on West Kettle River in British Columbia, Lesotho, Namibia, Premier, Kimberley and Jagersfontein in South Africa, Simcoe & New Mexico in USA and Massif Central in France and also several other regions reported by Bell and Rossman (1992b), Peslier et al. (2002) and Grant et al. (2007a), are compiled and illustrated in Fig. 7-1. The results indicate that the distribution of water in the lithospheric mantle beneath the NCC, or on a larger scale (e.g. globally), is laterally heterogeneous.

The water contents of mantle pyroxenes from the NCC are obviously lower than those from the other domains.

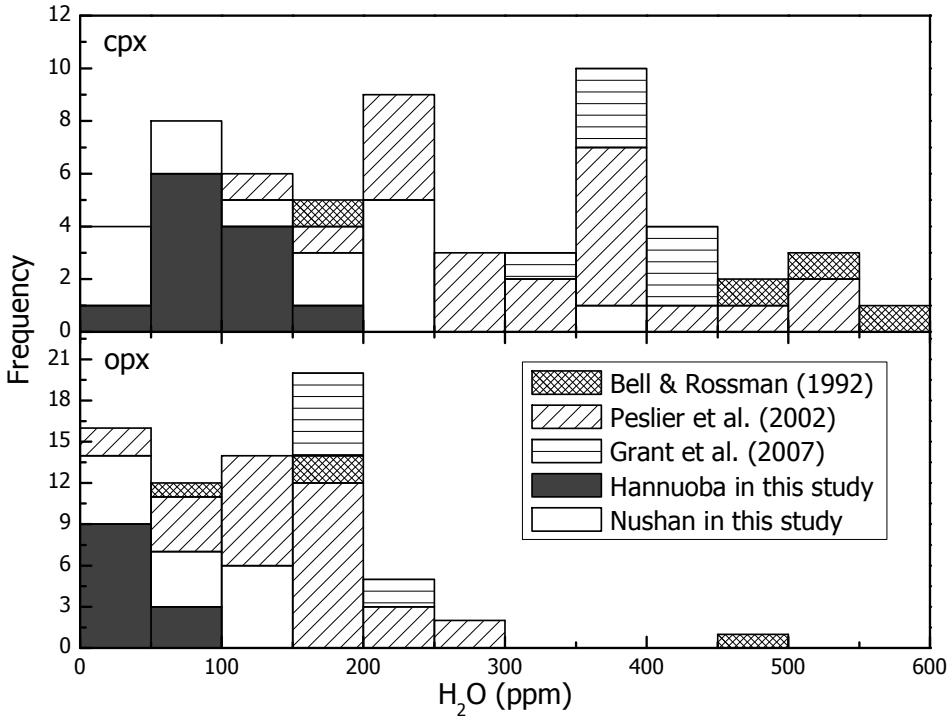

Fig. 7- 1 Lateral variation of water content in mantle pyroxenes

Such lateral variation may result from any of the following scenarios. (1) Distribution of water in the upper-most mantle depends on the geological environments, as argued by Skogby et al. (1990). The lithospheric mantle below Nushan may have been markedly influenced by subduction-released fluids, by contrast it seems absent beneath Hannuoba. This may affect, at least in part, their water contents. (2) Peridotites are the residues of different hydrous partial melting events in different regions, such as under normal mantle regions, in mantle wedges or in water-enriched regions (e.g. E-MORB or OIB), or they may have been disturbed by the later introduction of hydrogen (Bell and Rossman, 1992b). These source characteristics may be recorded or reflected in the water content of peridotites. (3) Variable extents of partial melting are involved in the generation of peridotites between different regions or even in the same area. This will influence the partitioning of H, because of its incompatible behavior,

between melts and residues, thereby producing variable OH contents. (4) If the water content of the upper-most mantle evolves as suggested by some studies (e.g. Stone et al., 1997), peridotites formed in different periods may dissolve different amounts of water. This requires a coupled chronological investigation on the sample subjecting to a water content measurement. (5) Metasomatism caused by melts/fluids can modify the hydrogen contents in peridotite minerals (Peslier et al., 2002), as mentioned before. The above several aspects are not totally exclusive and it is possible that all, or a few, of them have operated to some extent on the lithospheric mantle with respect to the lateral variations in water content.

In terms of the Hannuoba and Nushan samples, if the H_2O content of their mantle source was similar, differences in the extent of partial melting, heat perturbation from upwelling magma, and/or influences from subducted slabs may contribute to the different concentrations of water in them, implying that the average degree of partial melting was higher for the peridotites from Hannuoba than from Nushan, and/or that the dehydration loss of hydrogen in peridotites caused by heat flux from underplating magma was more evident at Hannuoba than at Nushan (or mantle upwelling was more violent at the former than at the latter). The markedly lower water content of pyroxenes from the lithospheric mantle below the NCC, relative to the other regions around the world (Fig. 7-1), is probably linked to its geological environment and tectono-thermal evolution. The widespread magmatic events or thermal reactivation/replacement from the Paleozoic to the Cenozoic have destroyed much of the lithospheric keel of this craton (see a recent review by Menzies et al., 2007), and the heat provided by these magmas may have induced further melting of the lithospheric mantle and diffusional loss of hydrogen, determining its characteristic lower water content.

7.4 Vertical variation of water content between the lower crust and upper mantle

The most interesting result from the FTIR measurements on the Hannuoba and Nushan xenolith samples is that cpx and opx, as well as the estimated bulk rock H_2O data (plag in the granulites commonly have higher water content than olivine in the peridotites), in the granulites contain obviously more water than those in the peridotites (Fig. 7-2), indicative of a more hydrous lower continental crust than the underlying lithospheric mantle, at least beneath the NCC.

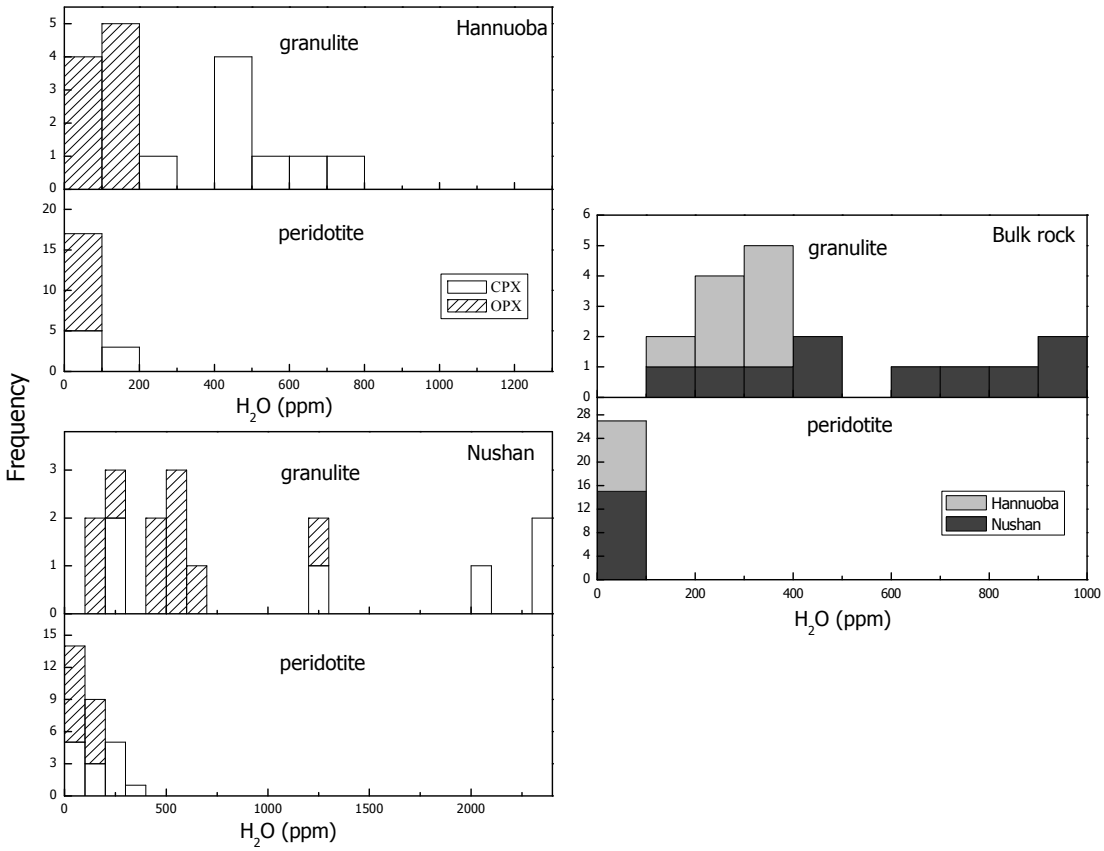

Fig. 7- 2 Water contrast between lower crust and upper mantle at Hannuoba and Nushan [The left panel illustrates the individual cpx and opx contrast for Hannuoba (upper) and Nushan (lower); the right panel illustrates the estimated bulk rock water content contrast]

The difference in water content between the lower crust and upper mantle, in terms of both the individual minerals and bulk rock, may be linked with the formation processes of granulites and peridotites. It is generally accepted that peridotites represent the residues of mantle partial melting after the extraction of basalt melts (e.g. Salters and Stracke, 2004; Workman and Hart, 2005), and

that H behaves incompatibly during mantle melting and subsequent shallow differentiation processes (Michael, 1995). Partial melting in the upper mantle will therefore markedly lower the water content of peridotite minerals. Here we do some calculations to illustrate the trends in water content variation during these processes. Assuming that: (1) the initial H_2O content of the upper mantle source is 50-600 ppm (e.g. Ingrin and Skogby, 2000; Hirschmann, 2006), (2) the partition coefficient of H_2O between peridotite and melts is ~ 0.02 (Michael, 1995; Danyuschevsky et al., 2000; Hauri et al., 2006), and (3) the melting process involves 5-25% batch partial melting (e.g. for the studied peridotites), the water content in the residual peridotites and melts is around 5-170 ppm and 200-8500 ppm, respectively. Considering the data in Table 5-10, the bulk water content of the Hannuoba and Nushan peridotites falls mostly in the 0-100 ppm range (only water in the main phases was included in the bulk value since that the hydrous amphibole was formed by later fluid-related metasomatism). If mafic granulites crystallized from these melts (many studies show that water in mantle melts varies from < 0.5% to > 6% (e.g. Wallace, 2005), and we here consider a water content of 200-8500 ppm for the purpose of estimation), assuming that the partition of H_2O between granulite and melts is similar to that between peridotite and melts and that 30-85% equilibrium fractional crystallization occurs, the water content in the crystallized products would be about 5-1000 ppm, which is similar to the estimated bulk water concentration in the studied granulites (Table 5-7); alternatively, if mafic granulites formed from subducted crustal materials, which are only rarely completely dehydrated and commonly contain some hydrous phases (e.g. amphibole), they would still preserve some water. In either case, the mafic granulites would contain a significant amount of water. Although these H_2O contents depend strongly on the initial H_2O content in the protoliths/melts, the extent of crystallization and the dehydration during granulite-facies metamorphism and subsequent partial melting in the deep crust (e.g. via the so-called intra-crustal differentiation), in most cases, including this one, the H_2O content in granulite minerals, and bulk

rock, is expected to be greater than in peridotites. This progressive enrichment in the water content, especially in melts during their evolution (e.g. by differentiation/crystallization), may also interpret why the upper continental crust (granite) is wetter than the lower crust (granulite).

Experimental studies have found that the solubility of water in minerals is strongly related to temperature, pressure and water activity (reviewed recently by Keppler and Bolfan-Casanova (2006)), as expressed by the following equation:

$$c_{OH} = A \cdot f_{H_2O}^{n} \cdot exp(-\frac{\Delta H^{1bar} + \Delta V^{solid} P}{RT})$$

where c_{OH} is water solubility, A is a temperature-dependent constant, f_{H2O} is the water fugacity, n is an exponential factor related to OH dissolution mechanisms, ΔH^{1bar} is the reaction enthalpy at 1 bar, ΔV^{solid} is the volume change of solids, P and T are pressure and temperature, and R is the gas constant. If applying the experimental results of cpx (Bromiley et al., 2004) and opx (Rauch and Keppler, 2002) into our estimations, and assuming that the water fugacities in the lower crust and upper mantle below the NCC are close to the experimental ones (this assumption is appropriate for only a very rough evaluation here), pyroxenes in the deep crustal xenolith granulites from both Hannuoba and Nushan are found to be mostly water saturated or even water super-saturated, and those in the mantle peridotites mostly water undersaturated. This implies the following: (1) water fugacities in the lower continental crust are much higher than previously estimated, and they greatly affect water content in the granulite minerals. (2) the crystal structure of the host minerals may be more important than T and P in determining water content. Cpx and opx in mantle peridotites are magnesian (close to the end-member composition of diopside and enstatite, respectively), so their structures are very close-packed and their ability to accommodate large OH anions is limited; in contrast, the Fe-rich pyroxenes in mafic granulites have less close-packed structures which allow a greater range of substitutions of

trivalent and quadrivalent ions, they can incorporate larger amounts of OH. (3) laboratory-simulated high-T (and P) experimental results cannot be applied to relatively low-T (and P) deep crustal conditions without any correction, because it is possible that at low-T totally different substitution mechanisms occur, which are not observed at high-T. In fact, a recent report found that a large amount of water can be incorporated into Al-opx at low-T (and P) (Mierdel et al., 2007). However, the marked difference in Al_2O_3 content between opx in the granulites and those in the experiments (Mierdel et al., 2007), e.g. by a factor up to ~ 10, probably makes it not appropriate to apply their new experimental parameters to the solubility equation for a quantitative estimation of the hydrous status of our natural granulite samples, because it is well known that Al^{3+} may have a critical role in dissolving H into minerals, especially for opx (Rauch and Keppler, 2002; Stalder and Skogby, 2002).

For a reference, the H_2O content saturation of minerals with depth is also illustrated in the below figure.

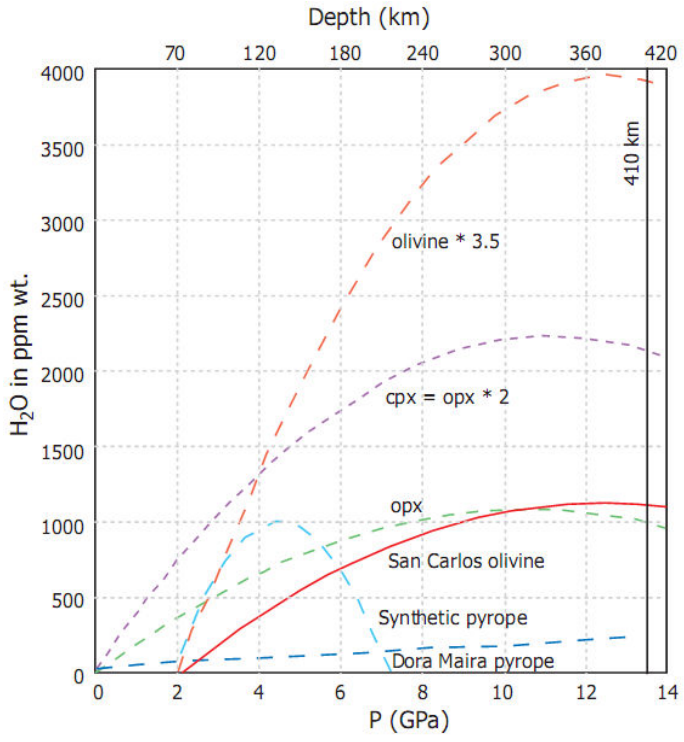

Figure illustration:

Water saturation of minerals with depth (after Bolfan-Casanova (2005)

7.5 Implications on the rheological viscosity of the deep continental

lithosphere

Quantitative estimates about the strength and/or viscosity of the Earth's lower crust and upper mantle in the present and past studies are largely based on the inversion of geophysical and geodetic data (e.g. Nishimura and Thatcher, 2003; Freed and Burgmann, 2004; Kenner, 2004) and on the extrapolation of laboratory measurements to natural environments (e.g. Kohlstedt et al., 1995; Hirth and Kohlstedt, 1996; Montesi and Hirth, 2003). Many recent studies on both natural and synthetic samples have established that the presence of even trace amounts of H_2O can dramatically enhance the deformation and therefore decrease the rheological strength of the dominant mineral constituents in the lower crust and upper mantle, such as feldspars (Tullis et al., 1996; Rybacki and Dresen, 2004; Rybacki et al., 2006), clinopyroxene (Hier-Majumder et al., 2005; Chen et al., 2006), and olivine (Mei and Kohlstedt, 2000a, 2000b; Karato and Jung, 2003).

The possible effects of water on the creep deformation of minerals and rocks can be approximated by a non-linear power law creep equation (Hirth and Kohlstedt, 1996; Mei and Kohlstedt, 2000a, 2000b; Hirth and Kohlstedt, 2003; Karato and Jung, 2003; Chen et al., 2006; see also a recent review paper by Kohlstedt, 2006):

$$\dot{\varepsilon} = A\frac{\sigma^n}{L^m} f_{H_2O}^r \exp\left(-\frac{E^* + PV^*}{RT}\right) \qquad (1a)$$

where $\dot{\varepsilon}$ is the strain rate, A is a constant, σ is the stress, n is the stress exponent, L is the grain size, m is the grain size exponent, r is the fugacity exponent, E^* and V^* are the activation energy and volume, respectively (the term "E^*+PV^*" is equal to the activation enthalpy, Q). Following the treatment generally used in many publications (Kohlstedt et al., 1995; Hirth and Kohlstedt, 1996; Mei and Kohlstedt, 2000b, 2000a; Karato and Jung, 2003; Dixon et al., 2004; Chen et al., 2006), the possible effects of oxygen fugacity on the strength are not considered in equation (1a). For dislocation creep, strain rate is inde-

pendent of grain size, so that the flow law can be simplified as follows:

$$\dot{\varepsilon} = A\sigma^n f_{H_2O}^r \exp\left(-\frac{E^* + PV^*}{RT}\right) \qquad (1b)$$

if Newtonian viscosity, η, is defined as $\eta = \sigma / \dot{\varepsilon}$, the strength at a given strain rate can be expressed as:

$$\eta = \dot{\varepsilon}^{\frac{1-n}{n}} f_{H_2O}^{-\frac{r}{n}} [A\exp\left(-\frac{E^* + PV^*}{RT}\right)]^{-\frac{1}{n}} \qquad (1c)$$

Equation (1c) was successfully applied by Dixon et al. (2004) to explain the low viscosity of the upper mantle beneath the western USA relative to the average global values, which was suggested by them to result from both higher water content and higher temperatures in the lithosphere mantle.

The rheological profile of the deep continental lithosphere beneath the NCC was defined based on equation (1c) and on the water data of minerals in the xenolith granulites and peridotites from Hannuoba and Nushan for different tectonic units (e.g. separated by the DTGL), respectively. For this purpose, the following assumptions and simplifications were proposed: (1) the strength of the deep crust and shallow mantle is dominated by dislocation creep (Ranalli, 1995); (2) water content variations with depth in the studied regions were not considered, and were assumed constant in the depth range of the lower crust and upper mantle (average values of the samples were used), respectively; (3) the strain rate in the continental lithosphere is $\sim 10^{-15}$ S^{-1} (Mackwell et al., 1998); (4) f_{H2O} in the deep crust was estimated on the basis of the relationship between H_2O content and H_2O fugacity suggested by Johnson et al. (2002) and revised recently by Johnson (2006); (5) the geothermal gradients at Hannuoba and Nushan are from Chen et al. (2001) and Huang et al. (2004), respectively; (6) the strength of the upper mantle is dominated by olivine (Hirth and Kohlstedt, 1996; Dixon et al., 2004), and the creep parameters are from Karato and Jung (2003) for water undersaturated conditions; (7) the strength of the lower crust at Nushan is dominated by plag (mafic granulites contain 60-85% plag: Table

3-3), and creep parameters are from Rybacki et al. (2006); and (8) the strength of the deep crust at Hannuoba is dominated by pyroxenes (mafic granulites contain up to 90% pyroxenes: Table 3-1), the water weakening of cpx and opx are assumed similar in the regime of dislocation creep for the lack of experimental data for opx, and creep parameters are from Chen et al. (2006) for cpx (assuming these parameters can also be applied to opx) and from Dimanov and Dresen (2005) for a 2-phase model with 75% diopside (An75Di in their report). If all the pyroxenes are regarded as cpx and considering the effects of grain size on the water content dissolved in the mineral grain (Rybacki and Dresen, 2004), the " average composition " (considering both the mineral proportion and water content) of the Hannuoba xenolith granulites (Tables 3-1 & 5-7) is comparable to the An75Di mixture. All the rheological parameters are compiled in Table 7-1. The neglect of oxygen fugacity in equation (1c) may not change the conclusion if assuming that, because the lowermost crust and uppermost mantle in each of the studied regions are very close, the oxygen fugacity in the two layers are similar and can thus be regarded as constant (Karato et al., 2008). The yielded rheological structure of the deep continental lithosphere below Hannuoba and Nushan are shown in Fig. 7-3a & b, respectively.

Table 7- 1 Material parameters used in the rheological calculation

	$A((Mpa)^{-n}/s)$	n	r	E^*(kJ/mol)	$V^*(cm^3/mol)$
cpx	$10^{6.7\pm0.1}$	2.7±0.3	3.0±0.6	670±40	0
olivine	$10^{0.56\pm0.02}$	3±0.1	1.2±0.05	410±40	11±3
plag	1.58	3	1.0±0.3	345	38
An75Di	$316^{\#}$	5.03±0.07	-	533	-

Data source: cpx, Chen et al. (2006); olivine, Karato and Jung (2003); plag, Rybacki et al. (2006); An75Di, Dimanov and Dresen (2005).

#: activation enthalpy, $Q=E^*+PV^*$; -: not reported.

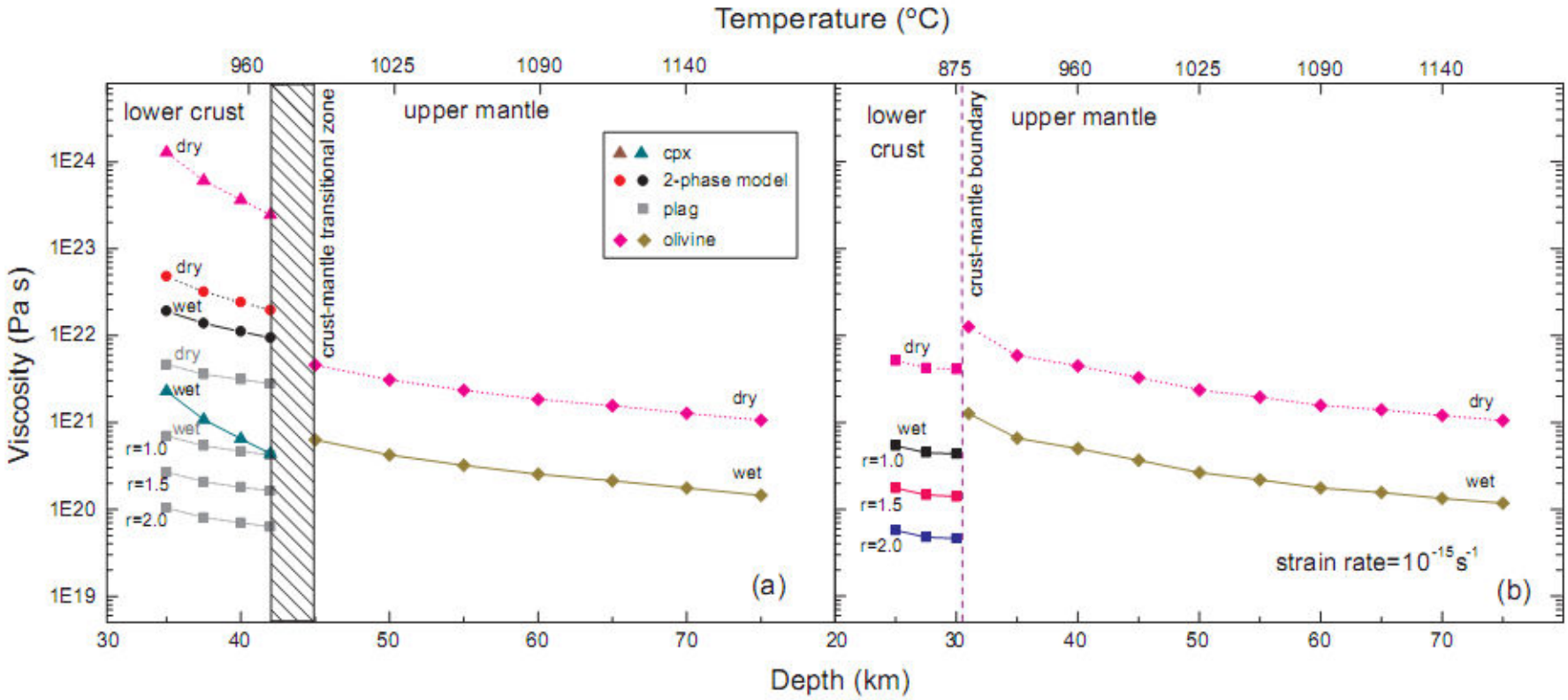

Fig. 7- 3 Rheological structure of the deep continental lithosphere at (a) Hannuoba and (b) Nushan

The estimated viscosity of the uppermost mantle beneath Hannuoba and Nushan are varying in the range of ~ 10^{20}~10^{21} Pa s, which are comparable to the viscosity structure for cratonic regions or global averages as compiled by Kaufmann and Lambeck (2002). The similarity in the viscosity profile between the Hannuoba and Nushan lithospheric mantle is probably related with the similar average water content for olivine, e.g. 10 vs. 15 ppm (Table 5-10), and the similar temperature gradients in these two regions (Fig. 7-3). Despite the resemblance in the lithospheric mantle, notable differences in the viscosity can be found for the lower crust between these two locations, which is on the order of magnitude of ~ 10^{21} to 10^{22} Pa s for Hannuoba and of ~ 10^{19} to 10^{20} Pa s for Nushan. The viscosity of the lower crust at Nushan is lower than that of the upper mantle, while at Hannuoba it is close to or higher than that of the upper mantle, depending on the model used. In the Hannuoba area, the viscosity yielded by the two-phase model of Dimanov and Dresen (2005) is higher by one order of magnitude than that of Chen et al. (2006). One interesting point is: if assuming that the rheological strength of the lower crust beneath Hannuoba were also dominated by plag as beneath Nushan, the viscosity-profile (illustrated by dotted-grey line in Fig. 7-3a) would be close to that in the latter (Fig. 7-3b) in spite of their significantly different water content (Table 5-7), implying that, in addition to water, temperature may as well have fundamental influences on the rheological viscosity of the lower crust, which conclusion is consistent with that proposed by Dixon et al. (2004) for the variation of rheology in the lithospheric mantle. Under dry conditions, the viscosity increases by about one order of magnitude in all these cases (Fig. 7-3a, b). These results indicate that the rheological strength of the deep continental lithosphere beneath the NCC is laterally heterogeneous, and that at this craton the lower crust can be stronger or weaker than the underlying lithospheric mantle. This sheds some light on the status of the lithosphere underneath the NCC.

The rheological difference between the deep crust and uppermost mantle

plays an important role in the stability/duration of the continental lithosphere (Burov and Watts, 2006). If the lower crust were stronger than the underlying uppermost mantle, or the strength of the lithosphere resided in the crust, the lithosphere would be thermally and mechanically unstable, and would easily disintegrate due to delamination/erosion of the mantle followed by its convective removal and replacement by the hot asthenosphere; by contrast, if a weak lower crust were sandwiched between a strong upper crust and a strong uppermost mantle and the total strength lay in the mantle region, the lithosphere would be dynamically stable for a longer time (Burov and Watts, 2006). In this context, an important implication from the predicted rheological architecture of Hannuoba and Nushan, e.g. relative to the lithospheric mantle the lower crust is stronger in the former and weaker in the latter, is that the lithospheric mantle beneath Hannuoba is not as stable as that beneath Nushan: the former can easily be modified, e.g. via delamination or thermo-chemical erosion, by mantle thermal convection or upwelling of the asthenosphere, whereas the latter may remain stable for a long period, possibly allowing the growth of newly accreted lithosphere beneath the previously reactivated mantle. Our results provide a critical basis for understanding the lithospheric model proposed for these two areas based on the geochemical investigation of basalts and mantle xenoliths (Xu et al., 2004a), which indicates that during the Cenozoic the continent has undergone lithospheric thinning at Hannuoba and lithospheric thickening at Nushan (Fig. 2-4). These contrasting lithospheric processes in the two regions may be easily triggered by the rheological structures established in this study, although further constraints from both experimental petrology and geophysics are required.

For a reference, stability test of the continental lithosphere below a normal (e.g. craton) region, from the numerical modeling of Burov and Watts (2006), is illustrated as following.

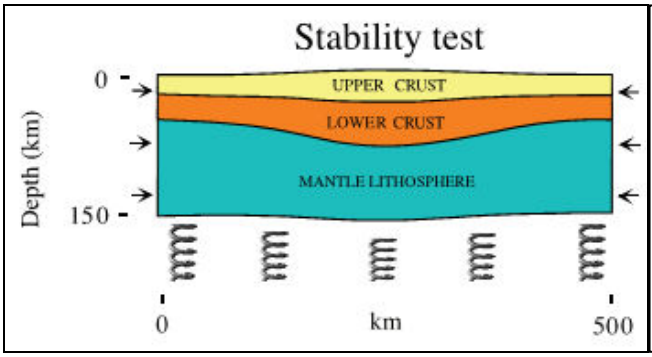

Starting conditions:
A mountain range height of 3 km and width of 200 km, initially in isostatic balance with a zero elevation of 36-km-thick crust, was disturbed by applying a horizontal compression to the edges of the lithosphere at a rate of 5 mm/yr.

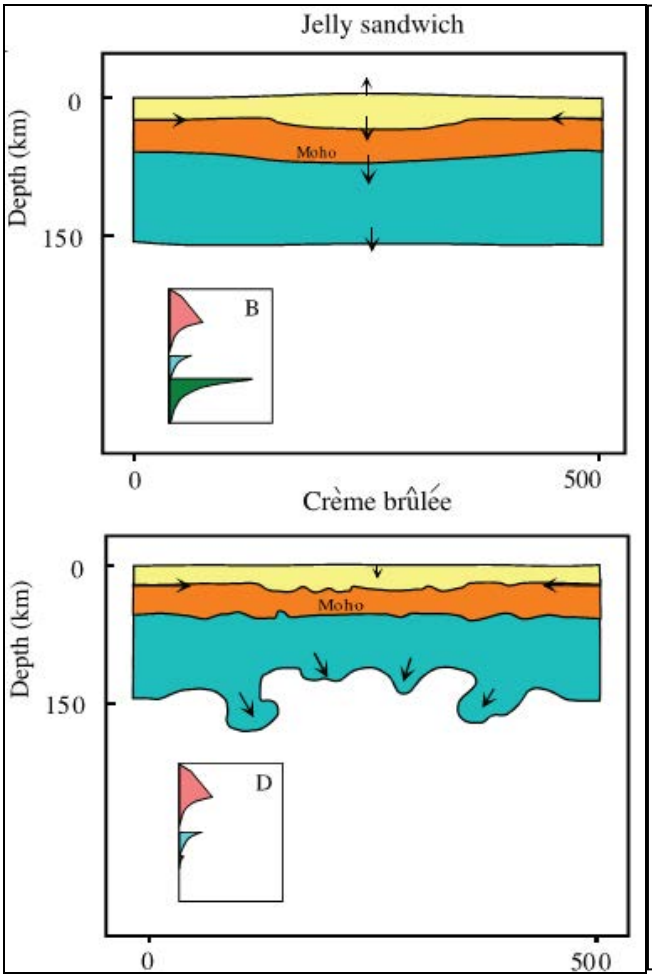

After 10 Ma:
The crust and mantle are stable if the lower crust is weaker than the upper mantle, and opposite state can be observed if the lower crust is stronger than the upper mantle

In the 2nd model, the lithosphere disintegrates due to delamination of the mantle followed by its convective removal and replacement with hot upwelling magma, which leads eventually to a flattening of the Moho and tectonic erosion of the crustal root that initially supported the topography.

The 1st model is more stable, and there is almost no modification of its initial status during such 10 Ma

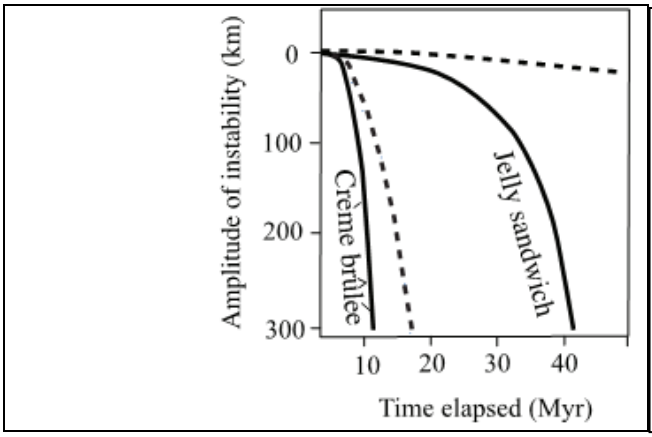

Stability of the mantle root.
The evolution of a marker that was initially positioned at the base of the mechanical lithosphere are in strong contrast between the 2 models, yielding the same result that the lithosphere is not that stable if the lower crust is stronger.

8 REE distribution and H-O-Li stable isotopes of lower crustal granulite minerals

In this chapter, the SIMS-yielded data, including REE partitioning between the coexisting lower crustal granulite minerals, and their hydrogen, oxygen and lithium isotopic compositions, are compiled toward a thorough discussion, such as the equilibrium of REE in the lower crust, the distribution and variation of these stable isotopic species and their possible origins and implications. To our knowledge, this is the first time to perform a detailed, systematic and coupled investigation of multi-stable isotopes into the lower crust; in especial attention are the hydrogen and lithium isotopes, for which the former is the first attempt towards the hydrogen isotopic compositions of the lower crust and the latter is the first attempt towards the lithium isotopic compositions of the coexisting lower crustal assemblages and especially the microscale variations in the lower crust.

8.1 Partitioning of REE between coexisting phases

Similar to the partitioning of H between coexisting minerals, the partition coefficient (K_D) of certain REE between phase A and B is defined as the ratio of their content within these two phases, e.g. $K_D=C_A/C_B$, where C_A and C_B are the content of the element in A and B, respectively.

The partition coefficients of REE between the coexisting mineral pairs in these granulites have been calculated and the results are given in Fig. 8-1. All these mineral pairs, e.g. cpx-plag, opx-plag and cpx-opx, display virtually consistent distribution patterns, and usually the variation of K_D for certain element within a mineral pair is smaller than the determined elemental variability (or the absolute content) for a given mineral. This observation is especially pronounced for elements whose contents are relatively higher and are thus more easily and accurately analyzed. For example in our data, the greater variability of HREE in

the cpx-plag pair (Fig. 8-1), in contrast to the narrow variation of LREE, is likely caused by the larger analytical uncertainty involved with the determination of HREE in the plag. The K_D patterns in Fig. 8-1 also indicate that cpx is enriched in REE relative to opx and plag, and plag is enriched in REE relative to opx, as observed from their ΣREE abundances (Table 5-12).

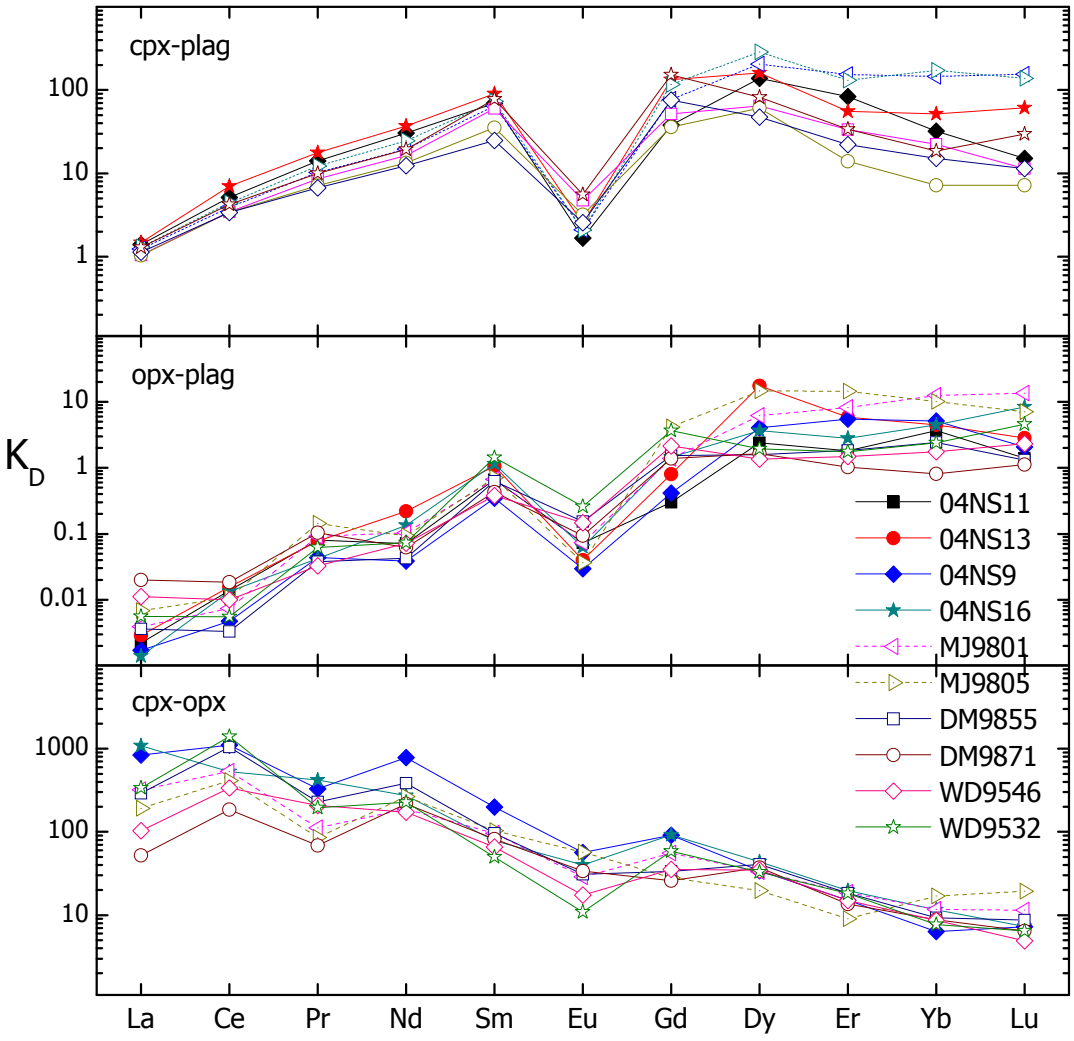

Fig. 8- 1 REE partitioning (K_D) between coexisting minerals in the granulite samples

The consistent K_D patterns and narrow K_D ranges for these mineral pairs (Fig. 8-1), and the similar REE distributions for individual minerals (Fig. 5-23) and the REE are mostly inter- and intra-grain homogeneous for each mineral in the same sample, imply that they approximate equilibrium in these granulites (Pride and Muecke, 1981).

8.2 Oxygen isotopic compositions

For each pyroxene grain under investigation, the $^{18}O/^{16}O$ ratios are mostly uniform according to the core to rim profile analyses, if considering the SIMS analytical uncertainty (Table 5-15).

8.2.1 Isotopic vs. cation exchange temperatures

The equilibrium isotopic temperatures recorded by the average $\delta^{18}O$ data of pyroxenes in the granulite samples are about 900°C (Fig. 8-2). If considering the possible analytical uncertainties and the resulting temperature errors, the estimated oxygen isotope temperatures concerning such refractory minerals as cpx and opx are in good agreement with the peak granulite-facies metamorphism temperatures derived from cation partitioning between these pyroxenes (800-950°C: Chapter 5) (Liu et al., 2001; Huang et al., 2004; and this study).

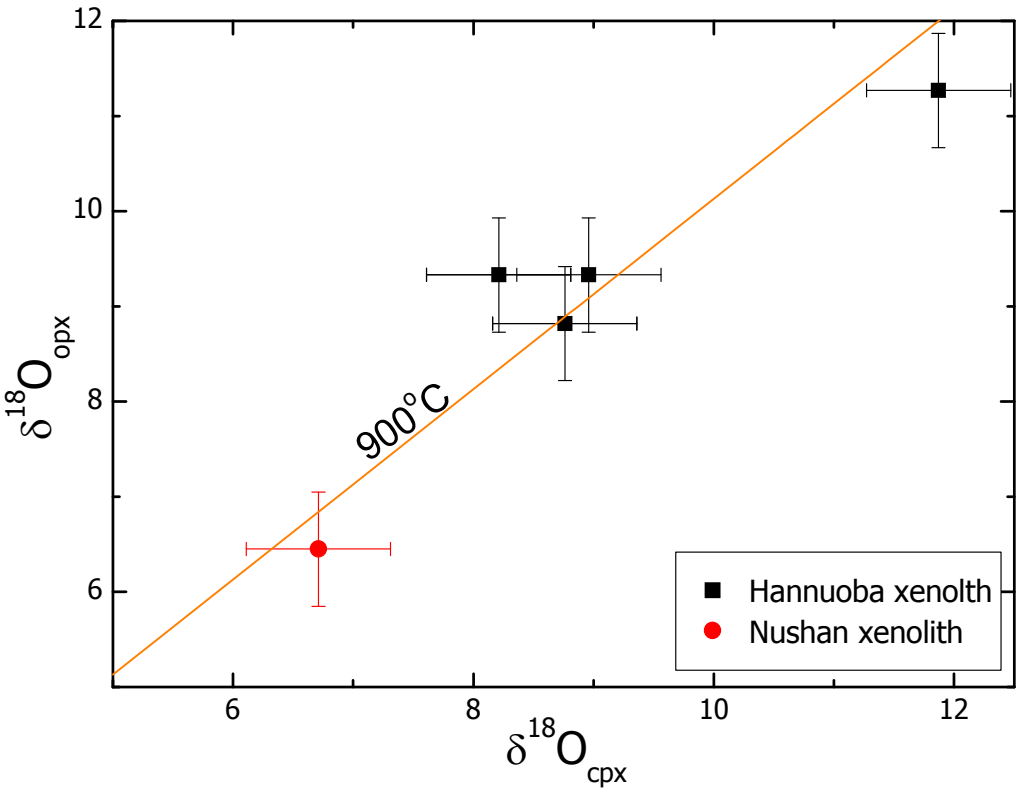

Fig. 8- 2 Isotherm plot for $\delta^{18}O$ fractionations between pyroxenes in the granulites (the theoretical 900°C equilibrium isotherm for pyroxenes is referred to Zheng (1993))

The consistency between the O-isotopic and petrological geothermometry strongly suggests that O-isotope equilibrium has been achieved and preserved at the formation temperatures of these granulites (e.g. Valley and O'Neil, 1984; Zheng et al., 2001). This not only points to a rapid cooling and ascent for these granulites during their transport/exhumation to the surface, but also rules out any significant later resetting, such as exchange between fluids (or melts) and minerals during these processes and the cooling of these samples. Presumably, we assume that this can be applied to all the other Nushan xenolith granulites, as well as the Hannuoba terrain granulites, in terms of the similarities in their formation ages, major and trace elements and H-, O- and Li-isotopic compositions (Huang et al., 2004; Guo et al., 2005; and data in this study). Further and more studies on minerals such as opx in the Nushan xenolith and Hannuoba terrain granulites, as well as plag in all these samples and the development of more suitable SIMS standards, may help clarifying these issues.

8.2.2 Recycled crustal materials during the petrogenesis

The oxygen isotopic compositions in the investigated granulite minerals are highly variable ranging from about 4.5 up to 12.5‰, and almost all of them are significantly higher than or nearly similar to the normal mantle of 5.7 ± 0.5‰ (Mattey et al., 1994; Harmon and Hoefs, 1995; Eiler, 2001). If assuming that plag in these granulites were in equilibrium with the coexisting pyroxenes in terms of their $\delta^{18}O$ values under the lower crustal conditions, on the basis of the equilibrium REE patterns and oxygen isotopic compositions in cpx and opx, the $\delta^{18}O$ of plag should be in the range of ~ 5 to 13‰ according to the theoretical equilibrium fractionation of O-isotopes between these minerals under high temperatures (Zheng, 1993). And therefore, the estimated whole rock $\delta^{18}O$ compositions of these granulites are approximately 5 to 12‰. Such variation is similar to the bulk $\delta^{18}O$ data of lower crustal granulite xenoliths from eight localities worldwide, 5.4~13.5‰, and nearly consistent with the range of mafic granulites, about 5~11‰ (Kempton and Harmon, 1992).

The large variations and markedly higher values (relative to normal mantle) of O-isotopic compositions in the studied mafic Hannuoba xenolith granulites cannot be accounted for by assimilation during their transport to the surface, because of the preservation of their peak-metamorphism isotopic values (Fig. 8-2) and the nearly constant $\delta^{18}O$ distributions within the sub-grain scales (Table 5-15); and furthermore, if such variations were produced during or after the exhumation by interactions with shallow/surface crustal rocks, the mafic compositions of these rocks, and their trace-element (e.g. REE) features, would have been strongly modified, which is obviously not the case in our samples. Therefore, the most likely mechanism which can result in such large range of higher $\delta^{18}O$ values, compared to the normal mantle, in the Hannuoba xenolith granulites under investigation is the hybridization of recycled crustal materials with the original mantle melts of granulite protoliths.

It is difficult to cast some constraints on the origin of such recycled crustal materials based on only the O-isotopic data here, e.g. continental or oceanic. Altered oceanic crusts are usually characterized by heavier $\delta^{7}Li$, e.g. more than 20‰ (Tomascak, 2004), and therefore the absence of high $\delta^{7}Li$ values in the granulites implies that their protoliths were not markedly influenced by oceanic crust. This agrees well with available studies from trace-element investigations which favor more the origin of continental crust for both Nushan and Hannuoba xenolith granulites (Liu et al., 2001; Huang et al., 2004). It is argued that the Nushan xenolith granulites were only weakly, if any, affected by such materials (Huang et al., 2004). This is consistent with our $\delta^{18}O$ data, which indicates that the Nushan xenolith granulites mostly have similar $\delta^{18}O$ as normal mantle (Table 5-15) and therefore they were not significantly modified by recycled crustal materials. If assuming similar origins and compositions between the Nushan xenolith and Hannuoba terrain granulites based on their similar major- and trace-elements, H- and Li-isotopic compositions (Chapter 5; shown later), the terrains should have not been modified to a large degree by crustal mate-

rials in terms of their protoliths.

8.2.3 Inter-grain $\delta^{18}O$ heterogeneities

The in situ SIMS analyses demonstrate that the pyroxene grains are nearly constant with their oxygen isotope compositions from core to rim regions (Table 5-15). Whether or not such intra-grain variations (0.6-1.0‰) denote within-grain zoning must await the improvement in the precision of ion microprobe analysis, however, relatively large differences in $\delta^{18}O$ up to ~ 2 to 3‰ (far beyond the SIMS analytical uncertainty) can be observed between different cpx grains even in the same sample, e.g. within less than 1 cm scale (Fig. 8-3).

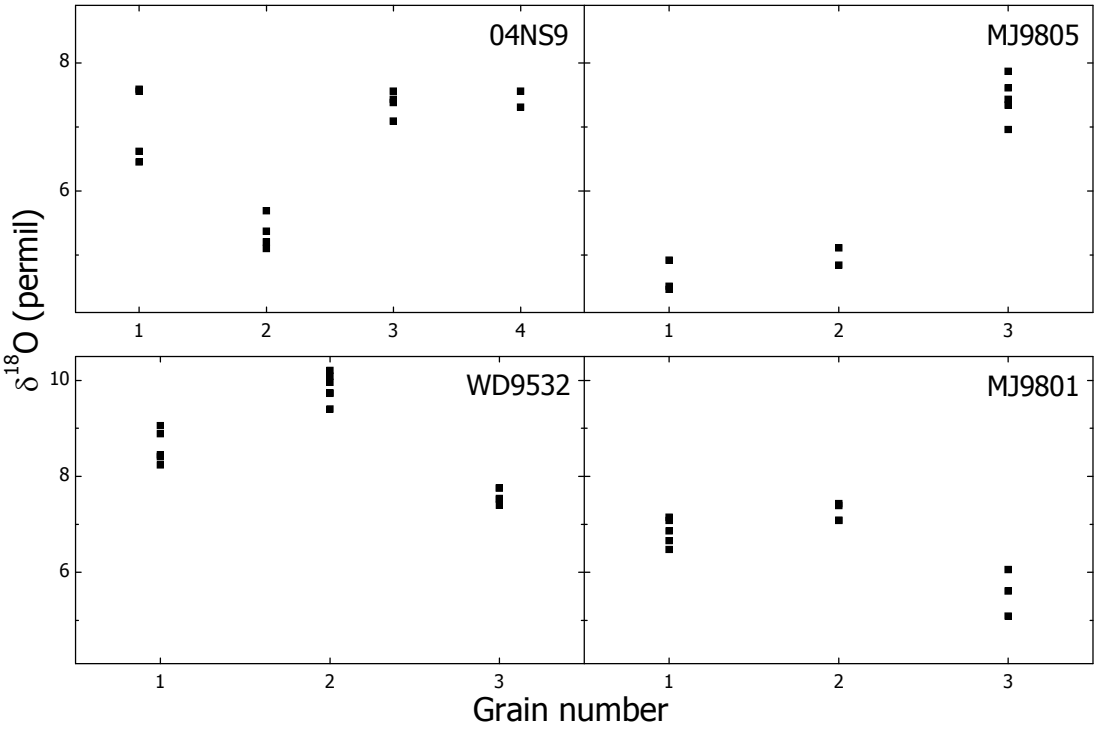

Fig. 8- 3 Inter-grain $\delta^{18}O$ variations of cpx in the granulites

The large, inter-grain $\delta^{18}O$ variations of cpx in the granulites, despite their formation ages, environments and localities, indicate the absence of pervasive fluids in the lower crust, even within very local scales (Valley and O'Neil, 1984; Kempton and Harmon, 1992). If in any cases fluids, derived either externally or by metamorphic devolatilization, are present in the lower crust, they flow most

probably along micro-channels but not pervasively, e.g. escape upwards rapidly (Valley and O'Neil, 1984; Yardley and Valley, 1997). Similar intra-grain uniform but inter-grain different distributions can also be found for Li contents, which have even larger variations, e.g. by a factor of 1-3 (Table 5-16).

The possible origins for the measured inter-grain $\delta^{18}O$ heterogeneities are difficult to address at present, probably including (1) the $^{18}O/^{16}O$ ratios of the melts were evolved with the growth of the mineral grains; (2) the original melts were not uniform in terms of the O-isotopic compositions; and (3) the $\delta^{18}O$ data of some grains were reset by micro-channelized fluids/melts. In spite of these issues, an important implication from such inter-grain heterogeneous but intra-grain homogeneous $\delta^{18}O$ data is that the diffusion-driven homogenization is probably active only in the subgrain scale, in this case the individual grains are uniform with their O-isotopic ratios along the core to rim transect, and cannot exert an apparent influence beyond one grain upon another one, so that the inter-grain $\delta^{18}O$ differences could have been maintained for long durations (e.g. since their peak metamorphic periods yielded by Zircon U-Pb dating).

One possible mechanism accounting for this is that the elemental/isotopic species (e.g. oxygen here), once diffusing out of one grain, would preferentially escape along the interspace between the neighboring grain boundaries rather than enter another grain (Fig. 8-4), especially when certain medium is present in the interstice in which the species are mobile. This can be further understood from the thermodynamic and kinetic aspects: obviously more activation energy (entropy) is required for the species, diffused out of one grain, to traverse the grain boundary of another grain, and thus go deep into its interior, than escape along the grain boundary or the space between the boundaries. It is very likely that some species, either elements or isotopes, do not have enough energy to penetrate into another grain. However, further studies including measurements on more grains and samples with respect to the inter-grain heterogeneities of O isotopes, as well as experimental investigations of grain boundary influences on

the mobility/diffusion of individual species, are seriously necessary for a better knowledge of the hypothesis presented here.

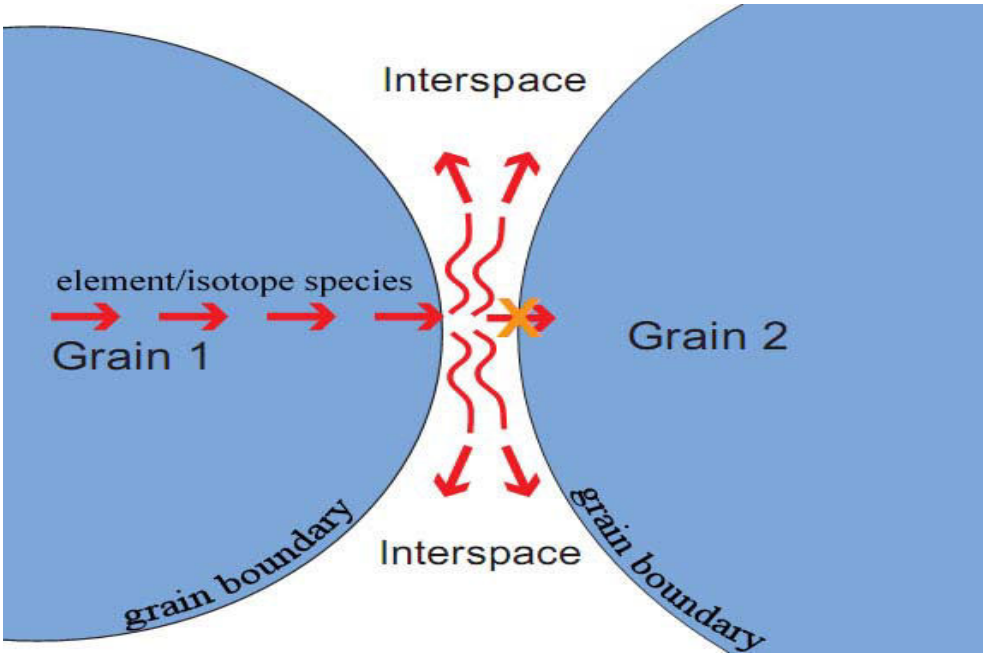

Fig. 8- 4 Cartoon illustrating diffusion-induced element/isotope mobility

8.3 Hydrogen isotopic compositions

The large δD variability for cpx and plag contrasts sharply with the relatively uniform major elements and REE contents in each sample, and with the narrow differences of these species between different samples from the same locality. Therefore, the δD variations should not be ascribed to the chemical differences (Suzuoki and Epstein, 1976). Besides, no regular zone of δD from core to rim in the mineral grains, and no systematic covariance between D/H ratios and IsH and/or between δD and H_2O for individual minerals (Table 5-13, Fig. 5-25), can be observed in these granulites. This, coupled with the unaltered/fresh nature of the analyzed phases and the small δD range for modern meteoric water in East China (-70 to -40‰: Zhang, 1985), also excludes the possibilities that the δD variations were caused by exchange of H with melts during eruption or with meteoric water at the earth surface, by slow cooling or by hydrothermal alterations (Kyser and O'Neil, 1984; Xia et al., 2002; Stone et al., 2005). The

yielded δD data, therefore, probably reflect their original compositions in the continental lower crust. This agrees well with that these granulites have probably preserved their primary hydrogen information, as predicted from H profile measurements conducted on mineral grains by FTIR and SIMS (Chapter 5).

8.3.1 Fractionation of H-isotopes between cpx and plag

Some samples show large intra-grain δD variations up to about 80‰ (Table 5-13). The diffusion of hydrogen under high temperatures, e.g. >800 °C, is so fast, 1-3 orders of magnitudes greater than Li (Ingrin and Blanchard, 2006; and references therein), that δD heterogeneities within sub-grain scales (e.g. 1 mm) could be eliminated within hundreds to thousands of years. The measured δD heterogeneities within some grains in the granulites are therefore suggested to result from recent events, such as shortly before or during their entrainment by host basalts. However, most grains show nearly homogeneous δD profiles (Table 5-13), indicating that they remain unmodified in terms of their initial δD compositions.

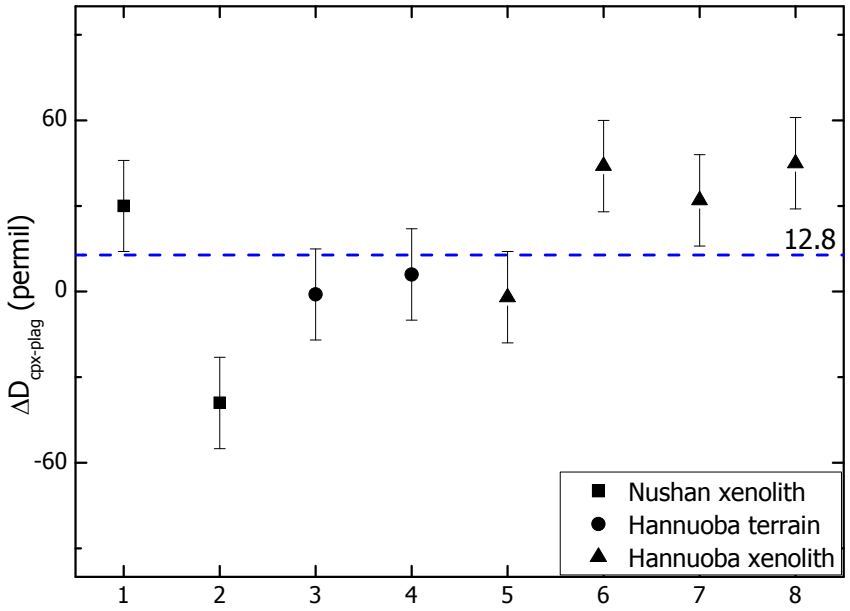

Fig. 8- 5 Isotopic fractionation of H between cpx and plag in the granulites (the dashed line was drawn at 12.8‰ for reference)

If following the relationship between the fundamental OH stretching frequency of a given mineral and the measured difference in isotopic composition between minerals and referred phase, established by Dobson et al. (1989) and revised recently by Bell and Ihinger (2000), and assuming that the weighted mean OH stretching frequency of plag is ~3400 cm^{-1} estimated from the data of Johnson and Rossman (2004) and this study, we will obtain that the theoretical D/H fractionation between cpx and plag ($\Delta_{A-B}= \delta D_A- \delta D_B$, which is constant at high temperature (Suzuoki and Epstein, 1976; Graham et al., 1984)) is ~ 12.8‰. The isotopic fractionation of hydrogen between cpx and plag in the granulites, using the average value for the approximation, is mostly around this value (Fig. 8-5). It can thus predicted that cpx and plag in the studied granulites acquired and preserved their equilibrium H-isotopic compositions for most of them, and that diffusion-related processes did not reset their δD to a large degree, as concluded by the δD profiles on most grains (Table 5-13).

The above discussions demonstrate that the lower crustal cpx and plag are characterized by relatively high δD values relative to the normal mantle (-80 to -10‰ vs. -90 to -60‰). The H-isotopic compositions of opx can be reasonably predicted to be in equilibrium with the coexisting cpx and plag, although more and further measurements on opx are necessary for this conclusion.

8.3.2 Possible origins for the δD variations

The distribution and variation of H-isotope compositions for cpx and plag in the lower crustal granulites are similar to each other for all the samples, in spite of their different mineral constitutions, formation ages, tectonic environments and exhumation histories (Table 5-13, Figs. 5-24 and 5-25). As a possible result, a general mechanism is expected for their δD characteristics.

Because possibilities of fractionations related to chemical compositions and processes during and/or after the eruption/exhumation can be totally excluded, the relatively heavier δD in the lower crustal cpx and plag, maybe also opx, can

be accounted for by the following several scenarios:

(1) D/H fractionations between different minerals and between minerals and melts. These fractionations may be important factors controlling the variation of δD in minerals and rocks (Kyser and O'Neil, 1984), but they could not result in the observed D/H enrichments within the lower crustal minerals, because D/H fractionations between NAMs and between NAMs and melts with relatively low water content are usually very small at high temperatures, e.g. less than 15‰ in the range of 800-1000 °C (Kyser and O'Neil, 1984; Bell and Ihinger, 2000).

(2) Exchange of H between NAMs and fluids in the lower crust. This process may lead to certain variations of δD in minerals and rocks; however, it is not applicable to those in the lower crust, which will be discussed later.

(3) Recycled crustal materials (continental and/or altered oceanic crust) with a wide range of possible H-isotopic compositions, e.g. -130 to -9‰ (Stakes and O'Neil, 1982; Sakai et al., 1990; Yui and Jeng, 1990; Putlitz et al., 2000), may produce large δD heterogeneity in the lower crust, e.g. through interaction with mantle melts prior to crystallization of granulite minerals. The marked influence of such materials on the Hannuoba xenolith granulites relative to the very weak, if any, effects on the Nushan xenolith and Hannuoba terrain granulites, as noted before, is in strong contrast to the similar δD compositions of minerals between these samples (Fig. 5-25); this possibility is therefore not favored. This can be further supported by the lack of any simple relationships between δD and δ^{18}O of cpx in the Hannuoba xenolith granulites which were modified significantly by recycled crustal materials, as illustrated in Fig. 8-6. Alternatively, the influences from recycled crustal materials on the H isotopic compositions of lower crustal minerals may have been overlapped by other processes, e.g. dehydration mechanism mentioned later in this section for H-isotopes, so that the relationships between the coupled isotopic species had been erased.

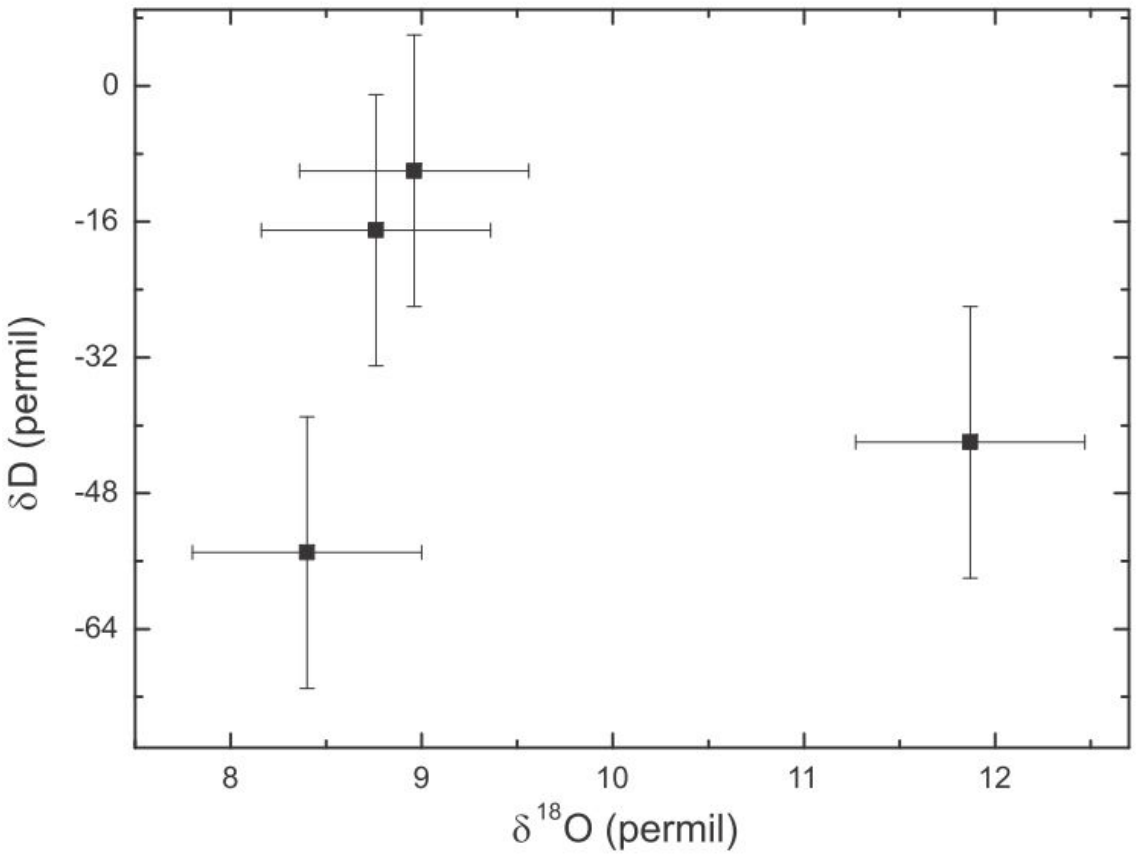

Fig. 8- 6 Relationships between δD and $\delta^{18}O$ of cpx in the Hannuoba xenolith granulites

(4) Dehydration or degassing in the petrogenesis of granulites. Devolatilization, or H release, may take place as loss of aqueous vapor (H_2O) or of reduced hydrogen species, e.g. H_2 and CH_4. Degassing of H_2O is expected to result in a preferential loss of D, while degassing of reduced gases is accompanied by a preferential loss of H from the remaining fractions (Kyser and O'Neil, 1984; Vennemann and O'Neil, 1996; Pineau et al., 1998). As a result, the release of hydrogen will decrease the δD values of the residual phases in the former and increase them in the latter case. Such processes have been widely proposed to explain the variation of δD in mantle minerals (e.g. Kyser and O'Neil, 1984; Xia et al., 2002; Stone et al., 2005; Demény et al., 2006).

The last scenario, degassing of reduced H-bearing gases, is the most likely mechanism for the enrichment of D in the lower crustal cpx and plag minerals. Differences in the D/H ratios between different minerals, samples and localities

(Table 5-13, Fig. 5-25) imply that variable extents of loss in H were involved. Such processes can be quantitatively approximated by the Rayleigh devolatilization equation described by (melt rather than mineral degassing is used, see later):

$$\frac{\left(D/H\right)_{final}}{\left(D/H\right)_{initial}} = f^{\alpha_{gas-melt}-1}$$

where f is the residual fraction of H in the melt, and $\alpha_{gas\text{-}melt}$ is the fractionation factor of hydrogen isotope between gas (e.g. H_2, H_2S) and melt. The isotopic fractionation between H_2/H_2S and melt, $\Delta_{gas\text{-}melt}$, is estimated to be -90‰ and -140‰ at 1000°C and 800°C, respectively (Richet et al., 1977; Pineau et al., 1998; see also data complied by Xia et al., 2002). If assuming the initial δD is about -80‰ (average of the normal mantle values: Kyser and O'Neil, 1984) and the final δD is ~ 5‰ (almost the highest in the granulites: Table 3, Fig. 4) for the melt, we can obtain that the remaining hydrogen, or more commonly water, in the melt is about 0.36 and 0.51, respectively. The possible notable contrast in water content between original mantle melts and final granulite products (see Chapter 7) actually favor this mechanism.

The hydrogen isotopic compositions of cpx and plag in the granulites offer some preliminary but critical constraints on the issue about when a significant amount of water was lost during the formation of granulites, e.g. during the evolution of their protolith melts or after the crystallization of granulite minerals. It has been advocated that the reduction of hydrogen species usually involves the oxidation of Fe (Feldstein et al., 1996; Ingrin and Skogby, 2000), via (using H_2 for an example)

$$2Fe^{2+} + 2OH^- \rightleftharpoons 2Fe^{3+} + 2O^{2-} + H_2$$

For Fe-rich minerals, such as pyroxenes, there is no difficulty for the proceeding of such reactions; however, plag is a mineral lacking (or absent) in Fe or other species that can be oxidized, a marked loss of H in plag through such reactions

is not available. The mineral degassing loss of reductive H-species is therefore not favored. Particularly, the nearly equilibrium δD fractionations between cpx and plag (Fig. 8-5) do not support variable extents of mineral degassing, because the property and behavior of H are so different between cpx and plag (e.g. Ingrin and Blanchard, 2006). Therefore, we favor more that the H_2O loss in the petrogenesis of granulites occurred mainly during the crystallization of granulite minerals from their original melts rather than after their formation, although further studies are required for a better knowledge.

Because these granulites derived from underplating magma, the reduction of H-species will be accompanied by the formation of Fe^{3+}, and the escape of such H-gases from the system will leave the residues in relatively high oxidation state. It is expected that the lower crust has high Fe^{3+}, Fe^{3+}/Fe^{total} and oxidation state relative to normal upper mantle. Available investigations show that the Hannuoba xenolith and terrain and Nushan xenolith granulites usually have higher Fe^{3+} contents and Fe^{3+}/Fe^{total} ratios than upper mantle (Canil et al., 1994; Huang et al., 2001; Zhou et al., 2002b; Huang et al., 2004; Bezos and Humler, 2005), and it is further argued that the lower crust generally has high Fe^{3+}, Fe^{3+}/Fe^{total} and oxidation state relative to normal upper mantle (McCammon, 2005). These observations provide some indirect supports for the degassing loss of reductive H-species during the genesis of granulites and thus the formation of lower crust, as the hypothesis presented here.

8.3.3 Constraints on fluids in the continental lower crust

The presence or absence, nature and composition of fluids in the continental lower crust and their possible effects on granulite facies metamorphism are crucial issues in the evolution of rocks at these highest grades of crustal metamorphism. Granulite-facies mineral assemblages indicate the absence of aqueous fluids during their lifetime and/or very low water activity in the lower crust, otherwise the fluids would be exhausted by retrograde reactions (Yardley

and Valley, 1997). And therefore, it is argued that the granulites were formed under water-absent conditions (Clemens et al., 1997). While on the other hand, it is proposed by many studies that CO_2-rich hydrous saline fluids are possibly pervasive in the deep crust (Touret, 1971; Collerson and Fryer, 1978; Newton et al., 1980), and that these fluids may result in the high electrical conductivity in the lower crust (Hyndman et al., 1993) and have tight relationships with the granulite-facies metamorphism (e.g. Newton et al., 1980; Rudnick and Presper, 1990).

The isotopic data of H, and Li and O, in this study may provide clues for these problems. The preservation of inter-grain heterogeneities and equilibrium isotopic fractionations in these samples indicates that a pervasive hydrous fluid in the lower crust is unlikely, or else the inter-grain isotopic differences, especially H, would be erased and the δD of all the mineral phases would be finally homogenized. The reason for this is that H-species in NAMs are so less and H is so mobile that only minor amounts of H in the fluids would markedly shift the H isotopic compositions of minerals, e.g. by exchange of H between minerals and fluids; the final result of this process would be that all the lower crustal minerals have the same δD value as that of the fluids. This is obviously not the case as shown from our data. In this scenario, if fluids were present in the lower crust, there should be no, or only in negligible amount of, H-related species (H_2O, CH_4, etc) dissolved in them, e.g. dominated by CO_2, unless these H are immobile and they cannot exchange with those in NAMs; however, this is inconsistent with the observed large inter-grain δ^{18}O heterogeneities, a CO_2-dominated fluid is thus not available. Alternatively, fluids are likely absent in the lower crust, as suggested petrologically by Yardley and Valley (1997). In either case, the most important is that water activity in the continental lower crust is very low (= ~0), and that hydrous fluids are absent, or if in any case the fluids are present, active H-bearing species in them are very little even far less than those in NAMs.

8.4 Lithium contents and isotopic compositions

The in situ ion microprobe measurements demonstrate that the Li contents and isotopic compositions of minerals in the granulites display quite different behaviors from those of O and H isotopes.

8.4.1 Li-abundance and isotopic systematics

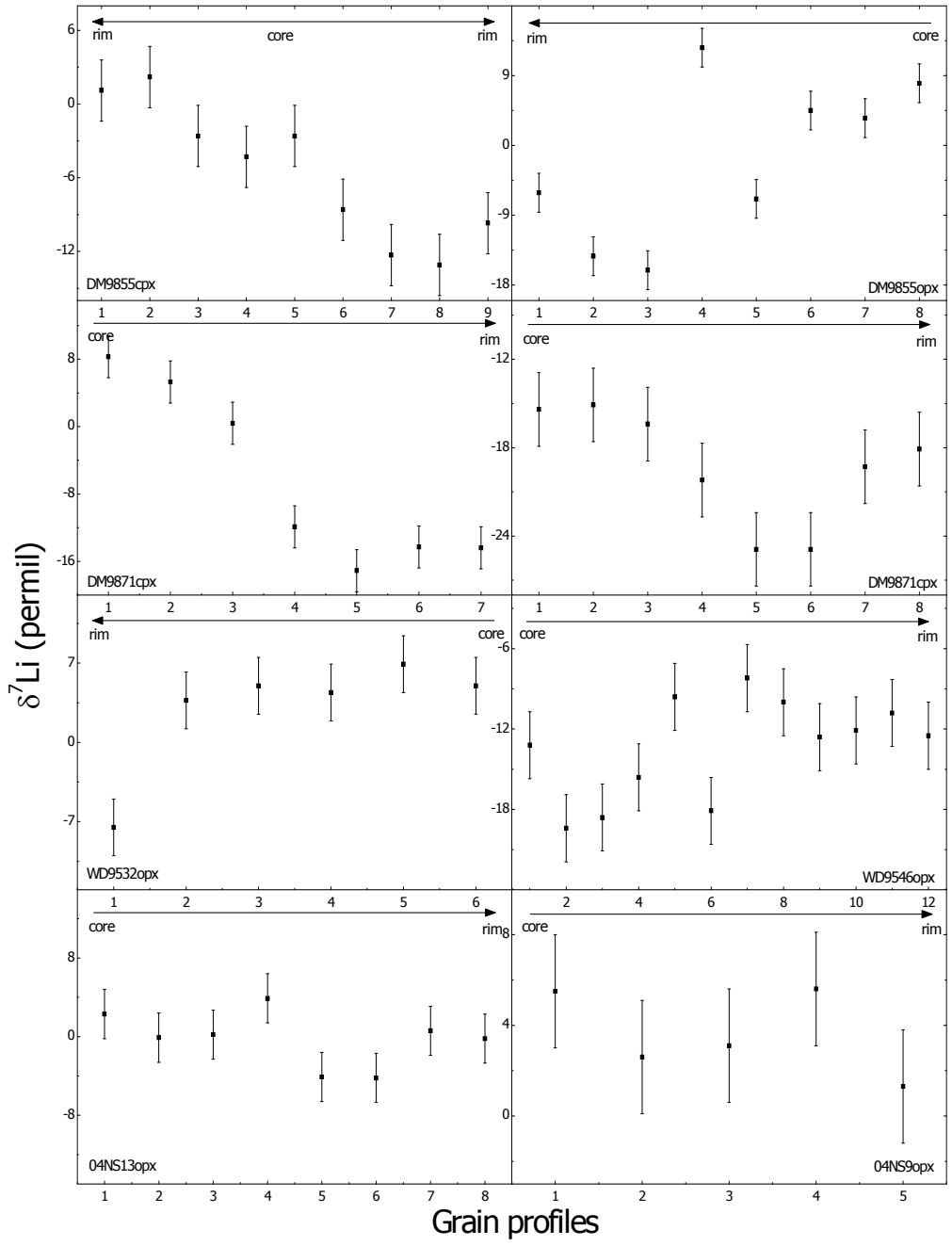

Fig. 8- 7 Profile analyses of δ^7Li on pyroxene grains in the granulites

Analyses of the granulites in terms of their Li contents show that the grains are usually uniform within sub-grain scales, although large variations far be-

yond the analytical uncertainty (20%) can be observed in some grains, e.g. cpx in MJ9801, opx in DM9855 and cpx in DM9871 (Table 5-16). On average, the Li contents are higher in cpx (~ 5-28 ppm) than in opx (~ 2-5 ppm) and then plag (mostly ~ 0.3-3 ppm, except MJ9801 whose content is ~ 10 ppm); the content of garnet in MJ9801 is ~ 3 ppm (Table 5-17). Cpx and plag in the Hannuoba terrain and Nushan granulites usually contain more Li than those in the Hannuoba xenolith granulites, with the highest contents in the terrain samples. By contrast, opx has similar Li content between these granulites (Tables 5-16 and 5-17). The estimated bulk contents are ~ 1.9 to 12.6 ppm, usually higher than those of mantle peridotites, about 0.7-2 ppm (e.g. Brenan et al., 1998; Seitz and Woodland, 2000; Seitz et al., 2004; Rudnick and Ionov, 2007; Tang et al., 2007; Wagner and Deloule, 2007; Ionov and Seitz, 2008), but lower than those of the upper continental crust, ~ 35 ppm (Teng et al., 2004). This is consistent with the incompatible behavior of Li during partial melting processes (e.g. Brenan et al., 1998). The average bulk Li content is ~ 5.2 ± 4.0 ppm, which is similar to the estimated average content of ~ 8 ± 4 ppm for the continental lower crust (Teng et al., 2008).

The in situ δ^7Li data of pyroxenes in the granulites are highly variable, with their total range from -24.9 to 10.9‰ for cpx and -20.2 to 12.6‰ for opx (Table 5-16). Such large variations resemble, to some extent, those measured on mantle pyroxenes, e.g. -10.3 to -1.0‰ for cpx and -22.4 to 8.3‰ for opx in mantle peridotites from Damaping, Hannuoba (Tang et al., 2007) and -11.1 to 19.9‰ for cpx and -10.4 to 22.8‰ for opx in mantle peridotites from Massif Central France (Wagner and Deloule, 2007). Profile analyses of δ^7Li over grain scales display complex variations from core to rim regions in these granulites, such as nearly constant along the core-to-rim profile, heavier (or lighter) in the core than in the rim, and/or a low trough between the core and rim areas (Fig. 8-7). Interestingly, the apparent variations in δ^7Li over some grains contrast sharply with the nearly constant distribution or only limited variation in their Li

contents (Table 5-16). This has also been observed for minerals in meteorites and mantle peridotites (Beck et al., 2004; Lundstrom et al., 2005; Beck et al., 2006; Parkinson et al., 2007; Tang et al., 2007; Wagner and Deloule, 2007).

The average δ^7Li of cpx and opx in the Nushan xenolith and Hannuoba terrain granulites are similar to each other but differ slightly from the Hannuoba xenolith granulites, e.g. -4.1 to 3.6‰ for cpx and -5.6 to 4.7‰ for opx in the former vs. -12.2 to -4.2‰ for cpx and -13.4 to -0.4‰ for opx in the latter; the δ^7Li of plag measured on two samples are ~ -13.5‰ and -0.4‰, respectively, and is about -3.3‰ for garnet in MJ9801 (Table 5-17). In general, except sample 04NS9 whose cpx and opx have δ^7Li values falling in the range of normal upper mantle, e.g. 2-6‰ defined by the isotopic compositions of oceanic basalts (Elliott et al., 2004; Tomascak, 2004; and refernences therein) and "equilibrated" intra-plate mantle peridotites (Seitz et al., 2004; Jeffcoate et al., 2007; Ionov and Seitz, 2008), minerals in the studied granulites are characterized by relatively depleted Li-isotopic compositions (Table 5-17). The average δ^7Li vs. Li content of cpx and opx in these granulites are illustrated in Fig. 8-8. No simple correlations are observed between δ^7Li and Li abundances for pyroxenes in each suite of samples.

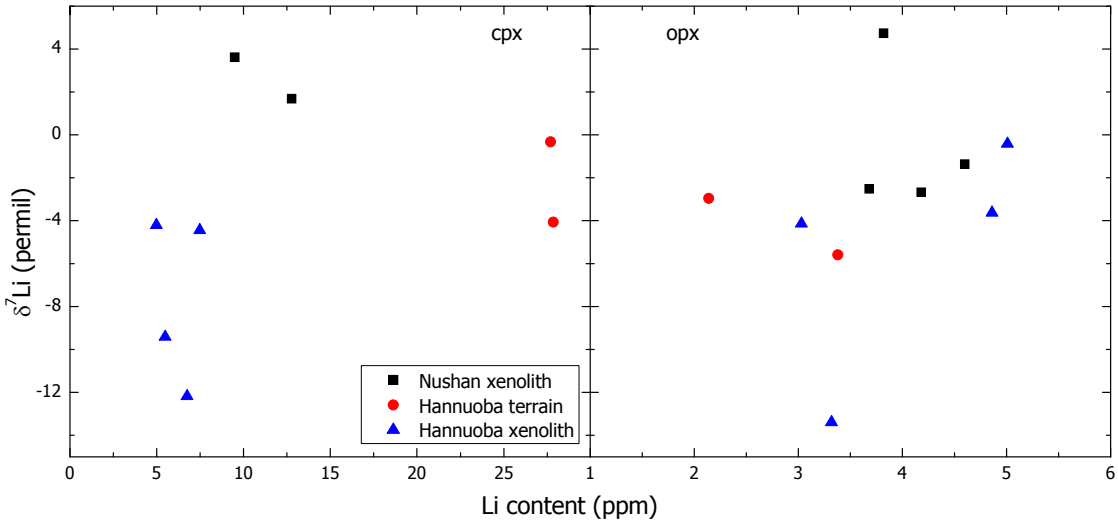

Fig. 8- 8 δ^7Li vs. Li abundances for cpx and opx in the granulites

8.4.2 Partitioning and isotopic fractionation of Li between lower crustal minerals

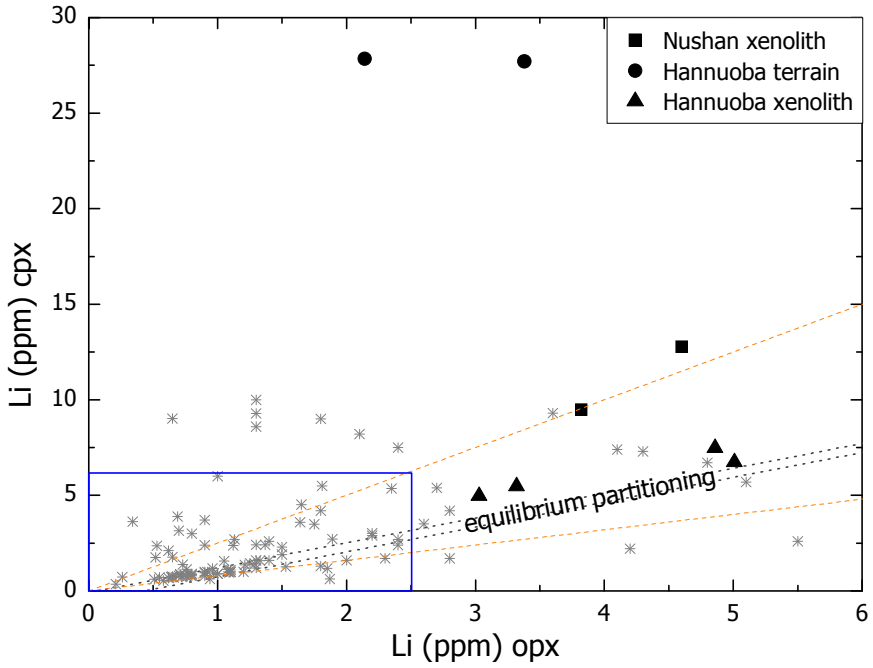

Fig. 8- 9 Partitioning of Li between cpx and opx in the granulites

(the dotted lines indicate equilibrium partitioning deduced from equilibrated mantle peridotites (Seitz and Woodland, 2000; Woodland et al., 2004); the dashed lines denote the boundaries where the mantle peridotites mostly fall in, while the squared area illustrating the region where mantle peridotites are mostly concentrated (Seitz and Woodland, 2000; Ottolini et al., 2004; Seitz et al., 2004; Rudnick and Ionov, 2007; Tang et al., 2007; Wagner and Deloule, 2007; Ionov and Seitz, 2008), the referred data shown by symbol "*" are for mantle peridotites from these literatures)

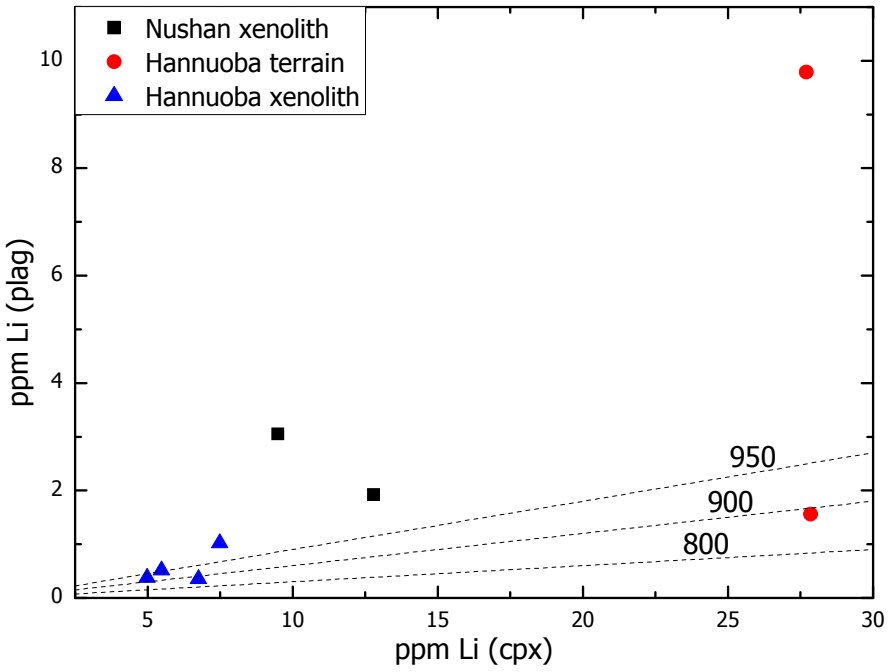

Fig. 8- 10 Partitioning of Li between plag and cpx in the granulites

(the three dotted lines are the experimentally measured partitioning coefficients under 800, 900 and 950 °C, respectively, from Coogan et al. (2005); these temperatures correspond to the equilibrium conditions of the samples calculated by two-pyroxene geothermometers)

The partitioning of Li between minerals in the lower crustal granulites, based on the average value of ion microprobe data (Table 5-17), is illustrated in Fig. 8-9 for the partitioning of Li between cpx and opx and 8-10 for the partitioning of Li between plag and cpx. In Fig. 8-9, the Hannuoba xenolith granulites project close to the trend of equilibrium partitioning defined by "equilibrated" mantle peridotites (Seitz and Woodland, 2000; Woodland et al., 2004), while the Nushan xenolith and Hannuoba terrain granulites deviate far from the equilibrium zone. In Fig. 8-10, the Hannuoba xenolith granulites fall into the equilibrium areas bounded by the experimentally measured coefficients of Coogan et al. (2005) under the temperature of 800-950 °C, while the Nushan xenolith and terrain granulites mostly fall outside these areas except MJ9805.

The equilibrium fractionations of $\delta^{18}O$, $\delta^{7}Li$ (will be discussed later) and δD (will be discussed in the next section), consistent REE patterns and equilibrium

REE partitioning and nearly constant core-to-rim distributions of both water and Li content over most grains in these granulites exclude any significant recent Li perturbations by any secondary processes (e.g. by metasomatism) and/or Li re-distribution between coexisting assemblages during their rapid cooling by temperature-dependent Li partitioning between plag and cpx (Coogan et al., 2005). For example, Li diffuses from plag into cpx as temperature decreases (Coogan et al., 2005), so that the re-distribution of Li between plag and cpx during cooling will result in a decrease of Li on the rims of plag and an increase on the rim of cpx; while at the same time, because ^{6}Li diffuses faster than ^{7}Li (Richter et al., 2003), the re-distribution of Li will also produce heavier δ^{7}Li on the rims of plag and lighter δ^{7}Li of cpx. Neither of these cases, however, was observed in our samples (Table 5-16). Consequently, the deviation of some Nushan xenolith and Hannuoba terrain granulites from the trend of equilibrium partitioning (Figs. 8-9 and 8-10) is probably related with the above mentioned inter-grain Li variations rather than other possible mechanisms. This suggests that, for minerals/samples which may have apparent inter-grain compositional differences, the in situ data obtained on limited grains may not be able to represent the bulk value. On the other hand, the deviation of the Nushan and terrain samples is probably caused by their high albite contents relative to the Hannuoba xenolith granulites, mainly 47-64 vs. 32-49 (Tables 5-1, 5-2 and 5-3), so that the method of Coogan et al. (2005) may be not applicable, as proposed by them: "*despite this apparent insensitivity of the partition coefficient to plagioclase major element composition we caution against using the measured partition coefficient for significantly more albitic plagioclase compositions without experimental verification*".

The faster diffusion of ^{6}Li relative to ^{7}Li (Richter et al., 2003) can result in large Li isotopic fractionations even during magmatic processes (Barrat et al., 2005; Lundstrom et al., 2005; Beck et al., 2006; Teng et al., 2006; Jeffcoate et al., 2007; Parkinson et al., 2007; Rudnick and Ionov, 2007; Tang et al., 2007;

Wagner and Deloule, 2007). Modeled results show that diffusion-driven Li isotopic fractionations can strongly shift δ^7Li and lead to large δ^7Li variations more than 20‰ even in very small scales (e.g. Lundstrom et al., 2005; Beck et al., 2006; Jeffcoate et al., 2007; Parkinson et al., 2007). If no sufficient time is allowed for re-equilibration, the variation in δ^7Li would be arrested by the deep-seated minerals. If considering the fast diffusion of Li under high temperatures, e.g. the diffusion coefficient of Li in cpx is on the 10^{-13} to 10^{-12} order of magnitude at about 900 °C (Coogan et al., 2005), it would take several hundred to dozens of thousands of years for the δ^7Li heterogeneity to disappear in ~ 1 mm scale. In this case, the diffusion events responsible for the Li isotopic fractionations of natural samples must have happened shortly before or during their transport to the surface. Accordingly, the intra-grain δ^7Li variations determined in the studied granulites (Fig. 8-7, Table 5-16) are proposed to result mainly from high-temperature diffusion-related isotopic fractionations by some recent events, e.g. before or during the entrainment of the xenoliths or the exhumation of the terrains.

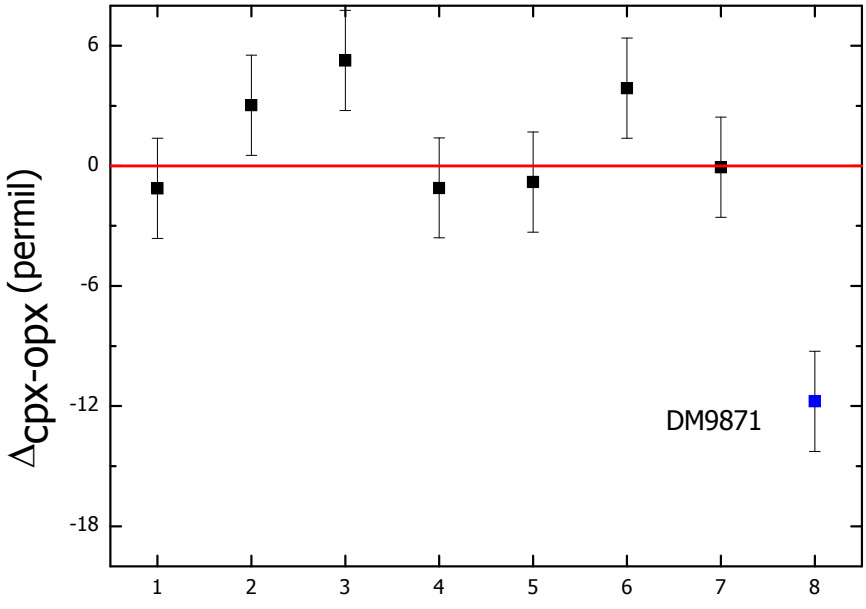

Fig. 8- 11 Li-isotopic fractionations between pyroxenes in the granulites (the vertical line is drawn at 0 for a reference)

The isotopic fractionations of Li between pyroxenes in the studied granulites are illustrated in Fig. 8-11. All the samples except DM9871 are projected around the value of 0. The equilibrium Li isotopic fractionations between coexisting phases at mantle or lower crustal temperatures are not well constrained, as no experimental data are yet available. Given the absence of large δ^7Li fractionations during partial melting, differentiation and subsequent crystallization under high temperatures down to ~ 720 °C (Tomascak et al., 1999; Teng et al., 2004; Wunder et al., 2006) and the knowledge that Li diffuses very fast under high temperatures, it can be reasonably assumed on the first order that the equilibrium isotopic fractionation of Li between coexisting minerals (either mantle or deep crust derived) at > 800 °C is around 0, as argued by Rudnick and Ionov (2007). This is further supported by empirical studies on equilibrated mantle peridotites xenoliths, which show that the Li isotopic fractionations between cpx, opx and olivine are all close to 0, as shown in Fig. 8-12 (e.g. Seitz et al., 2004; Ionov and Seitz, 2008). Under these assumptions, cpx and opx in the studied granulites are mostly in equilibrium with respect to their δ^7Li data (Fig. 8-11). The measured δ^7Li of plag and garnet of two samples are also in similar range and their fractionations relative to the coexisting cpx or opx are also close to 0 (except plag in MJ9801, Table 5-17); actually it can be reasonably predicted that the cpx and plag are in equilibrium in terms of their δ^7Li on the basis of their approximation in equilibrium REE partitioning and equilibrium H-isotopic fractionations. The deviation of DM9871 from the equilibrium fractionation is probably caused by analyzing too many points on a δ^7Li depleted cpx grain (Table 5-16) rather than indicative of disequilibrium, particularly when considering its composition of Li content (Figs. 8-9 and 8-10), δ^{18}O, REE and δD data.

The equilibrium δ^7Li fractionations between the coexisting minerals (mainly pyroxenes) and the relatively constant Li distributions on most grains, as well as the similar REE patterns and partitioning of individual minerals, the unzoned H content and the constant δD profiles on most grains and the equilibrium δD

fractionations between cpx and plag in these granulites, indicate that the diffusion-related fractionations were mainly produced by closed-system processes (Parkinson et al., 2007). During these processes, the difference in diffusion rate between ^{6}Li and ^{7}Li leads to large δ^{7}Li fractionations, but the total amount of Li in the grain remains nearly unmodified and so do the isotopic compositions of the whole grain. In this hypothesis, melts or fluids do not necessarily need to infiltrate the minerals/grains, or only the outmost rims of the grain were weakly modified in terms of the Li content while the composition of the whole grain remains nearly the same. To understand this model, we have to know clearly whether the host melt can completely wet the grains in the lower crust. The ability for melt to percolate a matrix is controlled by the dihedral angle (θ) between solid and melt, if θ>60º, melt cannot percolate at small melt fractions (Waff and Bulau, 1979). θ between lower crustal assemblages and melt are usually larger than 60º, e.g. θ is 98º between cpx and melt and is 76º between opx and melt (Toramaru and Fujii, 1986). Therefore, melt percolation of the lower crustal minerals can be effectively prevented. The high-temperature Li diffusions were probably driven mainly by Li-gradients between different grains as mentioned above rather than between melt and minerals so that Li isotopic fractionations occurred in a closed-system. For some grains which display large Li variations between their core and rim regions, e.g. opx in DM9855 and cpx in DM9871 (Table 5-16), they were probably penetrated by melts/fluids so that they were influenced significantly in terms of their Li contents.

Given the above documented scenario, the high-temperature diffusion-related fractionations may result in large δ^{7}Li variations from spot to spot within some mineral grain, but the bulk δ^{7}Li of the grain remains unmodified (e.g. in a closed system). In this case, the average δ^{7}Li of minerals from multi-point and multi-grain analyses in the granulites were not remarkably influenced by diffusion-related or other possible processes, and they could reflect their initial source compositions.

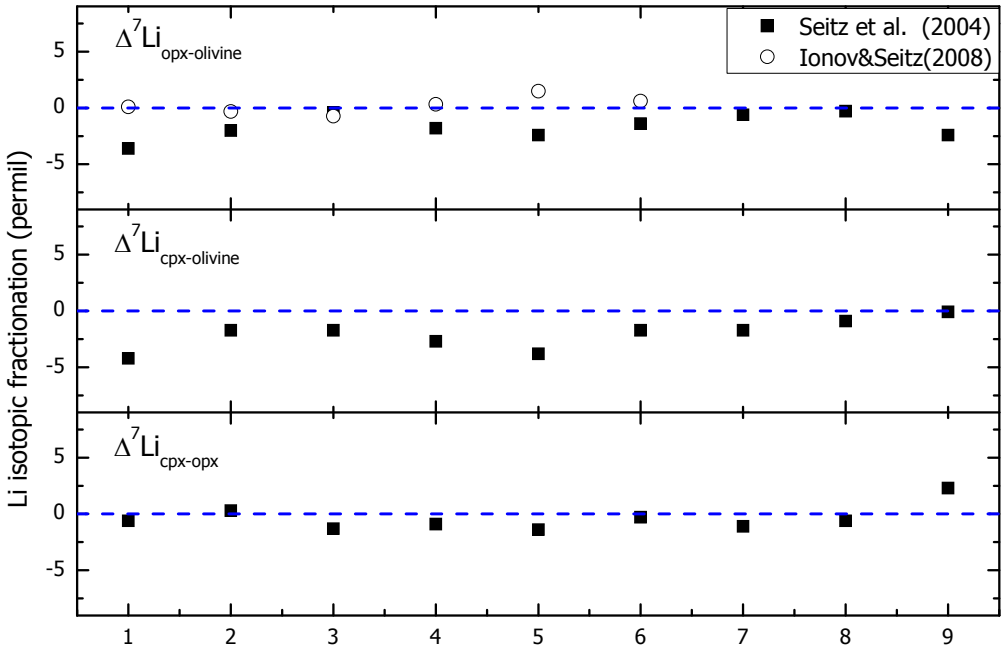

Fig. 8- 12 Li isotopic fractionations between equilibrated mantle peridotite minerals (the three dotted lines were draw at 0 fractionation for reference)

8.4.3 Possible origins for δ^7Li in the granulite minerals

Given equilibrium isotopic fractionations of Li between coexisting minerals and of H between cpx and plag (see last section), as well as REE equilibration, in the granulites, the δ^7Li of plag should, in principle, be in equilibrium with the coexisting pyroxenes in the samples. The measured δ^7Li of plag in two samples are -13.5 and -0.4‰, respectively, which are similar to those of pyroxenes (e.g. depleted compared to normal mantle) and therefore reasonable and believable. This, to some extent, offers evidence for the absence of large matrix effects on the lithium isotopic determination of plag by ion microprobe IMS 3f at the CRPG (Beck et al., 2004). If assuming similar δ^7Li for plag in the other samples, e.g. using -13.5‰, -0.4‰ and the average value of -7.0‰ for an approximation, the estimated bulk δ^7Li range from ~ -11.5 to 1.5‰ (Table 8-1), markedly lighter than the normal mantle, ~ 2 to 6‰ (Elliott et al., 2004; Seitz et al., 2004; Tomascak, 2004; Ionov and Seitz, 2008). The estimated bulk δ^7Li value for the Hannuoba xenolith granulites, -11.5~-2‰, is actually similar to the MC-ICP-MS measured whole rock δ^7Li range of mainly -9.6~2.2‰ for mafic xenolith gran-

ulites from this locality (Teng et al., 2008).

Table 8- 1 Estimated bulk δ^7Li values for the granulites

	estimated bulk δ^7Li (‰)		
	-13.5	**-7.0**	**-0.4**
04NS11	-10.5	-5.7	-1.0
04NS13	-11.3	-6.1	-0.9
04NS9	-5.5	-2.0	1.6
04NS16	-10.9	-5.7	-0.4
MJ9801	-5.3	-5.3	-5.3
MJ9805	-8.1	-5.2	-2.3
DM9855	-7.9	-5.3	-2.7
DM9871	-11.6	-7.6	-3.7
WD9532	-3.5	-3.5	-3.5
WD9546	-11.3	-10.8	-10.2

Note: the bulk Li-isotopic compositions were estimated under the given δ^7Li of plag, -13.5, -7.0 and -0.4‰, for the samples except MJ9801 and WD9532.

The notably lighter δ^7Li of the granulite pyroxenes, maybe also of plag and their bulk compositions, relative to the normal mantle is a subject deserving a thorough analysis. There are a few possible processes which might affect the Li isotopic compositions of granulite pyroxenes: (1) Weathering or alteration. This is not favored because the samples are mostly very fresh or the freshest parts were used for the study; furthermore, such processes would have even greater influences on O isotopes compared to Li (Halama et al., 2008), and their peak metamorphism O-isotopic equilibrium would be reset, which is not supported by the O-isotope data (Fig. 8-2). (2) Slow cooling after exhumation. This is not supported by the equilibrium Li (and H) isotopic fractionations between the coexisting minerals, no significant zoning of Li and water content on most grains. Furthermore, the well-preserved kelyphite in the terrain granulites (Guo et al., 2005) indicates a rapid cooling as mentioned above. (3) Re-distribution during the ascent. The nearly constant Li, and especially H, content profiles on most pyroxene grains, and the equilibrial Li partitioning between plag and cpx in the Hannuoba xenolith granulites under high temperatures (Fig. 8-10), ex-

clude notable exchange/re-distribution of Li (or H) between minerals (Coogan et al., 2005) or between minerals and melts; besides, the quick transport of xenolith samples, e.g. a few to dozens of hours, does not favor such processes. (4) Partial melting, differentiation and crystallization. Many studies have shown that Li isotopes will not fractionate significantly under high temperatures, e.g. >800°C, during such processes (Tomascak et al., 1999; Teng et al., 2004; Wunder et al., 2006). (5) Contamination with melt or wallrocks during ascent. The unzoned Li and water distribution on most grains, the lack of covariant δ^7Li and δD from core to rim and the lack of correlations between Li and δ^7Li and between δD and water content exclude this possibility. (6) Infiltration of fluids. The heterogeneities of Li content and δ^7Li indicate the absence of a pervasive fluid in the lower crust; in addition, it is difficult to imagine that the granulites, despite their formation ages and environments, generally interacted with certain fluids to decrease their δ^7Li values to a similar range.

Therefore, the large δ^7Li variations observed in the three suites of granulites most-likely reflect their source heterogeneities. The relatively depleted Li isotopic compositions could be accounted for by (i) recycled crustal materials involved with their protoliths, (ii) dehydration during the formation of granulites, and (iii) kinetic fractionations associated with high-temperature Li diffusion during the intrusion of their original melt(s). We will discuss these possibilities one by one.

(i) One possibility accounting for the lighter δ^7Li in the studied granulite minerals is the effects from recycled crustal materials in the mantle source from where the original melts of granulites derived. Because weathering usually leads to depleted δ^7Li in the continental rocks (e.g. Teng et al., 2004), recycling of sediments into the mantle source can lower its Li-isotopic compositions, which might be then inherited by derived granulites. While on the other hand, it is suggested that recycled crustal materials have greater influences on O relative to Li isotopes (Halama et al., 2008). In this case, if the lighter δ^7Li of these

granulites (minerals) were accounted for by recycled materials (such as sediments), their O-isotopes would have been modified to an even larger extent. However, our $\delta^{18}O$ data show that the Nushan xenolith and Hannuoba terrain granulites mostly have similar or only slightly heavier $\delta^{18}O$ relative to the normal mantle (Table 5-15); while for the Hannuoba xenolith granulites which generally have relatively high $\delta^{18}O$ (Table 5-15), no simple correlations exist between $\delta^{18}O$ and $\delta^{7}Li$ for both cpx and opx (Fig .8-13). The above discussions exclude significant influences from recycled crustal materials on the Li-isotope compositions of granulites from the North China Craton, or that their effects were overprinted by other processes.

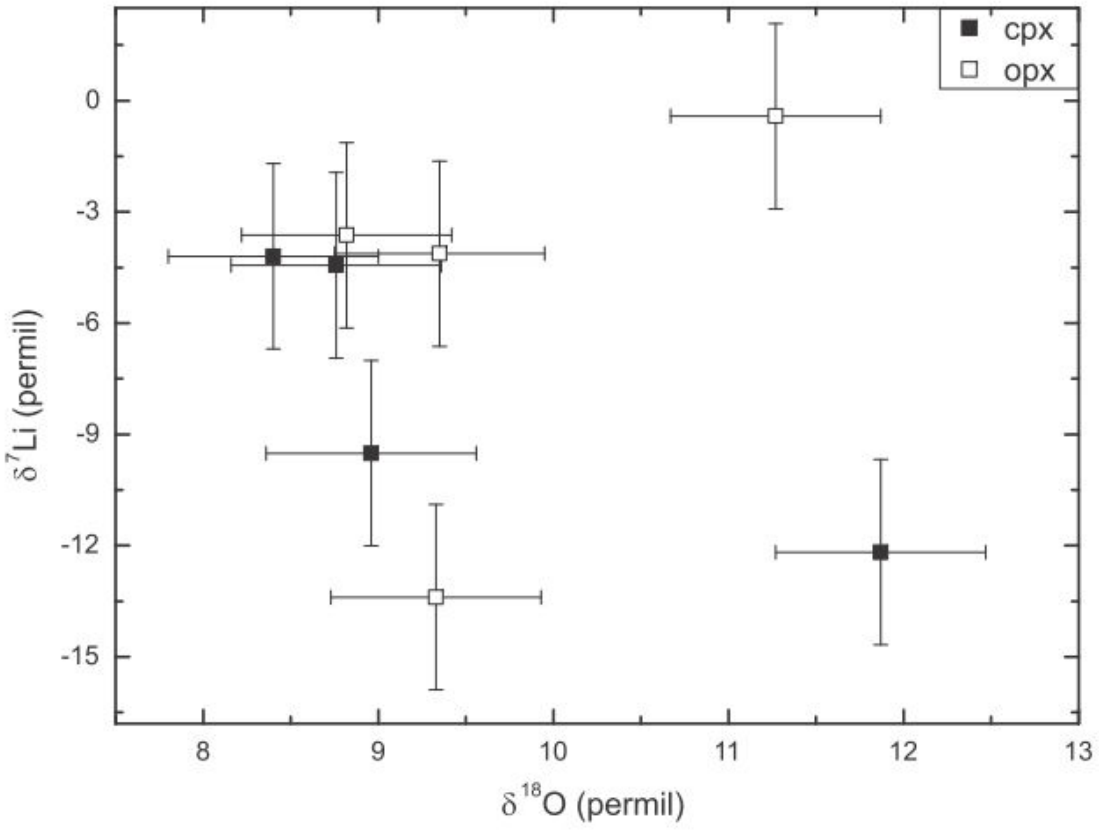

Fig. 8- 13 $\delta^{7}Li$ vs. $\delta^{18}O$ of pyroxenes in the Hannuoba xenolith granulites

(ii) Another possibility is the dehydration loss of water and Li during the formation of granulites. Because ^{7}Li is more sensitive to fluids relative to ^{6}Li, Li-isotopes may fractionate during dehydration and such processes can lower the original $\delta^{7}Li$ of minerals/rocks (Zack et al., 2003). This is supported by re-

cent experimental investigations (Wunder et al., 2006; Wunder et al., 2007), although the extent of such fractionations is a matter of debate at present (Marschall et al., 2007; Teng et al., 2007). Given granulites are concomitant with the loss of water through dehydration during their petrogenesis, it can be reasonably predicted that the low δ^7Li of granulite minerals may be related with such processes. However, the modeled results by Marschall et al. (2007) for eclogites and by Teng et al. (2007) for metapelites argue against noticeable effects from dehydration reactions on Li isotopic fractionations unless the loss of the original Li is larger than 50% (Teng et al., 2007). The estimated loss of the original water (or H) of these granulites is about 40-60%; and under similar conditions, the average loss of the original Li cannot exceed 10%, because the diffusion rate of H under high temperatures, e.g. >800 °C, is 1-3 orders of magnitude faster than Li in both minerals and melts (e.g. Coogan et al., 2005; Ingrin and Blanchard, 2006). Therefore, dehydration/degassing loss of Li in the formation of granulites is not a favored mechanism to result in their markedly depleted δ^7Li compositions.

As a possible result, the above mentioned scenario (iii), high-temperature diffusion-related kinetic Li-isotopic fractionation during the intrusion of original melt(s), is the most likely mechanism producing the depleted Li isotopic compositions of the granulite minerals. Several studies have documented kinetic Li isotope fractionation produced by Li diffusion from magmatic intrusions into country rocks (Lundstrom et al., 2005; Teng et al., 2006; Teng et al., 2008). The isotopic fractionations produced in this way can be up to ~ 20-30‰ (e.g. Lundstrom et al., 2005; Beck et al., 2006; Jeffcoate et al., 2007; Parkinson et al., 2007; Teng et al., 2007) and will be preserved so long as the system cooled quickly. Because the 3 suites of granulites studied here are interpreted to have originated from underplating magma, it is probably that such kinetic effects occurred in the lower crust at the time of their intrusion. On the other hand, because Li content in the lower crust is higher than that of mantle melts, e.g. 5-15 ppm for the former as revealed in this study vs. 1-5 ppm for the latter, it

can be assumed on the first order that Li diffuses from preexisting lower crust into the newly underplated intrusion; and such processes should result in lighter δ^7Li in the intrusion due to the faster diffusivity of ^{6}Li than ^{7}Li, while the country rocks immediately adjacent to the intrusion becomes heavier in δ^7Li for a preferential loss of ^{6}Li. The magnitude of the change in δ^7Li depends on the concentration ratio between the preexisting lower crust and intrusion as well as the diffusivity difference between Li isotopes (Richter et al., 2003). Assuming a Li content ratio of ~5 between preexisting lower crust (e.g. ~10 ppm, almost the highest value observed in the terrain granulites) and underplating magma (~2 ppm) and a diffusivity difference between Li isotopes (β) of 0.215 (β in silicate melts: Richter et al., 2003), a change in δ^7Li of 5-15‰ can be produced by diffusion along the diffusion path (Teng et al., 2008). And this can decrease the original δ^7Li from 2 to 6‰ of normal mantle to -15 to 1‰, which is nearly consistent with those determined in the mafic granulites from the NCC. Modeled results show that kinetic isotopic fractionations related with the original underplating events that formed the mafic granulites can survive for a long duration, e.g. a few to tens or hundreds of Ma (Teng et al., 2008), if the system cooled quickly. And in this case, the kinetic isotopic fractionation produced during underplating can lead to the depleted Li isotopic compositions of granulites from the NCC.

However, there is also another possibility that the lighter δ^7Li values of the mafic granulites result from the coupled effects from recycled crustal materials and kinetic Li isotopic fractionations during the intrusion on their protoliths. The recycled crustal materials to the original mantle source effectively decrease their δ^7Li compositions. The influences from recycled crustal materials are even larger on the Hannuoba xenolith granulites than on the Hannuoba terrain and Nushan xenolith granulites, as revealed by O-isotopic data (Table 5-15), and in this case the δ^7Li compositions of the former are generally lighter than the latter (Table 5-17). However, the subsequent kinetic isotopic effects during the mafic underplating erased the possible correlations between δ^7Li and δ^{18}O (Fig. 8-13).

9 Conclusions and future work

Over the past about 20 years, studies on water content and H-O-Li isotopic systematics have been largely concentrated on the hydrosphere, the shallower crust and the upper mantle. These studies provide fundamental information on the cycling and exchange of H_2O between the Earth's interior and exterior, the recycling of crustal materials and possibly related geodynamical processes. The continental lower crust is one of the most important layers inside the Earth, on the basis of the following philosophy: it is the interface between the continental mantle and crust, where crust-mantle exchange and interactions occur; it is the crystallized products of mantle differentiated melts, and can further differentiate into the upper and middle crusts. However, relatively scarce, if any, systematic investigations on H_2O content and H-O-Li species have been conducted on the lower crust, especially into the coexisting phases, which plays a critical role in determining if the information recorded by the samples were influenced by later processes, in the knowledge of crust-mantle interactions and exchange and in understanding the formation and evolution of granulites/lower crust.

It is the purpose of this thesis to characterize the water content and H-O-Li stable isotopes of the continental lower crustal minerals. This is the first time to systematically probe into the water-related species in the lower crust. The main conclusions drawn from this thesis are:

1. Nominally anhydrous minerals, such as pyroxenes, plagioclase and garnet, in the continental lower crust generally contain some structural H-species dominated by hydroxyl and less molecular H_2O, with their content (ppm H_2O by wt.) from 200 to 2330 for cpx, 60 to 1875 for opx, 65 to 900 for plag and 155 to 1100 for the whole rock compositions. The average bulk content is ~ 450 ppm, and the mafic lower crust is estimated to contain ~ 4.26×10^{18} kg H_2O in its nominally anhydrous minerals.

2. Significant contrast in water content is observed between Precambrian and Phanerozoic continental crust, implying a more hydrous ancient lower crust relative to the modern one.

3. Water contents of the main continental lower crustal minerals, and the bulk content, are notably higher than those in the underlying lithospheric mantle, in spite of their lateral variations. This water contrast may strongly influence the rheological behavior of deep continental lithosphere beneath the NCC, and results in different lithospheric processes between different zones below the NCC, e.g. lithospheric thinning vs. thickening.

4. The O-isotopes of the studied pyroxenes, and probably bulk samples, range from ~ 4.5 to 12.5‰, mostly higher than or roughly comparable to the normal mantle (5.7 ± 0.5‰), and indicate involvement of recycled crustal materials in their petrogenesis at least for some of them. Inter-grain $\delta^{18}O$ variations up to ~ 2-3‰ were observed for cpx in < 1 cm scale within some samples, in contrast to their constant distribution over each grain, implying grain-scale heterogeneities. Consistency between the O-isotopic and cation (Fe-Mg) exchange temperatures suggests preservation of peak-metamorphic compositions.

5. The lower crustal minerals are characterized by higher δD values relative to the normal mantle, e.g. -80 to -10‰ vs. -90 to -60‰. Intra-grain Variation of δD on some grains were likely produced by recent diffusion-related events, while the preservation of equilibrium fractionations between the coexisting minerals with respect to their D/H ratios indicates weak effects from these diffusion processes. The relatively heavier D/H ratios of the lower crustal minerals can be accounted for by melt degassing, e.g. during the crystallization, but mainly in the manner of losing reductive H-species (e.g. H_2, H_2S).

6. Li content varies from 3.2 to 34.2 ppm for cpx, 0.6 to 9.1 ppm for opx, 0.2 to 12.1 ppm for plag and ~ 1.9 to 12.6 ppm for bulk compositions, with an

average bulk value of ~ 5.2±4 ppm. The studied minerals are characterized by depleted Li-isotopic values relative to normal mantle, e.g. ~ -13 to 4.7‰ with estimated bulk values -11 to 2‰ vs. 2 to 6‰. Intra-grain variations of δ^7Li on some grains were related with diffusion-driven processes; however, the preservation of equilibrium δ^7Li fractionations indicates that the initial δ^7Li compositions reflected by the average of multi-points and multi-grains were not significantly modified by such diffusion-related fractionations. The lighter δ^7Li compositions were probably caused by kinetic Li isotopic fractionation during the intrusion of their original melts to the preexisting lower crust or by the coupled effects from recycled crustal materials and kinetic Li isotopic fractionation during the magma underplating.

7. The preliminary results by this thesis imply that recycled crustal materials, which have strong influences on O-isotopes, have no significant effects on Li- and H-isotopic ratios of lower crustal granulites unless their influences were erased by the dehydration processes.

8. The equilibrium REE distributions and H-O-Li isotope fractionations between coexisting minerals, and possible inter-grain isotopic heterogeneities, rule out the presence of pervasive fluids either on large or local scale in the lower crust.

The work done in this thesis provides a strong basis for understanding the H_2O content, H-O-Li stable isotopes and other fluid-associated processes in the continental lower crust, and for a knowledge of the recycling and interactions of water and H- and Li-isotopes between different layers of the Earth especially the crust and mantle. These are complementary to available studies performed on both the hydrosphere and upper mantle. This thesis on the one hand offers a lot of new data and resolves some questions, while on the other hand it raises many open problems, which are fundamental but need thorough investigations, including:

1. More samples globally are necessary for a more general understanding of the water content and H-O-Li isotopes in the continental lower crust.

2. Further studies both theoretically and experimentally are needed for better understanding the contrast in water content in the continental lower crust between Precambrian and Phanerozoic (or the evolution with time).

3. The possible contrast in water content between lower crustal minerals and underlying lithospheric mantle ones, especially from the same locality, are necessary for more investigations, as well as their effects on the rheological strength, and possible related geodynamical processes, of the continental lithosphere.

4. Experimental investigations about the possible effects of water in nominally anhydrous minerals on the high electrical conductivity in the continental lower crust are necessary.

5. The incorporation mechanisms of water into lower crustal minerals, relatively low T&P compared to mantle conditions, and the partitioning of H_2O between lower crustal phases, are necessary. Actually, we do not know if the notable difference in both mineral composition and crystal structure between mantle and lower crust minerals would exert any influences on the incorporation of H into minerals.

6. More measurements, from both natural samples and experimental simulation, are necessary for a better understanding of the inter-grain heterogeneities of both elements and isotopes on the intra-grain homogeneous samples, or diffusion processes under high temperatures.

7. A more detailed investigation of H and Li isotopes on other coexisting phases in the granulites may provide further constraints on the conclusions casted in this thesis. This, however, requires the establishment of more standards for ion microprobe measurement and the improvement of in situ techniques.

8. The equilibrium fractionations of H between coexisting minerals under high temperatures have been established, to some extent, by empirical and theoretical investigations, however, further experimental studies are necessary.

9. The equilibrium partitioning of Li contents and fractionation of Li isotopes between coexisting minerals under high temperatures are awaiting further investigations.

10. The significant contrast in lithium content between cpx and opx in the HP Hannuoba terrain granulites, coupled with their similar δ^7Li compositions, deserves a further investigation, especially into the possible redistribution of Li between coexisting minerals.

11. The possible behavior of hydrogen and lithium loss during metamorphic and dehydration processes of granulites deserves a careful investigation.

12. If accepting that the ancient crust and mantle contain more water than the modern ones, and assuming the mass of water in oceans remains constant ever since the late Archean, a significant contrast in water amount between ancient and modern hydrosphere + crust + mantle systems is produced. It is necessary to do some work about where such water was lost and about the continental freeboard model.

References

Afonso, J.C., Ranalli, G., 2004. Crustal and mantle strengths in continental lithosphere: is the jelly sandwich model obsolete? *Tectonophysics* **394**, 221-232.

Aimes, R.D., Rossman, G.R., 1984. Water in minerals: a peak in the infrared. *Journal of Geophysical Research* **89**, 4059-4071.

Alabi, A.O., Canfield, R.A., Gough, D.I., 1975. North American central plains conductivity anomaly. *Geophysical Journal of the Royal Astronomical Society* **43**, 815-833.

Andrut, M., Brandstatter, F., Beran, A., 2003. Trace hydrogen zoning in diopside. *Mineralogy and Petrology* **78**, 231-241.

Arndt, N.T., Ginibre, C., Chauvel, C., Albarede, F., Cheadle, M., Herzberg, C., Jenner, G., Lahaye, Y., 1998. Were komatiites wet? *Geology* **26**, 739-742.

Asimow, P.D., Stein, L.C., Mosenfelder, J.L., Rossman, G.R., 2006. Quantitative polarized infrared analysis of trace OH in populations of randomly oriented mineral grains. *American Mineralogist* **91**, 278-284.

Aubaud, C., Hauri, E.H., Hirschmann, M.M., 2004. Hydrogen partition coefficients between nominally anhydrous minerals and basaltic melts. *Geophysical Research Letters* **31**(20), L20611.

Barrat, J.A., Chaussidon, M., Bohn, M., Gillet, P., Gopel, C., Lesourd, M., 2005. Lithium behavior during cooling of a dry basalt: an ion microprobe study of the lunar meteorite Northwest Africa 479. *Geochimica et Cosmochimica Acta* **69**, 5597-5609.

Beck, P., Barrat, J.A., Chaussidon, M., Gillet, P., Bohn, M., 2004. Li isotopic variations in single pyroxenes from the Northwest Africa 480 shergottite (NWA 480): a record of degassing Martian magmas? *Geochimica et Cosmochimica Acta* **68**, 2925-2933.

Beck, P., Chaussidon, M., Barrat, J.A., Gillet, P., Bohn, M., 2006. Diffusion induced Li isotopic fractionation during the cooling of magmatic rocks: the case of pyroxene phenocrysts from nakhlite meteorites. *Geochimica et Cosmochimica Acta* **70**, 4813-4825.

Bell, D.R., Ihinger, P.D., 2000. The isotopic composition of hydrogen in nominally anhydrous mantle minerals. *Geochimica Et Cosmochimica Acta* **64**(12), 2109-2118.

Bell, D.R., Ihinger, P.D., Rossman, G.R., 1995. Quantitative analysis of trace OH in garnet and pyroxenes. *American Mineralogist* **80**(5-6), 465-474.

Bell, D.R., Rossman, G.R., 1992a. The distribution of hydroxyl in garnets from the subcontinental mantle of Southern Africa. *Contributions to Mineralogy and Petrology* **111**, 161-178.

Bell, D.R., Rossman, G.R., 1992b. Water in Earth's mantle: The role of nominally anhydrous

minerals. *Science* **255**, 1391-1397.

Bell, D.R., Rossman, G.R., Maldener, J., Endisch, D., Rauch, F., 2003. Hydroxide in olivine: A quantitative determination of the absolute amount and calibration of the IR spectrum. *Journal of Geophysical Research-Solid Earth* **108**(B2), -.

Bell, D.R., Rossman, G.R., Moore, R.O., 2004. Abundance and partitioning of OH in a high-pressure magmatic system: Megacrysts from the Monastery kimberlite, South Africa. *Journal of Petrology* **45**(8), 1539-1564.

Bezos, A., Humler, E., 2005. The $Fe^{3+}/\Sigma Fe$ ratios of MORB glasses and their implications for mantle melting. *Geochimica et Cosmochimica Acta* **69**, 711-725.

Bolfan-Casanova, N., 2005. Water in the Earth's mantle. *Mineralogical Magazine* **69**, 229-257.

Bolfan-Casanova, N., Keppler, H., Rubie, D.C., 2003. Water partitioning at 660 km depth and evidence for very low water solubility in magnesium silicate perovskite. *Geophysical Research Letters* **30**(17), -.

Brace, W.F., 1971. Resistivity of saturated crustal rocks up to 40 km based on laboratory measurements. In: Heacock, J.G. (Ed.), *Structure and Physical Properties of the Earth's Crust*. AGU Geophys. Monogr. Ser., Washington, DC. Vol., pp. 243-255.

Brenan, J.M., Ryerson, F.J., Shaw, H.F., 1998. The role of aqueous fluids in the slab-to-mantle transfer of boron, beryllium, and lithium during subduction: experiments and models. *Geochimica et Cosmochimica Acta* **62**, 3337-3347.

Brey, G.P., Kohler, T., 1990. Geothermobarometry in four-phase lherzolites II. New thermobarometers, and practical assessment of existing thermobarmeters. *Journal of Petrology* **31**, 1353-1378.

Bromiley, G.D., Keppler, H., McCammon, C., Bromiley, F.A., Jacobsen, S.D., 2004. Hydrogen solubility and speciation in natural, gem-quality chromian diopside. *American Mineralogist* **89**(8-9), 1352-1352.

Burns, R.G., 1993. Mineralogical and Applications of Crystal Field Theory (2nd edition). New York, Cambridge University Press.

Burov, E.B., Watts, A.B., 2006. The long-term strength of continental lithosphere: "jelly sandwich" or "crème brûlée"? *GSA Today* **16**(1), 4-10.

Canil, D., O'Neil, H.S.C., Rudnick, R.L., McDonough, W.F., Carswell, D.A., 1994. Ferric iron in peridotites and mantle oxidation states. *Earth and Planetary Science Letters* **123**, 205-220.

Cesare, B., Meli, S., Nodari, L., Russo, U., 2005. Fe^{3+} reduction during biotite melting in graphitic metapelites: another origin of CO_2 in granulites. *Contributions to Mineralogy and Petrology* **149**, 129-140.

Chan, L.H. (2003). Variation in lithium isotopic composition in terrestrial systems. 13th Goldschmidt Conference #A57 (abstract).

Chan, L.H., Edmond, J.M., 1988. Variation of lithium isotope composition in the marine environment: a preliminary report. *Geochimica et Cosmochimica Acta* **52**, 1711-1717.

Chaussidon, M., Robert, F., 1998. $^{7}Li/^{6}Li$ and $^{11}B/^{10}B$ variations in chondrules from Semarkora unequilibrated chondrites. *Earth and Planetary Science Letters* **164**, 577-589.

Chen, D.G., Peng, Z.C., 1988. K-Ar ages and Sr, Pb isotopic characteristics of Cenozoic volcanic rocks in Jiangsu and Anhui provinces. *Acta Petrologica Sinica* **4**, 3-12.

Chen, J.F., Foland, K.A., Xing, F.M., Xu, X., Zhou, T.X., 1991. Magmatism along the southeastern margin of the Yangtze block: Precambrian collision of the Yangtze and Cathysia blocks of China. *Geology* **19**, 815-818.

Chen, J.F., Jahn, B.M., 1998. Crustal evolution of southeastern China: Nd and Sr isotopic evidence. *Tectonophysics* **284**, 101-133.

Chen, S.H., O'Reilly, S.Y., Zhou, X.H., Griffin, W.L., Zhang, G.H., Sun, M., Feng, J.L., Zhang, M., 2001. Thermal and petrological structure of the lithosphere beneath Hannuoba, Sino-Korean Craton, China: evidence from xenoliths. *Lithos* **56**, 267-301.

Chen, S.S., Hiraga, T., Kohlstedt, D.L., 2006. Water weakening of clinopyroxene in the dislocation creep regime. *Journal of Geophysical Research* **111**, B08203, doi: 10.1029/2005JB003885.

Christensen, N.I., Mooney, W.D., 1995. Seismic velocity structure and composition of the continental crust - a global view. *Journal of Geophysical Research* **100**, 9761-9788.

Clemens, J.D., Droop, G.T.R., Stevens, G., 1997. High-grade metamorphism, dehydration and crustal melting: a reinvestigation based on new experiments in the silica-saturated portion of the system $KAlO_2$-MgO-SiO_2-H_2O-CO_2 at $P \leqslant 1.5$ GPa. *Contributions to Mineralogy and Petrology* **129**, 308-325.

Collerson, K.D., Fryer, B.J., 1978. The role of fluids in the formation and subsequent development of the early crust. *Contributions to Mineralogy and Petrology* **67**, 151-167.

Condie, K.C., 2004. Supercontinents and superplume event: distinguishing signals in the geologic record. *Physics of the Earth and Planetary Interiors* **146**, 319-332.

Connolly, J.A.D., Thompson, A.B., 1989. Fluid and enthalpy production during regional metamorphism. *Contributions to Mineralogy and Petrology* **102**, 347-366.

Coogan, L.A., Kasemann, S.A., Chackraoborty, S., 2005. Rates of hydrothermal cooling of new oceanic upper crust derived from lithium-geospeedometry. *Earth and Planetary Science Letters* **240**(2), 415-424.

Criss, R.E., Taylor, H.P., 1986. Meteoric-hydrothermal systems. In: Valley, J.W., Taylor, H.P., O'Neil, J.R. (Ed.), *Stable isotopes in high temperature geological processes*. Reviews in Mineralogy, Mineralogical Society of America, Washington, D.C. Vol. 16, pp. 373-424.

Dai, B.Z., Jiang, S.Y., Jiang, Y.H., Zhao, K.D., Liu, D.Y., 2008. Geochronology, geochemistry and Hf-Sr-Nd isotopic compositions of Huziyan mafic xenoliths, southern Hunan Province, South China: petrogenesis and implications for lower crust evolution. *Lithos*.

Danyuschevsky, L.V., Eggins, S.M., Falloon, T.J., Christie, D.M., 2000. H_2O abundance in depleted to moderately enriched mid-ocean ridge magmas, Part I: incompatible behaviour, implications for mantle storage, and origin of regional variations. *Journal of Petrology* **41**, 1329-1364.

Davis, G., 1994. Thermomechanical erosion of the lithosphere by mantle plume. *Journal of Geophysical Research* **99**, 15709-15722.

Decitre, S., Deloule, E., Reisberg, L., James, R., Agrinier, P., Mével, C., 2002. Behavior of Li and its isotopes during serpentinization of oceanic peridotites. *Geochemistry, Geophysics, Geosystems* **3**, doi:10.1029/2001GC000178.

Deer, W.A., Howie, R.A., Zussan, J., 1992. An introduction to the rock-forming minerals, 2nd edition. Essex, England, Longman Scientific and Technical.

Deloule, E., Albarède, F., Sheppard, S., 1991a. Hydrogen isotope heterogeneities in the mantle from ion probe analysis of amphiboles from ultramafic rocks. *Earth and Planetary Science Letters* **105**, 543-553.

Deloule, E., France-Lanord, C., Albarède, F., 1991b. D/H analysis of minerals by ion probe. In: Taylor, H.P., O'Neil, J.R., Kaplan, I.R. (Ed.), *Stable isotope gepchemistry: a tribute to Samuel Epstein*. The Geochemistry Society: Special Publication, 3, pp. 53-62.

Demény, A., Vennemann, T.W., Harangi, S., Homonnay, Z., Fórizs, I., 2006. H_2O-δD-Fe^{III} relations of dehydrogenation and dehydration processes in magmatic amphiboles. *Rapid Communications in Mass Spectrometry* **20**, 919-925.

Demouchy, S., Jacobsen, S.D., Gaillard, F., Stern, C.R., 2006. Rapid magma ascent recorded by water diffusion profiles in mantle olivine. *Geology* **34**(6), 429-432.

Dimanov, A., Dresen, G., 2005. Rheology of synthetic anorthite-diopside aggregates: implications for ductile shear zones. *Journal of Geophysical Research* **110**, B07203, doi: 10.1029/2004JB003431.

Dirks, P.H.G.M., Zhang, J.S., Passchier, C.W., 1997. Exhumation of high-pressure granulites and the role of lower crustal advection in the North China Craton near Datong. *Journal of Structural Geology* **19**, 1343-1358.

Dixon, J.E., Dixon, T.H., Bell, D., Malservisi, R., 2004. Lateral variation in upper mantle viscosity:

role of water. *Earth and Planetary Science Letters* **222**, 451-467.

Dobson, P.F., Epstein, S., Stolper, E.M., 1989. Hydrogen isotope fractionation between coexisting vapor and silicate glasses and melts at low pressure. *Geochimica Et Cosmochimica Acta* **53**, 2723-2730.

Duba, A.G., Heikamp, S., Meurer, W., Nover, H., Will, G., 1994. Evidence from borehole samples for the role of accessory minerals in lower-crustal conductivity. *Nature* **367**, 59-61.

Duba, A.G., Shankland, T.J., 1987. Analyzing electromagnetic data: suggestions from laboratory measurements. *Pure and Applied Geophysics* **125**, 285-289.

Eiler, M., 2001. Oxygen isotope variations of basaltic lavas and upper mantle rocks. In: Valley, J.W., Cole, D.R. (Ed.), *Stable Isotope Geochemistry*. Reviews in Mineralogy and Geochemistry, 43, pp. 319-364.

Elliott, T., Jeffcoate, A.B., Bouman, C., 2004. The terrestrial Li isotope cycle: light-weight constraints on mantle convection. *Earth and Planetary Science Letters* **220**, 231-245.

Elphick, S.C., Graham, C.M., Dennis, P., 1988. An ion-microprobe study of anhydrous O diffusion in anorthite: a comparison with hydrothermal data and some geological implications. *Contributions to Mineralogy and Petrology* **76**, 440-454.

Fahey, A.J., Goswami, J.N., McKeegan, K.D., Zinner, E., 1987. ^{26}Al, ^{244}Pu, ^{50}Ti, REE and trace element abundances in hibonite grains from CM and CV meteorites. *Geochimica et Cosmochimica Acta* **51**, 329-350.

Fan, Q.C., Liu, R.X., Li, H.M., Li, N., Sui, J.L., Lin, Z.R., 1998. Zircon chronology and REE geochemistry of granulite xenoliths from Hannuoba. *Chinese Science Bulletin* **43**(2), 133-137.

Fan, Q.C., Zhang, H.F., Sui, J.L., Zhai, M.G., Sun, J., Li, N., 2005. Magma underplating and composition of the present crust-mantle transitional zone: petrological and geochemical evidence from xenoliths. *Science in China (Series D)* **35**(1), 1-14.

Fan, W.M., Menzies, M.A., 1992. Destribution of aged lower lithosphere and accretion of asthenosphere mantle beneath eastern China. *Geotectonic et Metallogenia* **16**(3-4), 171-180.

Fan, W.M., Zhang, H.F., Baker, J., Jarvis, K.E., Mason, P.R.D., Menzies, M.A., 2000. On and off the North China craton: where is the Archean keel? *Journal of Petrology* **41**, 933-950.

Feldstein, S.N., Lange, R.A., Vennemann, T.W., O'Neil, J.R., 1996. Ferric-ferrous ratios, H_2O contents and D/H ratios of phlogopite and biotite from lavas of different tectonic regimes. *Contributions to Mineralogy and Petrology* **126**, 51-66.

Flesh, G.D., Anderson, A.R., Svec, H.J., 1973. A secondary isotopic standard for ^{7}Li/^{6}Li determination. *International Journal of Mass Spectrometry and Ion Processes* **12**, 265-272.

Freed, A.M., Burgmann, R., 2004. Evidence of power-law flow in the Mojave desert mantle.

Nature **430**, 548-551.

Freund, F., 2003. On the electrical conductivity structure of the stable continental crust. *Journal of Geodynamics* **35**(3), 353-388.

Frost, B.R., Fyfe, W.S., Tazaki, K., Chan, T., 1989. Grain-boundary graphite in rocks and implications for high electrical conductivity in the lower crust. *Nature* **340**, 134-136.

Gan, X., Li, H., Sun, D., Zhuang, J., 1993. Geochronological study on the Precambrian metamorphic basement in Northern Fujian. *Fujian Geol.* **12**, 17-32.

Gao, S., Lin, W.L., Qiu, Y.M., 1999. Contrasting geochemical and Sm-Nd isotopic compositions of Archean Metasediments from the Kongling high-grade terrain of the Yangtze craton: evidence from cratonic evolution and redistribution of REE during crustal anatexis. *Geochimica et Cosmochimica Acta* **13-14**, 2071-2088.

Gao, S., Rudnick, R., Carlson, R.W., McDonough, W.F., Liu, Y.S., 2002. Re-Os evidence for the replacement of ancient mantle lithosphere beneath the North China craton. *Earth and Planetary Science Letters* **198**, 307-322.

Gao, S., Rudnick, R.L., Yuan, H.L., Liu, X.M., Liu, Y.S., Xu, W.L., Ling, W.L., Ayers, J., Wang, X.C., Wang, Q.H., 2004. Recycling lower continental crust in the North China craton. *Nature* **432**(7019), 892-897.

Gao, S., Zhang, B.R., Jin, Z.M., Kern, H., Luo, T.C., Zhao, Z.D., 1998. How mafic is the lower continental crust? *Earth and Planetary Science Letters* **161**(1-4), 101-117.

Gayk, T., Kleinschrodt, R., Langosch, A., Seidel, E., 1995. Quartz exsolution in clinopyroxene of high-pressure granulite from the Munchberg Massif. *European Journal of Mineralogy* **7**, 1217-1220.

Glover, P.W.J., 1996. Graphite and electrical conductivity in the lower continental crust: a review. *Physics and Chemistry of The Earth* **21**(4), 279-287.

Glover, P.W.J., Vine, F.J., 1992. Electrical conductivity of carbon-bearing granulite at raised temperatures and pressures. *Nature* **360**, 723-726.

Glover, P.W.J., Vine, F.J., 1994. Electrical conductivity of the continental crust. *Geophysical Research Letters* **21**(22), 2357-2360.

Goldsmith, J.R., 1987. Al/Si interdiffusion in albite: effect of pressure and the role of hydrogen. *Contributions to Mineralogy and Petrology* **95**, 311-321.

Graham, C.M., Harmon, R.S., Sheppard, S.M.F., 1984. Experimental hydrogen isotope studies: hydrogen isotope exchange between amphibole and water. *American Mineralogist* **69**, 128-138.

Graham, C.M., Kinny, P., Harte, B., Valley, J.W., 1994. The nature and scale of stable isotope

disequilibrium in the mantle: ion and laser microprobe evidence. *Goldschmidt Conference Edinburgh*, 345-346.

Grant, K.J., Ingrin, J., Lorand, J.P., Dumas, P., 2007a. Water partitioning between mantle minerals from peridotite xenoliths. *Contributions to Mineralogy and Petrology*, doi: 10.1007/s00410-006-0177-1.

Grant, K.J., Kohn, S.C., Brooker, R.A., 2007b. The partitioning of water between olivine, orthopyroxene and melt synthesised in the system albite-forsterite-H_2O. *Earth and Planetary Science Letters* **260**, 227-241.

Griffin, W.L., Zhang, A.D., O'Reilly, S.Y., Ryan, C.G., 1998. Phanerozoic evolution of the lithosphere beneath the Sino-Korean craton. In: Flower, M., Chung, S.L., Lo, C.H., Lee, T.Y. (Ed.), *Mantle Dynamics and Plate Interactions in East Asia*. American Geophysical Union, Washington, DC. Vol., pp. 107-126.

Griggs, D.T., 1967. Hydrolytic weakening of quartz and other silicates. *Geophysical Journal International* **14**, 19-31.

Griggs, D.T., Blacic, J.D., 1965. Quartz: anomalous weakness of synthetic crystals. *Science* **147**, 292-295.

Guo, F., Fan, W.M., Lin, G., Lin, Y.X., 1997a. Chronology and petrogenesis of gabbro xenoliths from Daoxian, Hunan. *Chinese science bulletin* **42**(15), 1661-1664.

Guo, F., Fan, W.M., Lin, G., Lin, Y.X., 1997b. Sm-Nd dating and petrogenesis of mesozoic gabbro xenoliths in Daoxian County, Hunan Province. *Chinese Science Bulletin* **42**, 1661-1663.

Guo, F., Wu, Y.L., Fan, W.M., Lin, G., 1996. A petrological study of the gabbro xenoliths from Mesozoic basalts in Ningyuan-Daoxian, Hunan. *Geotectonica et Metallogenia* **20**(1), 38-45.

Guo, J.H., O'Brien, P.J., Zhai, M.G., 2002. High-pressure granulites in the Sanggan area, North China Craton: metamorphic evolution, P-T paths and geotectonic significance. *Journal of Metamorphic Geology* **20**, 741-756.

Guo, J.H., Sun, M., Chen, F.K., Zhai, M.G., 2005. Sm-Nd and SHRIMP U-Pb zircon geochronology of high-pressure granulites in the Sanggan area, North China Craton: timing of Paleoproterozoic continental collision. *Journal of Asian Earth Sciences* **24**, 629-642.

Guo, J.H., Zhai, M.G., Zhang, Y.G., Li, Y.G., Yan, Y.H., Zhang, W.H., 1993. Early Precambrian Manjinggou high-P granulite melange belt on the south edge of the Huai'an complex, North China craton: geological features, petrology and isotopic geochronology. *Acta Petrologica Sinica* **9**, 329-340.

Haak, V., Hutton, R., 1986. Electrical resistivity in continental lower crust. *Geological Society* **24**, 35-49.

Hacker, B.R., Ratschbacher, L., Webb, L., Ireland, T., Walker, D., Dong, S., 1998. U/Pb zircon ages constrain the architecture of the ultrahigh-pressure Qinling-Dabie Orogen, China. *Earth and Planetary Science Letters* **161**, 215-230.

Halama, R., McDonough, W.F., Rudnick, R.L., Bell, K., 2008. Tracking the lithium isotopic evolution of the mantle using carbonatites. *Earth and Planetary Science Letters* **265**, 726-742.

Harley, S.L., 1987. A pyroxene-bearing metaironstone and other pyroxene-granulites from Tonagh Island, Enderby Land, Antarctica: further evidence for very high temperature (> 980°C) Archaean regional metamorphism in the Napier Complex. *Journal of Metamorphic Geology* **5**, 341-356.

Harley, S.L., 1989. The origin of granulites: a metamorphic perspective. *Geological Magazine* **126**, 215-247.

Harmon, R.S., Hoefs, J., 1995. Oxygen isotope heterogeneity of the mantle deduced from global ^{18}O systematics of basalts from different geotectonic settings. *Contributions to Mineralogy and Petrology* **120**, 95-114.

Hauri, E.H., Gaetani, G.A., Green, T.H., 2006. Partitioning of water during melting of the Earth's upper mantle at H_2O-undersaturated conditions. *Earth and Planetary Science Letters* **248**, 715-734.

He, L.J., Hu, S.B., Wang, J.Y., 2001. Thermal structure of the continental lithosphere beneath east China. *Progress in Natural Science* **11**, 966-969.

Hercule, S., Ingrin, J., 1999. Hydrogen in diopside: diffusion, kinetics of extraction-incorporation, and solubility. *American Mineralogist* **84**, 1577-1587.

Hermance, J.F., 1979. The electrical conductivity of materials containing partial melt. *Geophysical Research Letters* **6**, 613-616.

Hermance, J.F., 1995. Electrical conductivity models of the crust and mantle. In: Ahrens, T.J. (Ed.), *Global Earth Physics: A handbook of physical constants*. American Geophysical Union, Washington, DC. Vol., pp. 190-205.

Hier-Majumder, S., Mei, S., Kohlstedt, D.L., 2005. Water weakening of clinopyroxeneite in diffusion creep. *Journal of Geophysical Research* **110**, B07406, doi: 10.1029/2004JB003414.

Hinton, R.W., 1990. Ion microprobe trace-element analysis of silicates: measurement of multi-element glasses. *Chemical Geology* **83**, 11-25.

Hirschmann, M., 2006. Water, melting, and the deep earth H_2O cycle. *Annual Review of Earth and Planetary Sciences* **34**, 629-653.

Hirschmann, M.M., Aubaud, C., Withers, A., 2005. Storage capacity of H2O in nominally anhydrous minerals in the upper mantle *Earth and Planetary Science Letters* **236**(1-2),

167-181.

Hirth, G., Kohlstedt, D.L., 1996. Water in the oceanic upper mantle: implications for rheology, melt extraction and the evolution of the lithosphere. *Earth and Planetary Science Letters* **144**, 93-108.

Hirth, G., Kohlstedt, D.L., 2003. Rheology of the upper mantle and the mantle wedge: A view from the experimentalists. In: Eiler, J. (Ed.), *Inside the Subduction Factory*. Geophysical Monograph, American Geophysical Union, 138, pp. 83-105.

Hoefs, J., 1997. Stable isotope geochemistry. Heidelberg, Springer-Verlag.

Holbrook, W.S., Mooney, W.D., Christensen, N.I., 1992. The seismic velocity structure of the deep continental crust. In: Fountain, D.M., Arculus, R., Kay, R.W. (Ed.), *Continental lower crust*. Elsevier, Amsterdam. Vol., pp. 1-44.

Hu, S., He, L., Wang, J., 2000. Heat flow in the continental area of China: a new data set. *Earth and Planetary Science Letters* **179**, 407-419.

Huang, J.L., Zhao, D.P., 2006. High-resolution mantle tomography of China and surrounding regions. *Journal of Geophysical Research* **111**, doi: 2005JB004066.

Huang, X.G., Xu, Y.S., Karato, S.I., 2005. Water content in the transition zone from electrical conductivity of wadsleyite and ringwoodite. *Nature* **434**(7034), 746-749.

Huang, X.L., Xu, Y.G., Chu, X.L., Zhang, H.X., 2001. Geochemical comparative studies of some granulite terrains and granulite xenoliths from North China craton. *Acta Petrologica et Mineralogica* **20**(3), 318-328.

Huang, X.L., Xu, Y.G., Liu, D.Y., 2004. Geochronology, petrology and geochemistry of the granulite xenoliths from Nushan, east China: Implication for a heterogeneous lower crust beneath the Sino-Korean Craton. *Geochimica Et Cosmochimica Acta* **68**(1), 127-149.

Hyndman, R.D., Shearer, P.M., 1989. Water in the lower continental crust: modelling magnetotelluric and seismic reflection results. *Geophysical Journal International* **98**, 343-365.

Hyndman, R.D., Vanyan, L.L., Marquis, G., Law, L.K., 1993. The origin of electrically conductive lower continental crust - saline water or graphite? *Physics of the Earth and Planetary Interiors* **81**, 325-344.

Ichiki, M., Baba, K., Obayashi, M., Utada, H., 2006. Water content and geotherm in the upper mantle above the stagnant slab: interpretation of electrical conductivity and seismic P-wave velocity models. *Physics of the Earth and Planetary Interiors* **155**, 1-15.

Ingrin, J., Blanchard, M., 2006. Diffusion of hydrogen in minerals. In: Keppler, H., Smyth, J.R. (Ed.), *Water in nominally anhydrous minerals*. Mineralogical Society of America, Washington D C. Vol. 62, pp. 291-320.

Ingrin, J., Hercule, S., Charton, T., 1995. Difffusion of hydrogen in diopside: results of dehydration experiments. *Journal of Geophysical Research* **100**, 15489-15499.

Ingrin, J., Skogby, H., 2000. Hydrogen in nominally anhydrous upper-mantle minerals: concentration levels and implications. *European Journal of Mineralogy* **12**(3), 543-570.

Ionov, D.A., Seitz, H.M., 2008. Lithium abundances and isotopic compositions in mantle xenoliths from subduction and intra-plate settings: mantle sources vs. eruption histories. *Earth and Planetary Science Letters* **266**, 316-331.

Jaffe, H.W., Robinson, P., Tracy, R.J., Ross, M., 1975. Orientation of pigeonite exsolution lamellae in metamorphic augite: correlation with composition and calculated optimal phase boundaries. *American Mineralogist* **60**, 9-28.

Jaupart, C., Mareschal, J.C., 2003. Constraints on crustal heat production from heat flow data. In: Rudnick, R.L. (Ed.), *Treatise on Geochemistry: The Crust*. Elsevier, Amsterdam. Vol., pp. 65-84.

Jeffcoate, A.B., Elliott, T., Kasemann, S.A., Ionov, D., Cooper, K., Brooker, R., 2007. Li isotope fractionation in peridotites and mafic melts. *Geochimica et Cosmochimica Acta* **71**, 202-218.

Jin, W., Sun, D., 1997. Deep Crustal Structure and its Evolution of South China. Beijing, Geological Publishing House.

Jochum, K.P., Stoll, B., Herwig, K., Willbold, M., Hofmann, A.W., Amini, M., Aarburg, S., 2006. MPI-DING reference glasses for in situ microanalysis: New reference values for element concentrations and isotope ratios. *Geochemistry Geophysics Geosystems* **7**, doi: 10.1029/2005GC001060.

Johnson, E.A., *Hydrogen in nominally anhydrous crustal minerals*. Ph. D. thesis, California Institute of Technology

Johnson, E.A., 2006. Water in nominally anhydrous crustal minerals: speciation, concentration, and geologic significance. In: Keppler, H., Smyth, J.R. (Ed.), *Water in Nominally Anhydrous Minerals*. Mineralogical Society of America, Washington D C. Vol. 62, pp. 117-154.

Johnson, E.A., Rossman, G.R., 2003. The concentration and speciation of hydrogen in feldspars using FTIR and H-1 MAS NMR spectroscopy. *American Mineralogist* **88**(5-6), 901-911.

Johnson, E.A., Rossman, G.R., 2004. A survey of hydrous species and concentrations in igneous feldspars. *American Mineralogist* **89**(4), 586-600.

Johnson, E.A., Rossman, G.R., Dyar, M.D., Valley, J.W., 2002. Correlation between OH concentration and oxygen isotope diffusion rate in diopsides from the Adirondack Mountains, New York. *American Mineralogist* **87**(7), 899-908.

Jones, A.G., 1992. Electrical Properties of the Lower Continental Crust. In: Fountain, D.M., Arculus, R.J., Kay, R.W. (Ed.), *Continental Lower Crust*. Elsevier, Amsterdam. Vol., pp. 81-143.

Karato, S., 1990. The role of hydrogen in the electrical conductivity of the upper mantle. *Nature* **347**(6290), 272-273.

Karato, S., Jung, H., 2003. Effects of pressure on high-temperature dislocation creep in olivine. *Philosophical Magazine* **83**, 401-414.

Karato, S.I., Jung, H., Katayama, I., Skemer, P., 2008. Geodynamic significance of seismic anisotropy of the upper mantle: New insights from laboratory studies. *Annual Review of Earth and Planetary Sciences* **36**, 59-95.

Katayama, I., Nakashima, S., Yurimoto, H., 2006. Water content in natural eclogite and implication for water transport into the deep upper mantle. *Lithos* **86**, 245-259.

Katsube, J.T., Mareschal, M., 1993. Petrophysical model of deep electrical conductors: Graphite lining as a source of its disconnection due to uplife. *Journal of Geophysical Research* **98**, 8019-8030.

Kaufmann, G., Lambeck, K., 2002. Glacial isostatic adjustment and the radial viscosity profile from inverse modeling. *Journal of Geophysical Research* **107**, doi: 10.1029/2001JB000941.

Kelley, S.I., Wartho, J.A., 2000. Rapid kimberlite ascent and significance of Ar-Ar ages in xenolith phlogopites. *Science* **289**, 609-611.

Kempton, P.D., Harmon, R.S., 1992. Oxygen isotope evidence for large-scale hybridization of the lower crust during magmatic underplating. *Geochimica et Cosmochimica Acta* **56**(3), 971-986.

Kenner, S.J., 2004. Rheological controls on fault loading rates in northern California following the 1906 San Francisco earthquake. *Geophysical Research Letters* **31**, L01606, doi: 10.1029/2003GL018903.

Keppler, H., Bolfan-Casanova, N., 2006. Thermodynamics of water solubility and partitioning. In: Keppler, H., Smyth, J.R. (Ed.), *Water in Nominally Anhydrous Minerals*. Mineralogical Society of America, Washington D C. Vol. 62, pp. 193-230.

Keppler, H., Smyth, J.R., 2006. Water in Nominally Anhydrous Minerals. Washington D C, Mineralogical Society of America.

Koga, K., Hauri, E., Hirschmann, M., Bell, D., 2003. Hydrogen concentration analyses using SIMS and FTIR: Comparison and calibration for nominally anhydrous minerals. *Geochemistry Geophysics Geosystems* **4**(2), 1019.

Kohlstedt, D.L., 2006. The role of water in high-temperature rock deformation. In: Keppler, H.,

Smyth, J.R. (Ed.), *Water in Nominally anhydrous minerals*. Mineralogical Society of America, Washington D C. Vol. 62, pp. 377-396.

Kohlstedt, D.L., Evans, B., Mackwell, S., 1995. Strength of the lithosphere: constrains imposed by laboratory experiments. *Journal of Geophysical Research* **100**, 17587-17602.

Kohlstedt, D.L., Mackwell, S.J., 1998. Diffusion of hydrogen and intrinsic point defects in olivine. *Zeitschrift Fur Physikalische Chemie* **207**, 147-162.

Kohlstedt, D.L., Mackwell, S.J., 1999. Solubility and diffusion of "water" in silicate minerals. In: Wright, K., Catlow, R. (Ed.), *Microscopic properties and processes in minerals*. Kluwer Academic Publishers, Dordrecht. Vol., pp. 539-559.

Kong, H., Jin, Z.M., Xi, X.S., 2002. Single grain zircon U-Pb dating of gabbro xenolith from Daoxian alkaline basalt, Hunan Province. *Acta Mineralogica Sinica* **22**(4), 350-352.

Kronenberg, A.K., 1994. Hydrogen speciation and chemical weakening of quartz. In: Heaney, P.J., Prewitt, C.T., Gibbs, G.V. (Ed.), *Silica: physical behavior, geochemistry and materials applications*. Mineralogical Society of American, Washington D C. Vol. 29, pp. 123-176.

Kronenberg, A.K., Kirby, S.H., Aines, R.D., Rossman, G.R., 1986. Solubility and diffusional uptake of hydrogen in quartz at high water pressures: implications for hydrolytic weakending. *Journal of Geophysical Research* **91**, 12723-12744.

Kronenberg, A.K., Yund, R.A., Rossman, G.R., 1996. Stationary and mobile hydrogen defects in potassium feldspar. *Geochimica Et Cosmochimica Acta* **60**, 4075-4094.

Kröner, A., 1985. Evolution of the archean continental crust. *Annual Review of Earth and Planetary Sciences* **13**, 49-74.

Kushiro, I., 1972. Effect of water on the composition of magmas formed at high pressures. *Journal of Petrology* **13**, 311-334.

Kushiro, I., 1990. Partial melting of mantle wedge and evolution of island arc crust. *Journal of Geophysical Research* **95**, 15929-15939.

Kusky, T.M., Li, J.H., Tucker, R.D., 2001. The Archean Dongwanzi opiolite complex, North China Craton 2.505-billion-year-old oceanic crust and mantle. *Science* **292**, 1142-1145.

Kyser, T.K., 1986. Stable isotope variations in the mantle. In: Valley, J.W., Taylor, H.P., O'Neil, J.R. (Ed.), *Isotopes in High Temperature Geological Processes*. Reviews in Mineralogy and Geochemistry, Mineralogical Society of America 16, pp. 141-164.

Kyser, T.K., O'Neil, J.R., 1984. Hydrogen isotope systematics of submarine basalts. *Geochimica Et Cosmochimica Acta* **48**, 2123-2133.

Langer, K., Robarick, E., Sobolev, N.V., Shatsky, V.S., Wang, W., 1993. Single-crystal spectra of garnets from diamondiferous high-pressure metamorphic rocks from Kazakhstan: indica-

tions for OH^-, H_2O, and FeTi charge transfer. *European Journal of Mineralogy* **5**, 1091-1100.

Lee, C.D., Vine, F.J., Ross, R.G., 1983. Electrical conductivity models for the continental crust based on laboratory measurements on high grade metamorphic rocks. *Geophysical Journal of the Royal Astronomical Society* **72**, 353-371.

Li, C.N., Zhong, C.S., Wang, F.Z., Liu, C.F., 2001a. Geochemistry and petrogenesis of Mesozoic basaltic rocks and their deep-source enclaves in northern Guangxi-southern Hunan. *Acta Petrologica et Mineralogica* **20**, 112-122.

Li, J.H., Hou, G.T., Huang, X.N., Zhang, Z.Q., Qian, X.L., 2001b. Constraints on the supercontinental cycles: evidence from Precambrian geology of North China Craton. *Acta Petrolei Sinica* **17**, 177-186.

Li, J.H., Qian, X.L., Huang, X.N., Liu, S.W., 2000. Tectonic framework of the North China Craton and its cratonization in the early Precambrian. *Acta Petrolei Sinica* **16**, 1-10.

Li, J.H., Zhai, M.G., Qian, X.L., Guo, J.H., 1998. The geological occurrence, regional tectonic setting and exhumation of late Archean high-pressure granulite with the high-grade metamorphic terranes, north to central portion of North China Craton. *Acta Petrologica Sinica* **14**, 176-189.

Li, W.X., Li, X.H., Li, Z.X., 2005. Neoproterozoic bimodal magmatism in the Cathaysia Block of South China and its tectonic significance. *Precambrian Research* **136**, 51-66.

Li, X.H., 1997. Timing of the Cathaysia Block initiation:Constraints from SHRIMP U-Pb zircon geochronology. *Episodes* **20**, 188-192.

Li, X.H., 1999. U-Pb zircon ages of granites from the southern margin of the Yangtze block: timing of Neoproterozoic Jinning, orogeny in SE China and implications for Rodinia assembly. *Precambrian Research* **97**, 43-57.

Li, X.H., Chung, S.L., Zhou, H.W., Lo, C.H., Liu, Y., Chen, C.H., 2004. Jurassic intraplate magmatism in southern Hunan-eastern Guangxi: $^{40}Ar/^{39}Ar$ dating, geochemistry, Sr-Nd isotopes and implications for the tectonic evolution of SE China. *Geological Society (London). Special Publication* **226**, 193-215.

Li, X.H., Li, Z.X., Ge, W., Zhou, H., Li, W., Liu, Y., Wingate, M.T.D., 2003a. Neoproterozoic granitoids in South China: crustal melting above a mantle plume at ca. 825 Ma? *Precambrian Research* **122**, 45-83.

Li, Z.X., Li, X.H., Kinny, P.D., Wang, J., Zhang, S., Zhou, H., 2003b. Geochronology of Neoproterozoic syn-rift magmatism in the Yangtze Craton, South China and correlations with other continents: evidence for a mantle superplume that broke up Rodinia. *Precambrian Research* **122**, 85-109.

Li, Z.X., Li, X.H., Zhou, H., Kinny, P.D., 2002. Grenvillian continental collision in South China:

new SHRIMP U-Pb zircon results and implications for the configuration of Rodinia. *Geology* **30**, 163-166.

Libowitzky, E., Rossman, G.R., 1996. Principles of quantitative absorbance measurements in anisotropic crystals. *Physics and Chemistry of Minerals* **23**(6), 319-327.

Libowitzky, E., Rossman, G.R., 1997. An IR absorption calibration for water in minerals. *American Mineralogist* **82**(11-12), 1111-1115.

Liu, D.Y., Nutman, A.P., Compston, W., Wu, J.S., Shen, Q.H., 1992. Remnants of >3800 Ma crust in the Chinese part of the Sino-Korean craton. *Geology* **20**, 339-342.

Liu, Y.S., Gao, S., Jin, S.Y., Hu, S.H., Sun, M., Zhao, Z.B., Feng, J.L., 2001. Geochemistry of lower crustal xenoliths from Neogene Hannuoba basalt, North China craton: implications for petrogenesis and lower crustal composition. *Geochimica Et Cosmochimica Acta* **65**, 2589-2604.

Liu, Y.S., Gao, S., Lee, C.T.A., Hu, S.H., Liu, X.M., Yuan, H.L., 2005. Melt-peridotite interactions: Links between garnet pyroxenite and high-Mg# signature of continental crust. *Earth and Planetary Science Letters* **234**(1-2), 39-57.

Liu, Y.S., Gao, S., Yuan, H.L., Zhou, L., Liu, X.M., Wang, X.C., Hu, Z.C., Wang, L.S., 2004. U-Pb zircon ages and Nd, Sr, and Pb isotopes of lower crustal xenoliths from North China Craton: insights on evolution of lower continental crust. *Chemical Geology* **211**(1-2), 87-109.

Lundstrom, C.C., Chaussidon, M., Hsui, A.T., Kelemen, P., Zimmerman, M.E., 2005. Observations of Li isotopic variations in the Trinity Ophiolite: evidence for isotopic fractionation by diffusion during mantle melting. *Geochimica et Cosmochimica Acta* **69**(3), 735-751.

Ma, X.Y., 1989. Lithospheric Dynamics Map of China and Adjacent Seas (1:4,000,000) and Explanatory Notes. Beijing, Geological Publishing House.

Mackwell, S., Zimmerman, M.E., Kohlstedt, D.L., 1998. High-temperature deformation of dry diabase with application to tectonics on Venus. *Journal of Geophysical Research* **103**, 975-984.

Magna, T., Wiechert, U., Halliday, A.N., 2006. New constraints on the lithium isotope compositions of the Moon and terrestrial planets. *Earth and Planetary Science Letters* **243**(3-4), 336-353.

Mareschal, M., Fyfe, W.S., Percival, J., Chan, T., 1992. Grain-boundary graphite in Kapuskaing gneisses and implications for lower-crustal conductivity. *Nature* **357**, 674-676.

Mareschal, M., Kellet, R.L., Kurtz, R.D., Ludden, J.N., Ji, S.C., Bailey, R.C., 1995. Archean cratonic roots, mantle shear zones and deep electrical anisotropy. *Nature* **375**, 134-137.

Marschall, H.R., Pogge von Stradmann, P.A.E., Seitz, H.M., Elliott, T., Niu, Y.L., 2007. The lithium

isotopic composition of orogenic eclogites and deep subducted slabs. *Earth and Planetary Science Letters* **262**, 563-580.

Martin, R.F., Donnay, G., 1972. Hydroxyl in the mantle. *American Mineralogist* **57**, 554-570.

Mattey, D., Lowry, D., Macpherson, C., 1994. Oxygen isotope composition of mantle peridotite. *Earth and Planetary Science Letters* **128**, 231-241.

McCammon, C., 2005. The paradox of mantle redox. *Science* **308**, 807-808.

McLennan, S.M., Taylor, S.R., 1999. Earth's Continental Crust. In: Marshall, C.P., Fairbridge, R.W. (Ed.), *Encyclopedia of Geochemistry*. Springer, New York. Vol., pp. 712.

Meade, C., Jeanloz, R., 1991. Deep-focus earthquakes and recycling of water into the Earth. *Science* **252**, 68-72.

Mei, S., Kohlstedt, D.L., 2000a. Influence of water on plastic deformation of olivine aggregates 1. diffusion creep regime. *Journal of Geophysical Research* **105**, 21457-21469.

Mei, S., Kohlstedt, D.L., 2000b. Influence of water on plastic deformation of olivine aggregates 2. dislocation creep regime. *Journal of Geophysical Research* **105**, 21471-21481.

Menzies, M.A., Fan, W.M., Zhang, M., 1993. Palaeozoic and Cenozoic lithoprobes and loss of > 120 km of Archean lithosphere, Sino-Korean craon, China. In: Prichard, H.M., Alabaster, T., Harris, N.B.W. (Ed.), *Magmatic processes and plate tectonics*. Geol Soc Spec Pub, 76, pp. 71-81.

Menzies, M.A., Xu, Y.G., 1998. Geodynamics of the North China craton. In: Flower, M., Chung, S.L., Lo, C.H., Lee, T.Y. (Ed.), *Mantle Dynamics and Plate Interactions in East Asia*. American Geophysical Union, Washington, DC. Vol. 100, pp. 155-165.

Menzies, M.A., Xu, Y.G., Zhang, H.F., Fan, W.M., 2007. Integration of geology, geophysics and geochemistry: A key to understanding the North China Craton. *Lithos* **96**, 1-21.

Michael, P.J., 1995. Regionally distinctive sources of depleted MORB: evidence from trace elements and H_2O. *Earth and Planetary Science Letters* **131**, 301-320.

Mierdel, K., Keppler, H., Smyth, J.R., Langenhorst, F., 2007. Water solubility in aluminous orthopyroxene and the origin of earth's asthenosphere. *Science* **315**, 364-368.

Montesi, L.G.J., Hirth, G., 2003. Grain size evolution and the rheology of ductile shear zones: from laboratory experiments to postseismic creep. *Earth and Planetary Science Letters* **211**, 97-110.

Morishita, T., Arai, S., Gervilla, F., 2001. High-pressure aluminous mafic rocks from the Ronda peridotite massif, southern Spain: significance of sapphirine- and corundum-bearing mineral assemblages. *Lithos* **57**, 143-161.

Mott, N.F., Gurney, R.W., 1948. Electronic Processes in Ionic Crystals, 2nd edition. London, Oxford University Press.

Newton, R.C., Smith, J.V., Windley, B.F., 1980. Carbonic metamorphism, granulites and crustal growth. *Nature* **288**, 45-50.

Nishimura, T., Thatcher, W., 2003. Rheology of the lithosphere inferred from postseismic uplift following the 1959 Hebgen Lake earthquake. *Journal of Geophysical Research* **108**(B8), 2389, doi: 10.1029/2002JB002191.

Niu, Y.L., 2005. Generation and evolution of basaltic magmas: some basic concepts and a new view on the origin of Mesozoic-Cenozoic basaltic volcanism in eastern China. *Geological Journal of China Universities* **11**, 9-46.

Nyblade, A.A., Pollack, H.N., Jones, D.L., Pdomore, F., Mushayandebvu, M., 1990. Terrestrial heat flow in East and Southern Africa. *Journal of Geophysical Research* **95**, 17371-17384.

O'Brien, P.J., Otzler, J.R., 2003. High-pressure granulites: formation, recovery of peak conditions and implications for tectonics. *Journal of Metamorphic Geology* **21**, 3-20.

Okay, A.I., Xu, S.T., Sengor, A.M.C., 1989. Coesite from the Dabie Shan eclogites, central China. *European Journal of Mineralogy* **1**, 595-598.

Olhoeft, G.R., 1981. Electrical properties of rocks. In: Touloukian, Y.S. (Ed.), *Physical Properties of Rocks and Minerals*. McGraw-Hill, New York. Vol., pp. 257-330.

Ottolini, L., Fèvre, B.L., Vannucci, R., 2004. Direct assessment of mantle boron and lithium contents and distribution by SIMS analyses of peridotite minerals. *Earth and Planetary Science Letters* **228**, 19-36.

Parkhomenko, E.I., 1982. Electrical resistivity of minerals and rocks at high temperature and pressure. *Reviews of Geophysics* **20**, 193-218.

Parkinson, I.J., Hammond, S.J., James, R.H., Rogers, N.W., 2007. High-temperature lithium isotope fractionation: insights from lithium isotope diffusion in magmatic systems. *Earth and Planetary Science Letters* **257**, 609-621.

Paterson, M.S., 1982. The determination of hydroxyl by infrared absorption in quartz, silicate glasses and similar materials. *Bullutin of Minéralogy* **105**, 20-29.

Peacock, S.M., 1993. Large-scale hydration of the lithosphere above subducting slabs. *Chemical Geology* **108**(49-59).

Percival, J.A., Fountain, D.M., Salisbury, M.H., 1992. Exposed cross sections as windows on the lower crust. In: Fountain, D.M., Arculus, R., Kay, R.W. (Ed.), *Continental lower crust*. Elsevier, Amsterdam. Vol., pp. 317-362.

Peslier, A.H., Luhr, J.F., 2006. Hydrogen loss from olivines in mantle xenoliths from Simcoe (USA)

and Mexico: mafic alkalic magma ascent rates and water budget of the sub-continental lithosphere. *Earth and Planetary Science Letters* **242**, 302-319.

Peslier, A.H., Luhr, J.F., Post, J., 2002. Low water contents in pyroxenes from spinel-perididtites of the oxidized, sub-arc mantle wedge. *Earth and Planetary Science Letters* **201**, 69-86.

Pineau, F., Shilobreeva, S., Kadik, A., Javoy, M., 1998. Water solubility and D/H fractionation in the system basaltic andesite-H_2O at 1250 ℃ and between 0.5 and 3 kbars. *Chemical Geology* **147**, 173-184.

Pouchou, J.L., Pichoir, F., 1985. 'PAP' ($\phi-\rho-Z$) correction procedure for improved quantitative microanalysis. In: Armstrong, J.T. (Ed.), *Microbeam Analysis*. San Francisco Press, pp. 104-106.

Pride, C., Muecke, G.K., 1981. Rare earth element distribution among coexisting granulite facies minerals, Scourian complex, NW Scotland. *Contributions to Mineralogy and Petrology* **76**, 463-471.

Priestley, K., Debayle, E., McKenzie, D., Pilidou, S., 2006. Upper mantle structure of eastern Asia from multimode surface waveform tomography. *Journal of Geophysical Research* **111**, doi: 2005JB004082.

Putlitz, B., Matthews, A., Valley, J.W., 2000. Oxygen and hydrogen isotope study of high-pressure metagabbros and metabasalts (Cyclades, Greece): implications for the subduction of oceanic crust. *Contributions to Mineralogy and Petrology* **138**(2), 114-126.

Qiu, Y.M., Gao, S., McNaughton, N.J., Groves, D.J., Ling, W.L., 2000. First evidence of >3.2 Ga continental crust in the Yangtze craton of South China and its implications for Archean crustal evolution and Phanerozoic tectonics. *Geology* **28**, 11-14.

Ranalli, G., 1995. Rheology of the Earth (2nd ed.), Chapman & Hall.

Rauch, M., Keppler, H., 2002. Water solubility in orthopyroxene. *Contributions to Mineralogy and Petrology* **143**, 525-536.

Reiitan, P.H., Roelandts, I., Brunfelt, A.O., 1980. Optimum ionic size for substitution in the M(2)-site in metamorphic diopside. *N. Jahrb. Mineral. Monat.* **4**, 181-191.

Richet, P., Bottinga, Y., JAvoy, V., 1977. A review of hydrogen, carobon, nitrogen, oxygen, sulfur, and cholrine stable isotope factionation among gaseous molecules. *Annual Review of Earth and Planetary Sciences* **5**, 65-110.

Richter, F.M., Davis, A.M., Depaolo, D.J., Watson, E.B., 2003. Isotope fractionation by chemical diffusion between molten basalt and rhyolite. *Geochimica et Cosmochimica Acta* **67**(20), 3905-3923.

Rietmejir, F.M.J., 1983. Chemical distinction between igneous and metamorphic orthopyroxenes

especially those coexisting with Ca-rich clinopyroxenes: a re-evaluation. *Mineralogical Magazine* **47**, 143-151.

Rollion-Bard, C., Chaussidon, M., France-Lanord, C., 2003. pH control on oxygen isotopic composition of symbiotic corals. *Earth and Planetary Science Letters* **215**, 275-288.

Rossman, G.R., 1996. Studies of OH in nominally anhydrous minerals. *Physics and Chemistry of Minerals* **23**(4-5), 299-304.

Rossman, G.R., Aines, R.D., 1991. The hydrous components in garnets: Grossular-hydrogrossular. *American Mineralogist* **76**, 1153-1164.

Rossman, G.R., Beran, A., Langer, K., 1989. The hydrous component of pyrope from the Dora Maira Massif, western Alps. *European Journal of Mineralogy* **1**, 151-154.

Rudnick, R.L., 1992. Xenoliths -- samples of the lower continental crust. In: Fountain, D., Arculus, R., Kay, R.W. (Ed.), *Continental Lower Crust*. Elsevier, Amsterdam. Vol., pp. 269-316.

Rudnick, R.L., 1995. Making continental crust. *Nature* **378**(6557), 571-578.

Rudnick, R.L., Fountain, D.M., 1995. Nature and composition of the continental crust: a lower crustal perspective. *Reviews of Geophysics* **33**(3), 267-309.

Rudnick, R.L., Gao, S., 2003. Composition of the continental crust. In: Rudnick, R.L. (Ed.), *Treatise on Geochemistry: The Crust*. Elsevier-Pergamon, Oxford. Vol., pp. 1-64.

Rudnick, R.L., Gao, S., Ling, W.L., Liu, Y.S., McDonough, W.F., 2004. Petrology and geochemistry of spinel peridotite xenoliths from Hannuoba and Qixia, North China craton. *Lithos* **77**, 609-637.

Rudnick, R.L., Ionov, D.A., 2007. Lithium elemental and isotopic disequilibrium in minerals from peridotite xenoliths from far-east Russia: product of recent melt/fluid-rock reaction. *Earth and Planetary Science Letters* **256**, 278-293.

Rudnick, R.L., McDonough, W.F., Mcculloch, M.T., Taylor, S.R., 1986. Lower crustal xenoliths from Queensland, Austrilia: evidence for deep crustal assimilation and fractionation of continental basalts. *Geochimica et Cosmochimica Acta* **50**, 1099-1115.

Rudnick, R.L., Presper, T., 1990. Geochemistry of intermedidate- to high-pressure granulites. Norwell, Kluwer Academic.

Rybacki, E., Dresen, G., 2004. Deformation mechanism maps for feldspar rocks. *Tectonophysics* **382**, 173-187.

Rybacki, E., Gottschalk, M., Wirth, R., Dresen, G., 2006. Influence of water fugacity and activation volume on the flow properties of ine-grained anorthite aggregates. *Journal of Geophysical Research* **111**(B03203), doi: 10.1029/2005JB003663.

Sakai, R., Kusakabe, M., Noto, M., Ishii, T., 1990. Origin of waters responsible for serpentinization of the Izu-Ogasawara-Mariana forearc seamounts in view of hydrogen and oxygen isotope ratios. *Earth and Planetary Science Letters* **100**(1-3), 291-303.

Salters, V.J.M., Stracke, A., 2004. Composition of the depleted mantle. *Geochemistry Geophysics Geosystems* **5: Q05004**, doi: 10.1029/2003GC000597.

Sandiford, M., Powell, R., 1986. Pyroxene exsolution in granulites from Fyfe Hills, Enderby Land, Antarctica: evidence for 1000°C metamorphic temperatures in Archean continental crust. *American Mineralogist* **71**, 946-954.

Seitz, H.M., Brey, G.P., Lahaye, Y., Durali, S., Weyer, S., 2004. Lithium isotopic signatures of peridotite xenoliths and isotopic fractionation at high temperature between olivine and pyroxenes. *Chemical Geology* **212**, 163-177.

Seitz, H.M., Woodland, A.B., 2000. The distribution of lithium in peridotitic and pyroxenitic mantle lithologies-- an indicator of magmatic and metasomatic processes. *Chemical Geology* **166**, 47-64.

Selverstone, J., Stern, C.R., 1983. Petrochemistry and recrystallization history of granulite xenoliths from the Pali-Aike field, Chile. *American Mineralogist* **68**, 1102-1112.

Sengor, A.M.C., 1999. Continental interiors and cratons: any relation? *Tectonophysics* **305**, 1-42.

Shankland, T.J., Ander, M.E., 1983. Electrical conductivity, temperatures and fluids in the lower crust. *Journal of Geophysical Research* **88**, 527-538.

Sheppard, S.M.F., Epstein, S., 1970. D/H and $^{18}O/^{16}O$ ratios of minerals of possible mantle or lower crustal origin. *Earth and Planetary Science Letters* **9**, 232-239.

Shu, L., Charvet, J., 1996. Kinematics and geochronology of the Proterozoic Dongxiang-Shexian ductile shear zone: with HP metamorphism and ophiolitic melange (Jiangnan Region, South China). *Tectonophysics* **276**, 291-302.

Skogby, H., Bell, D.R., Rossman, G.R., 1990. Hydroxide in pyroxene - variations in the natural environment. *American Mineralogist* **75**(7-8), 764-774.

Skogby, H., Rossman, G.R., 1989. OH^- in pyroxene: an experimental study of incorporation mechanisms and stability. *American Mineralogist* **74**, 1059-1069.

Song, Y., Frey, F.A., 1989. Geochemistry of peridotite xenoliths in basalt from Hannuoba, Eastern China: implications for subcontinental mantle heterogeneity. *Geochimica Et Cosmochimica Acta* **53**, 97-113.

Stakes, D.S., O'Neil, J.R., 1982. Mineralogy and stable isotope geochemistry of hydrothermally altered oceanic rocks. *Earth and Planetary Science Letters* **57**, 285-304.

Stalder, R., 2004. Influence of Fe, Cr and Al on hydrogen incorporation in orthopyroxene. *European Journal of Mineralogy* **16**(5), 703-711.

Stalder, R., Klemme, S., Ludwig, T., Skogby, H., 2005. Hydrogen incorporation in orthopyroxene: interaction of different trivalent cations. *Contributions to Mineralogy and Petrology* **150**, 473-485.

Stalder, R., Skogby, H., 2002. Hydrogen incorporation in enstatite. *European Journal of Mineralogy* **14**(6), 1139-1144.

Stalder, R., Skogby, H., 2003. Hydrogen diffusion in natural and synthetic orthopyroxene. *Physics and Chemistry of Minerals* **30**(1), 12-19.

Stesky, R.S., Brace, W.F., 1973. Eletrical conductivity of serpentinised rocks to 6 kbars. *Journal of Geophysical Research* **98**, 4301-4310.

Stone, W., Deloule, E., Larson, M., Lesher, C., 1997. Evidence for hydrous high-MgO melts in the Precambrian. *Geology* **25**(2), 143-146.

Stone, W.E., Deloule, E., Beresford, S.W., Fiorentini, M., 2005. Anomalously high δD values in an archean ferropicritic melt: implications for magma degassing. *The Canadian Mineralogist* **43**, 1745-1758.

Suzuoki, T., Epstein, A., 1976. Hydrogen isotope fraction between OH-bearing minerals and water. *Geochimica Et Cosmochimica Acta* **40**, 1229-1240.

Tang, Y.J., Zhang, H.F., Nakamura, E., Moriguti, T., Kobayashi, K., Ying, J.F., 2007. Lithium isotopic systematics of peridotite xenoliths from Hannuoba, North China Craton: implications for melt-rock interaction in the considerably thinned lithospheric mantle. *Geochimica et Cosmochimica Acta* **71**, 4327-4341.

Tarits, P., Hautot, S., Perrier, F., 2004. Water in the mantle: results from electrical conductivity beneath the French Alps. *Geophysical Research Letters* **31**, L06612, doi: 10.1029/2003GL019277.

Tatsumoto, M., Basu, A.R., Huang, W., Wan, J., Xie, G., 1992. Sr, Nd and Pb isotopes of ultramafic xenoliths in volcanic rocks of Eastern China: enriched components EMI and EMII in subcontinental lithosphere. *Earth and Planetary Science Letters* **113**, 107-128.

Taylor, S.R., Mclennan, S.M., 1995. The geochemical evolution of the continental crust. *Reviews of Geophysics* **33**(2), 241-265.

Teng, F.Z., McDonough, W.F., Rudnick, R.L., Dalpe, C., Tomascak, P.B., Chappell, B.W., Gao, S., 2004. Lithium isotopic composition and concentration of the upper continental crust. *Geochimica Et Cosmochimica Acta* **68**(20), 4167-4178.

Teng, F.Z., McDonough, W.F., Rudnick, R.L., Walker, R.J., 2006. Diffusion-driven extreme lithium

isotope fractionation in country rocks of the Tin Mountain pegmatite. *Earth and Planetary Science Letters* **243**(3-4), 701-710.

Teng, F.Z., McDonough, W.F., Rudnick, R.L., Wing, B.A., 2007. Limited lithium isotopic fractionation during progressive metamorphic dehydration in metapelites: a case study from the Onawa contact aureole, Maine. *Chemical Geology* **239**, 1-12.

Teng, F.Z., Rudnick, R.L., McDonough, W.F., Tomascak, P.B., 2008. Lithium isotopic composition and concentration of the deep continental crust. *Chemical Geology*, accepted.

Tomascak, P.B., 2004. Developments in the understanding and application of lithium isotopes in the Earth and Planetary sciences. *Reviews in Mineralogy and Geochemistry* **55**, 153-195.

Tomascak, P.B., Tera, F., Helz, R.T., Walker, R.J., 1999. The absence of lithium isotope fractionation during basalt differentiation: new measurements by multi-collector sector ICP-MS. *Geochimica et Cosmochimica Acta* **63**, 907-910.

Toramaru, A., Fujii, N., 1986. Connectivity of melt phase in a partially molten peridotite. *Journal of Geophysical Research* **91**, 9239-9252.

Touret, J.L.R., 1971. Le faciès granulite en Norvège Meridonale, II: Les inclusions fluids. *Lithos* **4**, 423-436.

Toussaint-Jackson, J.E., *Laboratory and theoretical studies of electrical conductivity in crystalline rocks*. Ph.D. thesis, University of East Anglia

Tullis, J., Yund, R.A., Farver, J., 1996. Deformation-enchanced fluid distribution in feldspar aggregates and implications for ductile shear zones. *Geology* **24**, 63-66.

Valley, J.W., Graham, C.M., 1991. Ion microprobe analysis of oxygen isotope ratios in granulite facies magnetites: diffusive exchange as a guide to cooling history. *Contributions to Mineralogy and Petrology* **109**, 38-52.

Valley, J.W., Graham, C.M., Harte, B., Eiler, J.M., Kinny, P.D., 1998. Ion microprobe analysis of oxygen, carbon, and hydrogen isotope ratios. In: McKibben, M.A., Shanks, W.C., Ridley, W.I. (Ed.), *Applicants of Microanalytical Technique to Understanding Mineralizing Processes*. S.E.G. Review in Economic Geology, 7, pp. 73-98.

Valley, J.W., O'Neil, J.R., 1982. Oxygen isotope evidence for shallow emplacement of Adirondack anorthosite. *Nature* **300**, 497-500.

Valley, J.W., O'Neil, J.R., 1984. Fluid heterogeneity during granulite facies metamorphism in the Adirondacks: Stable isotope evidence. *Contributions to Mineralogy and Petrology* **85**, 158-173.

Valley, J.W., O'Neil, J.R., 1986. Fluid heterogeneity during granulite facies metamorphism in the Adirondacks: stable isotope evidence. *Contributions to Mineralogy and Petrology* **85**,

158-173.

Van Zijl, J.S.V., 1978. The relationship between the deep electrical resistivity structure and tectonic provinces in southern Africa. Part 1: results obtained by Schlumberger soundings. *Transactions of the Geological Survey of South Africa* **81**, 129-142.

Vennemann, T.W., O'Neil, J.R., 1996. Hydrogen isotope exchange reactions between hydrous minerals and molecular hydrogen: I. A new approach for the determination of hydrogen isotope fractionation at moderate temperatures. *Geochimica Et Cosmochimica Acta* **60**(13), 2437-2451.

Vielzeuf, D., Champenois, M., Valley, J.W., Brunet, F., Devidal, J.L., 2005. SIMS analyses of oxygen isotopes: matrix effects in Fe-Mg-Ca garnets. *Chemical Geology* **223**, 208-226.

Waff, H.F., Bulau, J.R., 1979. Equilibrium fluid distribution in an ultramafic partial melt under hydrostatic stress conditions. *Journal of Geophysical Research* **84**, 6109-6114.

Wagner, C., Deloule, E., 2007. Behaviour of Li and its isotopes during metasomatism of French Massif Central lherzolites. *Geochimica et Cosmochimica Acta* **71**, 4279-4296.

Wallace, P.J., 2005. Volatiles in subduction zone magmas: concentrations and fluxes based on melt inclusion and volcanic gas data. *Journal of Volcanology and Geothermal Research* **140**, 217-240.

Wang, D.J., Mookherjee, M., Xu, Y.S., Karato, S.I., 2006. The effect of water on the electrical conductivity of olivine. *Nature* **443**, 977-980.

Wang, J., Li, Z.X., 2003. History of Neoproterozoic rift basins in South China: implications for Rodinia break-up. *Precambrian Research* **1-4**, 141-158.

Wang, X.M., Liou, J.G., Mao, H.K., 1989. Coesite-bearing eclogites from the Dabie Mountains in central China. *Geology* **17**, 1085-1088.

Wedepohl, K.H., 1995. The composition of the continental crust. *Geochimica Et Cosmochimica Acta* **59**(7), 1217-1232.

Wells, P.R.A., 1977. Pyroxene thermometry in simple and complex systems. *Contributions to Mineralogy and Petrology* **62**, 129-139.

Wilde, S.A., Zhou, X.H., Nemchin, A.A., Sun, M., 2003. Mesozoic crust-mantle interaction beneath the North China craton: a consequence of the dispersal of Gondwanaland and accretion of Asia. *Geology* **31**(9), 817-820.

Williams, Q., Hemley, R.J., 2001. Hydrogen in the deep earth. *Annual Review of Earth and Planetary Sciences* **29**, 365-418.

Wood, B.J., 1974. Solubility of alumina in orthopyroxene coexisting with garnet. *Contributions to Mineralogy and Petrology* **46**, 1-15.

Wood, B.J., Banno, S., 1973. Garnet-othopyroxene and orthopyroxene-clinopyroxene relationships in simple and complex symtems. *Contributions to Mineralogy and Petrology* **42**, 109-124.

Woodland, A.B., Seitz, H.M., Yaxley, G.M., 2004. Varying behaviour of Li in metasomatised spinel peridotite xenoliths from western Victoria, Australia. *Lithos* **75**, 55-66.

Woods, S.C., Mackwell, S., Dyar, D., 2000. Hydrogen in diopside: Diffusion profiles. *American Mineralogist* **85**(3-4), 480-487.

Workman, R.K., Hart, S.R., 2005. Major and trace element composition of the depleted MORB mantle (DMM). *Earth and Planetary Science Letters* **231**, 53-72.

Wu, F.Y., Lin, J.Q., Wilde, S.A., Zhang, X.O., Yang, J.H., 2005. Nature and significance of the Early Cretaceous giant igneous event in eastern China. *Earth and Planetary Science Letters* **233**, 103-119.

Wu, F.Y., Walker, R.J., Ren, X.W., Sun, D.Y., Zhou, X.H., 2003. Osmium isotopic constraints on the age of lithospheric mantle beneath northeastern China. *Chemical Geology* **196**, 107-129.

Wunder, B., Meixner, A., Romer, R.L., Feenstra, A., Schettler, G., Heinrich, W., 2007. Lithium isotope fractionation between Li-bearing staurolite, Li-mica and aqueous fluids: an experimental study. *Chemical Geology* **238**, 277-290.

Wunder, B., Meixner, A., Romer, R.L., Heinrich, W., 2006. Temperature-dependent isotopic fraction of lithium between clinopyroxene and high-pressure hydrous fluids. *Contributions to Mineralogy and Petrology* **151**, 112-120.

Xia, Q.K., Dallai, L., Deloule, E., 2004. Oxygen and hydrogen isotope heterogeneity of clinopyroxene megacrysts from Nushan Volcano, SE China. *Chemical Geology* **209**, 137-151.

Xia, Q.K., Deloule, E., Wu, Y.B., Chen, D.G., Cheng, H., 2002. Anomalously high δD values in the mantle. *Geophysical Research Letters* **29**(21), doi: 10.1029/2001GL013887.

Xia, Q.K., Sheng, Y.M., Yang, X.Z., 2005. Heterogeneity of water in garnets from UHP eclogites, eastern Dabieshan, China. *Chemical Geology* **224**, 237-246.

Xia, Q.K., Yang, X.Z., Deloule, E., Sheng, Y.M., Hao, Y.T., 2006. Water in the lower crustal granulite xenoliths from Nushan, eastern China. *Journal of Geophysical Research* **111**(B11202), doi:10.1029/2006JB004296.

Xie, M.M., Liu, C.G., Li, S., 2001. Geologic feature of Xiakengzi pluton of Anyuan, south Jiangxi and the geologic significance of Pb-Pb isotopic age of zircon. *Jiangxi Geol.* **15**, 256-259.

Xu, S.T., Okay, A.I., Ji, S.Y., Sengor, A.M.C., Su, W., Liu, Y.C., Jiang, L.L., 1992. Diamond from the Dabie Shan metamorphic rocks and its implication for tectonic setting. *Science* **256**, 80-82.

Xu, X.S., O'Reilly, S.Y., Griffin, W.L., Zhou, X.M., 2000. Genesis of young lithospheric mantle in southeastern China: an LAM-ICPMS trace element study. *Journal of Petrology* **41**(1), 111-148.

Xu, X.S., O'Reilly, S.Y., Griffin, W.L., Zhou, X.M., Huang, X.L., 1998. The nature of the Cenozoic lithosphere at Nushan, Eastern China. In: Flower, M.F.J., Chung, S.L., Lo, C.H., Lee, T.Y. (Ed.), *Mantle dynamics and plate interaction in east Asia*. American Geophysical Union, 27, pp. 167-196.

Xu, Y.G., 2001. Thermo-tectonic destruction of the Archean lithospheric keel beneath the Sino-Korean craton in China: evidence, timing and mechanism. *Physics and Chemistry of The Earth* **26A**, 747-757.

Xu, Y.G., 2002. Evidence for crustal components in the mantle and constraints on crustal recycling mechanisms: pyroxenite xenoliths from Hannuoba, North China. *Chemical Geology* **182**, 301-322.

Xu, Y.G., 2007. Diachronous lithospheric thinning of the North China Craton and formation of the Daxin'anling - Taihangshan gravity lineament. *Lithos* **96**, 281-298.

Xu, Y.G., Bodinier, J.L., 2004. Contrasting enrichments in high- and low-temperature mantle xenoliths from Nushan, Eastern China: results of a single metasomatic event during lithospheric accretion? *Journal of Petrology* **45**(2), 321-341.

Xu, Y.G., Chung, S.L., Ma, J., Shi, L., 2004a. Contrasting Cenozoic lithospheric evolution and architecture in the Western and Eastern Sino-Korean Craton: constraints from geochemistry of basalts and mantle xenoliths. *The Journal of Geology* **112**, 593-605.

Xu, Y.G., Huang, X.L., Ma, J.L., Wang, Y.B., Iizuka, Y., Xu, J.F., Wang, Q., Wu, X.Y., 2004b. Crustal-mantle interaction during the thermo-tectonic reactivation of the North China Craton: SHRIMP zircon U-Pb age, petrology and geochemistry of Mesozoic plutons in western Shandong. *Contributions to Mineralogy and Petrology* **147**, 750-767.

Xu, Y.G., Sun, M., Yan, W., Liu, Y., Huang, X.L., Chen, X.M., 2002. Xenolith evidence for polybaric melting and stratification of the upper mantle beneath South China. *Journal of Asian Earth Sciences* **20**, 937-954.

Yang, J.H., Wu, F.Y., Wilde, S.A., 2003. A review of the geodynamic setting of large-scale late Mesozoic gold mineralization in the North China Craton: an association with lithospheric thinning. *Ore Geology Reviews* **23**, 125-152.

Yang, X.Z., Deloule, E., Xia, Q.K., 2008a. Hydrogen isotope compositions of lower crustal granulite minerals: a case study from the North China Craton. *Geochimica et Cosmochimica Acta*, in preparation.

Yang, X.Z., Deloule, E., Xia, Q.K., Fan, Q.C., Feng, M., 2008b. Water contrast between Precambrian and Phanerozoic continental lower crust of eastern China. *Journal of Geophysical*

Research, in revision.

Yardley, B.W.D., 1981. Effect of cooling on the water content and mechanical behaviour of metamorphosed rocks. *Geology of Ore Deposits (Translation of Geologiya Rudnykh Mestrorozhdenii)* **9**, 405-408.

Yardley, B.W.D., 1986. Is there water in the deep continental crust? *Nature* **323**, 111.

Yardley, B.W.D., Valley, J.W., 1997. The petrologic case for a dry lower crust. *Journal of Geophysical Research* **102**, 12723-12185.

Ye, K., Cong, B.L., Ye, D., 2000. The possible subduction of continental material to depths greater than 200 km. *Nature* **407**, 734-736.

Yoshino, T., Manthilake, G., Matsuzaki, T., Katsura, T., 2008. Dry mantle transition zone inferred from the conductivity of wadsleyite and ringwoodite. *Nature* **451**, 326-329.

Yu, J.H., Xu, X.S., O'Reilly, S.Y., Griffin, W.L., Zhang, M., 2003. Granulite xenoliths from Cenozoic Basalts in SE China provide geochemical fingerprints to distinguish lower crust terranes from the North and South China tectonic blocks. *Lithos* **67**(1-2), 77-102.

Yui, T.F., Jeng, R.C., 1990. A stable-isotope study of the hydrothermal alteration of the east Taiwan ophiolite. *Chemical Geology* **89**, 65.

Yui, T.F., Rumble, D., Lo, C.H., 1995. Unusually low $\delta^{18}O$ ultrahigh-pressure metamorphic rocks from the Sulu terrain, eastern China. *Geochimica et Cosmochimica Acta* **59**, 2859-2864.

Zack, T., Tomascak, P.B., Rudnick, R.L., Dalpe, C., McDonough, W.F., 2003. Extremely light Li in orogenic eclogites: The role of isotope fractionation during dehydration in subducted oceanic crust. *Earth and Planetary Science Letters* **208**(3-4), 279-290.

Zhai, M.G., 1996. Granulites and Lower Continental Crust in North China Craton. Beijing, Seismological Press.

Zhai, M.G., Guo, J.H., Liu, W.J., 2001. An exposed cross-section of early Precambrian continental lower crust in North China craton. *Physics and Chemistry of the Earth, Part A: Solid Earth and Geodesy* **26**(9-10), 781-792.

Zhai, M.G., Guo, J.H., Liu, W.J., 2005. Neoarchean to Paleoproterozoic continental evolution and tectonic history of the North China Craton: a review. *Journal of Asian Earth Sciences* **24**, 547-561.

Zhai, Y.S., Xiong, Y.L., Yao, S.Z., Lin, X.D., 1996. Metallogeny of copper and iron deposits in the Eastern Yangtze Craton, east-central China. *Ore Geology Reviews* **11**, 229--248.

Zhang, H.F., Goldstein, S.L., Zhou, X.H., Sun, M., Zheng, J.P., Cai, Y., 2007a. Evolution of subcontinental lithospheric mantle beneath eastern China: Re-Os isotopic evidence from mantle xenoliths in Paleozoic kimberlites and Mesozoic basalts. *Contributions to Mineralogy*

and Petrology, doi: 10.1007/s00410-007-0241-5.

Zhang, H.F., Sun, M., Zhou, M.F., Fan, W.M., 2004. Highly heterogeneous late Mesozoic lithospheric mantle beneath the North China Craton: evidence from Sr-Nd-Pb isotopic systematics of mafic igneous rocks. *Geological Magazine* **141**, 55-62.

Zhang, H.F., Sun, M., Zhou, X.H., Fan, W.M., Zhai, M.G., Ying, J.F., 2002. Mesozoic lithosphere destruction beneath the North China Craton: evidence from major, trace element, and Sr-Nd-Pb isotope studies of Fangcheng basalts. *Contributions to Mineralogy and Petrology* **144**, 241-253.

Zhang, L.G., 1985. Applications of Stable Isotope to Geological Sciences. Xi'an, Press of Shanxi Science and Technology.

Zhang, M.J., Hu, P.Q., Niu, Y.L., Su, S.G., 2007b. Chemical and stable isotopic constraints on the nature and origin of volatiles in the sub-continental lithospheric mantle beneath eastern China. *Lithos* **96**, 55-66.

Zhang, S.B., Yong, Y.F., Wu, Y.B., Zhao, Z.F., Gao, S., Wu, F.Y., 2006. Zircon isotope evidence for ⩾3.5 Ga continental crust in the Yangtze craton of China. *Precambrian Research* **146**, 16-34.

Zhao, G.C., Cawood, P.A., Wilde, S.A., Lu, L.Z., 2001a. High-pressure granulites (retrograded eclogites) from the Hengshan Complex, North China Craton: petrology and tectonic implications. *Journal of Petrology* **42**, 1141-1170.

Zhao, G.C., Wilde, S.A., Cawood, P.A., 1998a. Thermal evolution of Archean basement rocks from the eastern part of the North China Craton and its bearing on tectonic setting. *International Geology Review* **40**, 706-721.

Zhao, G.C., Wilde, S.A., Cawood, P.A., Sun, M., 2000. Metamorphism of basement rocks in the Central Zone of the North China craton: implications for Paleoproterozoic tectonic evolution. *Precambrian Research* **103**, 55-88.

Zhao, G.C., Wilde, S.A., Cawood, P.A., Sun, M., 2001b. Archean blocks and their boundaries in the North China Craton: lithological, geochemical, structural and P-T path constraints and tectonic evolution. *Precambrian Research* **107**, 45-73.

Zhao, Z.F., Zheng, Y.F., Gao, T.S., Wu, Y.B., Chen, B., Chen, F.K., Wu, F.Y., 2006. Isotopic constraints on age and duration of fluid-assisted high-pressure eclogite-facies recrystallization during exhumation of deeply subducted continental crust in the Sulu orogen. *Journal of Metamorphic Geology* **24**, 687-702.

Zhao, Z.H., Bao, Z.W., Zhang, B.Y., 1998b. Geochemistry of the Mesozoic basaltic rocks in southern Hunan Province. *Science in China (Series D)* **41**, 102-112.

Zheng, J.P., 1999. Mesozoic-Cenozoic Mantle Replacement and Lithospheric Thinning Beneath

the Eastern China. Wuhan, Publishing House of China University of Geosciences.

Zheng, J.P., Griffin, W.L., O'Reilly, S.Y., Yang, J.S., Li, T.F., Zhang, M., Zhang, R.Y., Liou, J.G., 2006a. Mineral chemistry of peridotites from Paleozoic, Mesozoic and Cenozoic lithosphere: constraints on mantle evolution beneath Eastern China. *Journal of Petrology* **47**, 2233-2256.

Zheng, J.P., Griffin, W.L., O'Reilly, S.Y., Zhang, M., Pearson, N., Pan, Y.M., 2006b. Widespread Archean basement beneath the Yangtze craton. *Geology* **34**, 417-420.

Zheng, J.P., O'Reilly, S.Y., Griffin, W.L., Zhang, M., Lu, F.X., Liu, G.L., 2004a. Nature and evolution of Mesozoic-Cenozoic lithospheric mantle beneath the Cathaysia block, SE China. *Lithos* **74**, 41-65.

Zheng, Y.F., 1993. Calculation of oxygen isotope fractionation in anhydrous silicate minerals. *Geochimica et Cosmochimica Acta* **57**, 1079-1091.

Zheng, Y.F., Fu, B., Gong, B., Li, L., 2003. Stable isotope geochemistry of ultrahigh pressure metamorphic rocks from the Dabie-Sulu orogen in China: implications for geodynamics and fluid regime. *Earth-Science Reviews* **62**, 105-161.

Zheng, Y.F., Fu, B., Gong, B., Li, S.G., 1996. Extreme ^{18}O depletion in eclogite from the Su-Lu terrane in East China. *European Journal of Mineralogy* **8**, 317-323.

Zheng, Y.F., Fu, B., Li, Y.L., Wei, C.S., Zhou, J.B., 2001. Oxygen isotope composition of granulites from Dabieshan in eastern China and its implications for geodynamics of Yangtze plate subduction. *Physics and Chemistry of the Earth, Part A: Solid Earth and Geodesy* **26**(9-10), 673-684.

Zheng, Y.F., Wu, Y.B., Chen, F.K., Gong, B., Li, L., Zhao, Z.F., 2004b. Zircon U-Pb and oxygen isotope evidence for a large-scale ^{18}O depletion event in igneous rocks during the Neoproterozoic. *Geochimica et Cosmochimica Acta* **68**, 4145-4165.

Zhou, M.F., Yan, D.P., Kennedy, A.K., Li, Y., Ding, J., 2002a. SHRIMP U–Pb zircon geochronological and geochemical evidence for Neoproterozoic arcmagmatism along the western margin of the Yangtze Block, South China. *Earth and Planetary Science Letters* **196**, 51-67.

Zhou, X.H., Sun, M., Zhang, G.H., Chen, S.H., 2002b. Continental crust and lithospheric mantle interaction beneath North China: isotopic evidence from granulite xenoliths in Hannuoba, Sino-Korean craton. *Lithos* **62**(3-4), 111-124.

Zou, H.P., 2001. Continental marginal rifting along the northern South China Sea: the crustal response to the lower lithospheric delamination. *Marine Geology and Quaternary Geology* **21**, 39-44.

Appendix

The detailed information with respect to the ion microprobe measurements of hydrogen, oxygen and lithium isotopes and lithium abundances in the lower crustal granulite minerals from Hannuoba and Nushan, North China Craton are compiled and provided here.

Table A1 Hydrogen isotopic results of cpx and plag in the lower crustal granulites by ion microprobe

Sample	Mineral	x	y	Point*	IsH	D/H	sd	δD	Mean
Nushan xenolith granulites									
04NS11	plag	-6783	-1300	1-c	1.9E+05	99.20	1.05	-32	-55
		-6808	-1435	1-m	1.8E+05	93.91	1.03	-66	
		-6622	-1244	1-r	1.7E+05	94.42	1.17	-63	
		-2756	-250	2-c	1.8E+05	96.33	1.17	-50	
		-2759	-355	2-m	1.7E+05	93.93	1.17	-66	
		-2781	-435	2-r	1.7E+05	98.38	0.93	-37	
		-7365	2447	3-c	1.4E+05	96.73	0.81	-48	
		-7355	2343	3-m	1.5E+05	94.19	0.78	-64	
		-7264	2484	3-r	1.4E+05	94.19	1.18	-64	
04NS13	plag	3241	-671	1-c	6.8E+04	91.08	1.52	-84	-69
		3473	-729	1-m	7.8E+04	91.96	1.65	-79	
		3308	-1044	1-r	7.4E+04	86.33	2.03	-115	
		7908	-5620	2-c	4.1E+04	93.50	2.58	-69	
		7836	-5603	2-m	4.3E+04	92.18	1.85	-77	
		7765	-5578	2-r	5.0E+04	98.22	2.20	-38	
		-4084	3227	3-c	4.9E+04	100.25	2.12	-25	
		-4007	3274	3-m	6.0E+04	96.02	1.37	-52	
		-3824	3354	3-r	5.8E+04	92.01	1.29	-78	
04NS9	cpx	-4174	2366	1-c	3.0E+05	89.57	0.70	-58	-42
		-4283	2370	1-m	2.8E+05	96.60	0.76	-13	
		-4472	2482	1-r	2.7E+05	95.93	0.58	-17	
		-618	5164	2-c	2.4E+05	88.45	0.94	-65	
		1113	2419	3-c	2.7E+05	89.68	0.95	-57	
	plag	5143	758	1-c	1.4E+05	95.38	1.10	-57	-72
		5076	743	1-m	1.2E+05	91.89	1.33	-79	
		4991	760	1-r	1.2E+05	91.41	1.29	-82	
		3379	5831	2-c	1.1E+05	93.02	1.44	-72	
04NS16	cpx	-3622	-500	1-c	1.4E+05	84.60	1.30	-89	-96

		-3515	-475	1-r	1.4E+05	82.32	1.19	-104	
	plag	-3619	73	1-c	6.5E+04	93.67	2.62	-68	-57
		-4937	-190	1-r	6.6E+04	97.01	1.99	-46	
Hannuoba terrain granulites									
MJ9801	cpx	-889	1634	1-c	9.1E+04	90.48	1.70	-80	-44
		-901	1571	1-m	9.0E+04	91.55	1.35	-73	
		-973	1443	1-r	9.5E+04	92.10	1.19	-70	
		-3958	-1019	2-c	7.8E+04	94.55	1.48	-54	
		-3941	-1250	2-m1	5.6E+04	103.63	2.12	4	
		-3877	-1271	2-m2	7.8E+04	98.77	1.36	-27	
		-3925	-1336	2-r	6.8E+04	101.29	1.63	-11	
	plag	-5239	2478	1-c	1.6E+04	102.09	3.39	-13	-43
		-5293	2532	1-m	1.6E+04	94.24	2.73	-64	
		-5308	2614	1-r	1.7E+04	95.92	2.40	-53	
MJ9805	cpx	666	1236	1-c	5.7E+05	89.33	0.56	-59	-55
		726	1336	1-m	5.4E+05	89.69	0.61	-57	
		778	1372	1-r	5.3E+05	90.07	0.54	-54	
		-2600	1349	2-c	3.2E+05	89.96	0.93	-55	
		-2630	1284	2-r	2.6E+05	90.94	1.13	-49	
	plag	-8988	-591	1-c	6.6E+05	91.83	0.39	-79	-61
		-9020	-698	1-r	5.5E+05	93.68	0.37	-67	
		-8314	-478	2-c	3.9E+05	96.62	0.82	-49	
		-8371	-473	2-m	3.9E+05	95.03	0.60	-59	
		-8445	-531	2-r	3.8E+05	96.04	0.53	-52	
Hannuoba xenolith granulites									
DM9855	cpx	8229	3336	1-c	4.1E+05	91.84	0.69	-45	-55
		8029	3437	1-m	4.1E+05	93.48	0.66	-34	
		7838	3472	1-r	4.0E+05	94.58	0.63	-27	
		-4782	-830	2-c	6.2E+05	87.90	0.55	-70	
		-4682	-713	2-m	6.1E+05	87.13	0.58	-75	
		-4538	-633	2-r	6.1E+05	86.96	0.52	-76	
	plag	-9313	-2431	1-c	3.3E+05	98.02	0.66	-40	-53
		-9207	-2518	1-m	3.2E+05	98.19	0.51	-39	
		-9463	-2438	1-r	3.0E+05	97.50	0.82	-43	
		-5279	-69	2-c	2.8E+05	94.48	0.92	-62	
		-5102	-39	2-m	2.5E+05	93.90	0.79	-66	
		-4998	-6	2-r	2.3E+05	93.24	0.73	-70	
DM9871	cpx	-3283	-1992	1-c	7.8E+04	93.91	2.04	-32	-42
		-3256	-2124	1-m	7.1E+04	95.25	1.41	-23	
		-3262	-2198	1-r	6.8E+04	96.28	1.09	-16	
		8914	2207	2-c	3.9E+04	89.45	2.50	-60	
		8975	2122	2-m	4.1E+04	90.99	2.01	-50	
		9011	2036	2-r	3.9E+04	87.97	2.38	-70	
	plag	-3508	-2705	1-c	2.3E+04	89.21	1.56	-96	-86

		-3565	-2684	1-m	2.1E+04	88.94	3.35	-98	
		-3582	-2630	1-r	2.1E+04	94.44	3.39	-63	
WD9532	cpx	2825	-4102	1-c	3.8E+05	95.54	0.72	-20	-17
		2899	-4183	1-m	3.6E+05	98.07	0.74	-4	
		2985	-4248	1-r	3.5E+05	94.91	0.59	-24	
		-8945	2015	2-c	2.6E+05	96.55	0.95	-14	
		-8795	1946	2-r	2.6E+05	95.17	1.03	-23	
	plag	-4176	1576	1-c	1.6E+05	95.63	1.14	-55	-49
		-4117	1639	1-m	1.6E+05	98.07	0.83	-39	
		-4290	1734	1-r	1.6E+05	95.63	0.84	-55	
		-8472	1837	2-c	1.3E+05	96.58	0.95	-49	
		-8570	1871	2-r	1.4E+05	96.80	1.11	-47	
WD9546	cpx	651	1727	1-c	5.4E+04	90.21	1.63	-56	-10
		4554	3451	2-r	6.9E+04	99.61	1.04	5	
		4590	3325	2-m	6.0E+04	100.24	1.97	9	
		4642	3235	2-c	5.4E+04	99.57	2.65	4	
	plag	2632	-1405	1-c	1.6E+04	96.08	2.42	-52	-55
		2665	-1475	1-m	1.4E+04	103.59	3.49	-4	
		2659	-1516	1-r	1.4E+04	91.97	3.13	-78	
		5759	939	2-r	1.3E+04	90.58	3.39	-87	

Note: x and y denote the position of analyzed point in the μm unit; *: numbers denote different grains, c, r and m are core, rim and in the middle of them, respectively. IsH are the counts per second on H^+; D/H are the measured ratios by ion microprobe, δD are the instrumental calibrated H-isotopic values, and sd is the standard deviation.

Table A2 Oxygen isotopic results of cpx and opx in the lower crustal granulites by ion microprobe

	x	y	^{18}O_cps	$\delta^{18}O_{sims}$	sd		$\delta^{18}O_{corr}$	sd_{corr}
04NS9								
cpx1_1	1209	2845	6.52	7.39	0.08	c	6.45	0.50
cpx1_2	1172	2871	6.32	7.56	0.09		6.62	0.50
cpx1_3	1284	2838	6.08	8.50	0.12		7.56	0.51
cpx1_4	1344	2822	6.13	8.53	0.12	r	7.59	0.51
cpx2_1	-452	5567	5.50	6.14	0.11	c	5.20	0.51
cpx2_2	-372	5559	5.52	6.63	0.09		5.69	0.50
cpx2_3	-288	5557	5.73	6.31	0.11		5.37	0.51
cpx2_4	-219	5535	5.85	6.04	0.09	r	5.10	0.50
cpx3_1	-4060	2743	6.12	8.50	0.09	c	7.56	0.50
cpx3_2	-3971	2768	5.98	8.03	0.11		7.09	0.51
cpx3_3	-3913	2760	6.11	8.37	0.09		7.43	0.50
cpx3_4	-3839	2694	6.20	8.32	0.08	r	7.38	0.50
Cpx4_1	-9050	942	5.16	8.50	0.11		7.56	0.51
Cpx4_2	-9051	891	5.16	8.25	0.10		7.31	0.50
opx1_1	-560	2875	6.25	3.72	0.11	c	6.27	0.41
opx1_2	-625	2875	6.05	4.56	0.11		7.11	0.41
opx1_3	-676	2859	6.14	4.18	0.12		6.73	0.41
opx1_4	-751	2867	6.13	4.66	0.12		7.21	0.41
opx1_5	-295	2352	6.25	10.18	0.07		6.06	0.17
opx1_6	-322	2372	6.22	10.09	0.07		5.97	0.17
opx1_7	-280	2418	6.18	9.9	0.06	r	5.78	0.17
04NS16								
cpx1_1	-4539	3071	6.46	10.10	0.08	c	9.16	0.50
cpx1_2	-4545	3033	6.56	9.67	0.08	r	8.73	0.50
cpx1_3	-4586	3037	6.45	9.87	0.09	r	8.93	0.50
cpx1_4	-4572	3086	6.33	9.64	0.09	r	8.70	0.50
cpx2_1	-1870	3775	5.95	9.63	0.11	c	8.69	0.51
cpx2_2	-1901	3703	6.04	10.14	0.09		9.20	0.50
cpx2_3	-1937	3810	6.07	9.73	0.10	r	8.79	0.50
MJ9801								
cpx1_1	-3434	-1486	6.6	7.6	0.1	r	6.66	0.50

cpx1_2	-3505	-1487	6.61	8.09	0.08		7.15	0.50
cpx1_3	-3600	-1534	6.79	7.42	0.08	c	6.48	0.50
cpx1_4	-3594	-1654	6.49	8.02	0.06		7.08	0.50
cpx1_5	-3559	-1702	6.49	7.8	0.09	r	6.86	0.50
cpx2_1	-770	1210	6.67	8.02	0.08	c	7.08	0.50
cpx2_2	-749	1157	6.65	8.03	0.08		7.09	0.50
cpx2_3	-690	1110	6.5	8.33	0.09		7.39	0.50
cpx2_4	-650	1057	6.47	8.37	0.08	r	7.43	0.50
cpx3_1	-3830	-1465	6.36	11.49	0.08	c	5.09	0.80
cpx3_2	-3856	-1419	6.1	12.01	0.07		5.61	0.80
cpx3_3	-3886	-1387	5.98	12.46	0.09	r	6.06	0.81
MJ9805								
cpx1_1	983	871	6.49	11.32	0.09	c	4.92	0.81
cpx1_2	1007	898	6.59	10.86	0.06		4.46	0.80
cpx1_3	1092	860	6.8	10.91	0.08	r	4.51	0.80
cpx2_1	-2364	666	6.27	11.24	0.09	c	4.84	0.81
cpx2_2	-2450	656	6.07	11.51	0.09	r	5.11	0.81
cpx3_1	981	1290	6.59	7.9	0.09	c	6.96	0.50
cpx3_2	1016	1316	6.57	8.28	0.08		7.34	0.50
cpx3_3	1039	1234	6.56	8.55	0.08		7.61	0.50
cpx3_4	1147	1314	6.37	8.37	0.09		7.43	0.50
cpx3_5	1139	1183	6.25	8.81	0.12	r	7.87	0.51
WD9532								
cpx1_1	1677	1295	6.29	8.67	0.08	c	8.24	0.23
cpx1_2	1722	1387	6.17	8.84	0.10		8.41	0.24
cpx1_3	1786	1440	6.39	8.88	0.08		8.45	0.23
cpx1_4	1841	1502	6.14	9.49	0.15		9.06	0.26
cpx1_5	1891	1543	6.07	9.32	0.14	r	8.89	0.26
cpx2_1	-8140	3166	7.06	9.83	0.11	c	9.40	0.24
cpx2_2	-8061	3204	7.04	10.17	0.07		9.74	0.22
cpx2_3	-8000	3214	6.86	10.16	0.12		9.73	0.24
cpx2_4	-7938	3206	6.50	10.64	0.12		10.21	0.24
cpx2_5	-7887	3219	6.66	10.52	0.09		10.09	0.23
cpx2_6	-7835	3207	6.80	10.39	0.12	r	9.96	0.24
cpx3_1	3417	-3495	6.05	7.95	0.09	c	7.52	0.23
cpx3_2	3381	-3456	6.15	8.19	0.10		7.76	0.24

cpx3_3	3342	-3426	6.21	7.97	0.11		7.54	0.24
cpx3_4	3291	-3377	6.14	8.19	0.11		7.76	0.24
cpx3_5	3257	-3345	6.31	7.83	0.11	r	7.40	0.24
opx1_1	-3875	2181	5.39	6.17	0.13	r	8.72	0.42
opx1_2	-3811	2163	5.58	5.95	0.13		8.50	0.42
opx1_3	-3730	2127	5.86	5.84	0.11		8.39	0.41
opx1_4	-3639	2115	5.99	6.04	0.12		8.59	0.41
opx1_5	-3562	2092	6.01	6.24	0.12		8.79	0.41
opx1_6	-3397	2042	5.27	6.26	0.12		8.81	0.41
opx1_7	-3320	2012	5.36	6.19	0.10		8.74	0.41
opx1_8	-3258	1998	5.48	6.23	0.12	c	8.78	0.41
opx1_9	-3187	1984	5.09	6.84	0.14		9.39	0.42
opx1_10	-3107	1972	5.09	6.63	0.13		9.18	0.42
opx1_11	-3027	1967	5.10	6.56	0.13		9.11	0.42
opx1_12	-2934	1983	5.52	5.67	0.12		8.22	0.41
opx1_13	-2877	1970	5.35	6.71	0.13		9.26	0.42
opx1_14	-2789	1955	5.34	6.60	0.09		9.15	0.41
opx1_15	-2702	1953	5.55	5.58	0.10		8.13	0.41
opx1_16	-2617	1957	5.27	6.55	0.12		9.10	0.41
opx1_17	-3269	1888	6.54	6.49	0.08		9.04	0.40
opx1_18	-3205	1868	6.12	6.32	0.08	r	8.87	0.40
WD9546								
cpx1_1	-988	-1070	5.64	9.30	0.12	c	8.36	0.51
cpx1_2	-983	-1126	5.64	10.12	0.12		9.18	0.51
cpx1_3	-1012	-1168	5.51	10.24	0.12		9.30	0.51
cpx1_4	-1044	-1206	5.52	10.26	0.13		9.32	0.51
cpx1_5	-1070	-1260	5.60	9.60	0.11	r	8.66	0.51
opx1_1	-2460	1700	5.59	5.98	0.08	c	8.53	0.40
opx1_2	-2505	1653	5.32	7.00	0.10		9.55	0.41
opx1_3	-2522	1596	5.33	7.15	0.12		9.70	0.41
opx1_4	-2524	1532	5.38	7.02	0.11		9.57	0.41
opx1_5	-2529	-2462	5.37	6.73	0.08	c	9.28	0.40
cpx2_2	-8181	-2700	6.95	9.52	0.08		8.58	0.50
DM9855	-8188	-2745	6.92	9.79	0.06		8.85	0.50
cpx2_4	-8194	-2825	6.94	10.03	0.06	c	9.09	0.50
cpx2_5	-8196	-2879	6.97	12.32	0.08	r	11.28	0.50
cpx1_3	-721	3359	6.10	8.02	0.11		7.59	0.24
opx1_4	-4261	3305	5.47	6.58	0.09	c	8.15	0.41
opx1_5	-4251	3242	6.12	7.11	0.05		8.56	0.40
opx1_6	-4244	3178	5.90	8.51	0.08		8.07	0.40
opx1_7	-4252	3126	6.04	8.28	0.09	r	9.75	0.41

opx1_5	-4322	617	6.33	8.48	0.09		11.03	0.41
opx1_6	-4257	599	6.5	7.41	0.09	r	9.96	0.41
DM9871								
cpx1_1	-7361	-1837	3.99	13.42	0.14	c	12.48	0.51
cpx1_2	-7344	-1802	3.97	12.49	0.10		11.55	0.50
cpx1_3	-7331	-1757	3.84	12.43	0.13		11.49	0.51
cpx1_4	-7316	-1718	3.67	12.80	0.14		11.86	0.51
cpx1_5	-7314	-1660	3.90	12.16	0.10	r	11.22	0.50
cpx2_1	-5878	-4365	4.43	13.35	0.11	c	12.41	0.51
cpx2_2	-5796	-4366	4.55	12.99	0.11		12.05	0.51
cpx2_3	-5714	-4354	4.58	12.84	0.14	r	11.90	0.51
opx1_1	-7334	-1450	3.96	9.05	0.14	r	11.60	0.42
opx1_2	-7262	-1247	4.12	9.08	0.13		11.63	0.42
opx1_3	-7279	-1179	3.76	9.44	0.07		11.99	0.40
opx1_4	-7256	-1111	4.13	9.15	0.11		11.70	0.41
opx1_5	-7281	-1065	4.24	8.76	0.10	c	11.31	0.41
opx2_1	-1350	-3432	5.81	7.82	0.09	r	10.37	0.41
opx2_2	-1401	-3461	5.82	7.72	0.08	c	10.27	0.40

Note: x and y denote the position of analyzed point in the μm unit; ^{18}O_cps are the counts per second on ^{18}O in the 10^6 unit; $\delta^{18}O_{sims}$, sd, $\delta^{18}O_{corr}$ and sd_{corr} are ion microprobe measured δ^{18}O and standard variation and instrumental calibrated δ^{18}O and standard deviation, respectively.

Table A3 Lithium concentrations of cpx, opx and plag in the lower crustal granulites by ion microprobe

	x	y	Ip (nA)	7Li(cps)	30Si(cps)	7Li/6Li	sd	Lif/30Si ($*10^{-3}$)	sd	B/30Si ($*10^{-4}$)	sd	29Si/30Si	sd	Li (ppm)
04NS11														
opx1_1	-2495	2326	17.8	2309	10922	11.83	0.08	1.58	0.04	10.65	0.37	1.88	0.008	2.37
opx1_2	-2495	2234	19.2	1593	10618	12.31	0.13	1.58	0.04	20.72	3.39	1.8	0.001	2.37
opx1_3	-2467	2151	18.8	2420	12877	12.39	0.08	1.59	0.04	10.99	1.54	1.7	0.008	2.39
opx1_4	-2424	2048	18.5	3279	13911	12.32	0.09	1.86	0.05	8.14	1.02	1.66	0.006	2.79
opx1_5	-2405	1963	18.4	4171	14567	12.34	0.06	2.31	0.05	7.36	1.12	1.63	0.007	3.47
opx1_6	-2355	1879	17.9	4765	15130	12.35	0.08	2.2	0.06	7.64	0.9	1.63	0.005	3.30
opx2_1	3909	-4667	18.1	7506	12931	11.51	0.06	4.2	0.11	4.55	0.32	1.63	0.003	6.31
opx2_2	4010	-4667	18.4	9318	14133	11.91	0.04	4.3	0.1	12.01	1.68	1.61	0.005	6.46
plag1_1	-1956	2564	18	954	16180	12.1	0.14	0.72	0.03	1.88	0.23	1.56	0.004	1.24
plag1_2	-1873	2544	17.9	1253	18007	12.77	0.13	0.75	0.02	1.62	0.24	1.56	0.005	1.29
plag1_3	-1777	2544	18.3	1091	16684	12.46	0.11	0.8	0.03	1.82	0.22	1.56	0.004	1.38
plag1_4	-1665	2544	18.6	855	15712	11.82	0.18	0.71	0.02	2.43	0.3	1.57	0.004	1.22
04NS13														
opx1_1	-3641	4083	14.4	7543	20014	11.28	0.16	2.9	0.08	1.47	0.12	1.57	0.004	4.24
opx1_2	-3641	4004	14.3	6607	19765	12.15	0.07	3.09	0.06	4.33	0.59	1.58	0.002	4.52
opx1_3	-3641	3928	15.4	5247	19030	12.15	0.08	2.92	0.05	7.3	1.58	1.58	0.002	4.27
opx1_4	-3641	3843	15.1	7517	19907	11.91	0.05	3.33	0.05	8	1.33	1.59	0.004	4.87
opx1_5	-3599	3778	15.6	5118	17167	11.95	0.11	3.37	0.04	12.58	2.51	1.6	0.003	4.92

opx2_1	-5384	3742	16	2646	14635	12.35	0.08	2.48	0.03	2.88	0.3	1.54	0.003	3.62
opx2_2	-5411	3829	16	3756	14546	12.49	0.07	2.3	0.06	6.46	0.78	1.54	0.004	3.36
opx2_3	-5432	3895	16.5	3565	12563	12.41	0.08	2.47	0.04	8.89	1.04	1.57	0.005	3.61
plag1_1	-3570	3556	15.5	917	19477	11.94	0.15	0.68	0.03	4.54	0.82	1.56	0.004	1.18
plag1_2	-3642	3623	15.5	2182	20313	12.3	0.1	1.21	0.04	4.11	0.48	1.55	0.003	2.11
plag2_1	-4694	3560	15.5	2335	19096	12.15	0.13	1.09	0.03	1.36	0.13	1.55	0.002	1.90
plag3_1	-5329	3729	15.1	637	19860	12.07	0.12	0.52	0.04	8.97	1.1	1.56	0.004	0.91
plag3_2	-5355	3802	15.2	863	19191	12.14	0.15	0.58	0.03	8.01	1.03	1.55	0.004	1.01
plag3_3	-5380	3872	16.9	764	14712	12.33	0.19	0.73	0.03	27.99	2.56	1.55	0.003	1.27
plag3_4	-5358	3964	16.8	1069	14854	12.19	0.13	0.81	0.03	26.88	2.07	1.55	0.004	1.41
04NS9														
cpx1_1	-3703	2082	8.4	27750	80424	12.2	0.02	5.68	0.05	12.24	1.11	1.56	0.003	9.29
cpx1_2	-3797	1983	8.7	28528	78448	12.36	0.02	6.68	0.05	39.04	6.19	1.55	0.002	10.92
cpx1_3	-3872	1888	8.7	27237	71942	12.38	0.04	6.32	0.07	8.23	1.04	1.54	0.004	10.33
cpx1_4	-3967	1923	8.9	13980	56045	12.03	0.13	5.04	0.09	3.66	0.5	1.56	0.010	8.24
cpx1_5	-4019	1698	8.5	30246	54306	12.19	0.05	7.65	0.05	10.84	1.06	1.54	0.007	12.51
cpx2_1	-347	4656	7.4	20650	60740	12.26	0.04	4.32	0.01	6.38	0.75	1.55	0.018	7.06
cpx2_2	-375	4745	7.1	21915	66398	12.22	0.08	4.93	0.17	3.88	0.6	1.54	0.004	8.06
opx1_1	-8894	396	7.9	73043	122410	12.2	0.04	2.53	0.02	14.34	0.68	1.54	0.004	4.07
opx1_2	-8848	305	8.1	59446	123610	12.48	0.04	2.39	0.04	10.43	1.36	1.49	0.007	3.84

opx1_3	-8830	278		54025	114610	12.15	0.04	2.15	0.02	32.07	3.75	1.54	0.003	3.46
opx1_4	-8830	214		49961	94534	12.32	0.05	2.44	0.02	74.45	6.42	1.54	0.003	3.92
plag1_1	3624	4986	7.3	12230	107040	12.12	0.04	1.66	0.02	2.45	0.32	1.53	0.006	3.11
plag1_2	3697	5075	7.6	9866	104980	11.86	0.09	1.46	0.02	1.5	0.2	1.53	0.001	2.74
plag1_3	3699	5192	7.5	12580	97953	12.08	0.04	1.6	0.01	3.72	0.33	1.54	0.003	3.00
plag2_1	6711	3960	7.1	9306	104250	12.21	0.04	1.42	0.01	1.51	0.15	1.53	0.001	2.66
plag2_2	6821	3996	7.3	128560	109120	12.18	0.03	1.98	0.02	1.95	0.23	1.53	0.002	3.71
plag2_3	6906	4014	7.2	9995	106670	12.26	0.03	1.65	0.02	2.93	0.3	1.53	0.002	3.09
04NS16														
cpx1_1	-4118	2090	7.4	64418	55719	12.09	0.05	7.79	0.06	23.9	1.82	1.59	0.002	12.58
cpx1_2	-4174	2026	7.5	43645	62118	12.16	0.03	8.86	0.24	63.72	11.64	1.64	0.028	14.30
cpx2_1	-1510	2670	8.4	59985	73297	12.28	0.03	7.09	0.08	31.09	2.68	1.56	0.003	11.45
opx1_1	70	3597	8.5	57571	108030	12.22	0.02	3.77	0.04	29.29	3.03	1.54	0.002	6.06
opx2_1	-137	6204	8.9	31447	124890	12.14	0.02	1.95	0.03	31.55	2.99	1.55	0.001	3.13
plag1_1	-4760	1804	8	1171	123150	11.02	0.11	1.26	0.006	3.88	0.35	1.49	0.003	2.37
plag2_1	3192	5016	9.2	694	127010	11.59	0.18	0.87	0.02	3.79	0.6	1.54	0.008	1.64
plag3_1	3244	5209	9	237	132080	10.71	0.31	0.93	0.002	7.79	0.93	1.53	0.001	1.75

MJ9801

cpx1_1	-3268	-1893	13.1	47056	16894	12.12	0.06	15.76	0.32	6.1	0.64	1.54	0.005	22.84
cpx1_2	-3268	-1780	13	39266	15845	12.35	0.03	20.65	0.23	5.47	0.44	1.55	0.003	29.93
cpx1_3	-3310	-1621	13.1	57487	17666	12.44	0.02	22.83	0.18	8	0.96	1.54	0.004	33.09
cpx1_4	-3310	-1511	13.2	55640	18023	12.54	0.03	21.07	0.87	6.54	0.6	1.54	0.004	30.54
cpx1_5	-3363	-1430	13.3	53755	17519	12.54	0.01	21.05	0.12	8.5	0.86	1.54	0.004	30.51
cpx1_6	-3485	-1430	13.3	47586	17129	12.45	0.03	19.19	0.16	6.85	0.7	1.55	0.002	27.82
cpx1_7	-3411	-1547	13.1	63408	18396	11.36	0.15	17.19	0.43	8.12	0.65	1.54	0.002	24.92
cpx1_8	-3436	-1632	13.2	72694	19122	12.37	0.03	23.6	0.52	14.65	0.21	1.57	0.003	34.21
cpx1_10	-3467	-1723	14	48231	17440	10.37	0.2	13.9	0.41	5.68	0.56	1.53	0.003	20.15
cpx1_11	-3516	-1901	14.1	50490	17450	12.06	0.09	15.86	0.36	4.95	0.35	1.51	0.008	22.99
opx1_1	-4387	6760	14	5139	22054	11.81	0.1	1.9	0.07	12.15	0.55	1.61	0.002	2.79
opx1_2	-4387	6634	14.1	7144	23361	12.22	0.07	2.7	0.1	12.9	0.13	1.59	0.004	3.96
plag1_1	-4762	6666	14	8793	19458	12.23	0.05	4.01	0.05	8.32	1.07	1.55	0.002	6.34
plag1_2	-4762	6738	14.2	8330	17500	12.3	0.06	4.84	0.08	11.59	1.25	1.55	0.003	7.65
plag2_1	-3473	-1254	13.5	17253	21133	12.34	0.03	6.81	0.6	3.91	0.46	1.53	0.003	10.77
plag2_2	-3315	-1313	13.6	17969	19897	12.32	0.06	7.49	0.1	4.08	0.48	1.53	0.003	11.85
plag2_3	-3239	-1331	13.4	19957	21326	12.33	0.04	7.67	0.07	3.52	0.38	1.54	0.004	12.13
plag2_4	-3148	-1361	13.3	13428	22220	12.25	0.04	6.31	0.07	2.92	0.29	1.53	0.003	9.98
grt1_1	350	5234	13.9	5059	17292	11.87	0.08	1.9	0.04	1.27	0.12	1.53	0.002	2.14
grt1_2	419	5200	14	7334	18877	12.32	0.04	2.28	0.04	4.35	0.41	1.54	0.003	2.57

grt1_3	472	5171	14.1	7290	18516	12.11	0.05	2.4	0.04	4.41	0.39	1.54	0.002	2.70
grt1_4	552	5204	14	7904	18936	12.23	0.05	2.72	0.06	4.98	0.45	1.53	0.004	3.06
grt2_1	-787	4289	14.5	9866	17148	11.91	0.09	2.83	0.06	1.87	0.14	1.53	0.003	3.19
grt2_2	-844	4289	14.6	9756	17522	12.3	0.04	3.47	0.04	5.81	0.51	1.54	0.003	3.91
grt2_3	-903	4229	15.1	9056	16851	12.17	0.06	3.3	0.06	2.03	0.12	1.54	0.002	3.71
MJ9805														
cpx1_1	-2347	1332	17.2	37277	15189	11.93	0.08	17.21	0.27	4.73	0.2	1.53	0.004	25.79
cpx1_2	-2324	1409	17.3	42845	16096	12.39	0.02	18.56	0.19	8.49	0.52	1.54	0.002	27.81
cpx1_3	-2222	1404	17.1	41849	15731	12.43	0.01	18.87	0.18	7.95	0.6	1.54	0.002	28.27
cpx2_1	-2327	1640	17.1	39313	15690	12.43	0.01	18.58	0.17	8.91	0.78	1.54	0.002	27.84
cpx2_2	-2186	1721	17	39950	14911	12.41	0.01	19.71	0.18	3.47	0.41	1.55	0.003	29.53
opx1_1	-8480	-298	18	2909	13945	11.82	0.1	1.33	0.05	4.85	0.33	1.56	0.006	1.99
opx2_1	-8359	-433	17.2	5011	23005	12.5	0.06	1.17	0.03	3.87	0.28	1.54	0.003	1.75
opx2_2	-8288	-391	17	5464	35415	12.33	0.02	0.82	0.05	2.28	0.23	1.53	0.002	1.23
opx2_3	-8235	-291	17.1	5078	24141	12.35	0.05	1.22	0.04	4.81	0.33	1.54	0.003	1.82
opx3_1	-458	-2511	17.2	5374	17144	12	0.03	2.35	0.05	4.03	0.17	1.54	0.004	3.51
opx3_2	-292	-2509	17	5701	20328	12.39	0.04	1.79	0.04	5.72	0.45	1.54	0.003	2.68
opx3_3	-211	-2531	17.2	4274	20295	12.08	0.04	1.33	0.03	4.33	0.31	1.54	0.002	1.99
plag1_1	-8368	-702	16	1283	34152	12.17	0.11	0.31	0.01	0.3	0.03	1.5	0.007	0.52

plag1_2	-8312	-717	16.8	3974	44790	12.21	0.1	0.55	0.04	1.01	0.12	1.53	0.002	0.92
plag1_3	-8262	-760	16.9	8138	49465	12.35	0.09	1	0.05	0.97	0.09	1.53	0.002	1.68
plag2_1	-285	-2279	17.1	314	20680	11.89	0.16	0.14	0.001	5.55	0.3	1.53	0.003	0.24
plag2_2	-199	-2339	17.2	1193	21727	12.61	0.17	0.65	0.02	5.19	0.26	1.54	0.003	1.09
plag2_3	-77	-2359	16.1	4788	22168	12.24	0.04	1.96	0.04	4.88	0.31	1.54	0.002	3.29
plag2_6	-114	-2287	15.1	837	25669	11.58	0.22	0.35	0.01	5.98	0.35	1.53	0.002	0.59
plag3_1	-129	-2677	15.1	5016	24188	11.96	0.06	1.4	0.03	4.15	0.22	1.51	0.004	2.35
plag3_2	-63	-2657	15.1	4837	25468	12.54	0.08	1.8	0.03	5.34	0.22	1.53	0.003	3.02
plag3_3	-9	-2621	14.7	1887	25466	12.23	0.11	0.8	0.04	5.3	0.26	1.53	0.003	1.34
plag3_4	8	-2668	16.2	493	13692	11.9	0.08	0.96	0.21	98.48	30.28	1.52	0.009	1.61
plag3_5	52	-2641	15.2	2433	25284	12.43	0.26	1.16	0.01	5.21	0.22	1.54	0.004	1.95
plag3_6	117	-2641	15.3	2957	25861	12.36	0.08	0.98	0.02	5.95	0.39	1.53	0.003	1.65
DM9855														
cpx1_1	-8147	-2976	11	33805	94877	12.17	0.02	3.53	0.04	5.42	0.47	1.57	0.001	5.61
cpx1_2	-8197	-3062	11.2	38449	97204	12.17	0.01	3.9	0.01	10.67	1.71	1.56	0.001	6.20
cpx1_3	-8197	-3171	10.5	39623	95384	12.27	0.01	3.9	0.02	9.45	1.4	1.56	0.001	6.20
cpx1_4	-8206	-3239	10.9	25044	78102	12.33	0.02	3.93	0.03	10.53	1.67	1.57	0.002	6.24
cpx1_5	-8206	-3329	10.3	36010	85382	12.13	0.03	3.7	0.03	12.32	1.44	1.56	0.002	5.88
cpx1_6	-8206	-3427	10.1	42602	83467	12.06	0.01	4.6	0.03	10.96	1.29	1.57	0.001	7.31
cpx2_1	1437	-2516	8.5	27317	55645	12.16	0.03	5.08	0.29	8.6	0.47	1.6	0.070	8.07
cpx2_2	1440	-2407	8.7	31914	57735	12.12	0.02	6.29	0.04	16.59	2.94	1.55	0.009	9.99

cpx3_1	-1661	-3966	7.8	23413	52371	11.94	0.03	5.71	0.05	6.39	0.38	1.57	0.002	9.07
cpx3_2	-1718	-3966	7.8	18813	50716	12.04	0.03	6.48	0.09	22	4	1.57	0.002	10.30
opx1_1	-4894	588	12.1	34398	131270	12.26	0.01	2.36	0.02	11.18	1.93	1.59	0.001	3.94
opx1_2	-4797	588	12	72796	130200	12.22	0.01	5.44	0.03	8.54	1.23	1.59	0.001	9.09
opx1_3	-4698	576	12.3	78389	119360	12	0.02	4.97	0.006	1.76	0.07	1.6	0.001	8.30
opx1_4	-4586	473	12.3	40392	120770	11.99	0.03	4.34	0.04	6.21	0.62	1.58	0.001	7.25
opx1_5	-4480	276	11.5	74627	129170	12.09	0.02	4.83	0.05	5.65	0.48	1.58	0.001	8.07
opx1_6	-4550	220	11.6	56561	132720	12.35	0.02	4.55	0.02	10.83	0.8	1.57	0.001	7.60
opx1_7	-4632	133	11.3	4324	129060	12.02	0.08	0.34	0.006	8.59	1.06	1.57	0.001	0.57
opx1_8	-4685	102	11.3	11747	125290	12.16	0.03	1.23	0.01	19.61	0.15	1.58	0.002	2.05
opx2_1	-566	1073	9.8	18996	113030	12.15	0.04	1.04	0.02	3.38	0.38	1.57	0.001	1.74
opx2_2	-721	1073	9.7	16892	126830	12.39	0.03	1.3	0.01	11.39	1.94	1.57	0.001	2.17
opx2_3				16883	127340	12.08	0.09	0.56	0.01	10.22	1.67	1.57	0.002	0.94
opx3_2	-8627	-3068	7.9	72687	95521	12.27	0.02	5.25	0.02	27.44	5.08	1.78	0.003	8.77
opx3_3	-8700	-3012	8.1	52512	103840	12.21	0.02	3.51	0.02	22	3.57	1.71	0.001	5.86
opx3_4	-8727	-2930	8.3	15888	103970	12.1	0.02	0.98	0.01	17.37	2.47	1.68	0.002	1.64
plag1_1	-5366	638	11.6	4245	117470	11.92	0.05	0.48	0.07	2.08	0.15	1.6	0.001	0.86
plag1_2	-5278	616	11.6	4624	123020	11.93	0.05	0.55	0.01	7.05	0.52	1.58	0.001	0.98
plag1_3	-5185	563	11.8	4431	131230	11.92	0.04	0.52	0.01	4.46	0.65	1.57	0.001	0.93
plag1_4	-5062	592	12	4143	133070	11.91	0.04	0.5	0.01	7.63	1.27	1.57	0.001	0.89
plag1_5	-4989	552	12	4369	125480	11.97	0.04	0.38	0.006	16.52	0.4	1.59	0.002	0.68

plag2_1	-1076	1073	9.9	4282	109890	11.99	0.06	0.43	0.007	3.79	0.17	1.54	0.005	0.77
plag2_2	-1178	1108	9.1	3524	106100	11.85	0.08	0.48	0.01	11.49	1.62	1.55	0.008	0.86
plag2_3	-1024	1178	8.7	3477	104440	11.98	0.06	0.52	0.01	7.98	1.12	1.55	0.001	0.93
plag3_1	-8834	-2893	8.4	9387	109850	12.11	0.04	0.91	0.001	14.98	2.16	1.6	0.001	1.62
plag3_2	-8884	-2829	8.6	9795	116070	12.09	0.05	0.94	0.03	9.75	1.7	1.59	0.001	1.67
DM9871														
cpx2_1	-7678	-1467	14.4	12367	11443	11.69	0.04	6.41	0.08	3.89	0.49	1.63	0.004	9.48
cpx2_2	-7654	-1523	14.4	4911	11255	11.7	0.07	3.11	0.05	4.54	0.87	1.63	0.004	4.60
cpx2_3	-7643	-1625	14.5	4706	12425	12.11	0.06	2.19	0.03	8.88	1.33	1.61	0.003	3.24
cpx2_4	-7604	-1688	14.6	4756	11913	12.24	0.05	2.28	0.06	15.49	1.83	1.62	0.005	3.37
cpx2_5	-7564	-1747	14.7	10629	16056	12.16	0.05	2.98	0.03	23.9	2.66	1.59	0.004	4.41
cpx2_6	-7578	-1835	14.8	10476	11079	11.67	0.06	5.25	0.09	4.93	0.63	1.59	0.006	7.77
opx2_1	-7474	-580	14.9	2615	13014	12	0.21	2.14	0.06	3.58	0.38	1.6	0.003	3.34
opx2_2	-7439	-668	14.6	5355	13888	12.27	0.08	1.94	0.05	13.39	1.02	1.61	0.009	3.03
opx2_3	-7450	-739	15.4	3427	13081	12.15	0.13	2.08	0.04	16.65	3.06	1.62	0.003	3.25
opx2_4	-7450	-814	15	4748	13752	12.32	0.08	2.4	0.07	19.88	2.09	1.6	0.003	3.74
opx2_5	-7440	-879	15	3828	12927	12.13	0.09	2.64	0.04	18.78	2.88	1.62	0.004	4.12
opx2_6	-7453	-962	15.1	2539	13167	12.13	0.09	1.57	0.05	14.29	2.74	1.61	0.005	2.45
plag1_1	-7517	-2001	14.9	682	15393	11.86	0.15	0.32	0.03	2.81	0.47	1.58	0.004	0.51
plag1_2	-7491	-2066	14.8	698	15351	12.02	0.14	0.34	0.02	2.64	0.48	1.58	0.005	0.54
plag1_3	-7515	-2130	15	520	13784	11.89	0.28	0.28	0.02	2.88	0.49	1.54	0.007	0.45
plag1_4	-7474	-2217	15.1	818	15715	12.1	0.21	0.34	0.02	5.84	0.93	1.56	0.005	0.54

WD9532

cpx1_1	-7982	1667	11.5	13809	23396	11.69	0.07	3.45	0.08	6.65	0.47	1.71	0.002	5.05
cpx1_2	-7982	1454	11.5	12765	24346	12.38	0.02	3.29	0.05	21.8	4.4	1.67	0.004	4.81
cpx1_3	-7970	1361	11.6	13254	25088	12.4	0.03	3.52	0.07	26.3	4.29	1.64	0.005	5.15
cpx1_4	-7980	1194	11.8	11219	26247	12.38	0.03	3.35	0.06	20.17	3.81	1.63	0.003	4.90
opx1_2	-6482	1027	12.2	15432	35446	12.43	0.04	2.61	0.05	10.16	1.89	1.61	0.004	3.94
opx1_3	-6392	937	11.9	15140	34890	12.35	0.02	2.49	0.04	10.2	1.59	1.6	0.002	3.76
opx1_4	-6291	857	12	14838	34839	12.37	0.03	2.44	0.03	9.54	2.08	1.59	0.002	3.69
opx2_1				4484	24733	9.92	0.06	1.6	0.03	2.97	0.29	1.55	0.002	2.42
opx2_2				5217	24626	9.92	0.08	1.33	0.04	6.03	0.75	1.56	0.004	2.01
opx2_3				4812	24217	9.67	0.06	1.54	0.03	6.92	1.01	1.52	0.005	2.33
plag1_1	-5667	1462	12.2	824	32555	12.56	0.14	0.25	0.04	5.35	1.03	1.55	0.001	0.41
plag1_2	-5536	1462	12.4	814	32075	12.48	0.13	0.26	0.04	5.75	1.08	1.55	0.001	0.43
plag1_3	-5341	1462	12.2	808	31301	12.82	0.14	0.24	0.04	6.05	1.22	1.54	0.001	0.40
plag2_1			11.5	475	28183	11.49	0.19	0.17	0.02	4.3	0.36	1.52	0.005	0.28

WD9546

cpx1_1	4605	2527	15.2	13333	22106	11.89	0.07	3.74	0.09	9.73	0.64	1.53	0.003	5.53
cpx1_2	4587	2664	15	11593	17334	12.42	0.03	4.58	0.08	29.14	3.3	1.55	0.004	6.77
cpx1_3	4737	2743		10834	17522	12.37	0.04	4.65	0.07	34.94	5.69	1.54	0.002	6.88
cpx1_4	4840	2940	17	11400	17989	12.47	0.04	4.61	0.07	23.78	3.46	1.54	0.005	6.82

cpx2_1	759	1609	15.7	12239	18470	11.97	0.04	4.77	0.09	8.02	0.6	1.57	0.003	7.05
cpx2_2	821	1491	15.1	10645	18854	12.35	0.03	4.48	0.07	18.54	1.51	1.57	0.003	6.63
cpx2_3	957	1346	15.2	11814	19319	12.41	0.03	4.86	0.07	38.44	5.1	1.56	0.001	7.19
cpx2_4	1043	1371	15.6	12276	19910	12.38	0.02	4.7	0.07	25.73	3.23	1.56	0.003	6.95
cpx2_6	821	937	15.2	12124	20844	12.38	0.04	4.59	0.07	11.07	1.31	1.55	0.002	6.79
cpx2_7	958	679	15.4	12590	20846	12.32	0.02	4.66	0.05	11.67	1.31	1.55	0.003	6.89
opx1_1	2447	-1344	14.8	18432	31729	11.76	0.05	3.28	0.07	5.81	0.19	1.55	0.002	5.11
opx1_3	2486	-1659	14.7	17398	34294	12.42	0.03	3.2	0.05	8.39	0.93	1.54	0.003	4.98
opx1_4	2518	-1799	14.9	17968	34694	12.43	0.02	3.15	0.05	14.07	1.64	1.55	0.003	4.91
opx1_5	2583	-1952	14.9	17776	32341	12.27	0.06	3.23	0.05	11.78	1.43	1.55	0.004	5.03
plag1_1	833	976	14.9	692	25686	12.39	0.11	0.25	0.01	4.48	0.39	1.52	0.006	0.38
plag1_2	798	856	14.8	912	26937	12.63	0.19	0.33	0.02	7.38	1.02	1.53	0.003	0.50
plag2_1	923	780	14.8	711	26747	12.24	0.18	0.28	0.02	9.08	1.45	1.54	0.002	0.42
plag2_2	964	703	14.6	619	25813	12.34	0.12	0.25	0.01	5.99	0.77	1.54	0.003	0.38
plag3_1	2997	-1642	14.5	503	27599	11.1	0.17	0.18	0.01	2.16	0.27	1.53	0.002	0.27
plag3_2	2997	-1703	14.8	523	28045	10.47	0.42	0.17	0.01	6.31	1.08	1.54	0.001	0.26
plag3_3	2997	-1793	14.8	450	26744	10.76	0.24	0.17	0.01	5.28	1.12	1.54	0.002	0.26

Note: x and y denote the position of analyzed point in the μm unit; Ip is the beam current in the nA unit; ^{7}Li(cps) and ^{30}Si(cps) are the counts per second on ^{7}Li and ^{30}Si, respectively; ^{7}Li/^{6}Li, Lif/^{30}Si, B/^{30}Si and ^{29}Si/^{30}Si are the pre-specified index isotopic ratios to monitor the instrument status and calculate the lithium content, Li (ppm); sd is the standard deviation.

Table A 4 Lithium isotopic results of cpx and opx (and plag) in the lower crustal granulites by ion microprobe

	x	y	point	Ip (nA)	^{7}Li (cps)	δ^7Li	sd	δ^7Li_{corr}
04NS11								
opx1_1	-2425	1358	c	17.5	1.1E+04	30.14	0.89	4.9
opx1_2	-2370	1226	r	17.5	1.4E+04	31.00	0.81	5.8
opx2_1	4083	-4992	c	17.4	2.8E+04	22.34	0.86	-2.9
opx2_2	4167	-4992	r	17.1	3.1E+04	24.52	0.95	-0.7
opx2_1 #	-3120	5418	r		2.4E+04	23.83	0.88	-0.6
opx2_2 #	-3120	5359			2.1E+04	10.94	1.13	-13.5
opx2_3 #	-3112	5313			2.0E+04	4.19	1.69	-20.2
opx2_4 #	-3112	5246			1.8E+04	6.20	2.30	-18.2
opx2_5 #	-3112	5186			1.6E+04	10.73	1.56	-13.7
opx2_6 #	-3106	5100	c		2.1E+04	16.92	0.88	-7.5
opx2_7 #	-3086	5038			1.8E+04	25.76	1.22	1.3
opx2_8 #	-3065	4967			1.8E+04	33.85	1.04	9.4
opx2_9 #	-3065	4911	r		1.0E+04	35.08	1.63	10.6
opx3_1	-7820	1674	r		1.4E+04	25.25	1.04	0.8
opx3_2	-8411	1978			1.4E+04	10.25	0.89	-14.2
opx3_3	-8230	1891	c		2.3E+04	34.25	0.62	9.8
opx3_4	-8015	1782	r		2.2E+04	21.45	0.81	-3.0

	x	y	point	Ip (nA)	^{7}Li (cps)	δ^7Li	sd	δ^7Li_{corr}
cpx2_7 #	-2285	-2587			1.5E+04	12.14	0.67	-12.3
cpx2_8 #	-2285	-2466			1.9E+04	11.37	0.62	-13.1
cpx2_9 #	-2285	-2396	r		2.3E+04	14.72	0.54	-9.7
opx2_1	1089	-559	r		2.8E+04	18.32	0.55	-6.1
opx2_2	1089	-441			2.7E+04	10.10	0.58	-14.3
opx2_3	1089	-307			2.5E+04	8.32	0.57	-16.1
opx2_4	1089	-54			2.0E+04	37.04	0.76	12.6
opx2_5	1287	616			2.8E+04	17.50	1.54	-6.9
opx2_6	1287	804			2.9E+04	28.89	0.46	4.5
opx2_7	1287	924			2.6E+04	27.96	0.58	3.5
opx2_8	1287	1078	c		2.5E+04	32.42	0.54	8.0
DM9871								
cpx1_1	-7293	-5519	c	10.8	7.1E+03	29.29	1.07	4.1
cpx1_2	-7301	-5343	r	10.5	7.1E+03	26.52	1.17	1.3
cpx1_1 #	-6455	-5207	c	17.0	8.4E+03	32.78	1.11	8.3
cpx1_2 #	-6423	-5373		17.1	8.8E+03	29.71	0.99	5.3
cpx1_3 #	-6372	-5535		16.9	9.1E+03	24.86	0.90	0.4
cpx1_4 #	-6337	-5652		16.7	1.1E+04	12.50	0.72	-11.9
cpx1_5 #	-6312	-5774		16.7	2.0E+04	7.34	0.62	-17.1

opx4_1	-7694	1593	r		1.9E+04	32.21	1.10	7.8
opx4_2	-7644	1555			1.8E+04	28.16	1.02	3.7
opx4_3	-7564	1430	c		1.6E+04	14.39	1.10	-10.0
04NS13								
opx1_1	-5515	3335	c	14	2.3E+04	27.49	0.70	2.3
opx1_2	-5684	3364		13.8	2.7E+04	25.10	0.69	-0.1
opx1_3	-5736	3337		14.1	3.0E+04	25.35	0.61	0.2
opx1_4	-5791	3291		14	3.3E+04	29.09	0.78	3.9
opx1_5	-5852	3291		14.7	1.5E+04	21.09	0.74	-4.1
opx1_6	-5901	3285		14.1	1.3E+04	20.96	0.75	-4.2
opx1_7	-5980	3192		14.4	2.5E+04	25.78	0.64	0.6
opx1_8	-5980	3040	r	14.2	2.0E+04	24.96	0.62	-0.2
opx2_1	-6424	3180	c	13.9	3.8E+04	12.53	0.47	-12.7
opx2_2	-6364	3235	r	13.7	4.0E+04	12.88	0.57	-12.3
04NS9								
opx1_1	-253	2730	c	18.5	1.2E+04	31.27	0.92	6.1
opx1_2	-103	2833	r	18.5	1.4E+04	28.61	1.15	3.4
cpx1_1	-445	5490	c	13.9	9.4E+03	30.71	1.22	5.5
cpx1_2	-334	5417		12.7	1.2E+04	27.75	0.92	2.6
cpx1_3	-242	5417		12.7	9.6E+03	28.31	1.08	3.1
cpx1_4	-158	5469		12.7	6.5E+03	30.84	1.21	5.6
cpx1_6 #	-6283	-5878		17.0	4.1E+04	10.12	0.51	-14.3
cpx1_7 #	-6266	-6020	r	16.9	4.9E+04	10.01	0.58	-14.4
opx1_1	-1656	-3880	c	15.8	6.7E+03	21.11	0.91	-4.1
opx1_2	-1855	-3952	r	15.6	7.1E+03	29.29	1.07	4.1
opx1_1 #	-1745	-4184	r		1.2E+04	23.58	0.68	-0.9
opx1_2 #	-1818	-4188			1.4E+04	22.53	0.72	-1.9
opx1_3 #	-1878	-4157			4.1E+03	18.27	1.18	-6.2
opx1_4 #	-1907	-4124			3.6E+03	23.94	1.47	-0.5
opx1_5 #	-1950	-4093			3.3E+03	21.37	1.45	-3.1
opx1_6 #	-2001	-4080	c		4.9E+03	30.29	1.24	5.9
opx1_7 #	-2089	-3952			6.4E+03	29.70	0.94	5.3
opx1_8 #	-2135	-3908			3.6E+03	28.20	1.42	3.8
opx1_9 #	-2182	-3832			8.8E+03	21.37	0.89	-3.1
opx1_10 #	-2228	-3808	r		6.6E+03	20.39	0.92	-4.0
cpx2_1	-7690	-2469	c	15.8	1.4E+04	9.77	0.68	-15.4
cpx2_2	-7681	-2425		15.9	1.4E+04	8.78	0.80	-16.4
cpx2_3	-7665	-2370		15.4	1.6E+04	4.96	0.62	-20.2
cpx2_4	-7657	-2332		16.1	1.9E+04	0.28	0.58	-24.9
cpx2_5	-7657	-2285		16.4	3.5E+04	0.31	0.44	-24.9
cpx2_6	-7650	-2221		16.6	1.3E+04	5.88	0.32	-19.3
cpx2_7	-7631	-2184		16	1.1E+04	7.10	0.34	-18.1
cpx2_8	-7795	-2510	r	14.1	1.0E+04	10.10	1.47	-15.1

cpx1_5	-230	5651	r	12	5.2E+03	26.48	1.80	1.3
04NS16								
opx1_1	-392	7351	c	11	1.4E+04	26.84	0.84	1.6
opx1_2	-580	7330	r	11.6	1.4E+04	20.85	0.88	-4.4
cpx1_1	-1817	3639	c	18	3.6E+04	28.10	0.64	2.9
cpx1_2	-1721	3609	r	18.3	4.1E+04	25.65	0.62	0.4
MJ9801								
opx1_1	-4193	4726	c	20.4	1.1E+04	20.86	1.34	-4.3
opx1_2	-4089	4323	r	20.4	1.2E+04	18.36	1.32	-6.8
cpx1_1	-821	-1682	r	15.1	4.5E+04	27.39	0.84	2.2
cpx1_2	-675	-1639	c	15	4.3E+04	24.68	1.04	-0.5
cpx2_1	-3401	-4243	c	15.1	4.5E+04	27.07	1.01	1.9
cpx2_2	-3495	-4289		14.2	6.6E+04	19.81	0.73	-5.4
cpx2_3	-3495	-4157	r	14.3	4.9E+04	25.41	0.96	0.2
grt1	-2913	-4614		15.5	1.6E+04	21.88	1.21	-3.3
plag1_1	-3404	-4299		15.2	1.5E+04	12.01	1.60	-13.2
plag1_2	-3508	-4284		15.2	1.6E+04	11.44	1.38	-13.8

cpx2_1 #	-8081	-2553	*c*	16.7	6.6E+03	13.05	1.05	-11.4
cpx2_2 #	-6955	-2597		16.5	1.8E+04	0.91	0.78	-23.5
cpx2_3 #	-7052	-2752	*r*	16.5	1.5E+04	8.52	0.70	-15.9
opx2_1	-7631	-2032		15.6	8.4E+03	8.76	0.93	-16.4
opx2_2	-7617	-1970		16.2	5.7E+03	7.85	1.11	-17.4
opx2_3	-7601	-1774	r	15.7	1.5E+04	25.83	0.65	0.6
opx2_4	-7586	-1723		15.1	2.2E+04	31.59	0.68	6.4
opx2_5	-7636	-1648	c	14.2	2.5E+04	31.61	0.62	6.4
opx3_1 #	-7926	-1610	*c*		2.0E+04	42.28	0.74	8.0
opx3_2 #	-8077	-1610			2.3E+04	42.00	0.61	7.7
opx3_3 #	-8205	-1631	*r*		1.2E+04	35.36	0.72	1.1
WD9532								
cpx1_1	-8095	2297	c	8.1	8.4E+03	20.34	1.32	-4.9
cpx1_2	-8072	2530	r	8.2	6.9E+03	15.52	1.55	-9.7
cpx1_1 #			r		5.3E+03	22.24	1.38	-2.2
cpx1_2 #			c		1.0E+04	24.78	0.84	0.3
opx1_1	-6543	1903	c	7.9	1.2E+04	15.38	1.38	-9.8
opx1_2	-6543	2123	r	7.7	1.8E+04	8.43	1.01	-16.8
opx1_1 #	-6847	1600	r		9.8E+03	7.67	0.80	-16.8

MJ9805								
opx1_1	-8469	303	c	18.3	1.3E+04	20.21	1.08	-5.0
opx1_2	-8547	144	r	18.6	3.4E+04	17.66	0.78	-7.5
cpx1_1	-2561	2096	r	13.8	2.9E+04	22.17	1.02	-3.0
cpx1_2	-2588	2016	c	13.8	3.1E+04	21.34	1.12	-3.9
cpx2_1	-2476	2402	c	13	3.3E+04	20.98	0.99	-4.2
cpx2_2	-2411	2458	r	13	3.5E+04	20.07	0.95	-5.1
opx2	-419	-1775	c	13.8	5.5E+03	28.85	1.40	3.7
DM9855								
cpx1_1	-8165	-3251	c	14.1	1.1E+04	20.40	0.91	-4.8
cpx1_2	-8192	-3476	r	14	1.3E+04	14.82	0.79	-10.4
cpx1_1 #	-7885	-3148	r		1.3E+04	12.04	0.79	-12.4
cpx1_2 #	-7885	-3268			1.1E+04	20.38	1.10	-4.1
cpx1_3 #	-7885	-3355			2.7E+04	25.44	1.08	1.0
cpx1_4 #	-7885	-3547			2.6E+04	16.21	1.14	-8.2
cpx1_5 #	-7885	-3679	c		1.4E+04	26.28	1.39	1.8
cpx1_6 #	-7885	-3953			1.3E+04	32.65	1.43	8.2
cpx1_7 #	-7867	-4129			1.4E+04	35.36	1.31	10.9
cpx1_8 #	-7867	-4253			1.5E+04	10.80	1.22	-13.6
cpx1_9 #	-7867	-4372	r		2.6E+04	16.80	1.56	-7.6
cpx1_10 #	-7826	-4610	r		1.6E+04	30.16	1.81	5.7

opx1_2 #	-6739	1600			1.1E+04	25.76	0.85	1.3
opx1_3 #	-6635	1600			1.2E+04	25.76	0.82	1.3
opx1_4 #	-6535	1600	c		1.3E+04	22.70	0.70	-1.7
opx1_5 #	-6438	1600			1.4E+04	18.75	0.68	-5.7
opx1_6 #	-6350	1600			1.5E+04	18.78	0.66	-5.7
opx1_7 #	-6239	1600	r		1.1E+04	10.03	0.63	-14.4
opx2_1	-3399	2487	c	7.4	8.2E+03	17.56	1.39	-7.6
opx2_2	-3496	2695	r	7.9	8.0E+03	21.88	1.38	-3.3
opx2_1 #	-3450	2889	r		1.3E+04	16.95	0.77	-7.5
opx2_2 #	-3450	2723			9.8E+03	28.16	0.90	3.7
opx2_3 #	-3450	2492			9.4E+03	29.41	0.76	5.0
opx2_4 #	-3450	2303			1.0E+04	28.85	0.84	4.4
opx2_5 #	-3450	2178	c		1.0E+04	31.32	0.78	6.9
opx2_6 #	-3450	1937	r		9.3E+03	29.47	0.80	5.0
cpx2_1	1539	418	c	7.6	5.3E+03	21.92	1.94	-3.3
cpx2_2	1539	701	r	7.8	5.6E+03	23.30	1.48	-1.9
cpx2_1 #	1134	-557	r		3.5E+03	21.38	2.25	-3.1
cpx2_2 #	1134	-703			6.5E+03	24.64	2.33	0.2
cpx2_3 #	1082	-769			5.4E+03	15.96	1.80	-8.5
cpx2_4 #	1042	-863			4.4E+03	8.59	2.28	-15.9
cpx2_5 #	1042	-1116	c		8.5E+03	25.27	1.96	0.8
cpx2_6 #	1042	-1243			3.8E+03	21.64	1.63	-2.8

opx1_1	-4265	190	c	14.2	2.4E+04	10.91	0.64	-14.3
opx1_2	-4251	-4		14.4	1.9E+04	26.46	0.72	1.3
opx1_3	-4247	-97	r	14.2	2.0E+04	24.53	0.78	-0.7
opx1_1 #	-5382	445	r		1.8E+04	20.53	0.71	-3.9
opx1_2 #	-5015	445	c		3.2E+04	11.16	0.44	-13.3
opx1_3 #	-4866	445	r		3.2E+04	20.56	0.48	-3.9
opx1_4 #	-7873	350	r		1.9E+04	12.27	0.62	-12.2
cpx2_1	1378	-2773	c	14.1	9.4E+03	22.84	0.87	-2.4
cpx2_2	1370	-2702		12.4	9.5E+03	21.69	0.98	-3.5
cpx2_3	1463	-2802		12.8	9.6E+03	23.29	0.89	-1.9
cpx2_4	1355	-2849		12.7	9.0E+03	20.46	0.96	-4.7
cpx2_5	1261	-2780	r	13.3	9.5E+03	21.62	0.95	-3.6
cpx2_6	1150	-2726	c	11	9.8E+03	11.21	1.05	-14.0
cpx2_1 #	-2285	-3465	r		2.8E+04	25.54	0.54	1.1
cpx2_2 #	-2285	-3337			1.8E+04	26.65	0.67	2.2
cpx2_3 #	-2285	-3215			2.3E+04	21.88	0.57	-2.6
cpx2_4 #	-2285	-3108			1.9E+04	20.12	0.55	-4.3
cpx2_5 #	-2285	-2894	c		9.3E+03	21.80	1.11	-2.6
cpx2_6 #	-2285	-2694			1.1E+04	15.86	0.63	-8.6
cpx2_7 #	1000	-1345	r		3.8E+03	17.54	1.66	-6.9
plag1_1	-5466	2369	c	80.4	1.2E+04	24.76	1.09	-0.4
WD9546								
cpx1_1	-4701	-3670	c	8.6	7.6E+03	14.59	1.42	-10.6
cpx1_2	-4673	-3740		8.6	7.9E+03	15.43	1.39	-9.8
cpx1_2	-4562	-3858	r	8.8	8.1E+03	16.00	1.49	-9.2
cpx2_1	-1051	-1948	c	9.7	7.6E+03	16.77	1.46	-8.4
opx1_1	-2307	1045	c	8.9	9.0E+03	12.04	1.59	-13.2
opx1_2	-2439	999		9	4.0E+03	5.76	1.66	-19.4
opx1_3	-2453	934		9	2.8E+03	6.56	2.22	-18.6
opx1_4	-2481	894		8.9	2.2E+03	9.62	2.19	-15.6
opx1_5	-2496	840		8.5	5.1E+03	15.61	1.88	-9.6
opx1_6	-2520	798		8.1	2.6E+03	7.13	2.11	-18.1
opx1_7	-2526	748		8	7.8E+03	17.01	1.56	-8.2
opx1_8	-2526	684		8.1	9.4E+03	15.25	1.58	-10.0
opx1_9	-2517	641		8.3	9.7E+03	12.62	1.57	-12.6
opx1_10	-2529	608		8.4	1.1E+04	13.06	1.68	-12.1
opx1_11	-2513	720		9.3	1.2E+04	14.39	0.88	-10.8
opx1_12	-2595	762	r	9.1	1.5E+04	12.72	0.74	-12.5

Note: x and y denote the position of analyzed point in the μm unit; Ip is the beam current in the nA unit; ^{7}Li(cps) is the counts per second; c and r are core and rim, respectively; δ^{7}Li and $\delta^{7}Li_{corr}$ are the measured and calibrated Li-isotopic values, respectively; sd is the standard deviation.

Table A 5 correspondence in the grain number sequence between Li and H isotopic data

Li	H	Li	H
04NS9		DM9871	
cpx1	cpx2	cpx2	cpx2
MJ9801		WD9532	
cpx1	cpx1	cpx1	cpx2
cpx2	cpx2		
		WD9546	
MJ9805		cpx1	cpx2
cpx1	cpx1	cpx2	cpx1
DM9855			
cpx1	cpx1		

Note: the grain number sequence between the ion microprobe Li and H isotopic analyses are not always the same with each other, and their correspondence is illustrated here.

Related publications and manuscripts:

Yang Xiaozhi, Xia Qunke, Deloule Etienne, Dallai Luigi, Fan Qicheng, Feng Min. Water in minerals of continental lithospheric mantle and overlying lower crust: a comparative study of peridotite and granulite xenoliths from the North China Craton. Chem. Geol., 2008, in review.

Yang Xiaozhi, Deloule Etienne, Xia Qunke, Fan Qicheng, Feng Min. Water contrast between Precambrian and Phanerozoic continental lower crust in eastern China. J. Geophys. Res., 2008, doi:10.1029/2007JB005541,in press.

Yang Xiaozhi, Xia Qunke, Fan, Qicheng, Deloule E. Rheology of the continental lithosphere and effects of water in minerals: a review. Earth Science Frontiers, 2008, 15: 96-112. (in Chinese with English abstract)

Yang Xiaozhi, Xia Qunke, Deloule E., Fan Qicheng, Hao Yantao. Water in granulites: implications for the nature and evolution of the lower continental crust. Progress in Natural Sciences, 2007(17): 117-130.

Yang Xiaozhi, Xia Qunke. Comparison of H_2O in omphacite by two FTIR calibration coefficients. Acta Mineralogica Sinica, 2006(26): 210-214. (in Chinese with English abstract)

Yang Xiaozhi, Xia Qunke, Sheng Yingming, Yu Huimin, Hao Yantao. Water in the lower crustal granulite xenoliths from Nushan, Anhui Province. Acta Petrologica Sinica, 2005, 21(6): 1669-1676. (in Chinese with English abstract)

Yang Xiaozhi, Xia Qunke, Yu Huimin, Hao Yantao. Origin of high electrical conductivity in the lower continental crust: structural water in minerals? Advance in Earth Sciences, 2005, 2006, 21(1): 31-38. (in Chinese with English abstract)

Yang Xiaozhi, Xia Qunke, Cheng Hao, Wu Yuanbao. Application of SIMS in geochemistry: a review. Geology of Anhui, 2004, 14: 52-57. (in Chinese with English abstract)

Yang Xiaozhi, Xia Qunke, Deloule E.. Lithium isotopic composition of clinopyroxene megacrysts from Nushan, eastern China: An ion probe analysis. Acta Mineralogica Sinica, 2003, 23(4): 359-363. (in Chinese with English abstract)

Xia Qunke, **Yang Xiaozhi**, Hao Yantao et al. Water: distribution and circulation in the deep Earth, Earth Science Fronties, 2007, 14(2): 10-23. (in Chinese with English abstract)

Xia Qunke, **Yang Xiaozhi**, Deloule Etienne, Sheng Yingming, Hao Yantao. Water in the lower crustal granulite xenoliths from Nushan, eastern China. Journal of Geophysical Research, 2006, B11202, doi:10.1029/2006JB004296

Xia Qunke, Sheng Yingming, **Yang Xiaozhi**, Yu Huiming. Heterogeneity of water in garnets from UHP eclogites, eastern Dabieshan, China. Chemical Geology**,** 2005, 224: 237-246.

Sheng Yingming, Xia Qunke, Yu Huimin, **Yang Xiaozhi**. Water in clinopyroxenes from eclogites of Bixiling and Huangzhen, Dabieshan and geodynamic implications. Acta Petrologica Sinica, 2004, 20: 1133-1140. (in Chinese with English abstract)

Cheng Hao, Chen Daogong, Cheng Weiji, **Yang Xiaozhi**. Garnet chemical zoning in low-T eclogite: evidence for fast exhumation. Geochimica, 2003, 32: 81-85. (in Chinese with English abstract)

Yang Xiaozhi, Deloule Etienne, Xia Qunke. Ion microprobe investigations of O- and Li-isotopes in lower crustal granulite minerals of the North China Craton. In preparation to submit to Geochim. Cosmochim. Acta, 2008.

Yang Xiaozhi, Deloule Etienne, Xia Qunke. Hydrogen isotopic compositions of lower crustal granulite minerals: a case study from the North China Craton. In preparation to submit to Geochim. Cosmochim. Acta, 2008.

INSTITUT NATIONAL
POLYTECHNIQUE
DE LORRAINE

AUTORISATION DE SOUTENANCE DE THESE
DU DOCTORAT DE L'INSTITUT NATIONAL
POLYTECHNIQUE DE LORRAINE

o0o

VU LES RAPPORTS ETABLIS PAR :
Monsieur ZHANG Hongfu, Professeur, Institute of Geology and Geophysics, Chinese Academy of Sciences, Beijing, China

Monsieur Jannick INGRIN, Directeur de Recherche, Université Paul Sabatier, Toulouse

Le Président de l'Institut National Polytechnique de Lorraine, autorise :

Monsieur YANG XiaoZhi

NANCY BRABOIS
2, AVENUE DE LA
FORET-DE-HAYE
BOITE POSTALE 3
F - 54501
VANDŒUVRE CEDEX

à soutenir devant un jury de l'INSTITUT NATIONAL POLYTECHNIQUE DE LORRAINE, une thèse intitulée :

"Water content and H-O-Li isotopes in lower crustal granulite minerals"

en vue de l'obtention du titre de :

DOCTEUR DE L'INSTITUT NATIONAL POLYTECHNIQUE DE LORRAINE

Spécialité : « **Géosciences** »

Fait à Vandoeuvre, le 19 juin 2008
Le Président de l'I.N.P.L.,
F. LAURENT

TEL. 33/03.83.59.59.59
FAX. 33/03.83.59.59.55